NASA TECHNICAL MEMORANDUM

NASA TM X-62,094

NASA TM X-62,094

DIGITAL AUTOPILOTS: DESIGN CONSIDERATIONS AND SIMULATOR EVALUATIONS

Stephen Osder, Frank Neuman,
and John Foster

Sperry Flight Systems Division
Phoenix, Ariz. 85002

and

Ames Research Center
Moffett Field, Calif. 94

October 1971

DIGITAL AUTOPILOTS: DESIGN CONSIDERATIONS AND SIMULATOR EVALUATIONS

Prepared by

Stephen Osder
Sperry Flight Systems Divison

Frank Neuman
NASA Ames Research Center

John Foster
NASA Ames Research Center

Printed in U.S.A. October 1971 Pub. No. 70-1364-00-00

TABLE OF CONTENTS

TABLE OF CONTENTS (cont)

LIST OF TABLES

SUMMARY

This report describes the development of a digital autopilot program for a transport aircraft and the evaluation of that system's performance on a transport aircraft simulation. The digital autopilot includes three axis attitude stabilization, automatic throttle control and flight path guidance functions with emphasis on the mode progression from descent into the terminal area through automatic landing. The study effort involved a sequence of tasks starting with the definition of detailed system block diagrams and control laws followed by a flow charting and programming phase and concluding with performance verification using the transport aircraft simulation. The autopilot control laws were programmed in FORTRAN IV in order to isolate the design process from requirements peculiar to an individual computer. These control laws were grouped into the following categories:

- Longitudinal Stabilization (Pitch)
- Lateral - Directional Stabilization
- Autothrottle Control
- Vertical Guidance - Non-Landing
- Vertical Guidance - Landing
- Lateral Guidance

Stability, response time and accuracy performance criteria for these various functions were identified and the simulations verified that these criteria can be met using the specified digital autopilot program.

LIST OF SYMBOLS

A_y	Aircraft lateral acceleration in Y direction
b	Wing span (lateral normalizing length)
$\bar{c}$	Mean aerodynamic chord (pitch normalizing length)
C_D	Drag coefficient = $D/\frac{1}{2}\rho V^2 S$
$C_{D(\ )}$	$\partial C_D/\partial(\ )$
C_L	Lift coefficient $L/\frac{1}{2}\rho V^2 S$
$C_{L(\ )}$	$\partial C_L/\partial(\ )$
C_ℓ	Rolling moment coefficient = $L/\frac{1}{2}\rho V^2 Sb$
$C_{\ell(\ )}$	$\partial C_\ell/\partial(\ )$
C_m	Pitching moment coefficient = $M/\frac{1}{2}\rho V^2 S\bar{c}$
$C_{m(\ )}$	$\partial C_m/\partial(\ )$
C_n	Yawing moment coefficient = $N/\frac{1}{2}\rho V^2 Sb$
$C_{n(\ )}$	$\partial C_n/\partial(\ )$
C_Y	Side force coefficient = $F_y/\frac{1}{2}\rho V^2 S$
$C_{Y(\ )}$	$\partial C_Y/\partial(\ )$
D	Drag
F	Force (direction identified by subscript)

g	Gravitational acceleration = 32.2 ft/sec^2
$G(s)$, $H(s)$	Transfer function in Laplace format
h	Altitude (measurement source identified by subscript)
$k,a,b,c,d,e,f..$	Constants for gains etc, defined by subscript
L	Lift or roll moment
M	Pitch moment
m	Mass
N	Yawing moment
N_z or A_z	Aircraft normal acceleration in Z direction
p	Body axis roll rate
Q	Dynamic pressure = $\frac{1}{2}\rho V^2$
q	Body axis pitch rate
R	Slant distance to target point or to coordinate system origin
r	Body axis yaw rate
S	Wing area
s	Laplace operator
T	Thrust
t	Time
V	Velocity
V_c	Calibrated airspeed
V_T	True airspeed
W	Weight
x	Fore-aft distance - along flight path or along fore-aft aircraft axis as defined by coordinate system

y	Lateral distance - orthogonal to x distance
z	Downward distance - orthogonal to x distance
α	Angle of attack
β	Slideslip angle or lateral ILS beam deviation
γ	Flight path angle
Δ	Increment (prefix symbol)
δ	Control angle - general term defined by subscript
δ_A	Aileron or lateral control surface deflection angle
δ_E	Elevator or elevon deflection angle
δ_F	Flap deflection angle
δ_R	Rudder deflection angle
δ_{STAB}	Horizontal stabilizer deflection angle
δ_T	Throttle quadrant deflection angle
ζ	Damping ratio
θ	Pitch euler angle
λ	ILS glide slope deviation
ρ	Air density
τ	Time Constant
ϕ	Roll euler angle
ψ	Heading angle
ω	Frequency (rad/sec)
$\dot{(\ )}$	$\frac{d(\ )}{dt}$
$\ddot{(\ )}$	$\frac{d^2(\ )}{dt^2}$

SUBSCRIPTS

B	Barometric
C	command, computed or compensated
D/C	Decrab
E or ϵ	Error
F	Flare or final value (quantity at touchdown)
g	Gust
G/S	Glide Slope
i	Inertial
LOC	Localizer
MAX	Maximum value
MIN	Minimum value
o	Initial value
p	Phugoid
P	Predictive
R	Runway
REF	Reference (equivalent to command)
sp	Short period

SECTION I

INTRODUCTION

SECTION I

INTRODUCTION

This report summarizes work performed by Sperry Flight Systems Division and NASA Ames Research Center on a joint study to develop a simulation program for an advanced, three-axis, digital autopilot. The effort involved a sequence of tasks starting with the definition of detailed system block diagrams and control laws followed by a flow charting and programming phase and concluding with performance verification using a complete digital simulation of a representative transport aircraft. The digital autopilot includes three axis attitude stabilization, automatic throttle control, and flight path guidance functions, with special emphasis on the mode progression from descent into the terminal area through automatic landing.

The first phase of the study was performed by Sperry. It was a preliminary design activity in which all control laws and detailed system block diagrams were generated in Laplace Transform format. All filters and compensators associated with realistic requirements of airborne equipment were defined. Stability considerations for all control modes were identified in terms of generalized root loci which scoped the stability problems for the jet transport class of vehicles. Nonlinear constraints within the aircraft's flight controls such as actuator velocity and travel limits were identified for proper vehicle simulations. Appropriate non-linear controls such as maneuvering contraints and control authority limits were incorporated in the autopilot control laws in accordance with the program objectives of including practical operational considerations. Finally, quantitative and qualitative performance criteria and test procedures were specified to permit evaluation of the autopilot designs.

The second phase of the study involved the translation of control equations and system block diagrams into the mathematical form and flow charts needed to generate the digital autopilot program. This work was done by NASA Ames Research Center with Sperry participating in program review and debugging. It is noted that neither the scope of the problem or the programming procedures that were followed were fully representative of an actual airborne digital autopilot design

activity. The process of reducing Laplace Transform specified control laws and filters to flow charts and difference equations is certainly applicable to the real design procedure. In this study the difference equations were derived by converting the Laplace Transform equations to equivalent Z transforms as discussed in reference 5. Subroutines were used to compute difference equation coefficients for different sampling rates. In actual practice, when higher frequency compensators are programmed (such as those associated with elastic mode stabilization) it may be desirable to arrive at the required difference equation via the bilinear W transformation to the Z transform in order to improve the discrete representation of the continuous filter. (Reference 6).

A more significant departure from real design practice for an airborne system was the use of a high level language to code the guidance and control computations. In this study the autopilot control laws were programmed in FORTRAN IV in order to isolate the design process from requirements peculiar to an individual computer. The FORTRAN IV programs permitted the problem to run in nonreal time on the IBM 360/367 or in real time on the EAI 8400. While a higher level programming language is certainly a convenient approach to the problem, in actual design practice, compiler efficiencies do not seem able to compete with direct machine language or assembler coding in terms of computer time and memory consumption.

The most significant difference between the computer programs developed in this study and those that would be used in a practical airborne system relates to the fact that in this study the problem was restricted to guidance and control law computation. A practical airborne system would have to devote a major part of its computer program to data formatting, packing and unpacking, I/O operations, test, and monitoring routines. Experience in designs (such as the SST digital autopilot) shows that these functions would consume 50 to 90 percent of the airborne program.

The organization of this report is based on the autopilot control modes rather than on the chronological phases of the study. Six major groups of control functions are covered. They are:

- Longitudinal Stabilization (pitch)
- Lateral-Directional Stabilization
- Autothrottle Control
- Vertical Guidance - Nonlanding

- Vertical Guidance - Landing
- Lateral Guidance

The first two stabilization functions are the autopilot inner loops. The guidance functions may be viewed as commands applied to these inner loops. Trends in modern control theory tend to neglect this concept of multiple loop closures and instead, treat the entire problem in terms of a single state and control vector. In this study we have taken the approach of successive loop closures because it leads to a better perspective of the design problem. The criteria associated with these different loops are considerably different. The inner or stabilization loops are concerned primarily with stability and the interaction with the actuation system dynamics. In treating these loops we must recognize that aircraft rigid body equations are only approximations and due consideration must be given to the possibility of elastic mode coupling even when the elastic mode data is not available. The guidance modes are, in general, uncoupled from the higher frequency modes associated with attitude stabilization.

The criteria for guidance modes are essentially those related to accuracy. Guidance (or steering) system design involves such factors as selection and blending of the proper state measurements and the use of appropriate compensating techniques for winds and aircraft asymmetries. Stability considerations are important but different from those associated with the inner loops. While the damping ratios of some higher frequency modes associated with the inner loops may be tolerated at values of 0.3 or lower, the guidance mode damping ratios as high as 0.6 may be objectionable. Relatively low damping ratios associated with guidance modes can be made acceptable if special switching logic is used to prevent excitation of those modes.

In the case of the autothrottle modes, the criteria are accuracy and minimization of throttle activity. The constraints necessary to prevent excessive throttle activity necessitate the use of open loop or predictive controls to achieve the desired performance.

In this report the individual loops are considered separately and then in combination with the other modes. Thus longitudinal and lateral stabilization functions are treated first without the guidance modes engaged. The control laws are developed and stability factors identified. The digital programs are described and then performance is verified with the digital simulations. When this process is repeated for the guidance modes, the attitude stabilization and autothrottle modes are already included with their optimized parameters. The combination of all control modes defines a complete autopilot control law computation program. A brief discussion of mode controller and mode interlock requirements that provide for the proper integration and progression of the modes is given in the last section. The judicious application of the control laws and digital programs described in this report can, therefore, serve as a guide to the design of a digital autopilot. The parameters must, of course, be optimized for each vehicle and the actual airborne programs must be coded efficiently for the specific machine being used. The control functions defined herein and the techniques used, however, should be generally applicable to any transport aircraft.

SECTION II

LONGITUDINAL STABILIZATION

A. DESCRIPTION OF CONTROL LAWS

1. General

The longitudinal stabilization functions of the transport autopilot are those associated with pitch damping, pitch attitude control, and the pitch steering or guidance laws. The general form of these control functions for a transport employing powered (hydraulically boosted) elevator control is illustrated in Figure 2-1. Pitch control is achieved through an elevator/hydraulic servo system and pitch trim is accomplished through a movable horizontal stabilizer. Some jet transports operational today use aerodynamically-boosted flight controls. The particular aircraft used for the simulations in this study actually employs a servo tab system for controlling elevator deflection. Figure 2-1 suggests that the elevator servo dynamics are expressible as a linear transfer function with appropriate acceleration, velocity and position limits. For hydraulically-boosted controls a third order model is usually an adequate representation for rigid body simulation and stability studies. A similar third order model is also a reasonable representation of the aerodynamically-boosted system. In the case of the hydraulic servo a first order lag represents the power boost stage and a second order lag represents the secondary actuator (autopilot servo) that strokes the power boost control valve. In the case of the aerodynamic boost system, a first order lag represents the autopilot actuator while the second order lag represents the elevator-to-elevator tab dynamics although the elevator to tab dynamics are generally variable with flight condition. The resultant third order dynamic representation is, therefore, compatible with both types of boost systems. Since the more recent trends in transport aircraft has been toward the use of all hydraulically-powered control surfaces, the actuator model used in this study were assumed to represent hydraulic systems.

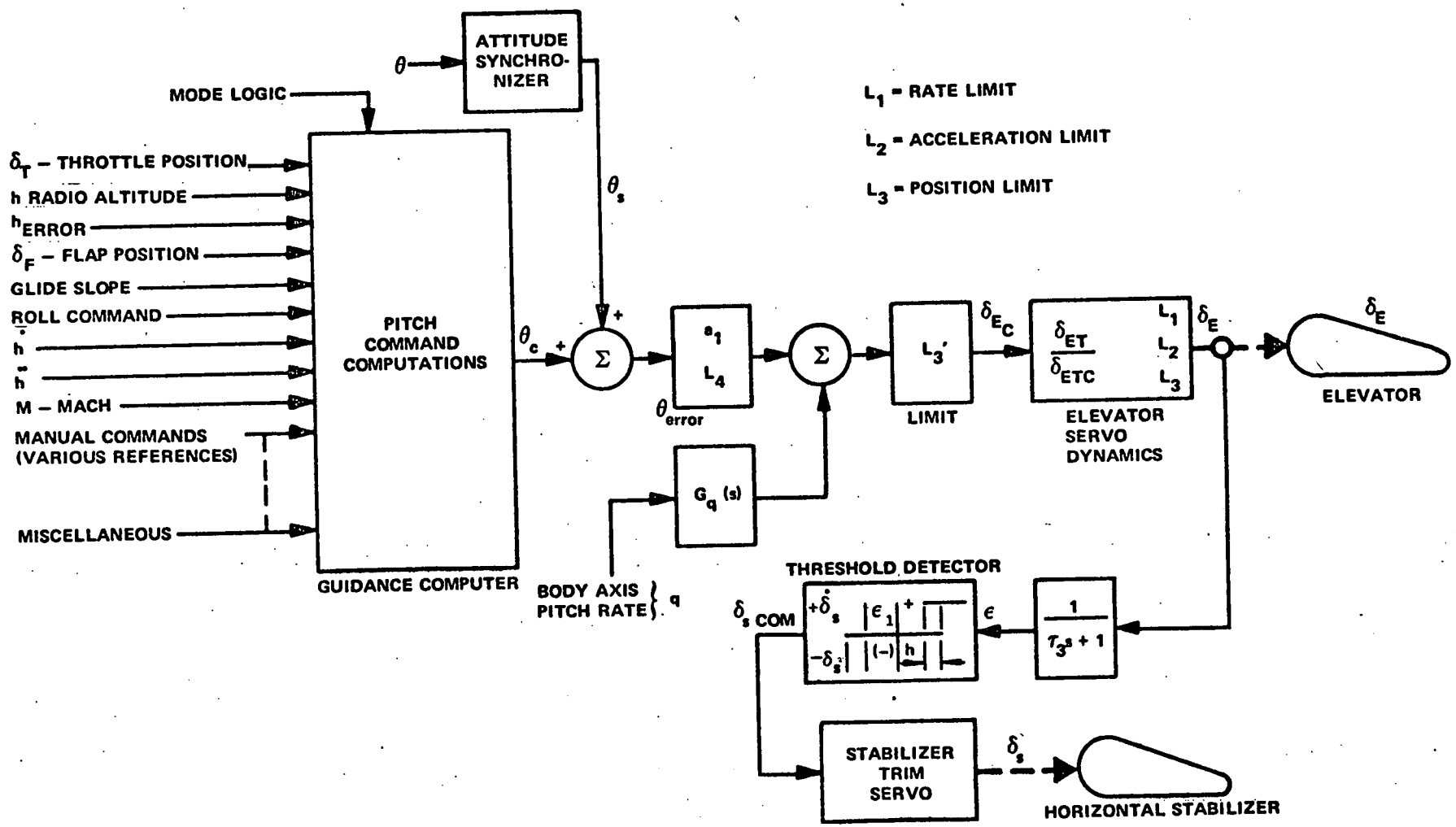

Figure 2-1
Basic Pitch Stabilization Block Diagram
Typical Transport

2. Servo Response

Elevator response to autopilot command

$$\left[\frac{\delta_E}{\delta_{EC}}\right] = \frac{1}{\left(\frac{s}{\omega_1} + 1\right)\left(\frac{s^2}{\omega_2^2} + \frac{2\zeta_2 s}{\omega_2} + 1\right)} \tag{2-1}$$

with the following constraints

$$\dot{\delta}_{E_{MAX}} = L_1$$

$$\ddot{\delta}_{E_{MAX}} = L_2$$

$$\delta_{E_{MAX}} = L_3$$

Note that $\delta_{E_{MAX}}$ results from force authority limiting if an autopilot parallel servo is used (servo moves the column). The $\delta_{E_{MAX}}$ would result from authority limit stops if an autopilot series servo is used (servo motion is not reflected at the stick). The prevalent commercial transport practice has been to use parallel servos although recent trends indicate that series servos are becoming more acceptable. When the limit L_3 is associated with a parallel servo, that limit is generally a function of flight condition if any aerodynamic load is reflected at the servo or if the feel spring is adjusted as a function of dynamic pressure.

3. Pitch Stabilization

The basic control law for pitch stabilization is

$$\delta_{E_C} = K_1 \left[K_R G_q(s) q + \theta_{error}\right] \tag{2-2}$$

where q = body axis pitch rate

$$G_q(s) = K_R \frac{\tau_1 s}{\left(\tau_1 s + 1\right)\left(\tau_2 s + 1\right)} \tag{2-3}$$

and

$$\theta_{ERROR} = \theta_E = (\theta_s + \theta_c)^* \tag{2-4}$$

with

$L_4 = \theta_E$ maximum constraint

θ_s = SYNCHRONIZED PITCH ATTITUDE

$= (\theta - \theta_i)$ (2-5)

where θ_i = pitch attitude existing at instant of autopilot engagement.

$$\theta_c = A_1 \theta_{c_1} G_1(s) + A_2 \theta_{c_2} G_2(s) + \ldots A_n \theta_{c_n} G_n(s) + \theta_{c_o} \tag{2-6}$$

where

θ_{c_o} = existing value of prior pitch command at time of mode engagement.

A_1 to A_n = mode logic = 1.0 for mode ON;
= 0 for OFF**

θ_{c_1} to θ_{c_n} = various pitch commands associated with different modes

$G_1(s)$ to $G_n(s)$ = transfer function (including gain) of various pitch guidance modes

---

*The polarity conventions that define the polarity of θ_E are not standardized. Since equation 2-4 sums rather than subtracts attitude and attitude command, it requires that the attitude command be defined as the difference between actual state and reference state as follows:

$$\theta_c = f(h - h_{REF})$$

If equation 2-4 had been written as $\theta_E = (\theta - \theta_c)$, then θ_c would, for the above illustration be defined as $\theta_c = f(h_{REF} - h)$.

**In practice, the engagement and disengagement of pitch command modes when finite error signals exist, must not cause transient disturbances to the aircraft. A function referred to as an easy engage, engage smoother, of fader, has been employed in analog type autopilots to achieve this requirement. The digital autopilot provides this capability by virtue of the attitude command accumulator function provided by the θ_{c_o} term in equation 2-6 and maneuver constraints to be discussed in the sections on guidance law descriptions.

The following typical pitch commands are associated with the various pitch guidance modes: (Note that the subscripts used are arbitrary and do not correspond to the notations used in the description of the guidance laws developed in subsequent sections of this report.)

$$\theta_{c_1} = \text{banking maneuver lift compensation} = C_1 \frac{(1 - \cos \phi_c)}{\cos \phi_c} \tag{2-7}$$

where

$C_1 = f(Q\ )$ (impact pressure or airspeed)

ϕ_c = roll command

$$\theta_{c_2} = \text{flap position lift compensation} = f(\delta_F) \tag{2-8}$$

$$\theta_{c_3} = \text{throttle compensation} = f(\delta_T) \tag{2-9}$$

$$\theta_{c_4} = \text{altitude control corrective command} = f(h_{error}, \dot{h}, M, \text{ or } V_T) \tag{2-10}$$

$$\theta_{c_5} = \text{glide path capture steering command} = f(\text{beam error}, \dot{h}) \tag{2-11}$$

$$\theta_{c_6} = \text{glide path control corrective command} = f(\text{beam error}, \dot{h}, h_{\text{radio alt}}) \tag{2-12}$$

$$\theta_{c_7} = \text{flare out control command} = f(h_{radio}, \dot{h}_{inertial}, \dot{h}_{baro}, \text{etc}) \tag{2-13}$$

θ_{c_8} = vertical speed control

θ_{c_9} = airspeed or Mach control

Automatic trim associated with pitch stabilization is provided in accordance with Figure 2-1 and the following control laws:

$$\delta_S = + B_1 \text{ deg/sec for } \epsilon > (\epsilon_1 + h) \text{ for turn ON} \tag{2-14}$$

$$\delta_S = + B_1 \text{ deg/sec for } \epsilon > \epsilon_1 \text{ for turn OFF} \tag{2-15}$$

$$\delta_S = 0 \text{ for } - \epsilon_1 \leqslant \epsilon \geqslant + \epsilon_1 \tag{2-16}$$

$$\delta_S = -B_1 \text{ deg/sec for } (-\epsilon_1 - h) < \epsilon_1 \text{ for turn ON} \tag{2-17}$$

$$\delta_S = -B_1 \text{ deg/sec for } -\epsilon_1 < \epsilon_1 \text{ for turn OFF} \tag{2-18}$$

(where h is the switch hystersis)

Note that the threshold ϵ_1, as shown in Figure 2-1, is based on elevator deflection. In autopilot practice where parallel servos are employed, the threshold is often based on elevator servo force or displacement of the feel spring. The use of an on-off autotrim system of this type is dictated by practical considerations regarding the stabilizer drive mechanizations. Aircraft that provide pitch trim by transferring the control moment from an elevator deflection to horizontal tail deflection employ fixed speed trim motor drives. While a proportional autotrim mode would have advantages from the standpoint of performance and stability, the on-off system is specified for compatibility with the actuating mechanisms that are used in practice.

4. Stability Considerations

The stability factors associated with the aircraft pitch stabilization functions can be derived from the basic block diagram shown in Figure 2-2. The body axis rate signal q is assumed to be equal to $\dot{\theta}$, the pitch Euler angle rate for the purpose of this analysis. Note that the washout (time constant τ_1) is added to the pitch rate feedback term in order to eliminate the steady state azimuth rate coupling that is sensed by the body axis pitch rate sensor during a constant altitude banking maneuver. In Figure 2-2, the aircraft dynamics are those obtained from three-degree-of-freedom perturbation equations (forward speed, pitching moment, and normal force). The stabilization of such a plant is easily obtained in theory with a simple attitude rate plus attitude displacement feedback. The phugoid poles are driven into the real axis with a relatively low gain attitude feedback. The sum of attitude rate plus displacement creates a zero on the real axis that draws the short period poles. This is illustrated in Figure 2-3, where servo dynamics and filter effects are neglected.

This ideal situation does not usually exist in practice. Even the phugoid mode which is easily stabilized with simple pitch attitude feedback leads to difficulties when pitch attitude is obtained from a vertical gyroscope that employs long term gravity slaving to maintain verticality. In that case, a new

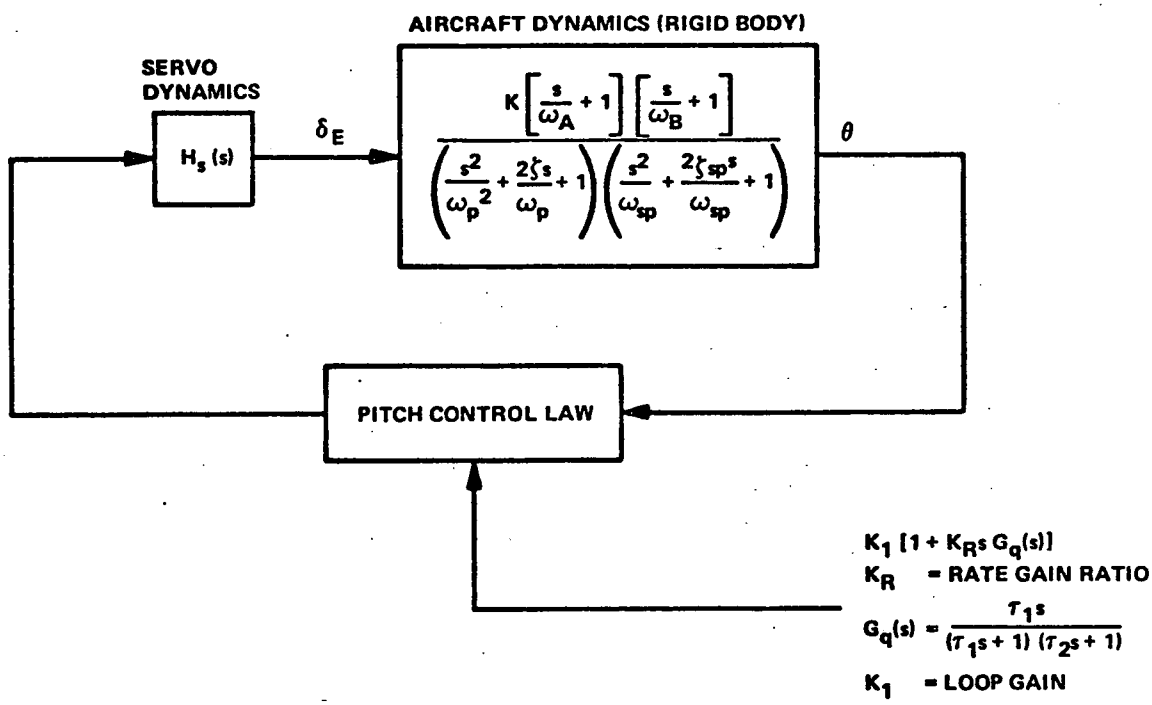

Figure 2-2
Block Diagram For Pitch Stability Analysis

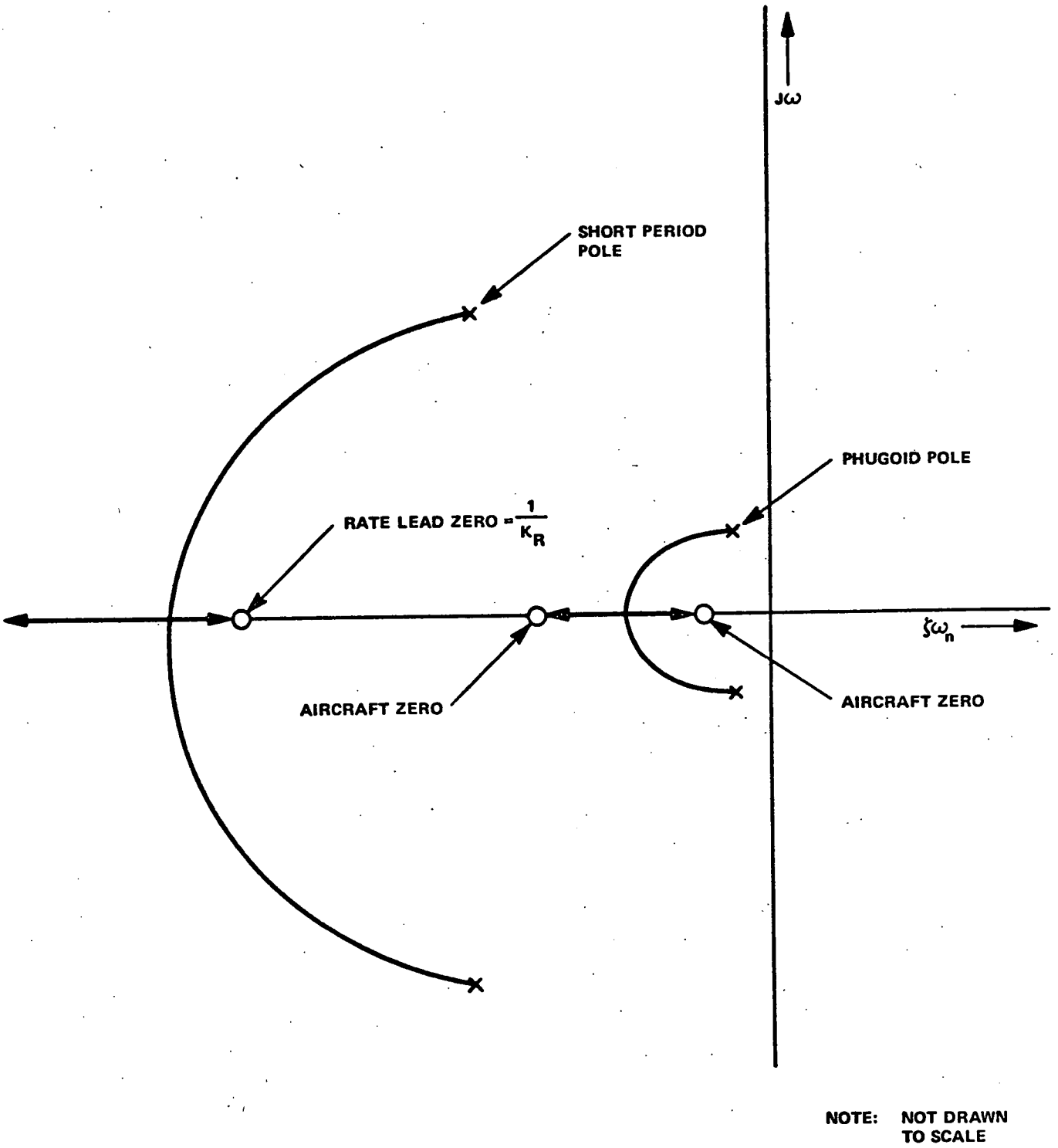

Figure 2-3
Idealized Pitch Stabilization Root
Locus with Servo and Filter Dynamics Neglected

pair of zeros appears in the open loop transfer function and, as the gravity slaving is increased in gain (faster erection to the pendulum), these zeros approach the phugoid poles. The dipoles formed in this manner prevent the damping of the phugoid poles. However, this phenomenon tends to be significant only at high cruise speeds where the phugoid period is very long. When a tight guidance loop such as glide path control or constant altitude control is used, the phugoid mode is eliminated as a source of any problem. Also, the use of airspeed control loops through the throttles prevents the excitation of a phugoid mode. The point of the gravity erecting gyro has been mentioned here because that phenomenon does represent one of the sources of difficulty in some automatic approach and landing systems. Erecting gyros, responding to speed transients, or correcting for previous speed transients are one of the contributors to flight path control errors. Even very small changes in the pitch angle reference can cause a few feet of error on final approach. This is a time when every foot of error seriously strains the total error budget.

The pitch stabilization root locus departs from the ideal form of Figure 2-3 when the various filters and servo dynamics are included. Now excessive gains will begin to excite high frequency modes created from the upward movement of the servo and aircraft short period poles (Figure 2-4). It is theoretically possible to design lead compensators that would appear to produce a more desirable situation, but this is generally not feasible or desirable because of the following factors. Elastic modes (not included in this analysis or incorporated in the simulations associated with this program) should be gain stabilized with about 10 to 12 db of margin. High frequency compensators aimed at correcting servo phase characteristics would result in coupling with elastic modes. Also, servo rate and acceleration limits and nonlinearities are usually incompatible with high frequency, high gain compensators. The approach, therefore, is to use roll-off filters (such as τ_2 of equation 2-3) to ensure gain stabilization of elastic modes and to accept the penalty of attitude stabilization loops that are not as tight as one could achieve with higher gains and idealized vehicle models.

Note that the stability analysis shown in Figures 2-2, 2-3, and 2-4 does not include the automatic stabilizer trim loop. This loop has the effect of an integration term. Its linearized representation would add a pole at the origin with a zero near the origin. Its effect is usually to draw the short period poles

toward the $j\omega$ axis at low gains. The destabilizing effect becomes less significant at higher gains. The low value of stabilizer trim rate plus a reasonable wide threshold helps eliminate any oscillatory problems as a result of the automatic trim loop.

5. Authority Limit Considerations

The acceleration, rate and displacement limits (L_1, L_2, and L_3, associated with equation 2-1) are usually variable with flight condition loading of the surfaces. In fully powered systems, actuator flow limits in both the power boost stages and autopilot actuators dictate L_2, the velocity limit. The acceleration limits are usually imposed by the static force limits (pressure x effective piston area) where the actuator is sized to handle the maximum anticipated surface loads. Control valve dynamics (pressure and flow characteristics in response to valve displacements) also enter into this limit. Finally, the displacement limit is imposed by physical stops or force limits on the autopilot servos. In aerodynamic boost systems (control tabs), the force limits of the autopilot servos usually impose the displacement limit L_3. Figure 2-1 shows servo physical limits L_1, L_2, and L_3, and an electronic command limit L_3'. In practice, it is easy to vary L_3' so that the electronic authority limit always corresponds to a reasonable aircraft acceleration limit. A more difficult problem is to achieve a variation of L_3 with speed. When electromechanical parallel servos are employed, the torque limits on these servos may be adjusted by controlling the current limits as a function of aircraft flight condition. Also, the reflection of changing aerodynamic loads on the servo or a Q spring feel system serves to change the value of L_3 with flight condition. A reasonable approach to simulating this requirement is to compute a continuous value of electronic limit L_3' and assume a second but larger physical constraint L_3 for safety purposes. If we select an incremental "g" limit for commercial transports of +0.7g's and -0.3g's, the passengers will certainly not object to these g levels. The surface deflection limits may then be estimated as follows.

Let α and δ_E represent incremental values from the existing equilibrium conditions. Then, to achieve an incremental normal acceleration N_Z,

$$C_{L_\alpha} \alpha QS + C_{L_{\delta_E}} \delta_E QS = \frac{W}{g} N_z \qquad (2\text{-}19)$$

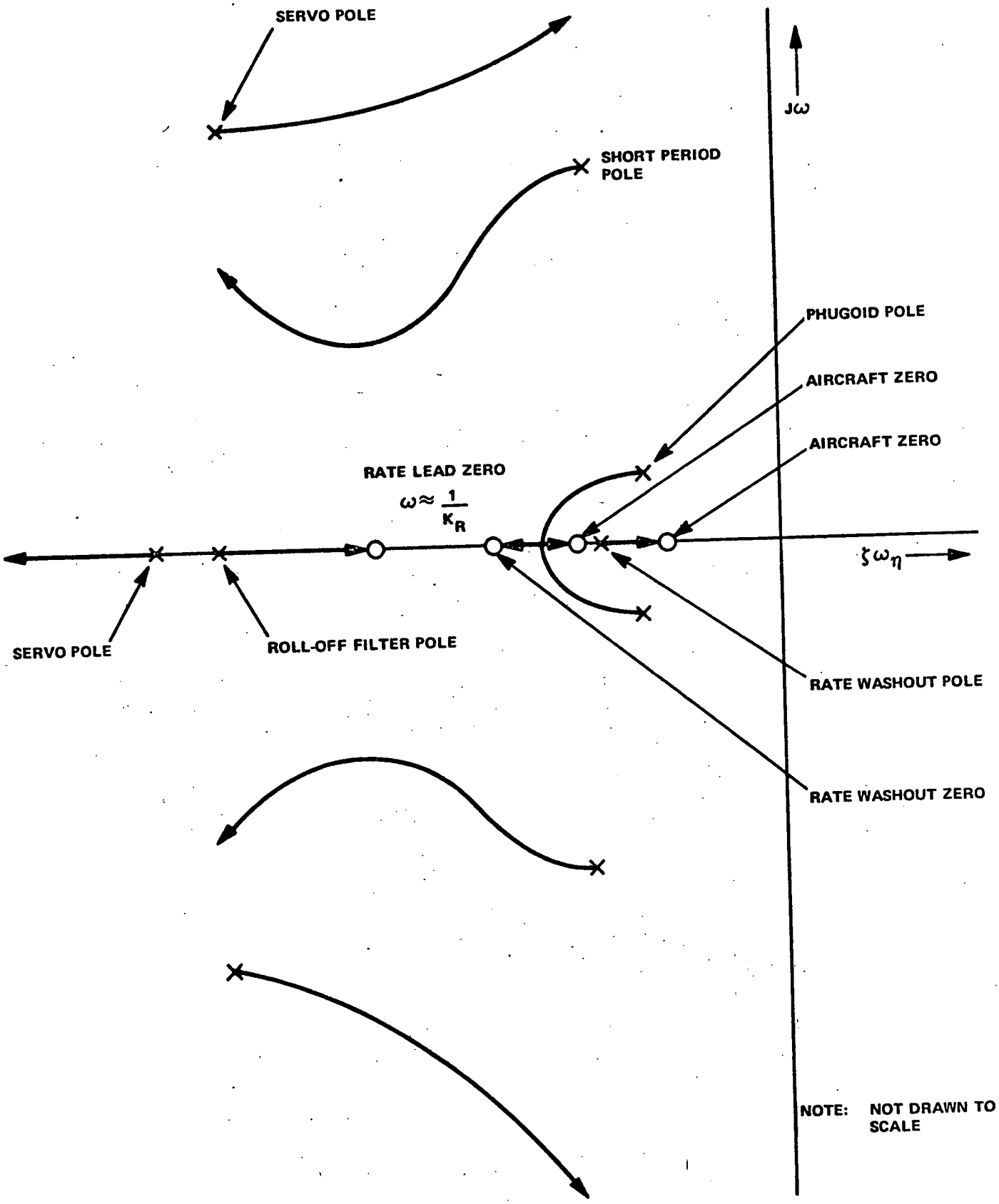

Figure 2-4
Pitch Stabilization Root Locus with
Servo and Filter Dynamics

and

$$C_{m_\alpha}\,\alpha = C_{m_{\delta_E}}\,\delta_E \tag{2-20}$$

or

$$\alpha = \frac{C_{m_{\delta_E}}}{C_{m_\alpha}}\,\delta_E$$

Substituting equation 2-20 into equation 2-19 and solving for δ_E gives

$$\delta_E = \frac{\left(\frac{W}{g}\right) N_z}{\left[C_{L_\alpha}\left(\frac{C_{m_{\delta_E}}}{C_{m_\alpha}}\right) + C_{L_{\delta_E}}\right] QS} \tag{2-21}$$

for (+)0.7g = 22.5 ft/sec^2 and (-)0.3g = 9.66 ft/sec^2 contraints

$$L_3'(+) = \delta^+_{E_{MAX}} = \frac{+22.5\left(\frac{W}{g}\right)}{\left[C_{L_\alpha}\left(\frac{C_{m_{\delta_E}}}{C_{m_\alpha}}\right) + C_{L_{\delta_E}}\right] QS} \tag{2-22}$$

and

$$L_3'(-) = \delta^-_{E_{MAX}} = \frac{-9.66\left(\frac{W}{g}\right)}{\left[C_{L_\alpha}\left(\frac{C_{m_{\delta_E}}}{C_{m_\alpha}}\right) + C_{L_{\delta_E}}\right] QS} \tag{2-23}$$

Note that these limits are functions of dynamic pressure Q. Note also, that equation 2-21 represents an approximation to the actual surface deflection that will give the specified acceleration limit. The approximation is only as good as the accuracy of the linearized coefficients. This accuracy is not adequate for defining the specific limit values to be incorporated in an autopilot design.

Equation 2-21 scopes the range of limits that must be considered and thereby aids in scaling the computation and control designs. The actual limits designed into the autopilot control logic should be determined by simulation studies where the non-linear aerodynamic effects can be considered more accurately.

Reasonable limits for L_1, the velocity limit, are 10 to 30 degrees per second. Acceleration limits should allow the peak velocity to be attained in 0.25 seconds.

6. Longitudinal Stabilization Response Criteria

There are no specifications or criteria for pitch autopilot response that have received wide acceptance. Military handling quality specifications (MIL-STD-8785, for example) are applicable to basic airframe response but they do not deal with phenomena that are specific to an autopilot. (For example, how should the aircraft's pitch response to a pitch command rather than stick command be specified.) In this section a set of somewhat arbitrary response criteria are defined. They are based on experience obtained with many autopilot designs. The suggested criteria are considered achievable and experience has shown that when this level of performance is attained, pilot evaluation is good and overall guidance accuracy objectives can generally be met.

For a step input pitch command, the vehicle attitude response should reach 90 percent of the commanded value within about 1.2 seconds. Overshoots associated with an oscillatory response should be governed by an equivalent second order system damping ratio criterion that permits the damping ratio to have a minimum value of about 0.5 (approximately 30 percent overshoot). The pitch response will tend to have a long tail associated with convergence to its final value. If tight airspeed control is maintained, this tail effect is usually negligible. A reasonable specification on this tail effect is that the response converges to within 95 percent of the commanded value within 6 seconds and must always remain within 90 percent of the final value within 2.5 seconds. An ideal response would be the transient that has the shape of a 0.8 damped second order system with frequency of about 4 to 6 radians per second.

7. Control Law Parameter Summary

The range of control law and control system parameters for pitch stabilization are fairly well bounded for all jet transports. Table 2-1 summarizes these parameters in terms of typical values and the possible range of variation for all jet transports.

TABLE 2-1

CONTROL LAW AND CONTROL SYSTEM PARAMETER SUMMARY
PITCH STABILIZATION

Parameter	Typical Minimum Value	Typical Nominal Value	Typical Maximum Value	Remarks
ω_1	10 Rad/Sec	15 Rad/Sec	20 Rad/Sec	May represent 1st order lag of hydraulic power servo.
ω_2	15 Rad/Sec	20 Rad/Sec	30 Rad/Sec	Represents auto-pilot servo or tab to elevator dynamics. Lower values typical of parallel servo. Higher values for series servo.
L_1	10 Deg/Sec	20 Deg/Sec	30 Deg/Sec	
L_2	40 Deg/Sec^2	60 Deg/Sec^2	100 Deg/Sec^2	
L_3	±10 Deg	±15 Deg	±25 Deg	
L_3'	15 percent Below Nominal	Per Equations 2-22 and 2-23	25 percent Above Nominal	$f(Q, C_{L_\alpha})$
K_1	2.0	3.0	6.0	Low Q
	1.4	2.0	4.0	Med Q
	0.6	1.0	2.0	High Q
K_R	0.2	0.5	1.0	Ratio of rate to displacement. These values can be increased at Low Q and decreased at Hi Q.
τ_1	2 Sec	4 Sec	6 Sec	Washout time constant - can be programmed as function of Q (increase for Low Q).

TABLE 2-1 (cont)

CONTROL LAW AND CONTROL SYSTEM PARAMETER SUMMARY
PITCH STABILIZATION

Parameter	Typical Minimum Value	Typical Nominal Value	Typical Maximum Value	Remarks
τ_2	0.02 Sec	0.05 Sec	0.1 Sec	Roll-off filter.
$\pm B_1$	0.03 Deg/Sec	0.06 Deg/Sec	0.1 Deg/Sec	$\dot{\delta}_{STAB}$ for auto-trim (lower for reduced K_1).
ϵ_1	0.1 Deg	0.25 Deg	0.5 Deg	Trim threshold in equivalent degrees of δ_E autopilot command.
h	0.05 Deg	0.08	0.15	Hysteresis of trim threshold.
τ_3 (See Figure 2-1)	0.25 Sec	0.75 Sec	1.5 Sec	Trim threshold detector filter on signal ϵ.
L_4 (See Figure 2-1)	±3 Deg	±5 Deg	±10 Deg	Attitude error limit.

B. DIGITAL PROGRAM - PITCH STABILIZATION

1. Control Law Conversion

In order to facilitate the programming of the control equations defined in the previous section, a notation compatible with the programming language must be defined. The mathematical symbols given thus far are convenient for analyzing systems and communicating concepts but for machine programming a more cumbersome set of symbols must be used. A set of FORTRAN permissible notations corresponding to the mathematical symbols used previously was defined. The FORTRAN notation has a mnemonic relationship to the original symbol when possible. A tabulation of the FORTRAN designations and their definitions is given in Table 2-2. A general description of the FORTRAN subroutines used for the combination of control modes that make up the autopilot is given in Appendix A. The equivalent pitch stabilization block diagram using the FORTRAN designations is shown in Figure 2-5. Note that this block diagram shows the specific dynamic pressure gain control function that optimized performance for the specific test vehicle used in the simulations.

2. Program Flow Chart

The initial condition computations which are performed in the SASIC subroutine for the pitch stabilization mode is given in the following summary and the flow chart is shown in Figure 2-6.

TABLE 2-2

PITCH STABILIZATION NAMELIST

Name	FORTRAN Name	Definition
q	QB	Body axis pitch rate.
θ	THET	Pitch angle.
δ_E	DELTE	Elevator angle; positive-nose down.
δ_S	XIH	Horizontal stabilizer angle.
θ_c	THECOM	Pitch angle command; positive-nose down.
δ_{EC}	DELTEP	Elevator command.
	QBW	Filtered body axis pitch rate.
$\dot{\delta}_{SC}$	DHSD	Horizontal stabilizer rate command signal.
ϵ_1	BKPT1	Breakpoint in threshold detector.
ϵ_2	BKPT2	Breakpoint in threshold detector.
$\dot{\delta}_s$	XMAXIH	Horizontal stabilizer drive rate.
	IETAB	Logic switch for horizontal stabilizer drive; -1 drive up, 1 drive down, 0 no drive.
$L_3(+)$	EL3UP	Upper elevator command position limit; function of dynamic pressure
$L_3(-)$	EL3DN	Lower elevator command position limit; function of dynamic pressure.
L_1	PL1	Elevator command rate limit.
Q	QBAR	Dynamic pressure.
K_1	PSK, PSKR	Forward pitch loop gain. PSKR = PSK $\cdot \frac{1}{57.3}$ rad/deg.
K_R	QFBK	Pitch rate feedback gain.
τ_1	TAUP1	Pitch rate filter time constant.
τ_2	TAUP2	Pitch rate filter time constant.
τ_3	TAUP3	Automatic trim filter.
	ITESTP	Logic variable for pitch loop synchronization.

TABLE 2-2 (cont)

PITCH STABILIZATION NAMELIST

Name	FORTRAN Name	Definition
C_{L_α}	CLALPH	Lift coefficient curve slope.
$C_{m_{\delta_e}}$	CMDE	Elevator moment stability derivative.
C_{m_α}	CMALPH	Angle of attack moment stability derivative.
$C_{L_{\delta_e}}$	CLDE	Elevator lift stability derivative.
W	WAIT	Aircraft weight.
S	AREA	Aircraft wing area.
---	DT2	Subroutine sample time interval.
---	R2D	Radian to Degree Conversion.
---	D2R	Degree to Radian Conversion.

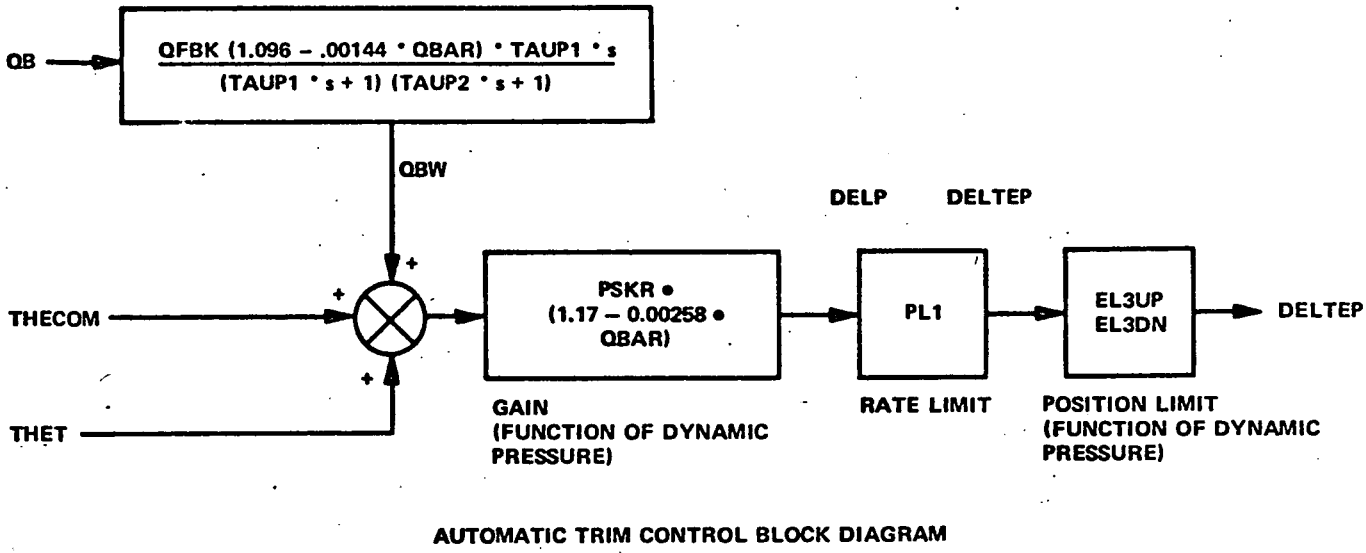

AUTOMATIC TRIM CONTROL BLOCK DIAGRAM

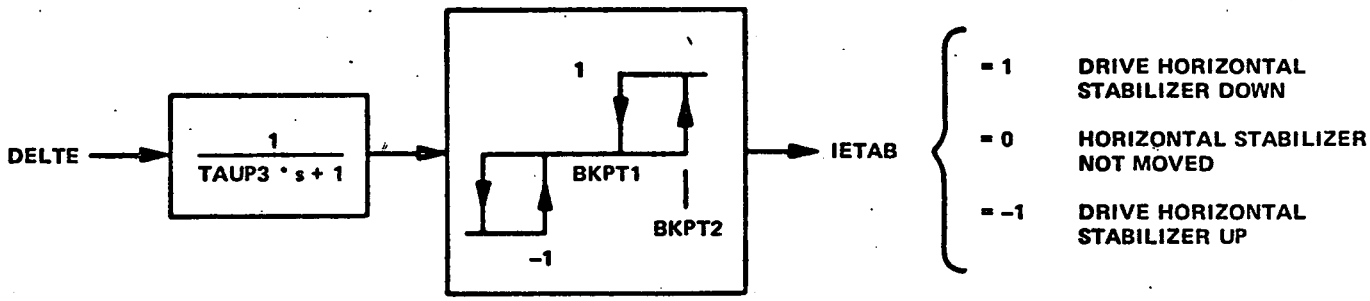

Figure 2-5
Pitch Stabilization Control
Block Diagram Fortran Notation

(a) Difference equation coefficients for pitch rate feedback filter.

```
CQ1 = EXP(-DT2/TAUP1) + EXP(-DT2/TAUP2)

CQ2 = EXP(-DT2/TAUP1 - DT2/TAUP2)

CQ3 = (QFBK * R2D/TAUP2)/(1/TAUP2 - 1/TAUP1) *
      (EXP(-DT2/TAUP1) - EXP(-DT2/TAUP2))
```

(b) Difference equation coefficients for horizontal stabilizer command filter.

```
CH1 = EXP(-DT2/TAUP3)

CH2 = 1 - CH1
```

(c) Elevator command rate limit

```
ERATE = PL1 * D2R * DT2
```

(d) Threshold detector limits (converted for input in radians)

```
BKPT1 = BKP1 * D2R

BKPT2 = BKP2 * D2R
```

(e) Feedback gain converted for input in radians

```
PSKR = PSK * D2R
```

(f) Position limits for elevator commands. (Must be multiplied by dynamic pressure to get actual value.)

```
WSCL = WAIT/((CLAPH/CMALPH * CMDE + CLDE) * AREA)

EL3UP = -0.7 * WSCL

EL3DN = 0.3 * WSCL
```

(g) Initialize elevator deflection

```
DELTEP = 0
```

The chosen pitch control loop parameters for best performance are:

TAUP1 = 4.0	BKP1 = 0.3
TAUP2 = 0.05	BKP2 = 0.45
PL1 = 20.0	XIHDOT = 0.06°/sec
TAUP3 = 0.75	PSKR = 5.0
	QFBK = 0.6

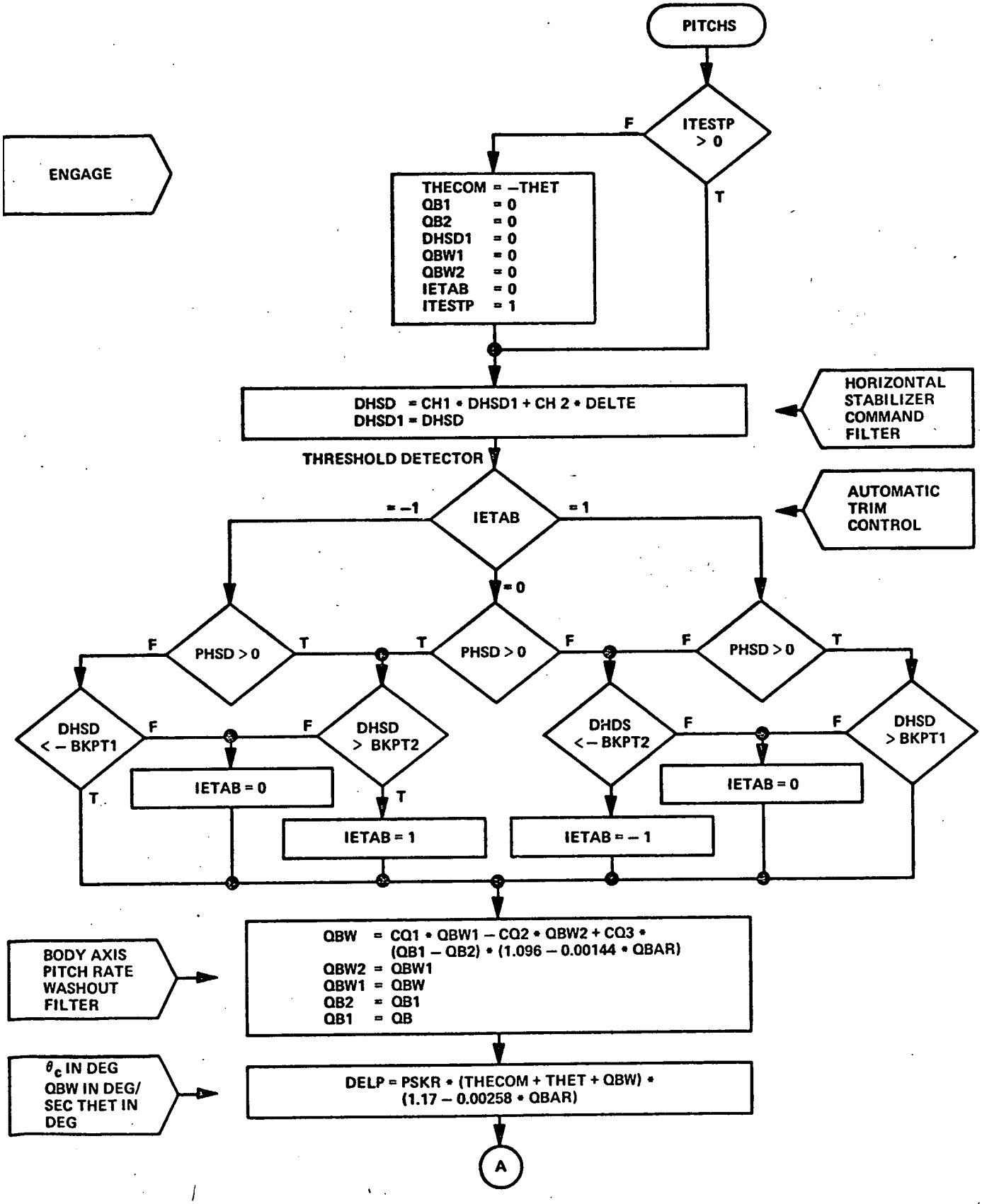

Figure 2-6a
Pitch Stabilization Flow Chart

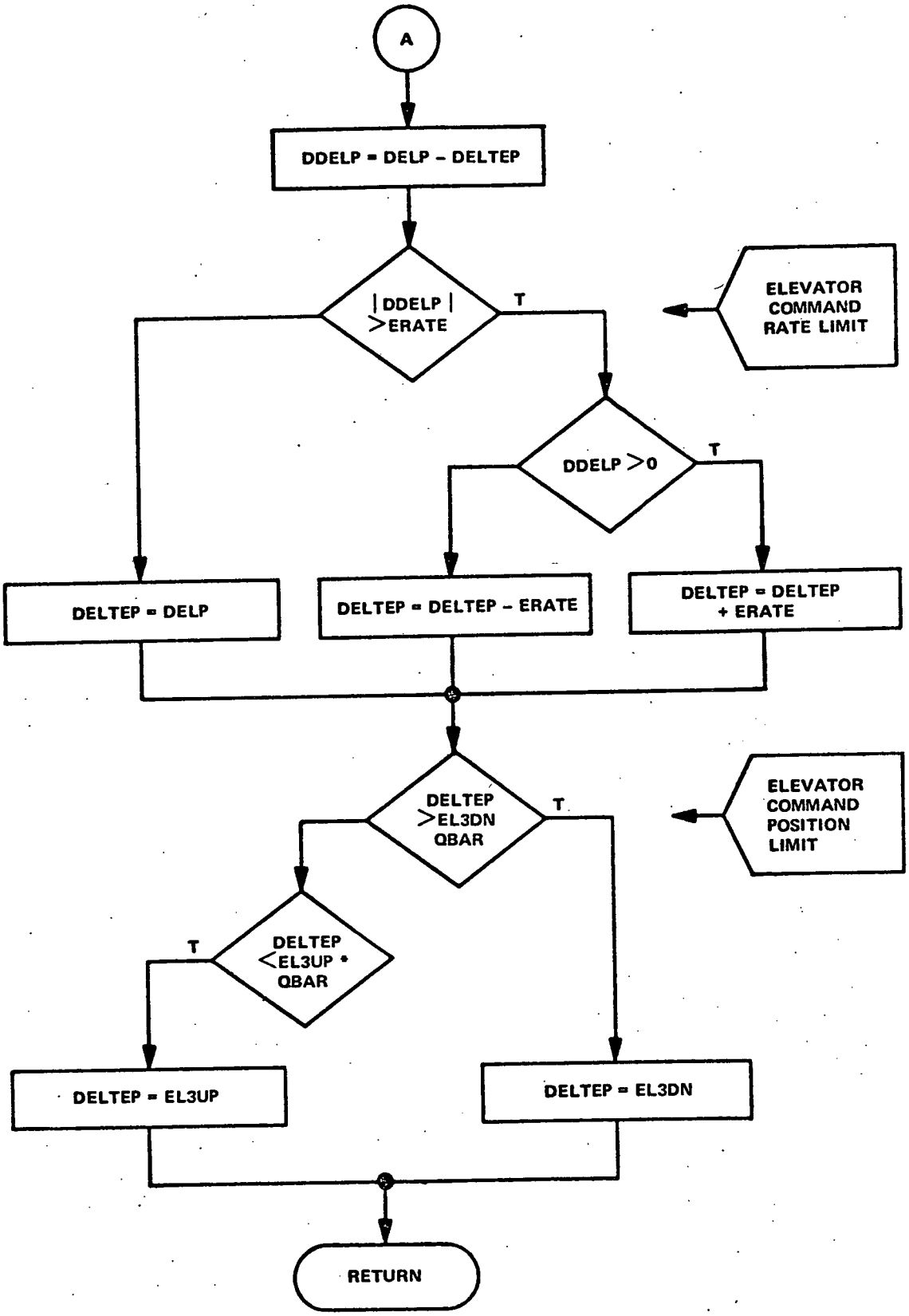

Figure 2-6b
Pitch Stabilization Flow Chart (cont)

C. SIMULATION TEST RESULTS

The pitch stabilization response was determined using the reference jet transport simulator described in Appendix B. The pitch command response at the approach condition (V = 141 knots, 50 degree flaps deployed, autothrottle engaged and h = 1500 feet is illustrated in Figure 2-7. The response time criteria specified in Section IIA-6 are shown shaded. It is apparent that the response time objective is met but at the expense of a deterioration in the high frequency mode damping. This high frequency mode response can be improved theoretically with a lead-lag compensator designed to expand control bandwidth. Removing the pitch rate feedback high frequency roll-off filter would also help. However, these techniques cannot be considered practical without taking the vehicle's elastic mode characteristics into account. Also, precise definitions of the actuator dynamics and sensor dynamics must be included in any such compensator design. Consequently, the most practical method of improving the damping of the high frequency mode is a loop gain reduction of about 20 percent. This would compromise the time response. The results shown in Figure 2-7, however, are not unacceptable. With a parallel autopilot servo there might be some pilot objection to excessive control activity in turbulence. With a series autopilot servo, pilot comment on such a system might be an opinion that the autopilot is "too tight" but would otherwise be quite acceptable.

A more interesting phenomenon is observed in the responses illustrated in Figure 2-7. The response is characteristic of a statically unstable vehicle but the reference jet transport has adequate static margin. The pitch attitude overshoots the 5.0 degree reference value after the up-elevator command is inserted. The elevator must reverse polarity to hold the new attitude; consequently the overshoot error must occur. This phenomenon is a characteristic that had actually been encountered in the design of the autopilot and autothrottle system used in the real vehicle. The problem is the result of the pitch moment coupling from the autothrottle system. As pitch attitude increased, the aircraft started to decelerate. In order to maintain speed, the autothrottle system commanded a thrust increase. The location of the engines below the aircraft c.g. resulted in a nose-up pitching moment. This moment must be countered by down elevator; hence the sustained overshoot. The overshoot would eventually be minimized by the autotrim system. The correction for this problem would have been the incorporation of the throttle compensation pitch command per equation 2-9.

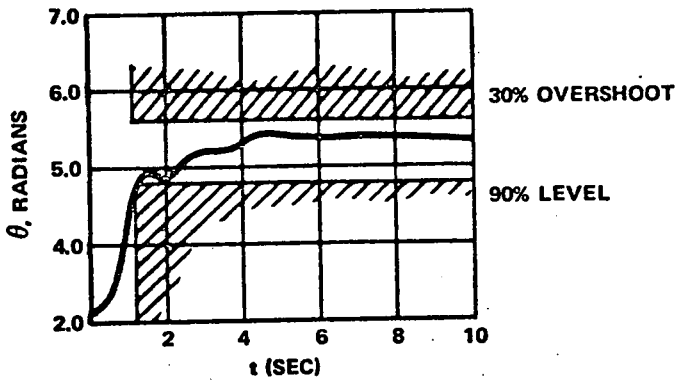

FLIGHT CONDITION: V = 141 KNOTS
h = 1500'

PARAMETER VALUES: PSK = 5.0
QFBK = 0.6
PL1 = 20.0

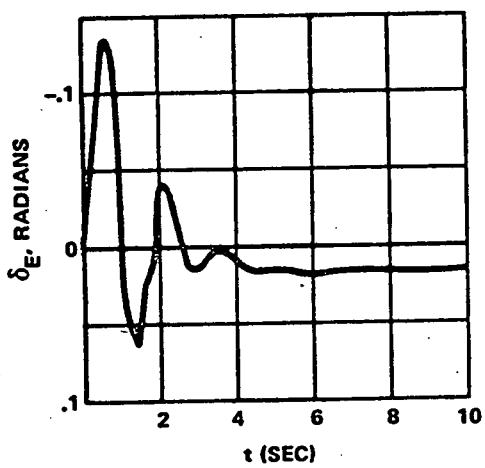

Figure 2-7
Pitch Stabilization Test Approach Condition

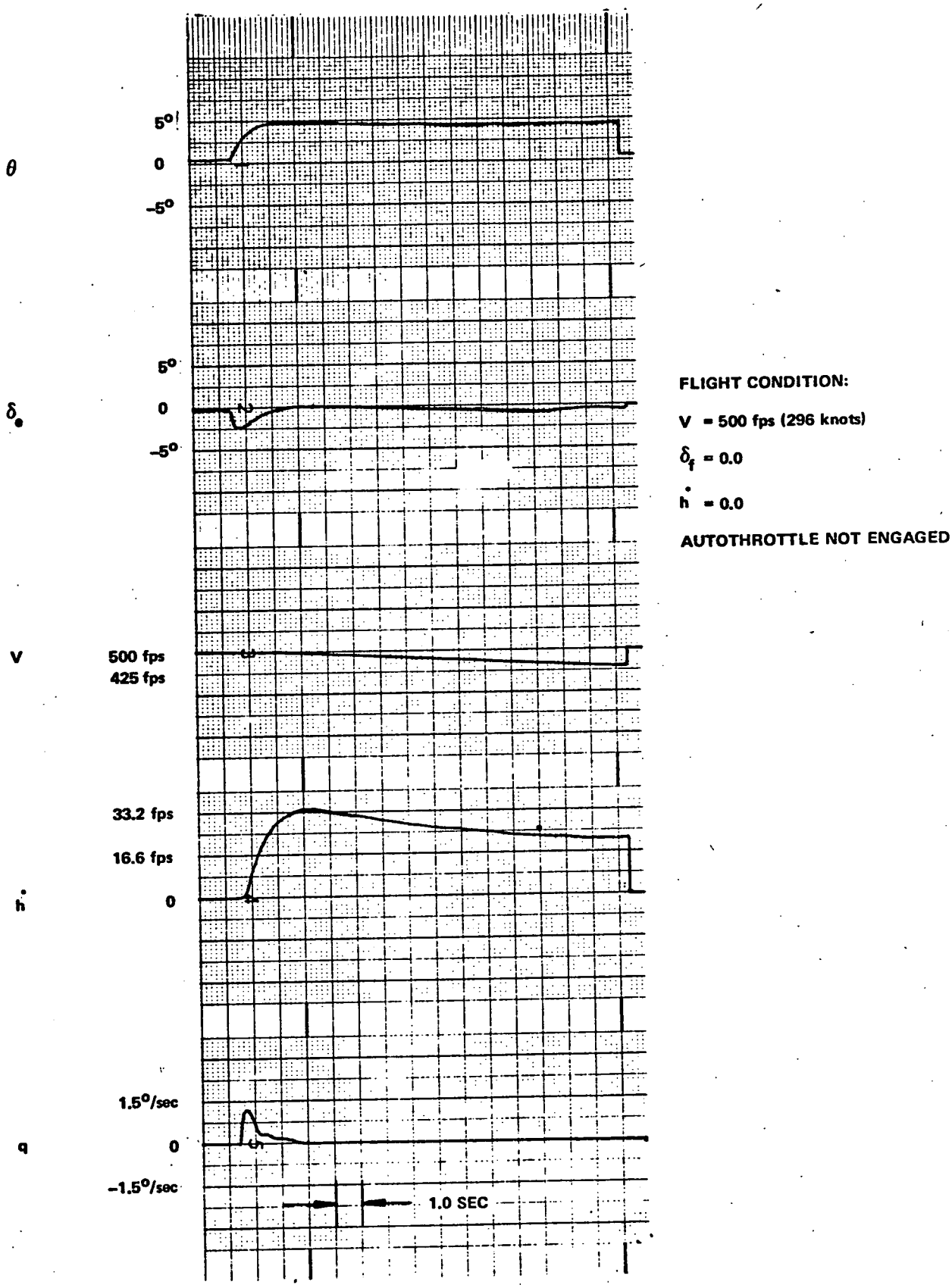

Figure 2-8
Pitch Response of Aircraft to a Step
Change in Theta Command of ≈ 5°, V = 500 fps

This compensation was not used for this test. It is noted that in the actual autopilot design for the reference jet transport, a compensation term having the form of equation 2-9 was included after this phenomenon was encountered in flight tests.

The response at a higher speed condition prior to entering final approach is illustrated in Figure 2-8. At this condition, the speed is 296 knots, clean (zero flaps) and autothrottle is not engaged. The pitch response meets the time and damping criteria. Note that the elevator position limit is reached and consequently the initial response is slowed somewhat by saturation. Also, the absence of the autothrottle pitch moment coupling prevented the type of overshoot seen in Figure 2-7.

SECTION III

LATERAL STABILIZATION

A. DESCRIPTION OF CONTROL LAWS

1. General

The lateral stabilization functions of the transport autopilot are those associated with yaw (or dutch roll) damping, turn coordination, and roll attitude control. The dutch roll damping is provided by a yaw damper that drives the rudder in response to various sensor inputs. For many flight conditions, a roll damper is also an effective dutch roll damper. The use of a separate roll damper, however, has significance only for manual control. Roll damping is implicit in the roll attitude control function and is not treated as a separate stabilization loop in the subsequent description of lateral stabilization control laws.

Turn coordination is considered as part of the yaw stabilization function. In addition to providing for damping of dutch roll oscillations, the yaw (or rudder) channel is also used to turn the aircraft into the relative wind for coordinated (zero sideslip) turns. (Note that zero sideslip and zero lateral accelerometer or pendulum angle are not identical. The differences are illustrated in Appendix C.

Roll attitude stabilization is achieved through the actuation of rolling moment producing surfaces, generally ailerons. Many of the jet transports use combinations of ailerons and spoilers. Supersonic vehicles use differential tail controls or elevons where roll and pitch controls are accomplished with common surfaces. The reference vehicle on this study uses inboard and outboard ailerons that are controlled by aerodynamic tabs. For aerodynamically-boosted control, the control surface deflection is determined by the hinge moment equations. Rolling moment characteristics associated with ailerons and spoilers tend to be quite nonlinear and very dependent upon other variables such as angle of attack, flap deflection, and sideslip. These nonlinear effects could easily be masked by high gain, roll rate, and roll displacement feedback loops, but the problem is usually compounded by mechanical nonlinearities in the control system (backlash, cable stretch,

friction, etc). In large transports, these mechanical nonlinearities often determine the quality of an autopilot's roll control performance. In the present study, an idealized control actuation system is assumed. It is represented by realistic, linearized dynamic transfer functions. This linear representation of the control system will permit performance that is, in general, better than that which is obtainable in the real environment of control nonlinearities. The roll performance results obtained in this study should therefore be viewed as an upper bound or goal that may be difficult to achieve with state-of-the-art mechanical and hydromechanical controls.

2. Yaw Stabilization and Turn Coordination

a. Feedback Variables

The yaw stabilization and turn coordination control laws are those associated with the δ_R (rudder) feedback on Figure 3-1. These feedbacks include the following information:

- r = body axis yaw rate (yaw rate gyro)
- A_Y = lateral acceleration (cg, mounted accelerometer)
- ϕ = roll angle
- δ_{AC} = commanded aileron deflection
- δ_R = rudder deflection
- $\Delta\psi$ = skid command (from lateral steering system)

These variables may be used in different combinations ranging from the simple, single variable (r) yaw rate dampers to the use of all of the above variables in a computed $\dot{\beta}$ (sideslip rate) damper.

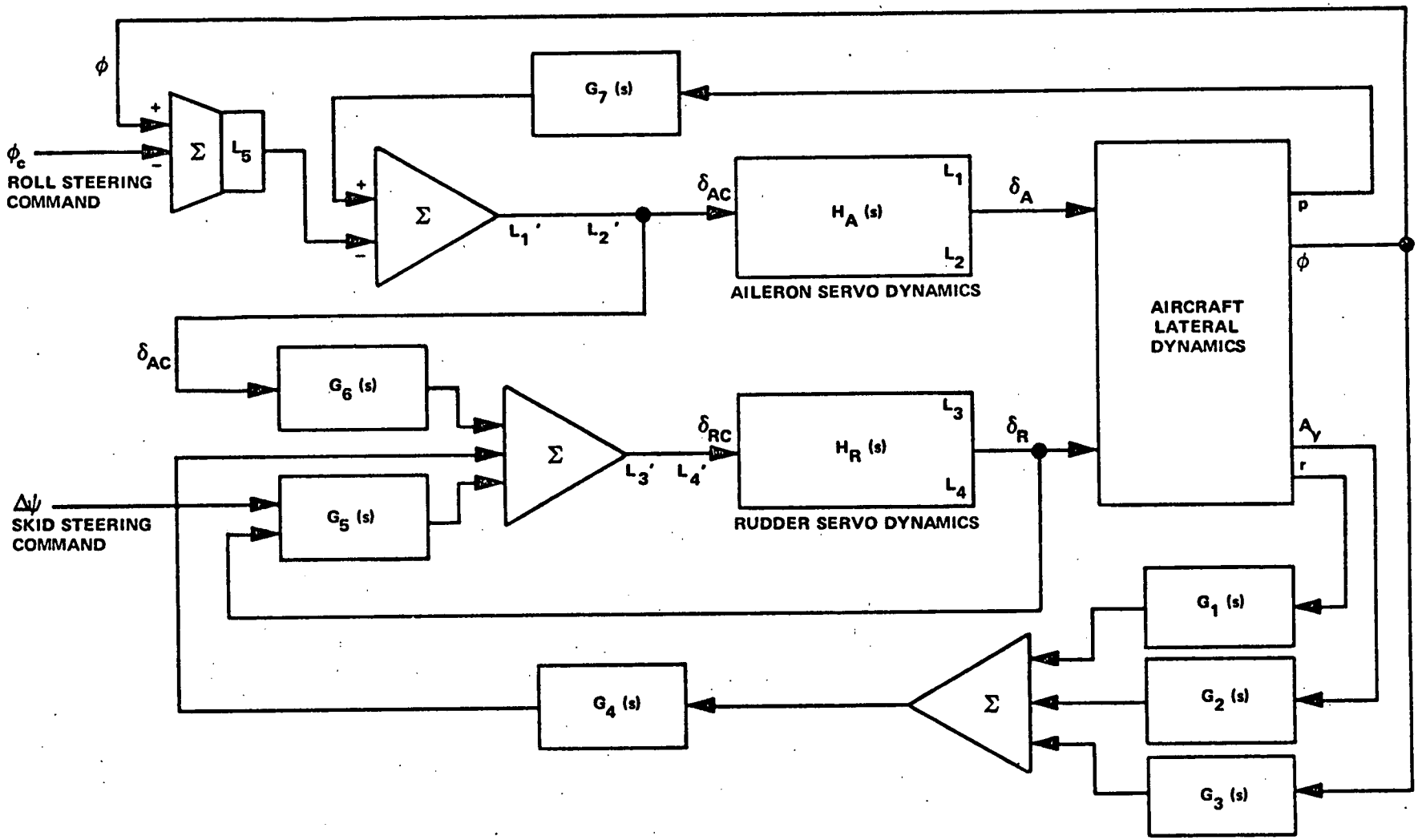

Figure 3-1
Lateral Stabilization System

b. Yaw Rate Damper

The typical jet transport dutch roll mode is readily damped with yaw rate feedback as illustrated in Figure 3-2a. The $[r/\delta_R](s)$ aircraft dynamics are of the form:

$$\left[\frac{r}{\delta_R}\right](s) = k \frac{(\tau_\psi s + 1)\left(\frac{s^2}{\omega_\psi^2} + \frac{2\zeta_\psi s}{\omega_\psi} + 1\right)}{(\tau_R s + 1)(\tau_s s + 1)\left(\frac{s^2}{\omega_D^2} + \frac{2\zeta_D s}{\omega_D} + 1\right)} \tag{3-1}$$

where

τ_R = is the roll convergence time constant

τ_s = is the spiral mode time constant (usually slightly negative)

ω_D = is the dutch roll frequency

ζ_D = is the dutch roll damping ratio

The location of the numerator quadratic zeros determine the effectiveness of the yaw damper in damping the dutch roll. When ω_ψ approaches ω_D to form a dipole, the yaw damper becomes ineffective. This often occurs at high angles of attack for some transports and is also a common phenomenon in vehicles designed for hypersonic flight. The optimum yaw damper gain is usually the one yielding maximum damping, as illustrated on Figure 3-2a. Higher gains cause the dutch roll period to be stretched with the response becoming more oscillatory.

It is noted that the simple yaw rate-to-rudder feedback described in Figure 3-2a also provides good spiral mode stabilization. It will be demonstrated, however, that this spiral mode stabilization effect is not generally attained when some of the practical problems begin to be considered. The first problem (not revealed in the root locus diagrams) relates to achieving good turn coordination. In a steady state, coordinated turn, the steady body yaw rate would deflect the rudder to cause the aircraft to develop sideslip in a direction that drives the aircraft out of the turn. That is, if the yaw damper control equation is

$$+\delta_R = k_1 r \tag{3-2}$$

and the steady yaw rate (for a constant altitude, coordinated turn) is

$$r = \frac{g}{V} \sin \phi \cos \theta \tag{3-3}$$

the steady rudder deflection would be

$$+ \delta_R = k_1 \frac{g}{V} \sin \phi \cos \theta \tag{3-4}$$

This is, of course, unacceptable. The standard practice for coping with this problem has been to incorporate a washout function in the yaw rate feedback control law. Thus, in terms of the control law functions identified on Figure 3-1, the simple yaw rate damper with washout to eliminate steady turning rates would have the following control law

$$+ \delta_R = r\, G_1(s)\, G_4(s)\, H_R(s) \tag{3-5}$$

where

$$G_1(s) = \text{lag filter} = \frac{1}{\tau_1 s + 1} \tag{3-6}$$

$$G_4(s) = \text{washout} = \frac{\tau_2 s}{\tau_2 s + 1} k_2 \tag{3-7}$$

$$H_R(s) = \text{rudder servo transfer function}$$

$$= \frac{1}{\left(\frac{s}{\omega_1} + 1\right)\left(\frac{s^2}{\omega_R^2} + \frac{2\zeta_R s}{\omega_R} + 1\right)} \tag{3-8}$$

Neglecting the rudder servo dynamics and the lag filter (for elastic mode and noise attenuation), the root loci for the yaw damper with washout (τ_2) are illustrated on Figures 3-2b and 3-2c. Note that for fast washout time constants, the attainable damping improvement decreases. Fast washouts are desirable for sideslip minimization following turn entry and exit, but they are undesirable because of the loss in attainable damping. One method often used to help minimize sideslip, both in turns or in response to gust disturbances, is lateral acceleration feedback.

c. Lateral Acceleration Feedback

The transfer function of lateral acceleration for rudder deflection inputs is

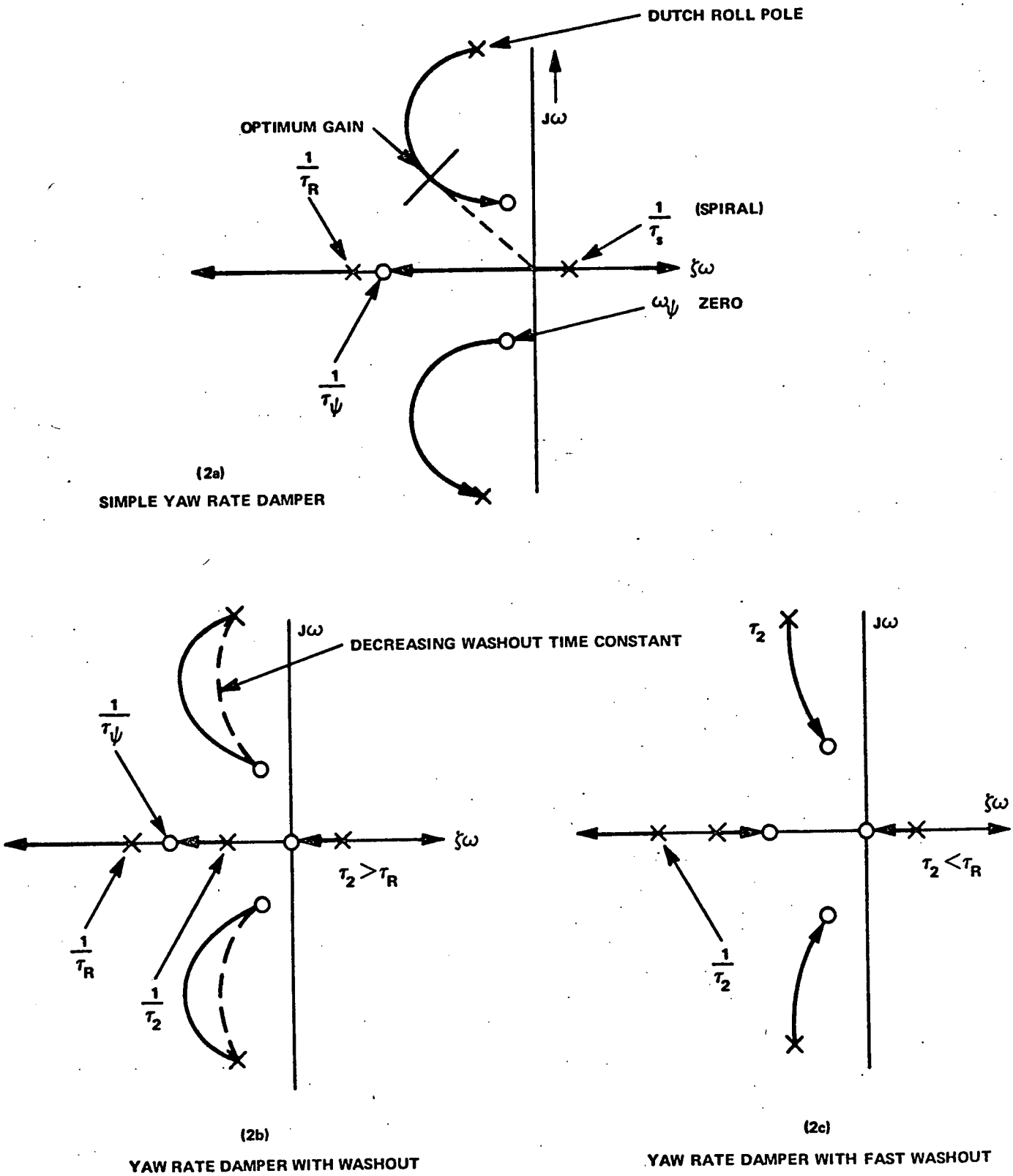

Figure 3-2
Yaw Rate Damper Root Loci
(Not to Scale)

$$\left[\frac{A_y}{\delta_R}\right] = K_{A_y} \frac{(\tau_A s + 1)(\tau_B s + 1)(\tau_C s + 1)(\tau_D s + 1)}{(\tau_s s + 1)(\tau_R s + 1)\left(\frac{s^2}{\omega_D^2} + \frac{2\zeta_D s}{\omega_D} + 1\right)} \tag{3-9}$$

where typically

$\tau_A \approx \tau_s$

$\tau_B \approx \tau_R$

τ_C and τ_D are approximately equal and of opposite polarity

Of the two possible polarities for A_y feedback, one provides sideslip minimization, but usually at the expense of dutch roll damping. The other polarity of A_y feedback can damp the dutch roll, but it will cause sideslip divergence by driving the spiral mode pole deeper into the right-half plane. This is illustrated in Figures 3-3a, and 3-3b, which show the root loci for both polarities of feedback. Figure 3-3a, the correct control for sideslip minimization, causes a deterioration in dutch roll damping, but the yaw rate feedback associated with the complete control law should have adequate gain to compensate for the adverse shift in the dutch roll poles. The proper polarity for sideslip control is:

Right rudder command for aircraft acceleration to the left. (Acceleration to the left is caused by $+\beta$.)

d. The $\dot{\beta}$ Damper

In large jet transport aircraft, the problem of achieving adequate dutch roll damping without sideslip deterioration is aggravated by the size of the aircraft. The larger values of yaw and roll inertias result in longer period dutch roll oscillations. Washout time constants on the yaw rate feedback should be sufficiently high so that the proper phase of the yaw rate feedback exists at the dutch roll frequency. For example, a 12.56-second ($\omega = 0.5$ rad/sec) dutch roll period may not be adequately damped by a yaw rate feedback signal with a 2.0-second washout. The phase of the yaw rate signal would be the phase of

$$\left[\frac{2s}{2s + 1}\right]$$

where $s = j\omega = 0.5j$

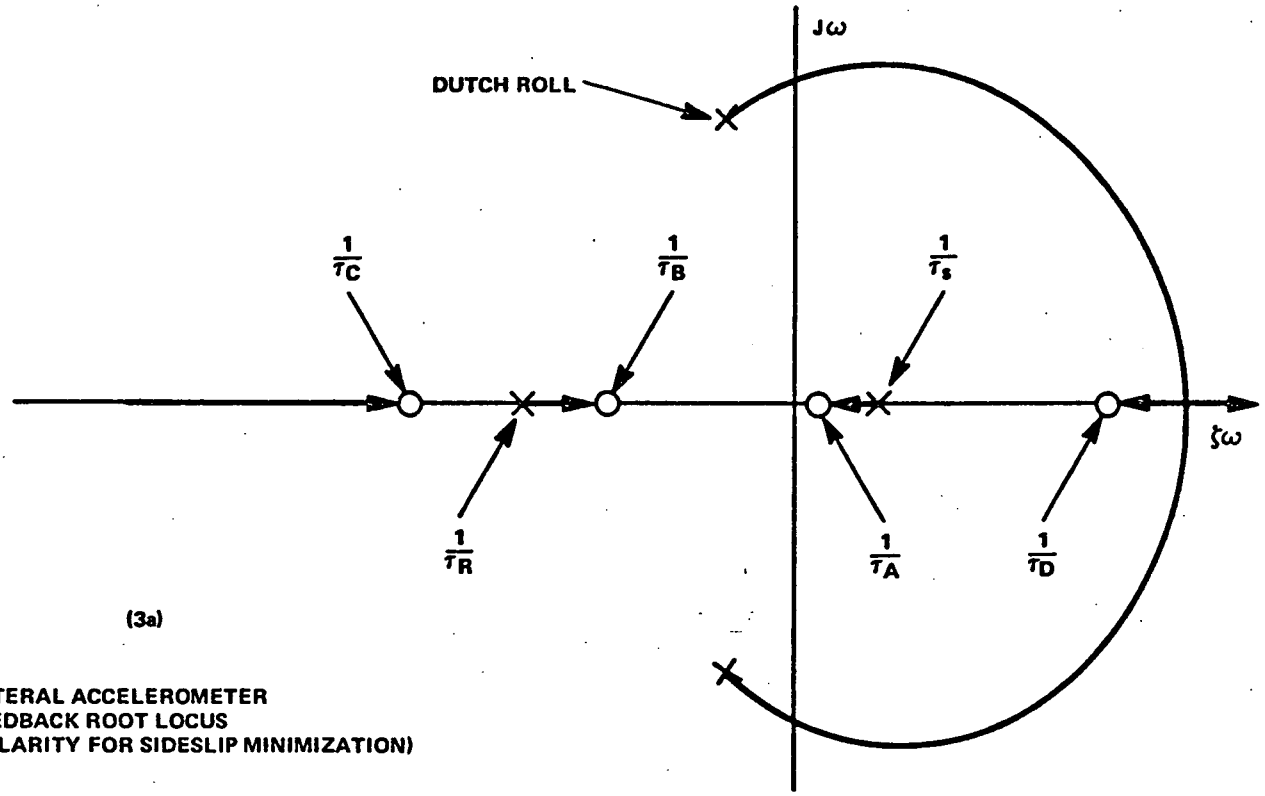

(3a)

LATERAL ACCELEROMETER
FEEDBACK ROOT LOCUS
(POLARITY FOR SIDESLIP MINIMIZATION)

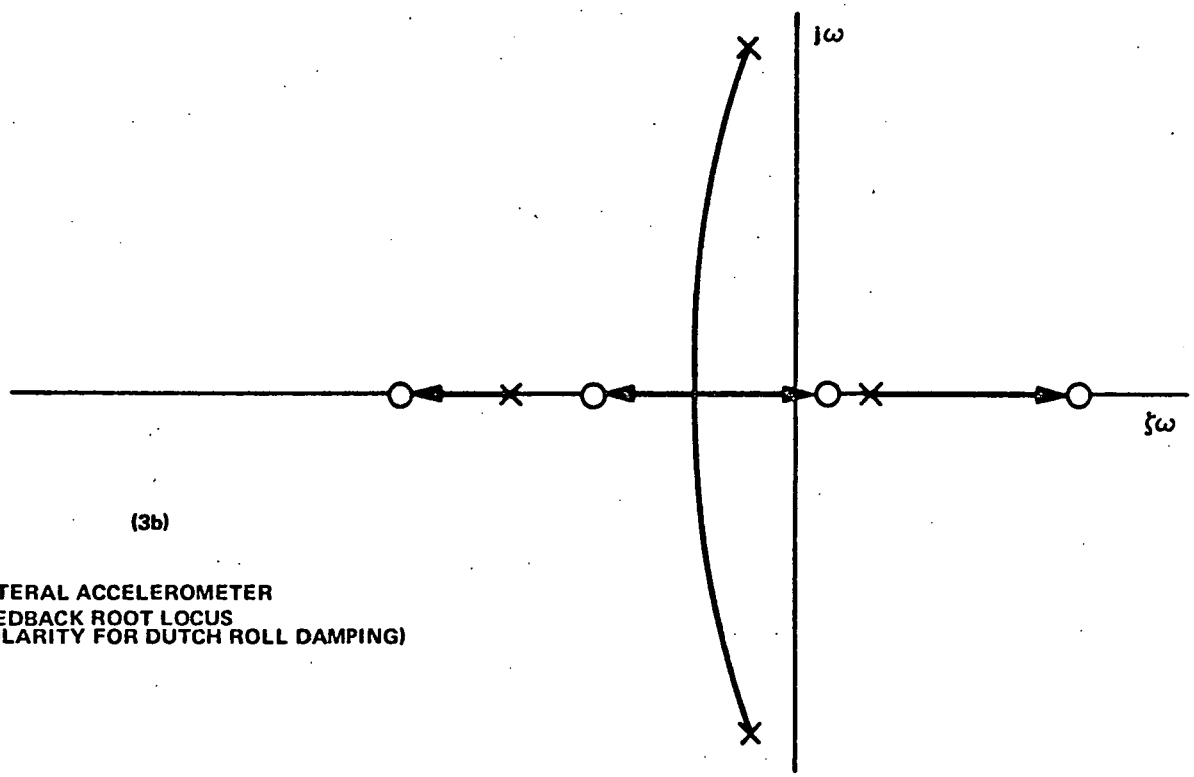

(3b)

LATERAL ACCELEROMETER
FEEDBACK ROOT LOCUS
(POLARITY FOR DUTCH ROLL DAMPING)

Figure 3-3
Lateral Accelerometer Root Loci
(Not to Scale)

The desirable phase at the dutch roll frequency is zero degrees; but in the above case, it would be +45 degrees.

One method of coping with this problem is to account for the steady yaw rate during a bank angle maneuver in some manner other than with a washout filter. An intuitive solution would be the establishment of a dynamic yaw rate reference other than zero. That is, let the yaw rate reference be zero only when the aircraft is in nonbanking flight. The yaw damper feedback signal would therefore be r_{error} where

$$r_{error} = r - r_{REF.} \tag{3-10}$$

$$r_{REF.} = \frac{g}{V} \sin \phi \tag{3-11}$$

Such an approach is often referred to as the $\dot{\beta}$ damper because subtracting the steady turn rate from the damping signal approximates a damping signal proportional to sideslip rate. In principle, therefore, the damper would be responsive to motions with respect to the relative wind rather than to an inertial reference frame. Even if perfect compensation is not achieved, a longer time constant ($G_4(s)$ in Figure 3-1) could be used without causing the adverse yaw sideslip effect encountered with the conventional yaw rate feedback plus long washout time constant.

The $\dot{\beta}$ damper is not commonly used because of its computation complexity. It should be noted that yaw dampers are generally simple devices that do not contain the computation sophistication of an autopilot. There is also a problem regarding access to a bank angle signal and to a velocity signal since yaw dampers must usually be autonomous of other aircraft subsystems. The perfect $\dot{\beta}$ damper equations can be derived from the small perturbation side force equation (in body axis coordinates)

$$\sum F_y = mV\dot{\beta} + r - \alpha_o p - \frac{g}{V}\phi \tag{3-12}$$

or

$$\dot{\beta} = \frac{\sum F_y}{mV} - r + \alpha_o p + \frac{g}{V}\phi \tag{3-13}$$

where

F_y is the sum of aerodynamic and thrust forces.

Since a lateral accelerometer is responsive to the sum total of aerodynamics and thrust forces on the aircraft (see Appendix C), we can substitute for F_y using the following relationship

$$\frac{\sum F_y}{mV} = \frac{A_y}{V} \tag{3-14}$$

where

A_y is the effective acceleration sensed by a lateral accelerometer.

Substituting equation 3-14 into equation 3-13 and solving for $(-\dot{\beta})$, the correct polarity for a damping feedback term yields

$$-\dot{\beta} = r - \frac{g}{V}\phi - \frac{A_y}{V} - \alpha_o p \tag{3-15}$$

Note that the first two terms represent the simple or approximate $\dot{\beta}$ damper defined by equations 3-10 and 3-11. Adding the lateral accelerometer with its sensitivity inversely proportional to V helps converge the result to perfect $\dot{\beta}$. The $\alpha_o p$ term can be significant at landing angles of attack although roll rates p, for transports in landing approaches are usually kept low. Feeding back perfect $\dot{\beta}$ (even if it can be computed) has one slight disadvantage. (Note that the polarity of the A_y term is opposite that required for sideslip minimization, as discussed in the previous paragraph.)

This is seen from the $\left[\frac{\dot{\beta}}{\delta_R}\right]$ transfer function

$$\left[\frac{\dot{\beta}}{\delta_R}\right] = k_{\dot{\beta}} \frac{s\left(\tau_E s + 1\right)\left(\tau_F s + 1\right)\left(\tau_G s + 1\right)}{\left(\tau_s s + 1\right)\left(\tau_R s + 1\right)\left(\frac{s^2}{\omega_D^2} + \frac{2\zeta_D s}{\omega_D} + 1\right)} \tag{3-16}$$

where

$$\tau_E \approx \tau_R$$

$$\tau_F \approx \tau_s$$

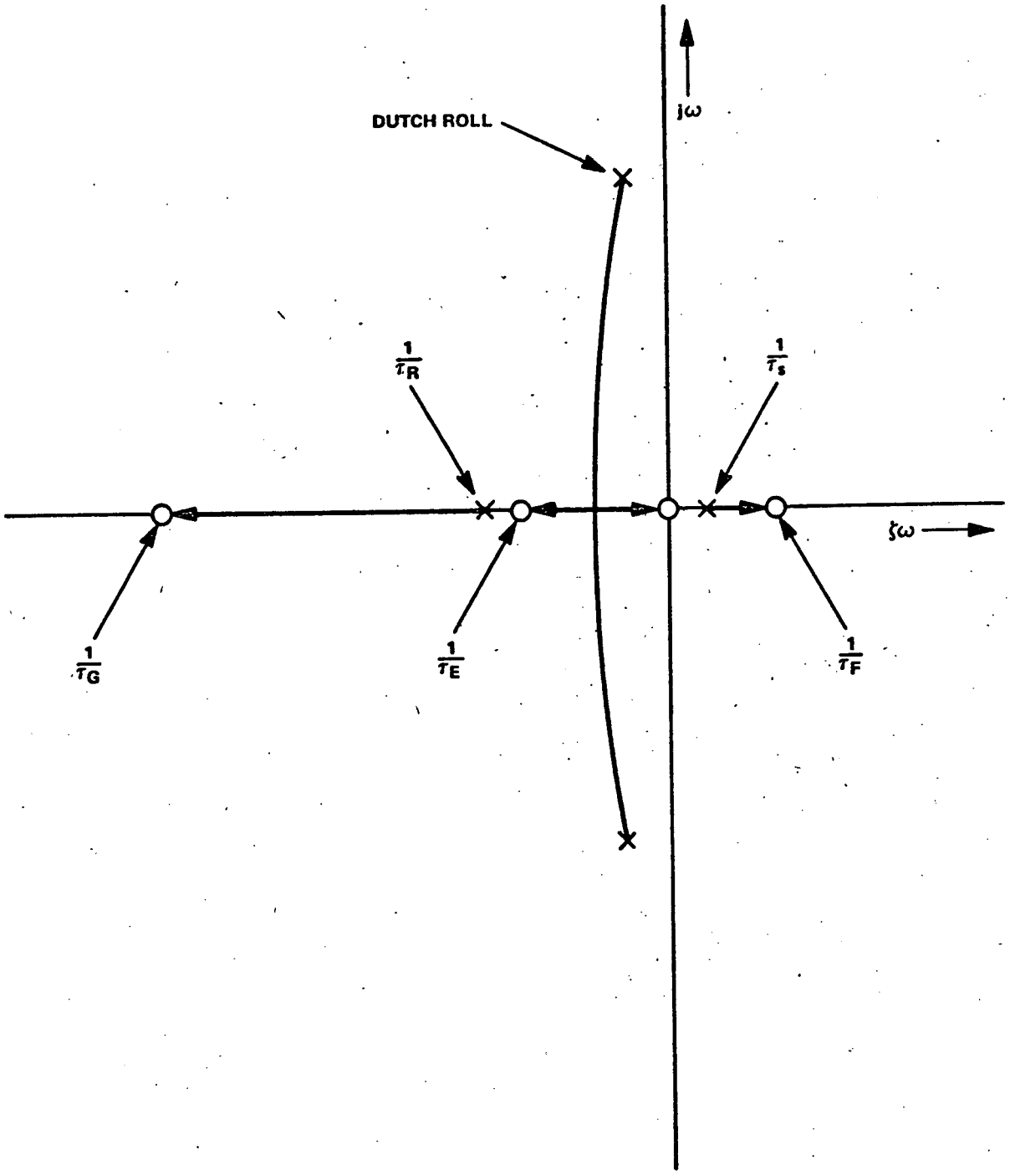

Figure 3-4
$\dot{\beta}$ Damper Root Locus
(Not to Scale)

The root locus for a typical $\dot{\beta}$ damper is shown on Figure 3-4. It is seen that unlike the typical yaw rate damper, the spiral mode divergence may be increased slightly. Damping capability for the dutch roll mode, however, is excellent.

e. Other Sideslip Control Techniques

Major sources of sideslip in turning maneuvers are the yawing moments and side forces associated with turn entry and exit. Yawing moments due to ailerons, spoilers, and roll rate cause sideslip. The $\alpha_o p$ term in equation 3-13 can result in large sideslip transients if the roll rates are high. In jet transports, these dynamic turn coordination effects are minimized by restricting roll rate maneuvers to relatively low values. If maneuvering roll rates above about 10 degrees/second are allowed and if large deflections of ailerons (or spoilers) are permitted, then a corrective, feedforward compensation proportional to aileron displacement should be fed into the rudder channel.

As shown on Figure 3-1, the compensation term is:

$$\delta_{R_1} = \delta_{AC}\, G_6(s) \tag{3-17}$$

where

$$G_6(s) = k_6 \left[\frac{\tau_3 s}{\tau_3 s + 1}\right]\left[\frac{1}{\tau_4 s + 1}\right] \tag{3-18}$$

The required compensation gain can be computed approximately as follows:

$$N_{\delta A}\,\delta_A + N_{\delta R}\,\delta_{R_1} = 0 \tag{3-19}$$

$$\delta_{R_1} = -\frac{N_{\delta A}\,\delta_A}{N_{\delta_R}} \approx -k_6\,\delta_{AC} \quad \text{(neglecting washout)} \tag{3-20}$$

or

$$k_6 \approx \frac{N_{\delta A}}{N_{\delta R}} = \frac{C_{n_{\delta_A}}}{C_{n_{\delta_R}}} \tag{3-21}$$

f. Rudder Centering

A typical yaw damper may develop offset errors as a result of the accumulation of electronic and electrohydraulic unbalances. To insure a zero steady state rudder deflection for undisturbed flight, the position feedback associated with the rudder servo mechanization may incorporate an integration term. This will provide the effect of a washout on all rudder commands. It is represented on Figure 3-1 as $G_5(s)$. This long term washout should be at least ten times larger than the yaw damper washout time constant (τ_2). In Figure 3-1, the rudder servo dynamics $H_R(s)$ are represented as having unity static gain. Hence, the effective long term washout time constant will be the reciprocal of the integrator loop gain. Thus,

$$G_5(s) = \frac{k_5}{s} \tag{3-22}$$

and

$$\tau_x = \frac{1}{k_5} \tag{3-23}$$

where τ_x is the effective long term washout time constant on rudder commands. Since this function is added to cope with specific equipment mechanization problems it need not be included in the present study; hence k_5 should be assumed to be zero.

3. Roll Stabilization

With an effective yaw damper operating through the rudders, roll attitude stabilization is usually a very simple task if a linear control system can be mechanized. Reference to the roll-to-aileron transfer function illustrates this point:

$$\left[\frac{\phi}{\delta_A}\right] = k_\phi \frac{\left(\frac{s^2}{\omega_\phi^2} + \frac{2\zeta_\phi s}{\omega_\phi} + 1\right)}{\left(\tau_s s + 1\right)\left(\tau_R s + 1\right)\left(\frac{s^2}{\omega_D^2} + \frac{2\zeta_D s}{\omega_D} + 1\right)} \tag{3-24}$$

for the undamped vehicle. This transfer function retains the same form (in the lower frequency regions) when a yaw damper loop is closed through the rudder.

However, the yaw damper loop closure moves both the poles and zeros of equation 3-24 into regions that considerably simplify the achievement of a tight roll attitude system. With yaw damper operative, the roll transfer function becomes

$$\left[\frac{\phi}{\delta_A}\right]_{Y.D.} = k_\phi \frac{\left(\frac{s^2}{\omega_\phi'^2} + \frac{2\zeta_\phi' s}{\omega_\phi'} + 1\right)}{\left(\tau_s' s + 1\right)\left(\tau_R' s + 1\right)\left(\frac{s^2}{\omega_D'^2} + \frac{2\zeta_D' s}{\omega_D'} + 1\right)} \tag{3-25}$$

Where the notation ( )' represents the new value due to yaw damper loop closure. The root loci for a roll attitude control law of the form

$$\delta_A = k_7 \left[\phi + G_7(s)p\right] H_A(s) \tag{3-26}$$

are shown on Figure 3-5. $G_7(s)$ is a cutoff filter that may be approximated by a first order lag and $H_A(s)$ may be represented by a third order model identical to that of equation 3-8. On Figure 3-5, the lag in $G_7(s)$ is neglected and it is assumed that

$$G_7(s) = a_1 \tag{3-27}$$

and

$$p = s\phi \tag{3-28}$$

Note that the effect of the yaw damper loop closure is to move ω_D and ω_ϕ into well damped regions where they form a dipole that is essentially uncoupled from the roll stabilization dynamics. Also, the spiral root has been moved from the right-half plane to near the origin. However, even if the spiral root remained in the right-half plane, the closure of a roll loop rapidly moves the spiral pole into a stable region.

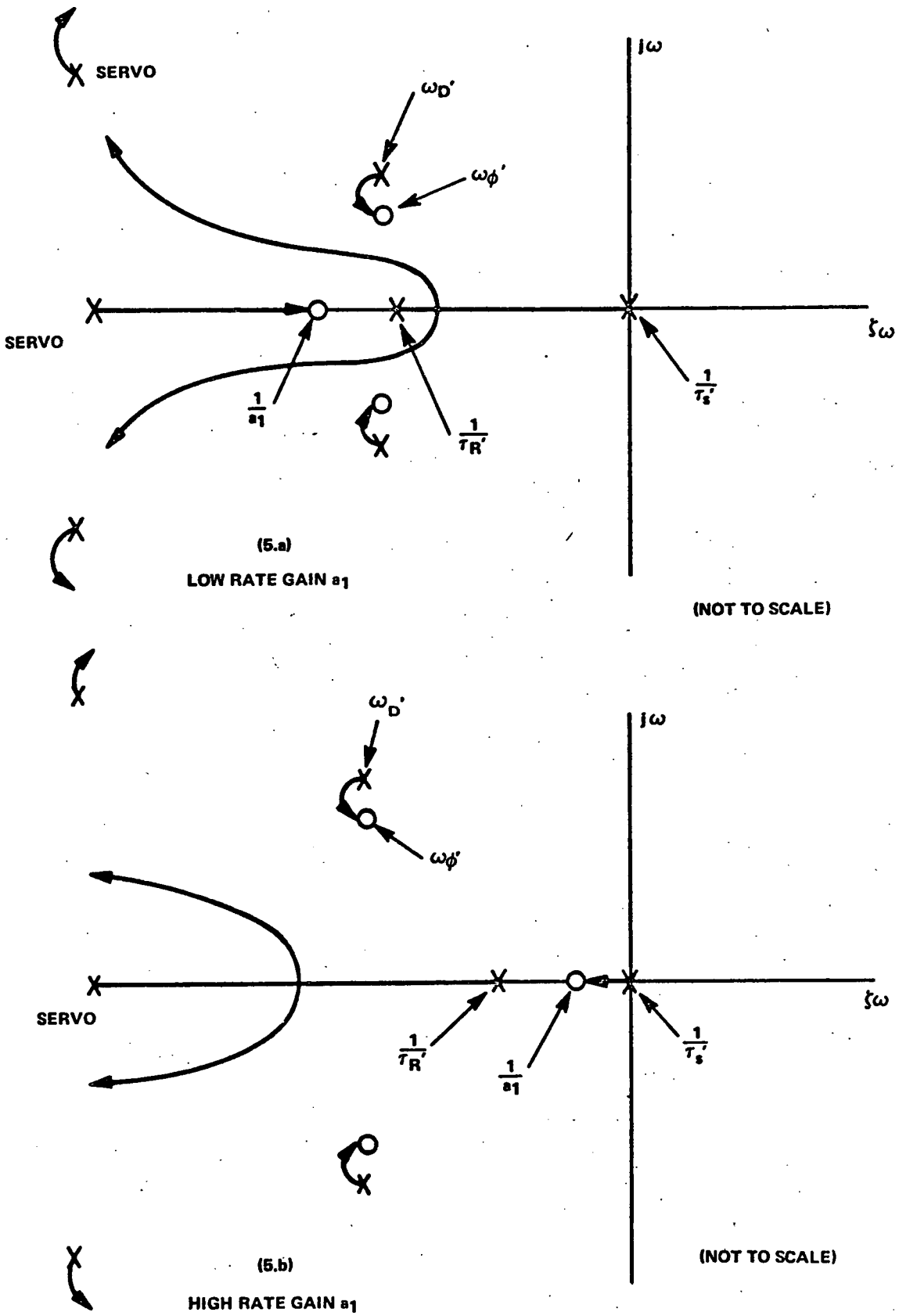

Figure 3-5
Roll Stabilization Root Loci with Yaw Damper Loop Closed

4. Lateral Stabilization Control Law Summary

The recommended control laws are*:

Rudder

$$+\delta_{RC} = (r - r_c)\left[\frac{\tau_2 s}{\tau_2 s + 1}\right]\left[\frac{1}{\tau_1 s + 1}\right] k_2 + A_y\left[\frac{1}{\tau_5 s + 1}\right] k_3$$

$$+\delta_{AC}\left[\frac{\tau_3 s}{\tau_3 s + 1}\right]\left[\frac{1}{\tau_4 s + 1}\right] k_6 \qquad (3\text{-}29)$$

where

$$r_c = \frac{g}{V}\sin\phi_c\left(\frac{1}{57.3}\right) \text{ deg/sec} \qquad (3\text{-}30)$$

Aileron

$$-\delta_{AC} = k_7\left[\phi_{error} + \frac{a_1}{\tau_7 s + 1}\, p\right] \qquad (3\text{-}31)$$

Typical values for lateral stabilization parameters are summarized in Table 3-1.

*The polarity of the surface commands depend upon the polarity convention used for the vehicle equations. There is no universally accepted convention for these polarities. The rudder and aileron control laws given here assume that positive rudder is trailing edge to the left and positive aileron is left wing aileron trailing edge down (right rolling moment).

TABLE 3-1

PARAMETER SUMMARY

Parameter	Typical Minimum Value	Typical Nominal Value	Typical Maximum Value	Remarks
k_2	1.0 deg δ_R per deg/sec r	2.0 deg δ_R per deg/sec r	4.0 deg δ_R per deg/sec r	Approach Condition Values (decrease with Q) Yaw Rate Gain
τ_2	1.5 sec	2.4 sec	4.0 sec	Washout on Yaw Damper
τ_1	0.05 sec	0.1 sec	0.2 sec	High Frequency Cutoff
k_3 for Sideslip Minimization	0.5 deg δ_R/ft/sec^2	1.0 deg δ_R/ft/sec^2	2.0 deg δ_R/ft/sec^2	Lateral Acceleration Gain (positive polarity)
τ_5	0.1 sec	0.15 sec	0.3 sec	Accelerometer Filter
k_5	0.02	0.025	0.05	Rudder Centering Integration
k_6	0.05 nom	$C_{n_{\delta_A}}/C_{n_{\delta_R}}$	2 x nom	
τ_3	1.0 sec	2.0 sec	4.0 sec	Aileron Compensation Washout
τ_4	0.1 sec	0.2 sec	0.4 sec	Aileron Compensation Filter
ω_1	10 rad/sec	15 rad/sec	20 rad/sec	Rudder or Aileron Servo - 1st Order
ω_R, ω_A	15 rad/sec	20 rad/sec	30 rad/sec	Rudder or Aileron Servo - 2nd Order
L_1, L_1'*	20 deg/sec	30 deg/sec	50 deg/sec	Aileron Rate Limit L_1' = Electrical Limit
L_2, L_2'*	20% full authority	50% full authority	70% full authority	Aileron Displacement Limit L_2' = Electrical Limit
L_3, L_3'*	10 deg/sec	20 deg/sec	30 deg/sec	Rudder Rate Limit L_3' = Electrical Limit
L_4, L_4'*	10% full authority	25% full authority	50% full authority	Rudder Displacement Limit L_4' = Electrical Limit
k_7 hi Q	1	2 deg δ_A per deg ϕ	4.0	Roll Error Gain - (should be reduced with dynamic pressure, Q)
k_7 lo Q (approach)	2.5	5.0 deg δ_A per deg ϕ	8.0	
a_1	0.4	0.8	1.5	Ratio of Rate-to-Displacement Gain
τ_7	0.05	0.1	0.15	Roll Rate Filter
L_5	5 deg/sec	10 deg/sec	20 deg/sec	Cruise — Roll Rate Limit
	3 deg/sec	5 deg/sec	8 deg/sec	Final Approach — Roll Rate Limit

*Values are given for mechanical limit. Electrical limit should be set about 15 percent below mechanical limit.

5. Lateral Stabilization Performance Criteria

a. Procedure for Establishing Yaw Damper

- Establish free-aircraft simulation and obtain transient response using initial condition of 2.0 degrees in sideslip

- Close yaw rate feedback loop without washout

- Increase yaw rate gain until damping ratio of greater than 0.5 is obtained, or until damping begins to deteriorate with long-period oscillation detectable, or until signs of high frequency mode appear on δ_R response. The δ_R response should never show oscillations with damping below 0.20.

- Add yaw rate washout time constant, starting with value of about 4.0 seconds and decreasing until dutch roll damping ratio shows deterioration to below about 0.5.

b. Procedure for Establishing Roll Stabilization Parameters

- Use nominal control law - $\delta_A = k\ (\phi_e + 0.5\ p)$.

- Apply 5-degree step roll command (with roll rate constraint L_5).

- Raise k to nominal or higher value until roll overshoot is held to less than 10 percent. Roll angle should settle at final value within 3.0 seconds. If any evidence of high frequency oscillations appear on the δ_A response, the gain k should be lowered. High frequency δ_A motions with damping ratios below 0.2 are objectionable.

c. Turn Coordination

- Apply 20-degree bank command, ϕ_c, through a 1.0-second lag filter plus a command constraint that restricts $\dot{\phi}_c$ to 10 deg/sec.

- Observe peak excursions of β and A_y. The lateral acceleration A_y should not exceed 0.1g (3.2 ft/sec^2) during this maneuver.

- Observe the effect of the yaw rate washout time constant on β and A_y during the bank maneuver. If reduction in washout time constant improves turn coordination but causes a dutch roll damping deterioration, then the $\dot{\beta}$ damper may be desirable or the inclusion of an A_y loop should be considered.

- If transient turn coordination is poor because of yaw moments due to aileron, then aileron compensation loop should be added. The criterion should be 0.1g peak lateral accelerometer reading for the most severe bank maneuver. Steady state g's in the turn for 20-degree bank should always be below 0.5 to 1.0 ft/sec^2.

B. DIGITAL PROGRAM - LATERAL STABILIZATION

1. Control Law Conversion

The representation of the lateral stabilization block diagram and control laws in FORTRAN notation is summarized in Figure 3-6 with a tabulation of the FORTRAN namelist given in Table 3-2. Note that, as in the case of the pitch stabilization control laws, a proportional gain program as a function of dynamic pressure Q is incorporated.

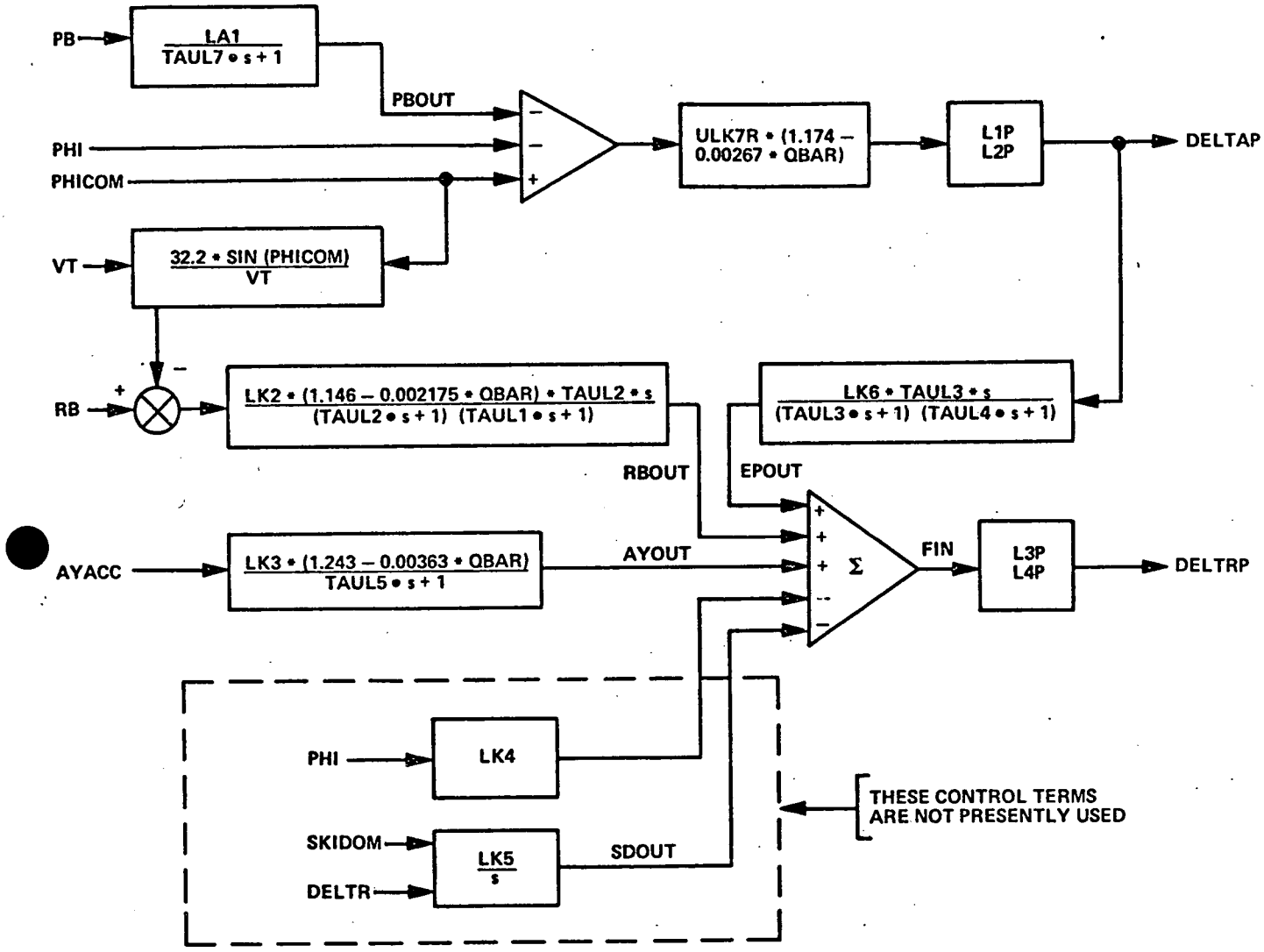

Figure 3-6
Lateral Stabilization Block Diagram
with Fortran Notation

TABLE 3-2

VARIABLE NAMELIST
SUBROUTINE LATSTB

Variable	FORTRAN Name	Definition
p	PB	Body axis roll rate
ϕ	PHI	Euler roll angle
ϕ_c	PHICOM	Roll angle command
r	RB	Body axis yaw rate
A_y	AYACC	Lateral body-mounted accelerometer output
V	VT	Aircraft ground speed
δ_R	DELTR	Rudder angle
δ_{RC}	DELTRP	Rudder angle command
δ_{AC}	DELTAP	Aileron angle command
a_1	LA1 (ULA1)*	Roll rate gain
K_7	ULK7R (ULK7)	Roll stabilization gain
K_2	LK2	Yaw damper gain
K_3	LK3	Accelerometer feedback gain
K_4	LK4	Roll angle feedback gain; $\dot{\beta}$ damper
K_5	LK5	Rudder centering integrator gain
K_6	LK6	Aileron feedback gain
L_1'	L2P (P1P)	Aileron command rate limit
L_2'	L2P (P2P)	Aileron command position limit
L_3'	L3P (P3P)	Rudder command rate limit
L_4'	L4P (P4P)	Rudder command position limit
τ_1	TAUL1	Yaw damper filter time constant
τ_2	TAUL2	Yaw damper filter time constant
τ_3	TAUL3	Aileron compensation filter time constant
τ_4	TAUL4	Aileron compensation filter time constant

*Fortran variables in parenthesis are unscaled values.

TABLE 3-2 (cont)

VARIABLE NAMELIST
SUBROUTINE LATSTB

Variable	FORTRAN Name	Definition
τ_5	TAUL5	Accelerometer filter time constant
τ_7	TAUL7	Roll rate filter time constant
-	DT2	Subroutine sample time
-	R2D	Radians-to-degrees conversion
-	D2R	Degrees-to-radians conversion
-	ITESTL	Logic variable for lateral stabilization loop synchronization
Q	QBAR	Dynamic Pressure

2. Program Flow Chart

The initial condition computations which are performed in the SASIC subroutine (see Appendix A) for the lateral stabilization mode is given in the following summary. The flow charts are shown in Figure 3-7.

Lateral Stabilization Subroutine LATSTB IC Calculation

a. Set Outputs

SKIDCM = 0

DELTRP = 0

DELTAP = 0

b. Scale Limits

L1P = P1P * D2R * DT2

L2P = P2P * D2R

L3P = P3P * D2R * DT2

L4P = P4P * D2R

c. Scale Gains

ULK7R = ULK7 * D2R

LK3 = ULK3 * D2R

LK4 = 32.2 * LK2 * NOP

d. Difference Equation Coefficients

- Roll Rate Filter

```
CP1 = EXP (-DT2/TAUL7)
DP1 = LA1 * (1.0 - CP1) * R2D
```

- Aileron Compensation Filter

```
CEP1 = EXP(-DT2/TAUL3) + EXP(-DT2/TAUL4)

CEP2 = EXP[-DT2 * (1.0/TAUL3 + 1.0/TAUL4)]

DEP1 = LK6/TAUL4 * [EXP(-DT2/TAUL3) -EXP(-DT2/TAUL4)]/
       (1.0/TAUL3 - 1.0/TAUL4)
```

- Rudder Centering Integrator

```
LK5 = ULK5 * DT2
```

- Yaw Rate Filter

```
CRB1 = EXP(-DT2/TAUL1) + EXP (-DT2/TAUL2)

CRB2 = EXP[-DT2 * (1.0/TAUL1 + 1.0/TAUL2)]

DRB1 = LK2/TAUL2 *[EXP (-DT2/TAUL1) - EXP (-DT2/TAUL2)]/
       (1.0/TAUL2 - 1.0/TAUL1)
```

- Lateral Accelerometer Filter

```
CA1 = EXP(-DT2/TAUL5)
DA1 = LK3* (1.0 - CA1)
```

The chosen Lateral Stabilization parameters for best performance are:

TAUL1 = 0.1	P1P = 25.5	ULK7 = 3.0
TAUL2 = 2.4	P2P = 14.9	LK2 = -2.0
TAUL3 = 2.0	P3P = 17.0	ULK3 = -3.0
TAUL4 = 0.2	P4P = 15.3	
TAUL5 = 0.15	LK6 = -0.15	
TAUL7 = 0.1	LA1 = 0.5	

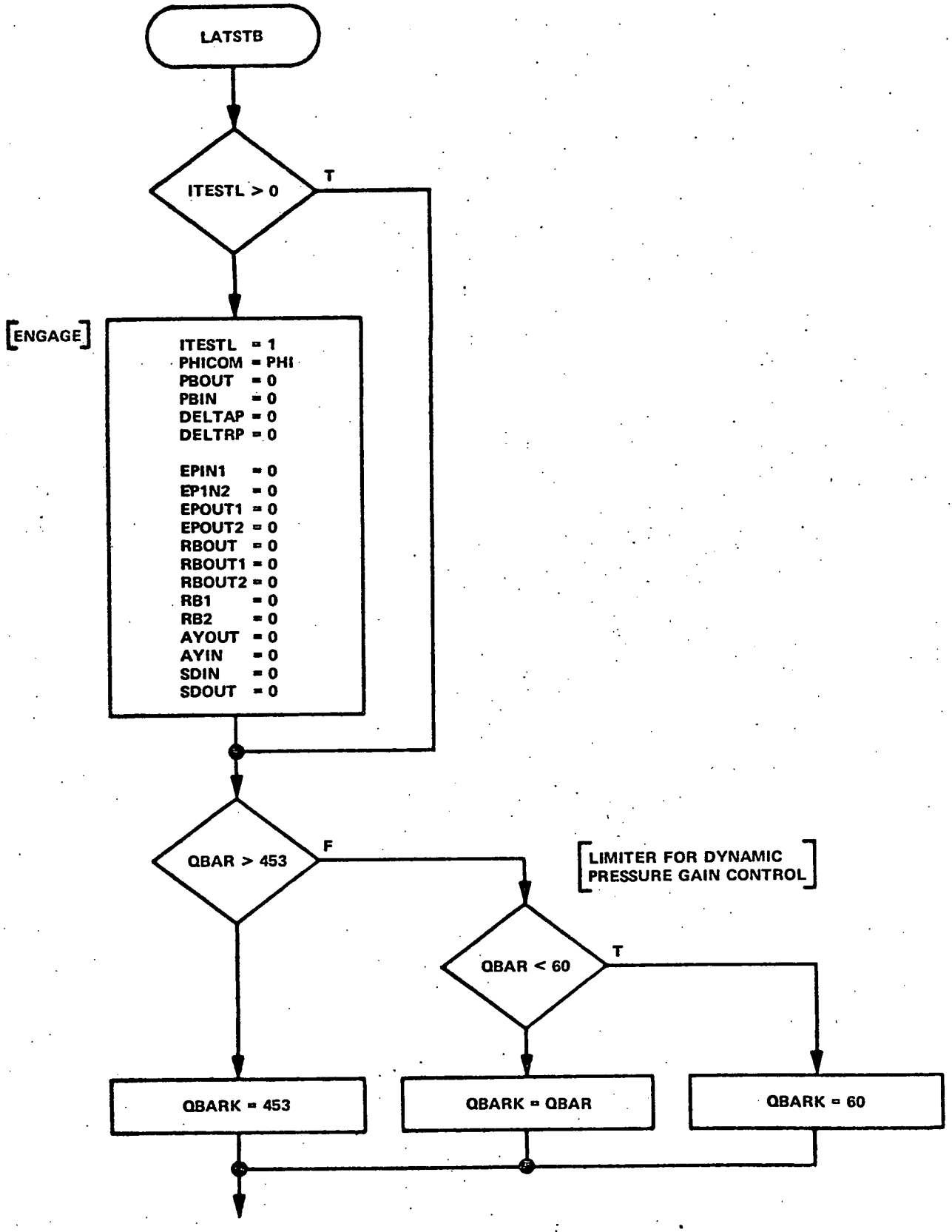

Figure 3-7a
Lateral Stabilization Flow Chart

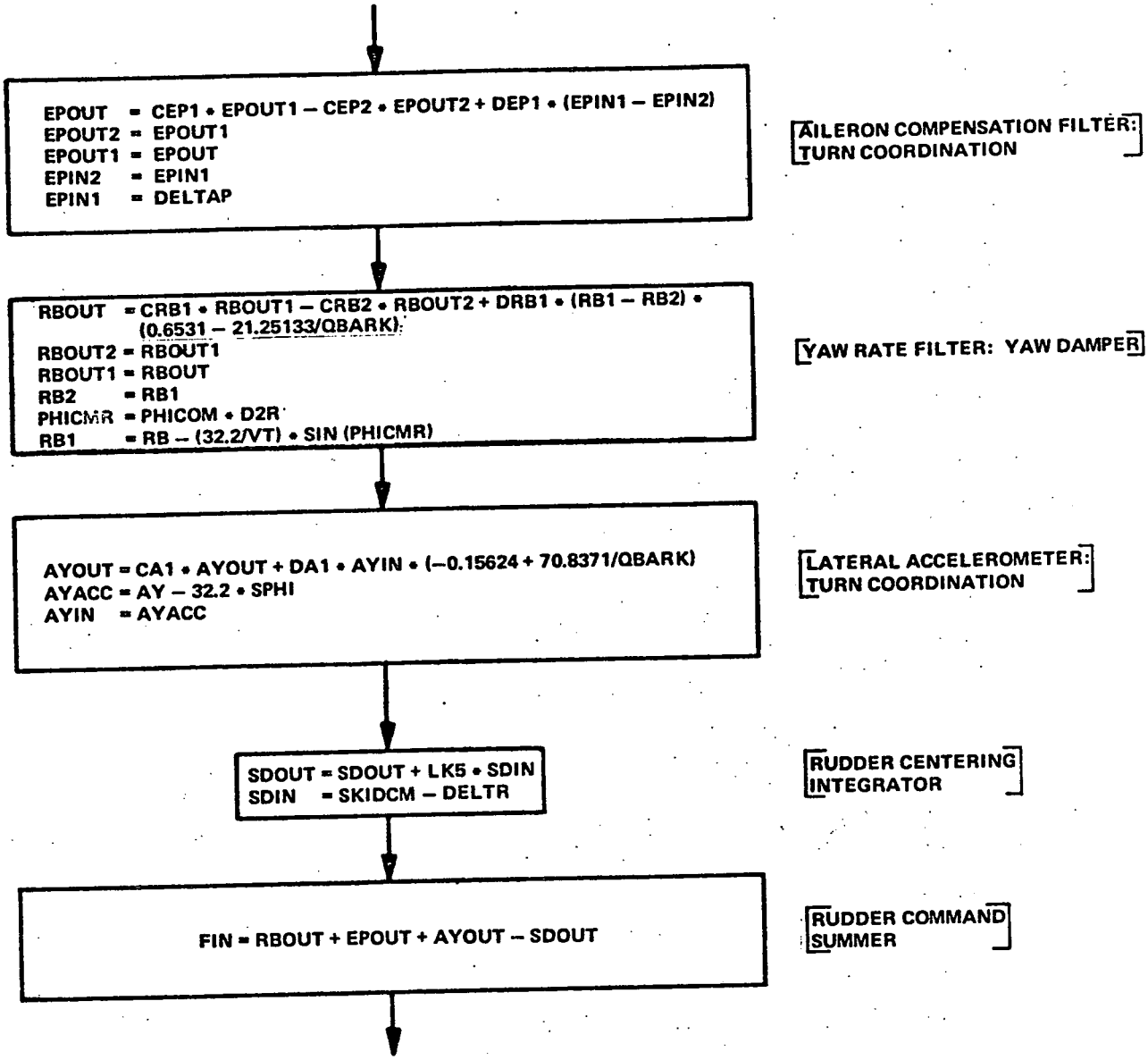

Figure 3-7b
Lateral Stabilization Flow Chart (cont)

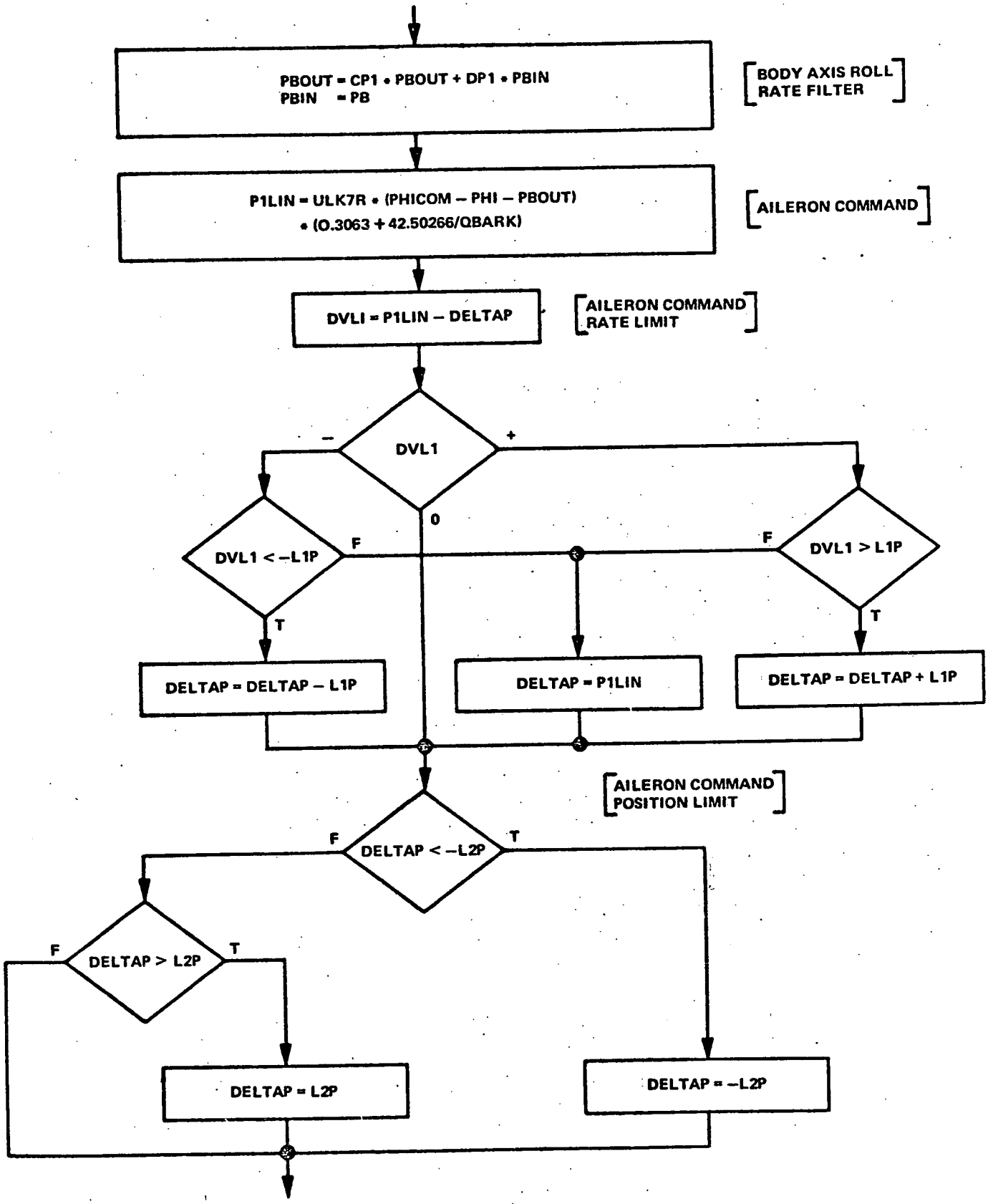

Figure 3-7c
Lateral Stabilization Flow Chart (cont)

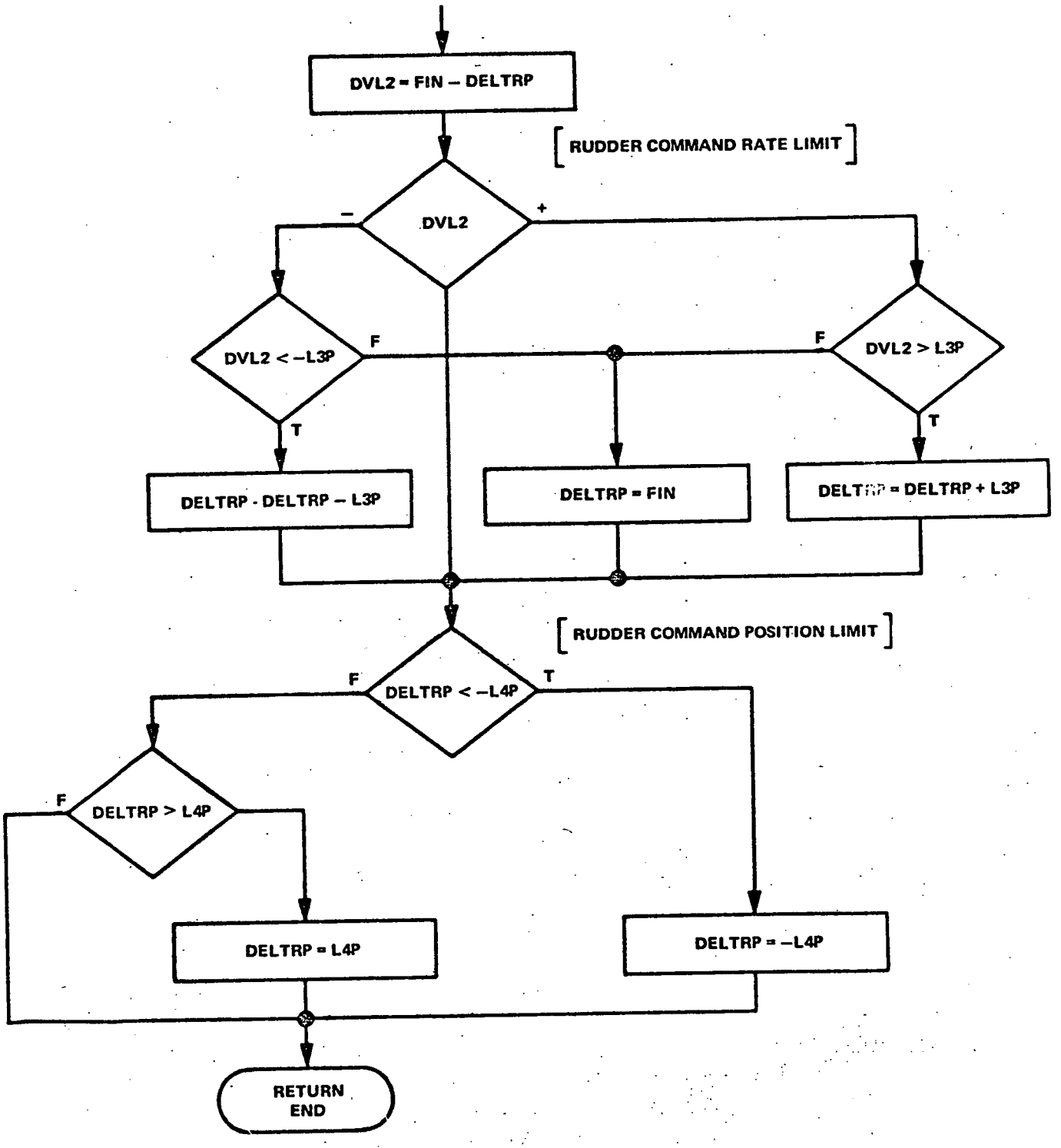

Figure 3-7d
Lateral Stabilization Flow Chart (cont)

C. SIMULATION TEST RESULTS

1. Yaw Damper

Yaw damper performance achieved with the recommended control law parameter is illustrated in Figure 3-8. The transient responses are at the 141-knot and 295-knot, sea level flight conditions. They illustrate sideslip in response to a step gust corresponding to 2.0 degrees of sideslip. It is apparent from these responses that dutch roll damping (by the yaw damper) is excellent at the higher speed condition but only marginally acceptable at the low speed condition. The relative ineffectiveness of the yaw rate into rudder loop as a dutch roll damper at the landing approach flight condition is a common aircraft phenomenon. It is a consequence of the close proximity of the ω_ψ zeros to the ω_D poles in equation 3-1. Fortunately, this does not cause any autopilot problems because the dutch roll is readily damped at this flight condition by a roll rate feedback into the ailerons. This feedback is inherent in the roll stabilization system.

2. Roll Stabilization

The absence of any dutch roll oscillations and hence the effectiveness of the roll stabilization loop as a dutch roll damper at low speeds is apparent from the roll stabilization test results illustrated in Figure 3-9. Roll angle responses to filtered 5.0-degree bank angle commands are shown for the 141-knot and 296-knot flight conditions. Damping is excellent and static accuracy is perfect.

3. Turn Coordination

The turn coordination criteria defined in Section III A-5 were easily achieved as illustrated in Figures 3-10(a) and 3-10(b) for the low and high speed conditions respectively. Those criteria can probably be viewed as worst case numbers. The level of performance achieved in Figures 3-10(a) and 3-10(b) would probably be rated good to excellent by a flight test pilot who would evaluate turn coordination performance on the basis of his ball-bank inclinometer. One "ball" on this instrument is equal to a 4.7-degree deflection of the apparent gravity angle. The apparent gravity (or pendulum) angle, σ, is

$$\sigma = \frac{A_y}{\left(\frac{g}{\cos \phi}\right)} = \frac{A_y}{g} \cos \phi$$

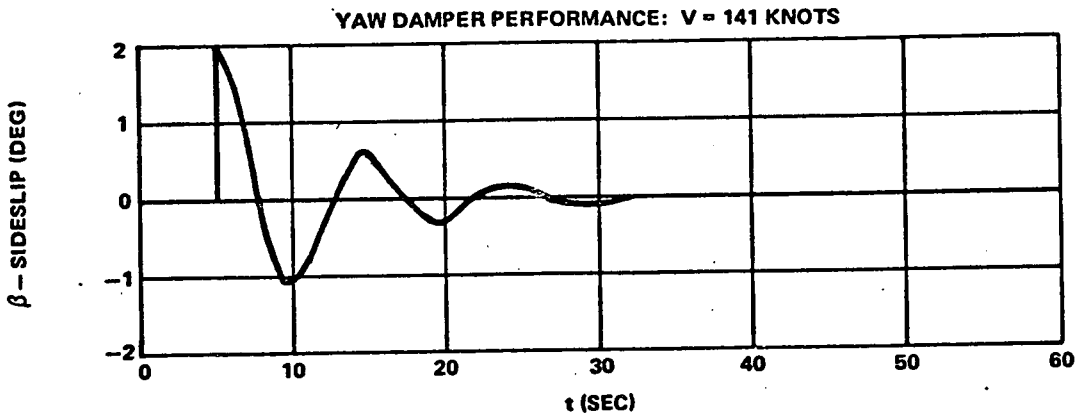

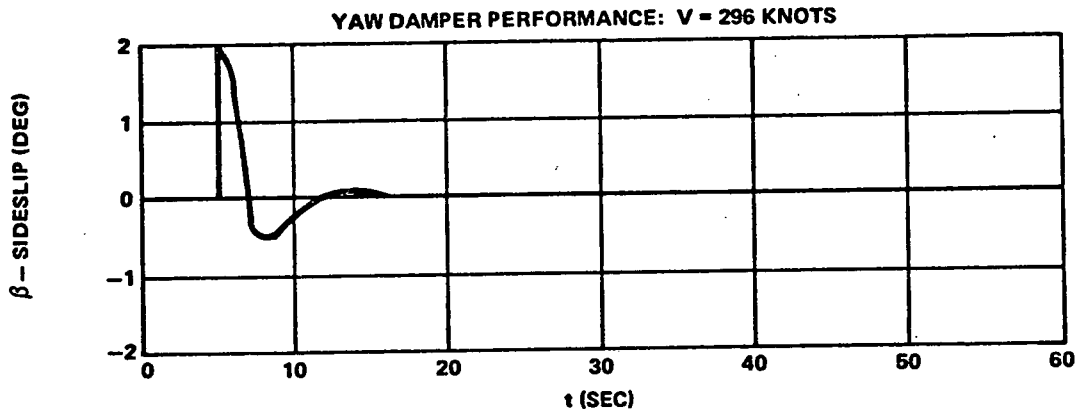

NOTE: IN BOTH OF THE ABOVE TESTS, A STEP SIDE GUST EQUIVALENT TO β = 2.0 DEGREES WAS APPLIED AT t = 5.0 SECONDS

YAW DAMPER PARAMETERS:

TAUL1 = 0.1 SEC
TAUL2 = 2.5 SEC
LK2 = –2.0 (THE YAW DAMPER GAIN IS REDUCED AUTOMATICALLY AS THE DYNAMIC PRESSURE INCREASES)
P3P = 17.0 DEG/SEC
P4P = 15.3 DEG

Figure 3-8
Yaw Damper Performance

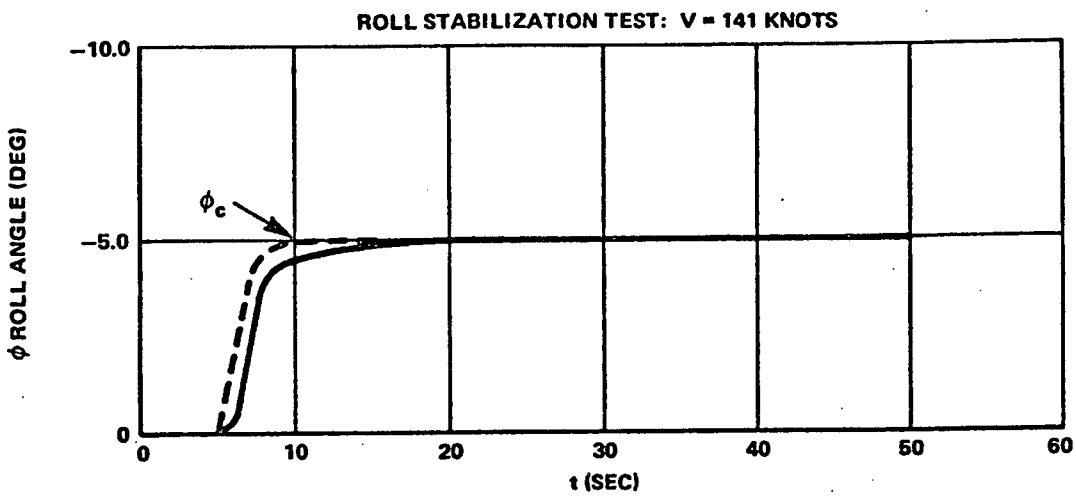

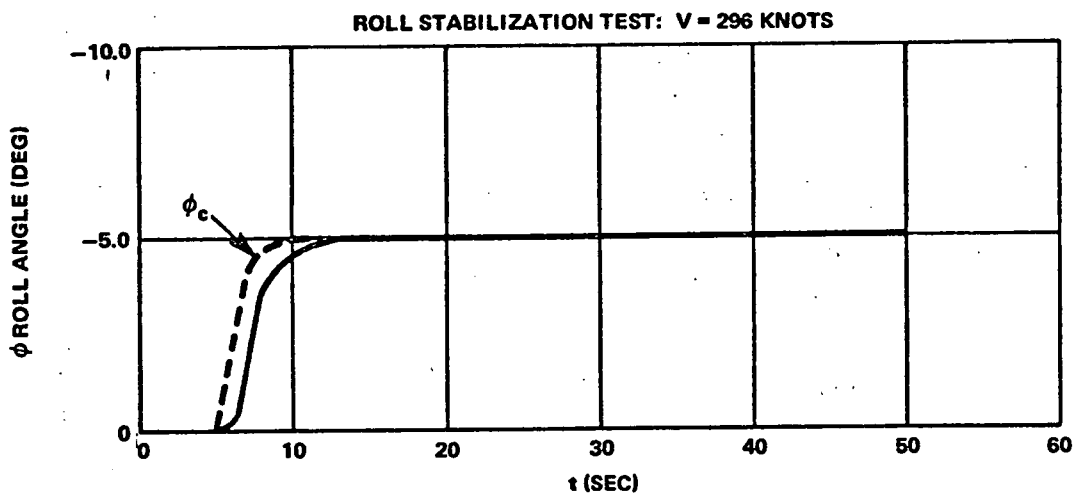

ROLL STABILIZATION ON PARAMETERS:

TAUL7 = 0.1 SEC
LA1 = 0.5 SEC^{-1}
ULK7 = 3.0 DEG/DEG (GAIN REDUCED AS DYNAMIC PRESSURE INCREASES)
P1P = 25.5 DEG/SEC
P2P = 14.9 DEG

YAW DAMPER AS GIVEN IN YAW DAMPER TESTS

Figure 3-9
Roll Stabilization Performance

A pilot would consider turn coordination good if his inclinometer shows less than 1/8 ball. At ϕ = 30 degrees, 1/8 ball corresponds to 0.0118 g's or 0.38 ft/sec^2. At the low speed condition the transient acceleration reaches a peak of 0.039 g's but always reduces to less than 0.01 g's steady state. The rudder control system's turn coordination includes the lateral acceleration (gain controlled with Q) and the aileron-to-rudder crossfeed. Any additional sophistication to improve turn coordination performance does not appear to be warranted.

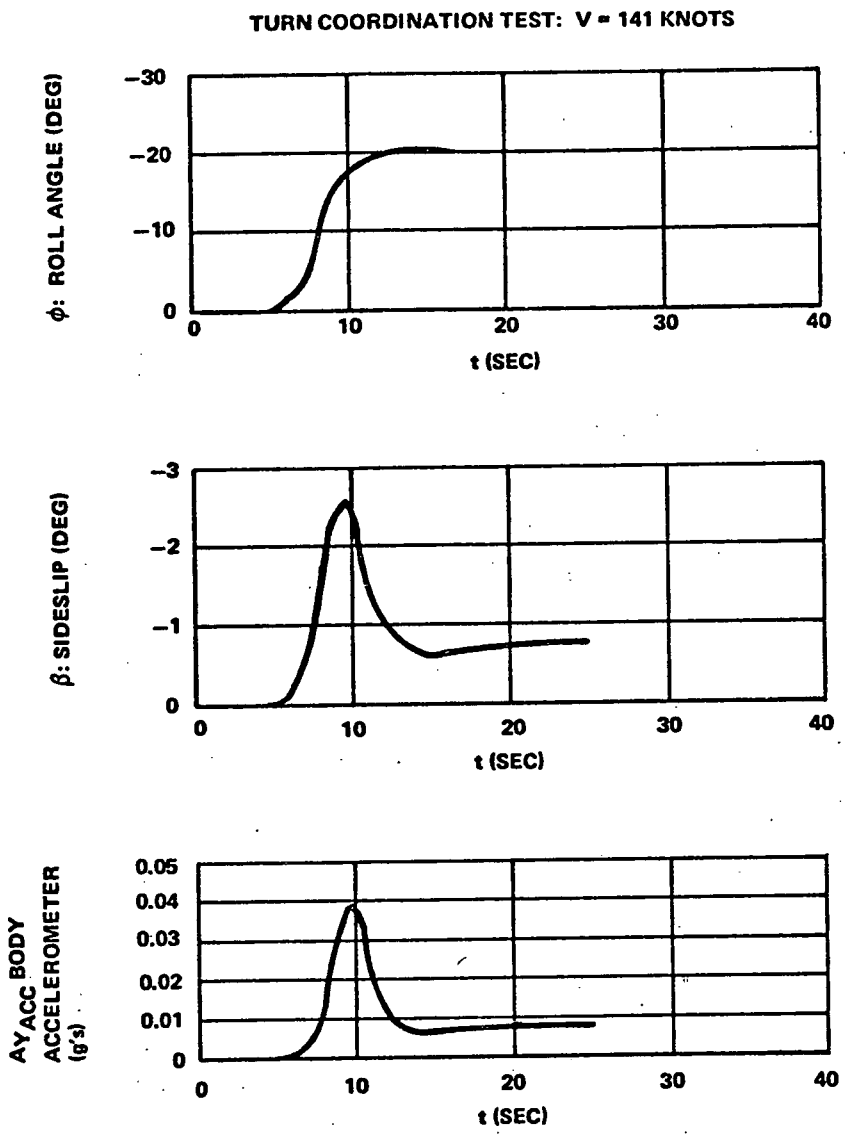

TURN COORDINATION PARAMETERS:

TAUL5 = 0.15 SEC
TAUL3 = 4.0 SEC
TAUL4 = 0.1 SEC
LK6 = 0.1
ULK3 = 3.0 DEG/FT/SEC^2

YAW DAMPER AND ROLL STABILIZATION PARAMETERS GIVEN IN PREVIOUS TESTS.

Figure 3-10a
Turn Coordination Performance
(141 Knot Condition)

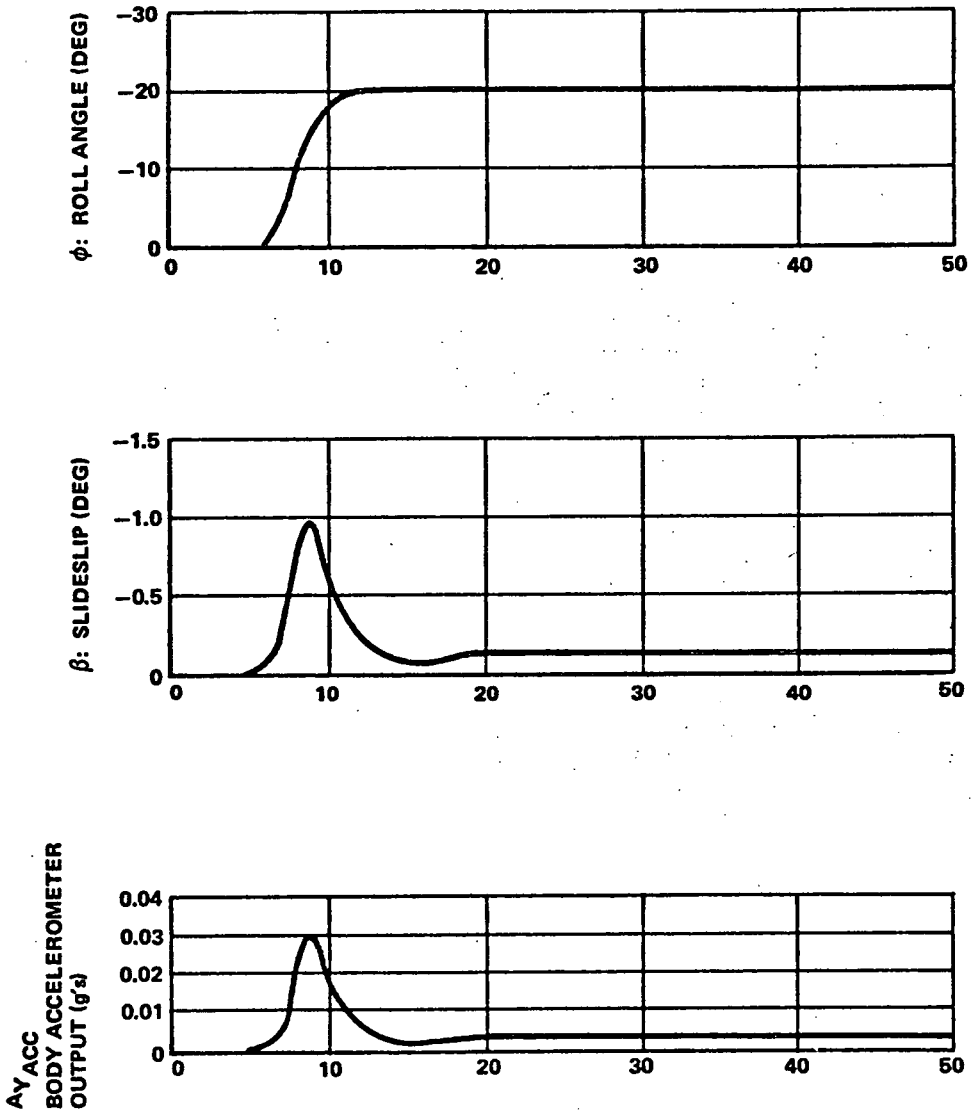

TURN COORDINATION PARAMETERS SAME AS IN LOW SPEED TEST.
GAIN LK3 IS REDUCED BY A FACTOR OF SIX (LK3 = −0.5) WITH DYNAMIC PRESSURE.

Figure 3-10b
Turn Coordination Performance
(296 Knot Condition)

SECTION IV

AUTOTHROTTLE SYSTEM

A. DESCRIPTION OF CONTROL LAWS

1. General

The general autothrottle system block diagram is shown in Figure 4-1. The basic inputs are calibrated airspeed $\left(V_c\right)$ in knots. a commanded airspeed reference $\left(V_{c_{REF}}\right)$, compensated inertial acceleration $(\ddot{x})$, pitch angle (θ), and elevator position (δ_E). Compensated forward acceleration refers to the subtraction of the component of gravity due to pitch angle from the body-mounted fore-aft accelerometer. This resolution of the required acceleration signal from an accelerometer is shown in Figure 4-2. The cosine of the angle-of-attack compensation is not required for the usual range of angle of attack.

2. Control Laws

The complete throttle control equation may be expressed as

$$V_{c_{ERROR}} \left[G_{1A}(s)\right] + \ddot{x}_c \left[G_{1B}(s)\right] - \theta \left[G_2(s)\right] + \delta_{T_P} + \delta_E \left[G_3(s)\right] = -\delta_{T_c} \tag{4-1}$$

where δ_{T_P} is a predictive feedforward command based on computation of future throttle requirements

$$\frac{\delta_T}{\delta_{T_c}} = G_4(s) = \frac{1}{\left[\frac{S}{\omega_T} + 1\right]^2} = \text{Throttle Servo Dynamics} \tag{4-2}$$

with following constraints

$$\dot{\delta}_{T_{MAX}} = L_2 \tag{4-3}$$

$$\delta_{T_{MAX}} = L_3 \tag{4-4}$$

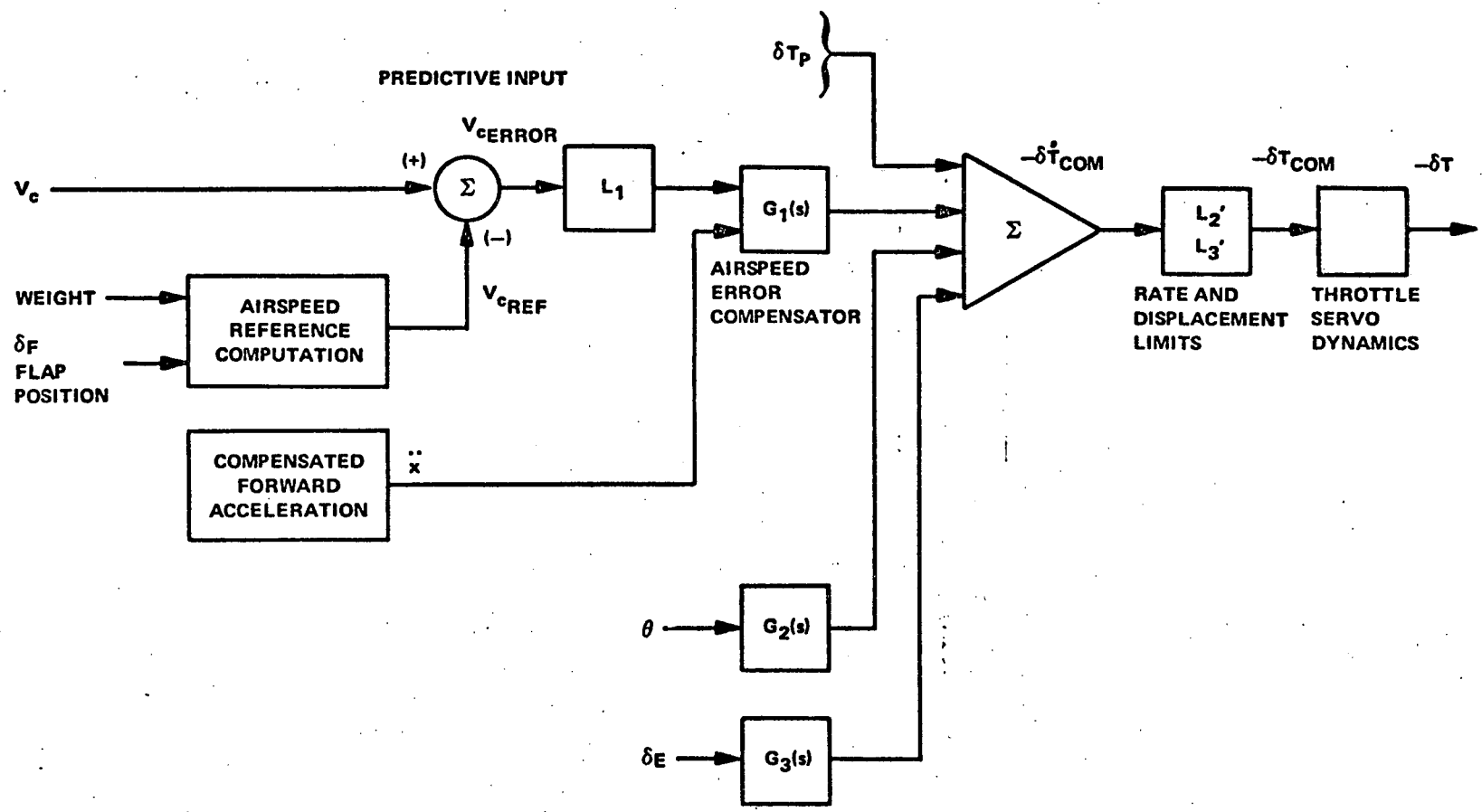

Figure 4-1
Autothrottle System Block Diagram

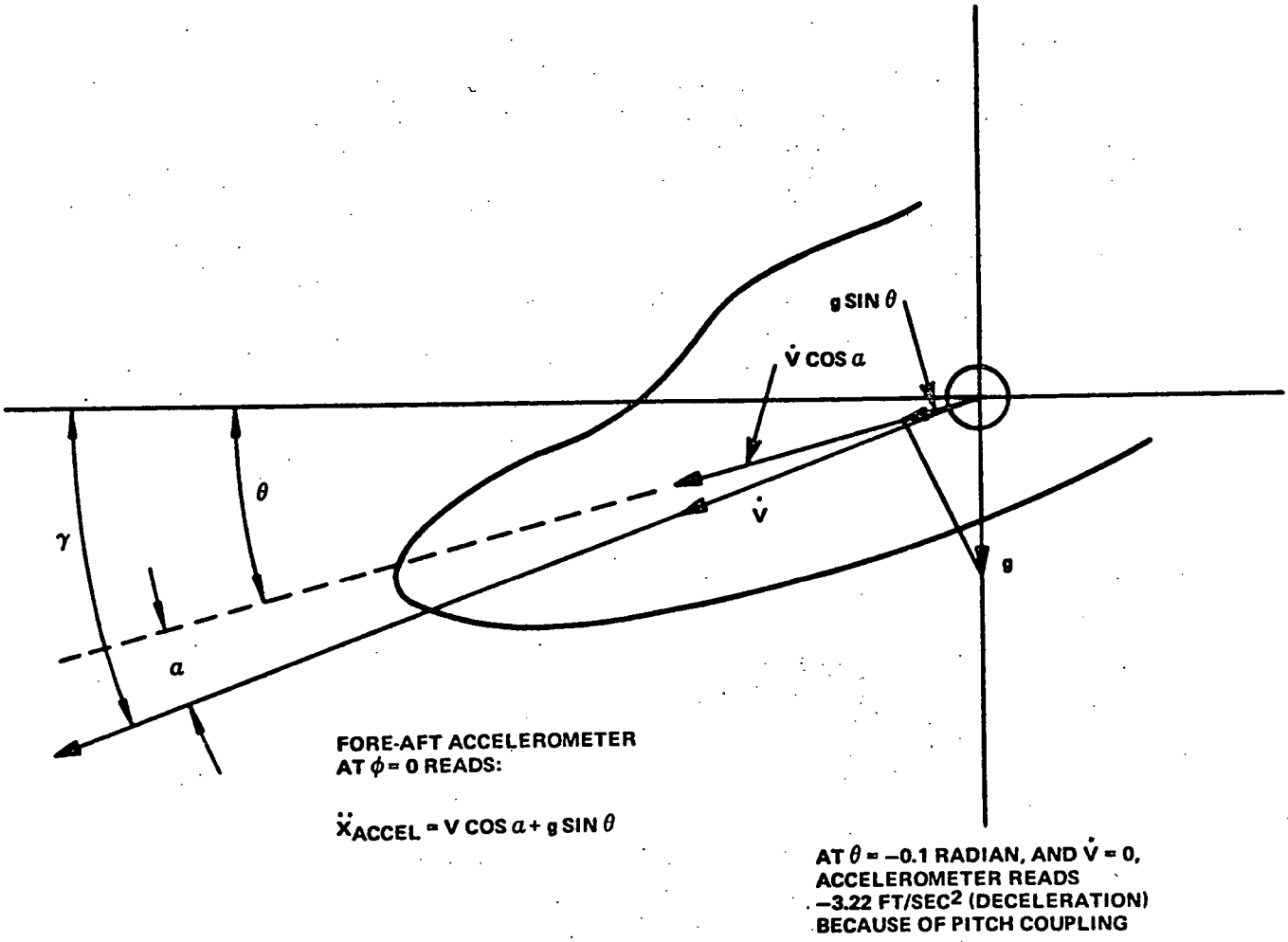

Figure 4-2
Pitch Coupling In Fore-Aft Body
Mounted Accelerometer

It is noted that most mechanizations of autothrottle servo systems use velocity servos rather than position servos (equation 4-2). This is a practical consequence of the requirement that the throttle servo have a floating reference position established by the manual throttle input. The velocity servo mechanization usually eliminates the need for specifying an integral compensation term. For the purposes of this study, however, the mathematical form of the control laws as throttle increments will be valid and all peculiarities of mechanization will be omitted.

The combination of $G_{1A}(s)$ and $G_{1B}(s)$ includes a complementary filter that creates a wide bandwidth speed error signal using inertial data for short term and pressure data for long. A detailed block diagram of this function is shown in Figure 4-3. As seen in this figure

$$G_{1A}(s) = \left[\frac{1}{\tau_c s + 1} + \frac{K_I}{s}\right] K_V \tag{4-5}$$

and

$$G_{1B}(s) = \frac{K_V \tau_c}{\tau_c s + 1} + K_A \tag{4-6}$$

where K_A provides for a lead compensator, if required.

The compensated signal $\ddot{x}_c$ is defined as

$$\ddot{x}_{ACCEL} - g \sin \theta = \ddot{x}_c \tag{4-7}$$

and

$$\ddot{x}_{ACCEL} = \dot{V} \cos \alpha + g \sin \theta \tag{4-8}$$

where $\dot{V}$ is true inertial acceleration along the velocity axis. A problem is often encountered because of imperfect cancellation of the pitch angle coupling term. The higher the complementary filter time constant τ_c, the higher the accelerometer loop gain. Any erroneous null signal including the imperfect measurement, scaling and subtraction of g sin θ can cause large errors in the airspeed control loop accuracy. Hence, in practice, a washout prefilter is often added to the $\ddot{x}_c$ filter. This filter produces a new signal $\ddot{x}_c'$ of the form

$$\ddot{x}_c' = \frac{\ddot{x}_c \tau_w}{\tau_w s + 1} \tag{4-9}$$

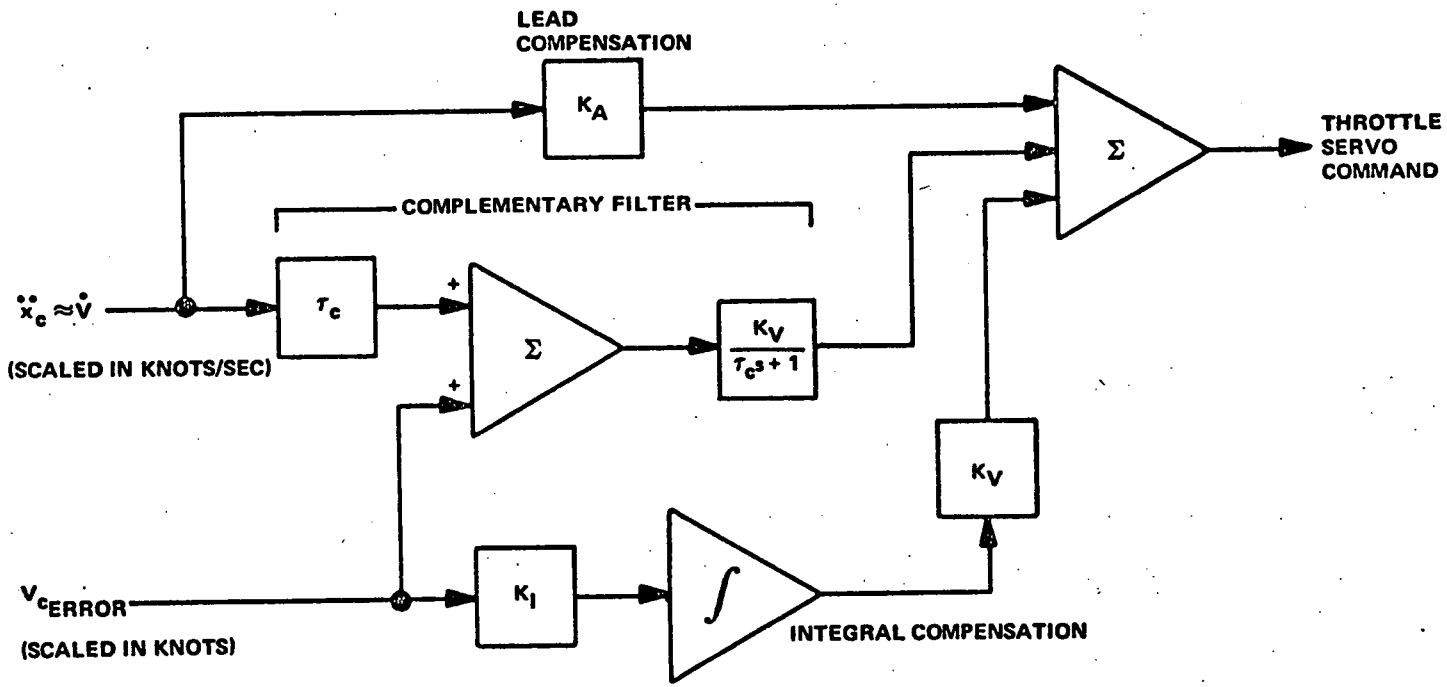

Figure 4-3
Block Diagram of Airspeed
Error Compensator

where τ_w is about 100 seconds. Since this is a problem encountered in actual aircraft installations but need not appear in simulator studies (unless one wishes to simulate instrument installation accuracies, etc.), there is no reason to include this filter in a study of control laws.

The elevator compensation control, $G_3(s)$ is

$$G_3(s) = \delta_E \left[\frac{\tau_7 s}{\tau_7 s + 1} \right] \left[\frac{1}{\tau_8 s + 1} \right] k_2 \qquad (4\text{-}10)$$

The washout is needed to remove steady state elevator deflections from the control signal. Time constants in the order of about 30 seconds are needed.

The pitch compensation $G_2(s)$ has a similar form as $G_3(s)$. If τ_8 above is sufficiently large, the elevator compensator actually provides the same speed change anticipation that would be obtained from the pitch signal. Both are shown for generality, but it is quite possible that only one would suffice. The θ or δ_E control inputs act as feedforward predictors that allow the throttle loop to begin correcting for an anticipated error. That is, the correction occurs before the error develops. In aircraft where the engine thrust change produces a pitching moment, the possiblity of coupling the pitch-to-throttle compensation and throttle-to-pitch compensation into a throttle-pitch instability exists. The filters on the compensation signals must be set for the proper phasing and attenuation that avoids this type of instability.

An important computational requirement for an autothrottle control law is the definition of the calibrated airspeed reference command, $V_{c_{REF}}$. Even if the speed reference is selected on a display device by the pilot, the effective command to the autothrottle system must be processed for inclusion of a rate constraint before being applied to the autothrottle control law. In general, a command rate limit, often referred to as the retard rate limit, should be about 1 knot per second. If the airspeed reference program is automated to follow the correct speed requirements as flaps are deployed, the actual value of $\dot{V}_c$ can be determined using the following procedure on a simulator:

- Hold throttles fixed.
- Deploy flaps at standard flap rates.
- Constrain flight path to desired trajectory (hold aircraft on glide path).

- Measure actual $\dot{V}$

- Use this value of $\dot{V}$ as $\dot{V}_{c_{REF}}$, and the final value of calibrated airspeed as the new $V_{c_{REF}}$.

- The V_c program will therefore be

$$V_{c_{REF}} = V_{c_o} + \dot{V}_{c_{REF}} t \tag{4-11}$$

until the desired final value is reached. The $V_{c_{REF}}$ is held at that final value.

The effect of this type of $V_{c_{REF}}$ programming is to allow the aircraft to decelerate in response to flap deployment without necessitating any throttle adjustments. In effect, the airspeed error is maintained zero by predicting the airspeed transient and using that transient as the reference airspeed.

The reference airspeed may be adjusted as a function of weight. A method that allows the correct reference speed to be determined for any aircraft weight uses an angle-of-attack outer loop on the $V_{c_{REF}}$ as follows

$$V_{c_{REF}} = V_{c_{REF_{NOMINAL}}} + k_\alpha \int \left(\alpha - \alpha_{REF}\right) \, dt \tag{4-12}$$

where α_{REF} is the desired or optimum angle of attack for the approach condition. The α_{REF} value must be adjusted as a function of flap position. A practical problem associated with this method involves the accurate measurement of α for various flap conditions.

3. Throttle-Thrust Scaling and Authority Limits

For simulation purposes, the suggested relationship between the throttle limits and thrust is illustrated in Figure 4-4. Note that this figure shows that full throttle quadrant can produce greater than 100 percent rated thrust. The 42-degree throttle limit is selected to provide 100 percent rated thrust under the most optimistic conditions favoring increased thrust (cold day, high barometric pressure). For nominal conditions, it is suggested that the 42-degree limit correspond to 90 percent full rated thrust. The 13-degree lower limit would then

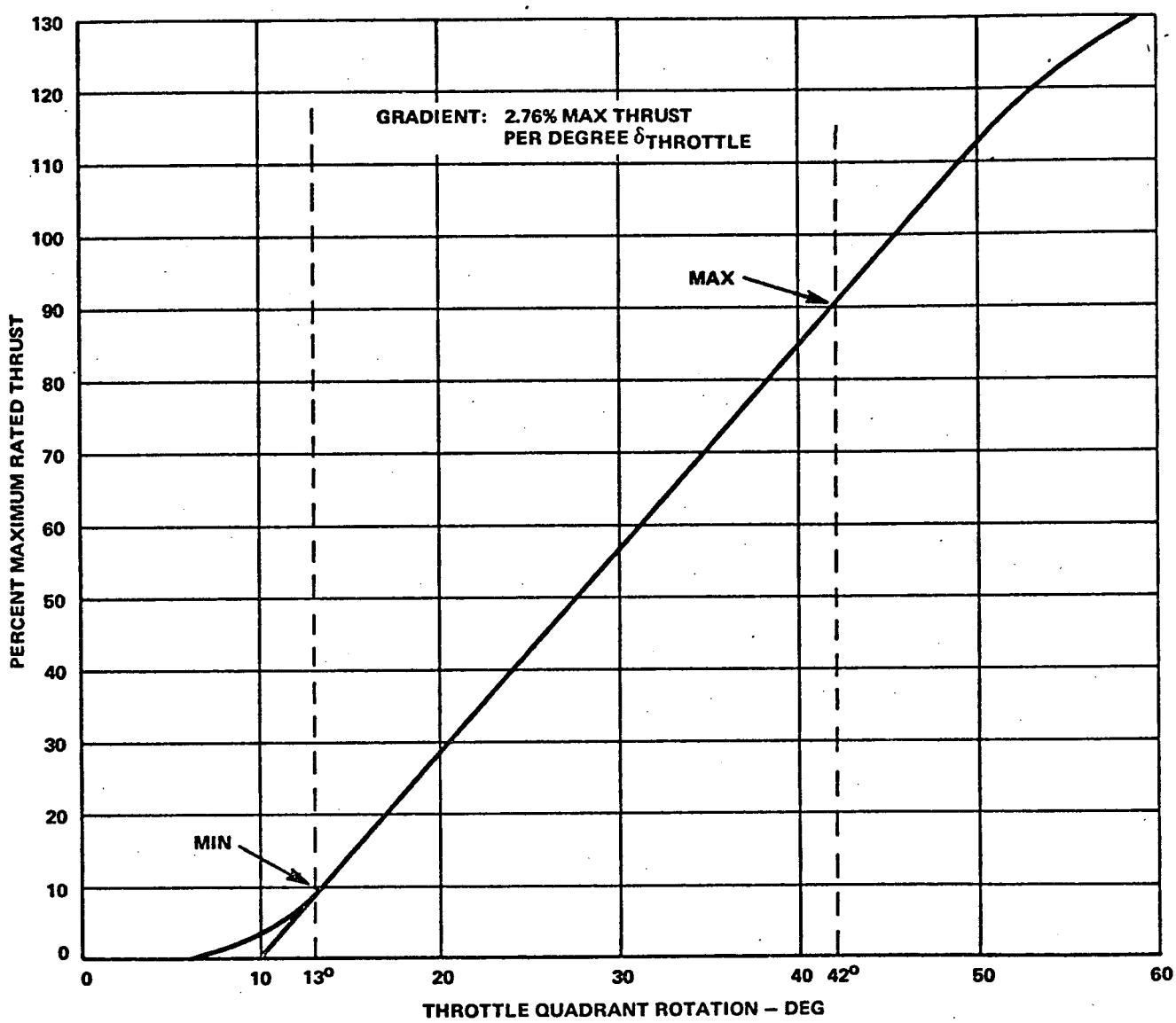

Figure 4-4
Autothrottle Servo Thrust Authority
Limits (Nominal Day)

correspond to about 10 percent full rated thrust. Note that for about the first ten degrees of throttle quadrant rotation, the thrust output is about zero; the engine output drives only the accessory loads.

4. Autothrottle Control Law Summary

In summary, the autothrottle control law is

$$-\delta_{T_c} = \left[V_{c_{ERROR}} + \tau_c \ddot{x}_c\right]\left[\frac{1}{\tau_c s + 1}\right]\left[1 + \frac{K_I}{s}\right] K_v$$

$$+k_A \ddot{x}_c + k_2 \delta_E \left[\frac{\tau_7 s}{\tau_7 s + 1}\right]\left[\frac{1}{\tau_8 s + 1}\right] + \delta_{TP} \qquad (4\text{-}13)$$

where $-k_2' \theta$ may be used in place of $k_2 \delta_E$.

The range of typical control law parameters is summarized on Table 4-1.

TABLE 4-1

AUTOTHROTTLE PARAMETER SUMMARY

Parameter	Typical Minimum Value	Typical Nominal Value	Typical Maximum Value	Remarks
ω_T	4 Rad/Sec	6 Rad/Sec	12 Rad/Sec	High bandwidth not important
L_2	4 Deg/Sec	8 Deg/Sec	12 Deg/Sec	Throttle rate limit - (degrees of throttle quadrant rotation)
L_3		13 Degrees above idle stop to 42 Degrees		Throttle limits
τ_c	2 Sec	4 Sec	8 Sec	Complementary filter
k_v	1.0 Deg δ_T per knot	3 Deg δ_T	6 Deg δ_T	Air speed error gain

TABLE 4-1 (cont)

AUTOTHROTTLE PARAMETER SUMMARY

Parameter	Typical Minimum Value	Typical Nominal Value	Typical Maximum Value	Remarks
k_I	0.025 Deg/Sec δ_T per knot	0.1 Deg/Sec δ_T per knot	0.25 Deg/Sec δ_T per knot	Airspeed integral gain
k_A	2 Deg δ_T per knot/sec	5 Deg δ_T per knot/sec	10 Deg δ_T per knot/sec	Acceleration compensation gain
k_2	1.0 Deg δ_T per deg δ_E	2 Deg δ_T per deg δ_E	5 Deg δ_T per deg δ_E	Elevator compensation
L_1	2.0 knot	5 Knots	10 Knots	Error limit
τ_W	30	100	150	If this washout is used, it should be disabled for large errors
τ_7	15	30	50	Elevator washout
τ_8	20	4	6.0	Compensation filter
$\dot{V}_{c_{REF}}$	0.75 Knots/Sec	1.0 Knots/Sec	2.0 Knots/Sec	Slew rate of calibrated airspeed reference (may also be computed for perfect compensation)

5. Autothrottle Control Response Criteria

a. Airspeed Transients

Because speed control uses a frequency-weighted combination of pressure references and inertial references, the dynamic response to speed changes depends upon the actual inertial and wind velocity. In general, the control law is designed to respond to inertial changes at high frequency and impact pressure changes in the lower frequency region. A step increase in calibrated airspeed because of a step input of forward wind will cause an aircraft inertial velocity deceleration. The inertial terms of the control law will then tend to increase throttles while the pressure terms will tend to retard them. Ideally, a wind pulse of about 0.5 second duration should cause no throttle response. A step increase in headwind should produce a response compatible with the final determination of the required equilibrium speed. If pitch attitude is constrained, a step increase in headwind will cause a positive normal acceleration with a resulting increase in flight path angle. With no throttle adjustment the aircraft will experience a deceleration until the original airspeed equilibrium is restored. An autothrottle system will retard throttles initially, permitting a faster restoration of the original airspeed. The throttles will then return to their original value. If flight path angle with respect to a ground reference is constrained, then changes in the equilibrium throttle position will be required. Consider descent on a 3-degree glide path, for example. A step increase in headwind will cause a deceleration with respect to the ground track. In order to maintain the aircraft's position on the glide path an increased angle of attack is needed. If the aircraft is on the stable side of the thrust required curve, it can continue on the original glide path but at a lower airspeed. If airspeed is to be maintained, the throttles must be advanced. The autothrottle system should provide that advance with a minimum of initial retard activity trying to cope with the initial airspeed increase. The complementary filter blend of inertial acceleration and airspeed helps achieve this desired response.

The dynamic coupling between the longitudinal stabilization modes and the throttle control loops is always significant. Ultimately, the best response criteria are those which result in the tightest flight path control. However, for initial throttle loop adjustment, the following transient response criteria are suggested.

Input	Response Criteria
• 0.5 second step wind pulse	• Minimum throttle activity
• Step 5 knot speed change (pitch attitude constrained via maximum gain pitch autopilot)	• Minimum forward throttle transient. • Airspeed error reduced by 90 percent in 8 seconds. • Maximum 10 percent speed overshoot (0.5 knots).
• Apply 5.0 knot speed reference change in the form of a 1.0 knot/second ramp command	• Airspeed error should never exceed 1.5 knots. • Speed overshoot should not exceed 0.5 knots. • Final value within 0.25 knots should be attained within 8 seconds of ramp command completion. Error should be within 0.5 knots after 4 seconds of ramp completion.

B. DIGITAL PROGRAM - AUTOTHROTTLE CONTROL

1. Control Law Conversion

The representation of the autothrottle block diagrams and control laws in FORTRAN notation is summarized in Figure 4-5 and the FORTRAN namelist is given in Table 4-2. Note that in the system configuration shown in Figure 4-5, the pitch compensation loop rather than the elevator compensation loop is used. As discussed previously these two loops may usually be used interchangeably (with appropriate gains). Also noted on Figure 4-5 is the absence of a feedforward throttle predictive input. The predictive input could be used advantageously for improving command response but it will have no bearing on the disturbance response.

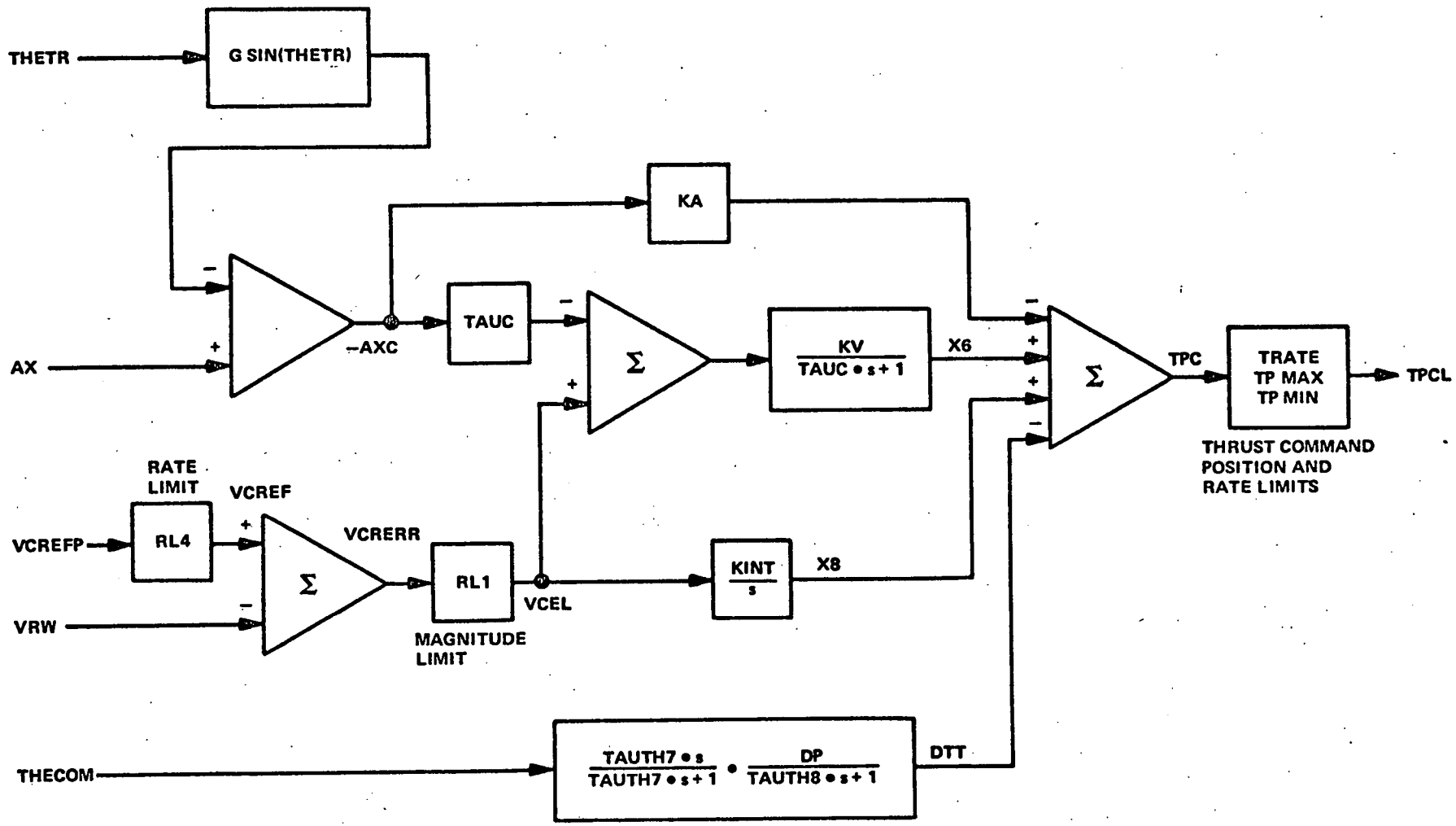

Figure 4-5
Autothrottle Block Diagram with
Fortran Notation

TABLE 4-2

AUTOTHROTTLE NAMELIST

Name	FORTRAN Name	Definition
$\ddot{x}_{ACCEL}$	AXB	Body axis longitudinal accelerometer output.
V	VRW	Aircraft airspeed.
V_{cREF}'	VCREFP	Airspeed reference command.
$\dot{V}_{cREF}$	RL4 (UTH4)	Slew rate of airspeed reference command.
L_1	RL1 (UTH1)	Airspeed error magnitude limit.
L_2'	TRATE (UTHR)	Thrust command rate limit.
L_3'	TPMIN	Thrust command position limit.
L_4'	TPMAX	Thrust command position limit.
$\ddot{x}_c$	AXC	Compensated body axis longitudinal accelerometer output.
θ_c	THECOM	Pitch angle command.
-	STHET	Sine of pitch angle command.
-	TPCTR	Trim thrust value in percent.
-	TPCL	Position and rate limited total thrust command in percent.
-	TPC1,2,3,4	Individual engine thrust commands in percent.
-	DTMAX	Percent thrust change per degree throttle change.
-	ITESTT	Logic variable for synchronizing autothrottle at engagement.
K_a	KA	Longitudinal acceleration feedback gain.
K_v	KV	Airspeed error feedback gain.
$K_v \cdot K_I$	KINT (KV·KI)	Integral error feedback gain.
τ_c	TAUC	Time constant for complementary airspeed filter.
K_2	DP (UDP)	Feed-forward pitch compensation gain.

TABLE 4-2 (cont)

AUTOTHROTTLE NAMELIST

Name	FORTRAN Name	Definition
τ_7	TAUTH7	Pitch compensation filter time constant.
τ_8	TAUTH8	Pitch compensation filter time constant.
	DT3	Subroutine sample time interval.

2. Program Flow Chart

The initial condition computations which are performed in the SASIC subroutine (See Appendix A) for the autothrottle mode is given in the following summary. The flow charts are shown in Figure 4-6.

Autothrottle I.C. Calculations

a. Set Engine Thrust Commands to Trim Value

```
TPC1 = TPCTR
TPC2 = TPCTR
TPC3 = TPCTR
TPC4 = TPCTR
```

b. Convert Gains and Limits to Proper Units

```
RL1   = UTH1 *1,688
RL4   = UTH4 *1,688 *DT3
DP    = UDP/DTMAX
KA    = UKA/DTMAX/1.688
KV    = UKV/DTMAX/1.688
TRATE = UTHR/DTMAX *DT3
```

c. Airspeed Error Integrator Gain

```
KINT = KI*KV*DT3
```

d. Pitch Compensation Filter Difference Equation Coefficients

```
C1 = EXP(-DT3/TAUTH7) + EXP(-DT3/TAUTH8)
C2 = EXP(-DT3*(1.0/TAUTH7 + 1.0/TAUTH8))
D1 = DP/TAUTH8/(1.0/TAUTH8 - 1.0/TAUTH7)
     *(EXP(-DT3/TAUTH7) - EXP(-DT3/TAUTH8))
```

e. Complementary Airspeed Filter Difference Equation Coefficients

C = EXP(-DT3/TAUC)

D = KV*(1.0-C)

The autothrottle parameter test values selected for best performance are:

UDP	2.5	Deg Throttle/Deg Theta
UKA	4.08	Deg Throttle/Knot/Sec
UKV	6.0	Deg Throttle/Knot
KI	0.05	Dimensionless
UTH1	5.0	Knots
UTH4	1.0	Knots/Sec
DTMAX	36.2	Deg Throttle/% Max Thrust
UTHR	8.0	Deg/Sec
TAUTH7	30.0	Seconds
TAUTH8	2.0	Seconds
TAUC	4.0	Seconds

C. SIMULATION TEST RESULTS - AUTOTHROTTLE

Figures 4-7 and 4-8 summarize the autothrottle transient responses for approach and cruise speeds achieved with the control law parameters listed in paragraph B.2 above. At both speeds, the 5-knot step headwind response shows a small overshoot of about 10 percent maximum. This is within the specified criteria but it could have been improved with a higher gain (degrees throttle per knot) and switching logic on the integration function. The higher autothrottle loop gain would tend to move the response characteristics into the range where excessive throttle activity occurs. Logic switching of the integrator involves holding the integral gain at zero until an error plus error rate criterion is satisfied. With such a technique the integrator would not have started until the speed returned to about 240 ft/second in Figure 4-7 or 502 ft/second in Figure 4-8.

The 0.5-second pulse response illustrates the effect of the complementary filter in minimizing throttle activity although it obviously has not done the job completely. The effectiveness can be demonstrated with a simple calculation. The error is 5 knots for 0.5 second. Without the complementary filter

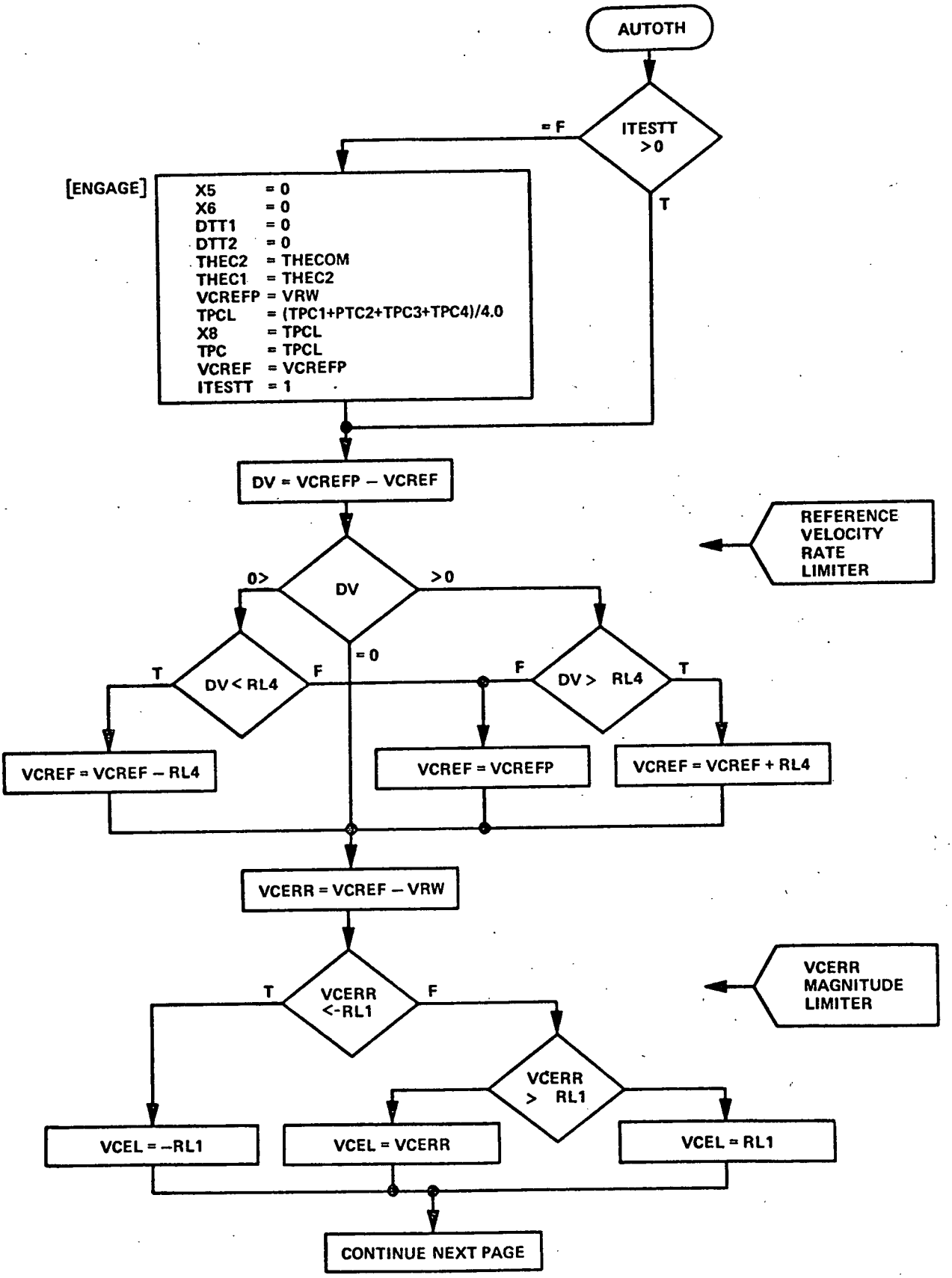

Figure 4-6a
Autothrottle Flow Chart

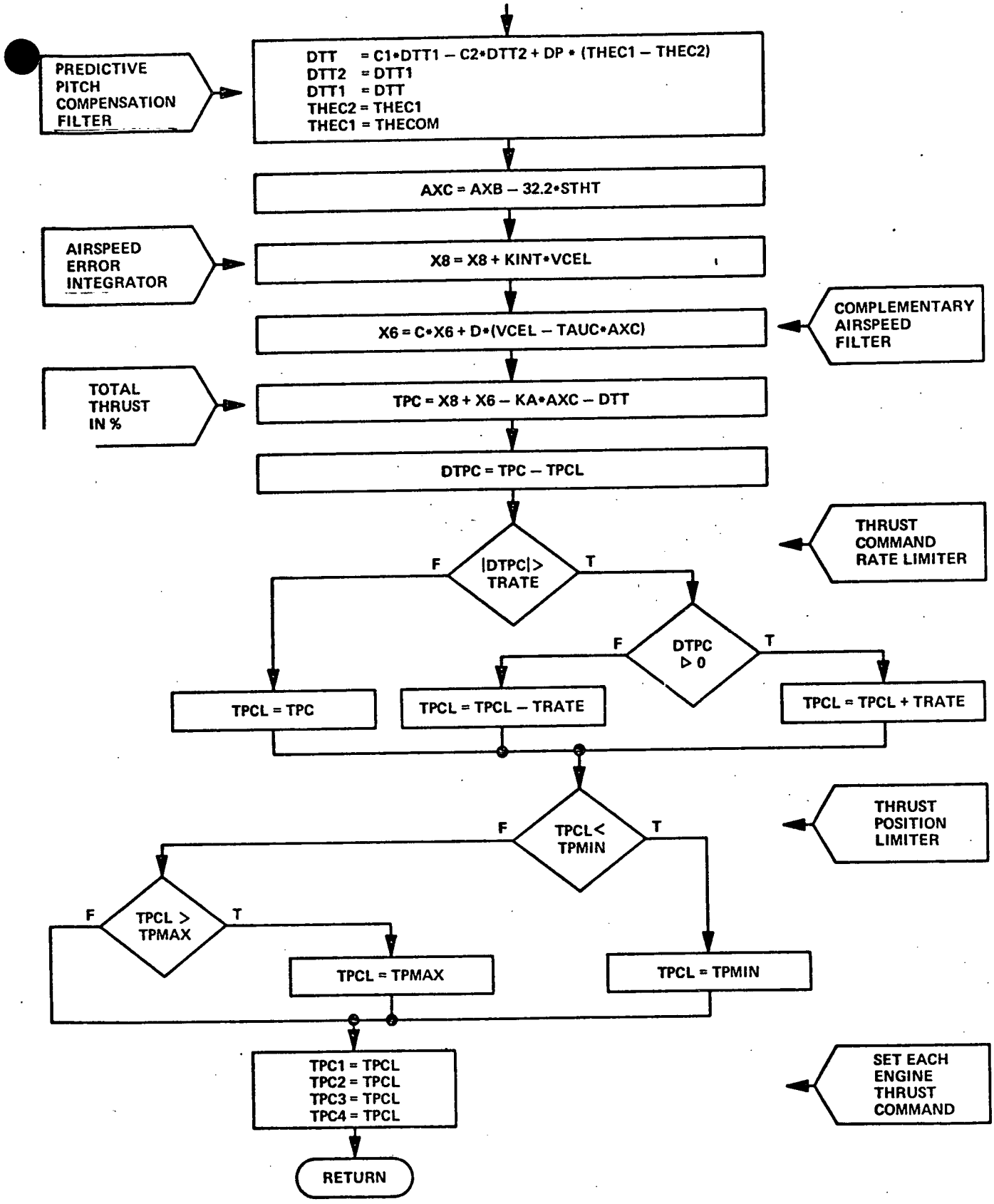

Figure 4-6b
Autothrottle Flow Chart (cont)

the throttle retard rate would have been 8 degrees per second (neglecting throttle servo dynamics). With a thrust gradient of 2.76 percent full thrust command per degree of throttle, the commanded thrust change in 0.5 second would have been 11 percent. As shown in the response, the blend of inertial and air data results in a significant attenuation of this throttle activity. A high time constant on the complementary filter would result in greater throttle motion attenuation but at the expense of excessive stretching of the recovery time to a step wind change.

The airspeed command responses shown on the third set of traces in Figures 4-7 and 4-8 do not meet the desired response time criteria but this can easily be remedied with the use of a feedforward compensator. The responses obtained in the simulation tests depended entirely on the closed loop system. Thus, an airspeed error had to exist before throttle movement is initialed. Also, the acceleration loops, both in the complementary filter and in the damping loop (KA), oppose the build-up of the corrective throttle. The use of a predictive feed-forward compensator would eliminate this problem by providing the throttle change needed to yield the 1.0 knot/second change in airspeed reference plus the Δ throttle needed to bias the acceleration loop (4.08 degrees of throttle per knot/second). It is also noted that the use of the switching logic on the integral loop, as discussed previously, would help eliminate the small overshoot and the long tail in the convergence to the reference airspeed.

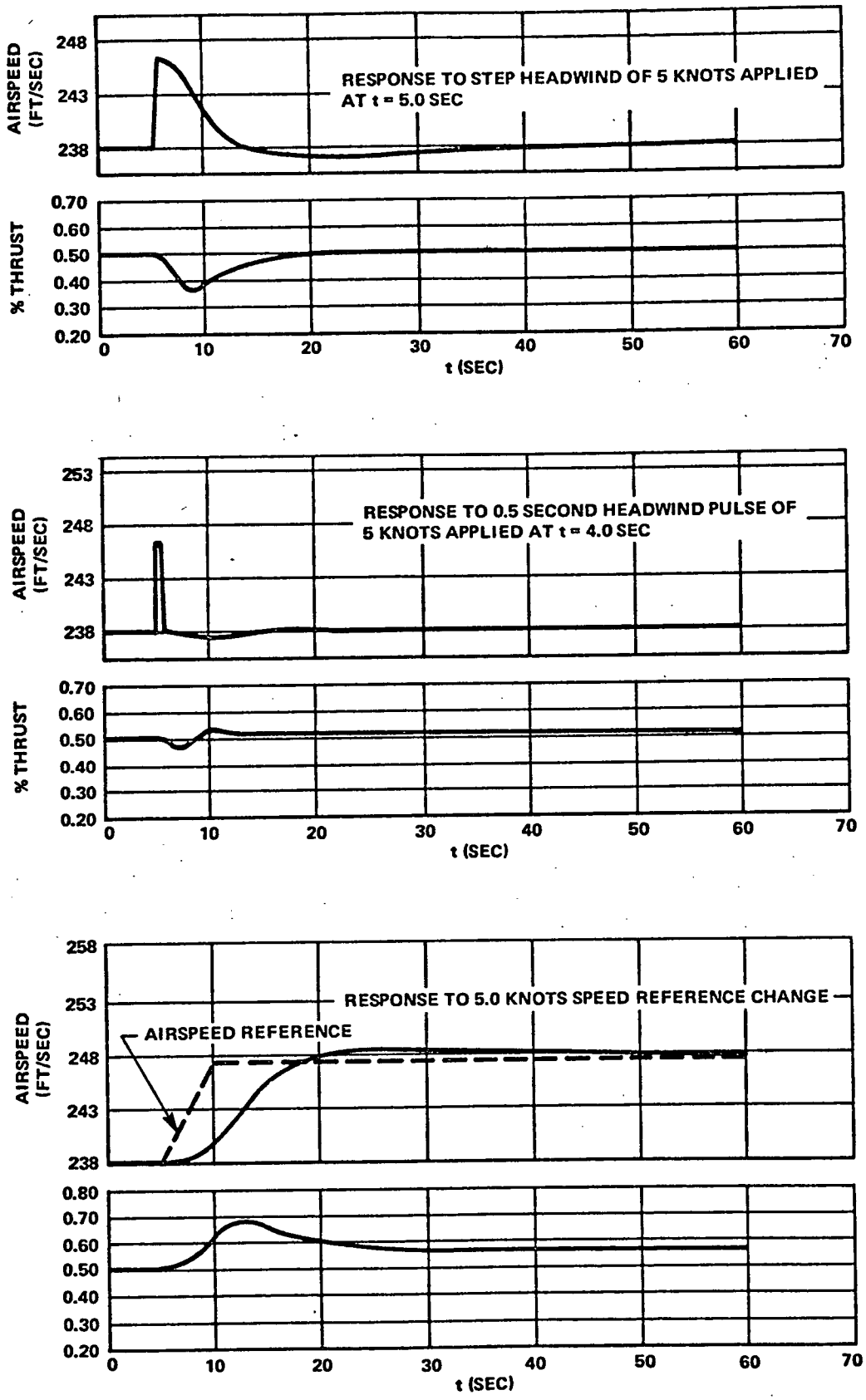

Figure 4-7
Autothrottle Tests (Landing Approach Speed)

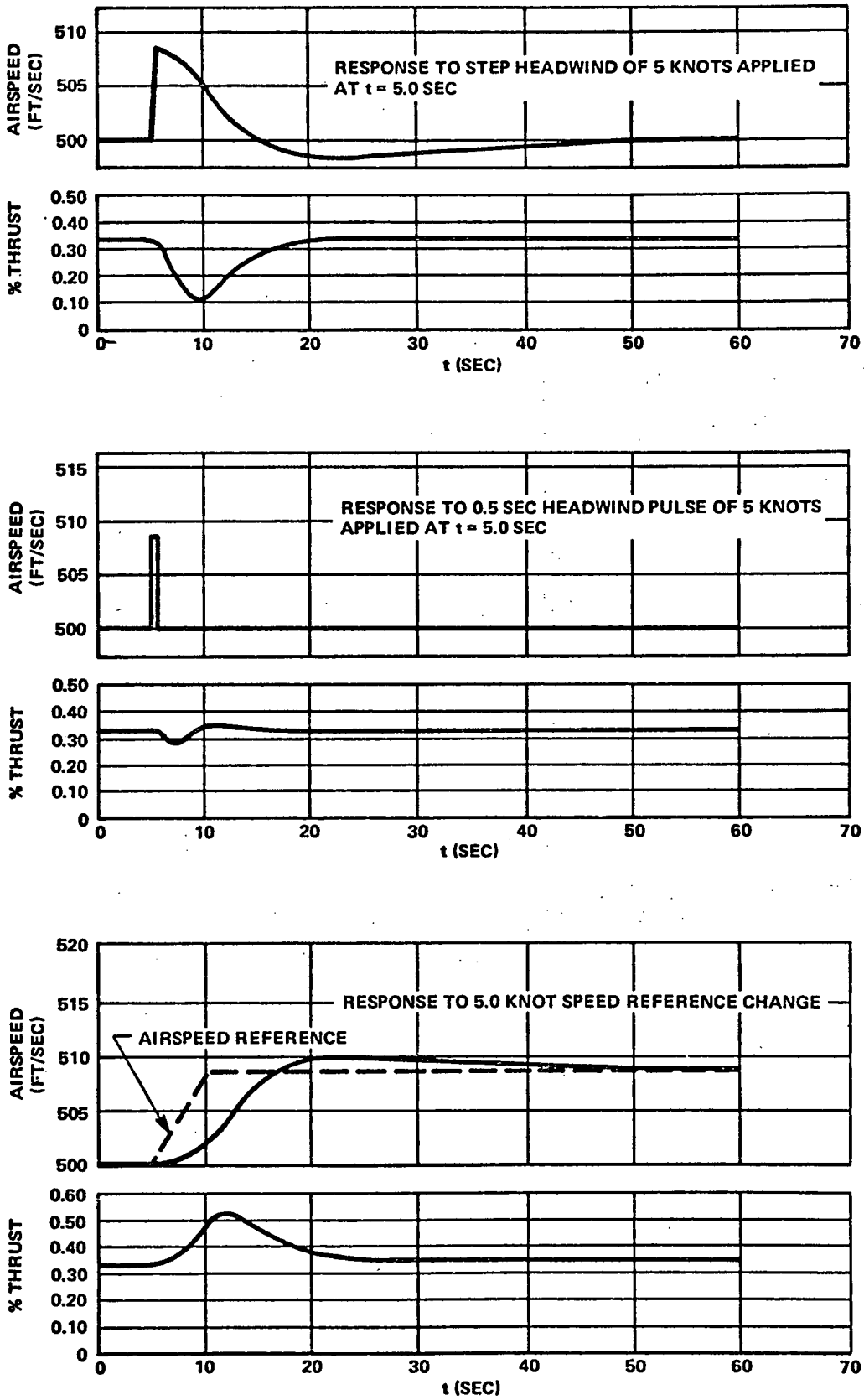

Figure 4-8
Autothrottle Tests (Cruise Speed)

SECTION V

VERTICAL FLIGHT PATH GUIDANCE LAWS (NONLANDING)

A. DESCRIPTION OF CONTROL LAWS

1. General

The vertical guidance functions covered in this section relate to the flight path steering commands associated with climb and descent, and the acquisition and holding of constant altitude. Not covered herein are the final approach glide path descents or cruise modes based on airspeed and Mach control.

Vertical guidance laws are represented as pitch steering commands into the autopilot pitch stabilization inner loop. Figure 5-1 shows how the series of pitch command outputs of specific modes are transmitted through a synchronizing function and summed with incremental pitch attitude to create the pitch error signal of the pitch stabilization loop. The synchronization function causes the last value of pitch command to be held as the initial value for a new control mode during mode transitions. (Note that the polarity of the summation of pitch command and pitch attitude is positive. See the discussion in Section II for the explanation of this polarity.)

In general, the performance of the vertical guidance modes is dependent upon good forward speed control. This may be achieved through the use of the automatic throttle control system.

2. Vertical Speed Control

a. Control Laws

Vertical speed control is accomplished with two submodes: Vertical Speed Hold and Vertical Speed Command. Both submodes are represented by the block diagram on Figure 5-2. The basic vertical speed control law is:

$$\theta_c = \dot{h}_{error} \left[1 + \frac{a_1}{s} \right] k_{\dot{h}} + \theta_{c_p} \qquad (5\text{-}1)$$

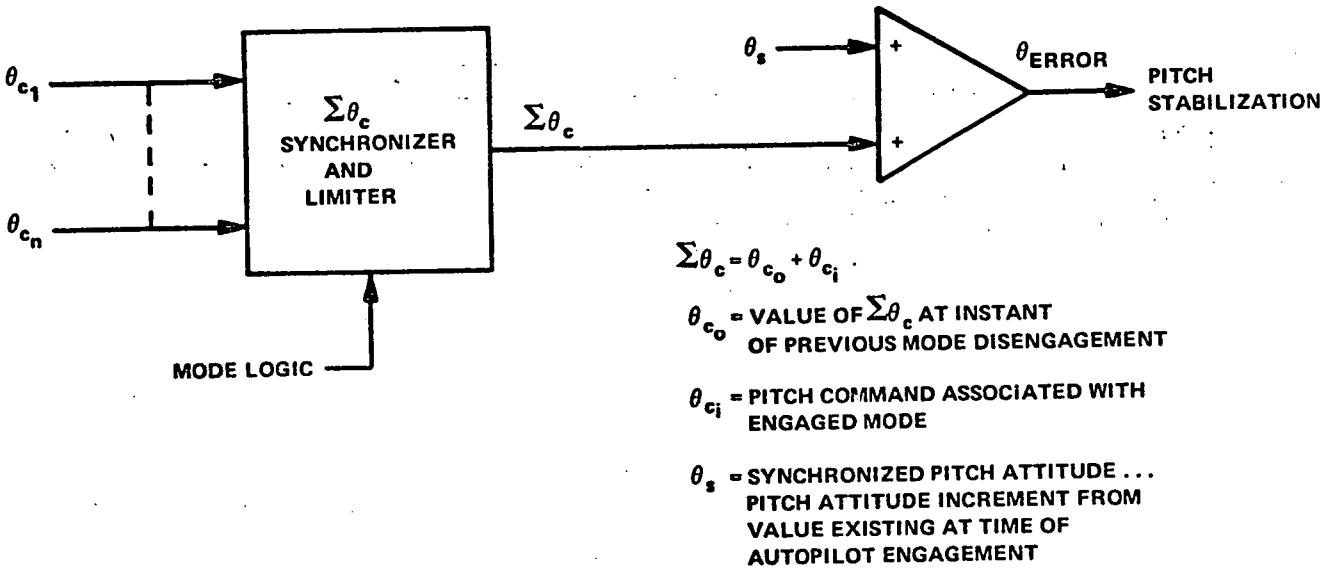

Figure 5-1
Pitch Guidance Function Engage Synchronization

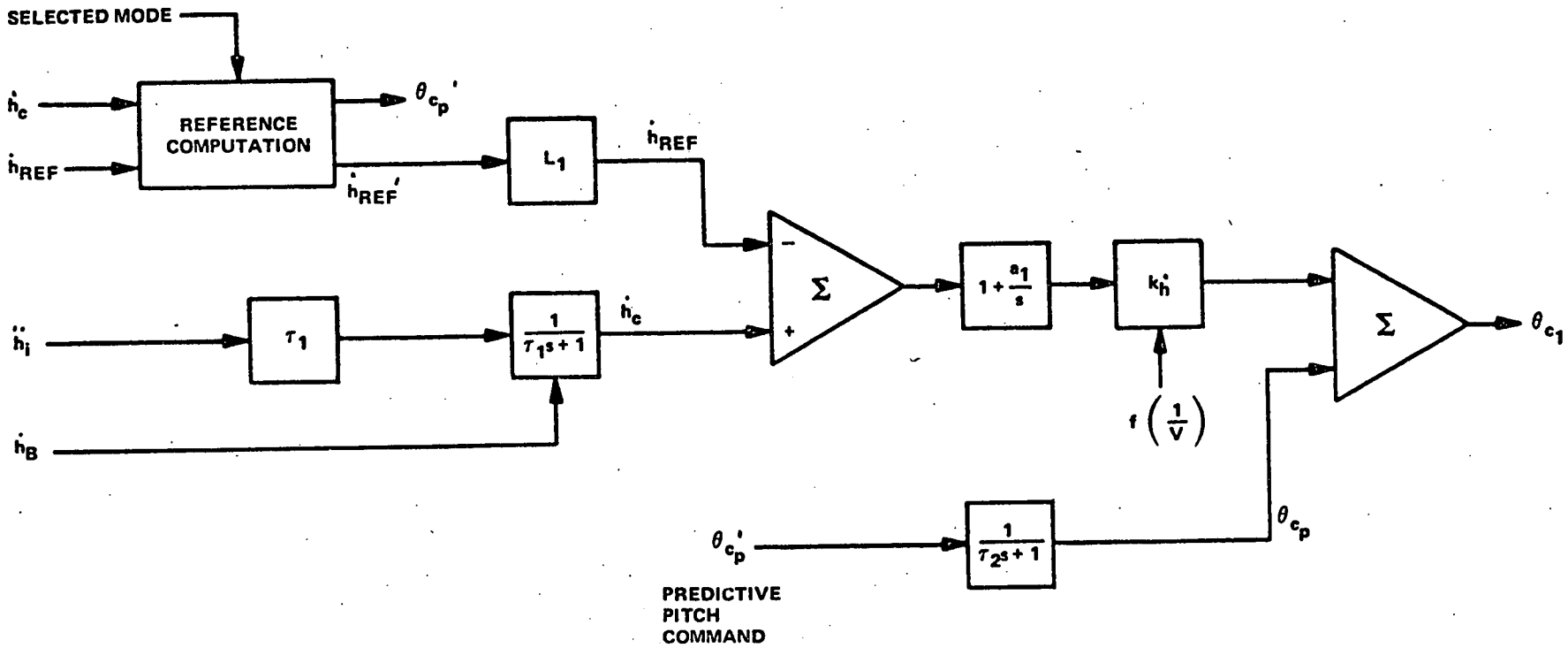

Figure 5-2
Vertical Speed Control Block Diagram

where

$$\dot{h}_{error} = \left[\dot{h}_c - \dot{h}_{ref}\right] \tag{5-2}$$

$\dot{h}_c$ = compensated vertical speed

$$= \frac{\ddot{h}_i \tau_1 + \dot{h}_B}{\tau_1 s + 1} \tag{5-3}$$

$\dot{h}_{ref}$ = reference vertical speed

$\ddot{h}_i$ = inertial vertical acceleration

$\dot{h}_B$ = barometric vertical velocity

θ_{c_P} = predictive pitch command ... based on mode sequencing and recognition of changes in $\dot{h}_{ref}$

The gain $k_{\dot{h}}$ should be made a function of velocity with the following characteristic:

$$k_{\dot{h}} = \frac{V_o}{V} k_{\dot{h}_{nominal}} = \frac{200}{V} k_{\dot{h}_{nominal}} \tag{5-4}$$

for $V > V_o$ or $V > 200$ ft/sec

$$k_{\dot{h}} = k_{\dot{h}_{nominal}} \tag{5-5}$$

for $V < 200$ ft/sec

Note that in many practical mechanizations, continuous gain programs on $k_{\dot{h}}$ are not used. The gain is switched at two or three discrete velocity (or Mach number) points to achieve an approximate gain program that permits reasonable stability and performance.

b. Vertical Speed Reference

For the hold mode, $\dot{h}_{ref}$ is synchronized to the existing $\dot{h}$ (using $\dot{h}_c$) prior to vertical speed hold engage. Thus,

$$\dot{h}_{ref_o} = \dot{h}_c \text{ at } t = t_o \tag{5-6}$$

where

t_o = time of vertical speed hold engage

For the vertical speed command mode, the vertical speed reference is established as a numerical input to the autopilot via a Mode Control Panel. In that case,

$$\dot{h}_{ref} = [L]\,\dot{h}'_{ref} \tag{5-7}$$

where [L] represents a limiting function based on an acceleration constraint and $\dot{h}'_{ref}$ is the numerical input value of desired vertical speed. The limit L provides the following function:

$$\dot{h}_{ref} = \dot{h}_{ref_o} + \left[\text{sign}\,(\dot{h}'_{ref} - \dot{h}_{ref})\right] \left|\ddot{h}_{max}\right| (t - t_o)$$

$$\text{for } \left|\dot{h}'_{ref}\right| > \left|\dot{h}_{ref}\right| \tag{5-8}$$

where $\left|\ddot{h}_{max}\right|$ represents the maneuvering acceleration constraint in feet/sec^2, $(t - t_o)$ represents the time from the entry of the new $\dot{h}$ reference, and $\dot{h}_{ref_o}$ is the initial value of the $\dot{h}$ reference.

For $\dot{h}_{ref} = \dot{h}'_{ref}$, the ramp function described by equation (5-8) is terminated and the $\dot{h}$ reference is clamped at the desired value until a new reference is entered at the Mode Control Panel. When programmed in a digital autopilot, equation (5-8) is implemented as:

$$\dot{h}_{ref_n} = \dot{h}_{ref_{n-1}} + \left[\text{sign}\left(\dot{h}'_{ref} - \dot{h}_{ref_{n-1}}\right)\right] \left|\ddot{h}_{max}\right| \Delta T \tag{5-9}$$

where ΔT is the computation cycle time.

A typical value for $\ddot{h}_{max}$ = 0.07g's = 2.25 ft/sec^2.

c. Predictive Pitch Commands

To minimize the $\dot{h}$ error when the $\dot{h}$ reference is changed, a feed-forward (or predictive) pitch command θ_{c_p} is added to the $\dot{h}$ control law. A good approximation of the required angle-of-attack increment that will yield the $\ddot{h}_{max}$ associated with the ramp change in $\dot{h}_{ref}$ can be computed from the following equations:

$$C_{L_\alpha} QS\,\Delta\alpha + C_{L_{\delta_E}} QS\,\Delta\delta_E = \frac{W}{g}\ddot{h} \tag{5-10}$$

$$C_{m_\alpha}\Delta\alpha + C_{m_{\delta_E}}\Delta\delta_E = 0 \tag{5-11}$$

Substituting (11) into (10) yields

$$\Delta\alpha = \left[\frac{W}{QS}\right]\left[\frac{1}{\left(C_{L_\alpha} - C_{L_{\delta_E}}\dfrac{C_{m_\alpha}}{C_{m_{\delta_E}}}\right)}\right]\frac{\ddot{h}}{g} \tag{5-12}$$

Using approximate values for C_{L_α}, $C_{L_{\delta_E}}$, C_{m_α}, and $C_{m_{\delta_E}}$ can yield a reasonable estimate of the aerodynamic coefficient part of equation (5-12). The main variables that will change over the different flight conditions will be weight, W, and dynamic pressure, Q, although there is also a variation in the aerodynamic terms. The predictive pitch term must include the $\Delta\alpha$ of equation (5-12), plus the flight path angle change associated with the acceleration maneuver.

For $\left|\dot{h}'_{ref} - \dot{h}_{ref}\right| > 2$ ft/sec

$$\theta'_{c_P} = \theta'_{c_{P_\alpha}} + \theta'_{c_{P_\gamma}} \tag{5-13a}$$

or

$$\theta'_{c_{P_\gamma}} = \int\left(\frac{\ddot{h}}{V}\max\right)dt \tag{5-13b}$$

$$\theta'_{c_{P_\alpha}} = \frac{W}{Q}(C)\left|\frac{\ddot{h}_{max}}{g}\right|\left[\text{sign}\left(\dot{h}'_{ref} - \dot{h}_{ref}\right)\right] \tag{5-13c}$$

where

$$C = \frac{1}{S}\left(\frac{1}{C_{L_\alpha} - C_{L_{\delta_E}}\dfrac{C_{m_\alpha}}{C_{m_{\delta_E}}}}\right) \tag{5-14}$$

and the control input is

$$\theta_{c_P} = \theta'_{c_P}\left(\frac{1}{\tau_2 s + 1}\right) = \left(\theta'_{c_{P_\alpha}} + \theta'_{c_{P_\gamma}}\right)\left(\frac{1}{\tau_2 s + 1}\right) \tag{5-15}$$

For

$$\left|\dot{h}'_{ref} - \dot{h}_{ref}\right| \leqslant 2 \text{ ft/sec}$$

$$\theta'_{c_{P_\alpha}} = 0$$

The significance of bounding the range of $\dot{h}_{ref}$ errors for which the predictive feedforward correction is made is the recognition that equations (5-13) and (5-14) are approximations. Hence, as the maneuver approaches terminal conditions, the predictive or open-loop command is removed and the closed-loop control takes over the entire task of error correction.

3. Altitude Preselect and Capture

a. General

Preselect altitudes are entered at a Mode Control Panel. When the altitude preselect mode is engaged, the autopilot is armed to automatically capture the reference altitude. The vertical steering mode that directs the aircraft toward the preselected reference altitude may then be selected by the pilot. The aircraft is not automatically maneuvered to a descent or climb toward the target. The pilot must select the manner in which the preselected altitude will be approached. With the altitude preselect mode engaged, the autopilot will automatically sense the approach to the preselected altitude and initiate an altitude capture maneuver.

The computational requirements for the altitude preselect mode involve four programs. They are:

- Compute Capture Initiate Altitude
- Capture Phase (A) Control Law Computation (Vertical Speed Command)
- Capture Phase (B) Control Law Computations (Exponential Flare)
- Capture Phase (C) Altitude Hold Computation

b. Altitude Capture Computations and Control Laws

Phase A - Initial Capture Maneuver

In order to acquire the reference altitude without exceeding an acceleration limit, the capture maneuver must be started at a distance from the desired altitude that is proportional to the square of the vertical speed. For a fixed vertical acceleration maneuver representing the maximum acceleration constraint, $\ddot{h}_{max}$, the maneuver must be initiated at an altitude displacement Δh from the reference given by:

$$\left|\Delta h\right| = \left|\frac{\dot{h}_o^{\,2}}{2\ddot{h}_{max}}\right| \tag{5-16}$$

If we make provision for the response time required to achieve the maximum $\ddot{h}$ and recognize that the final flare into the reference altitude involves accelerations below $\ddot{h}_{max}$, then Δh should be biased on the high side by assuming an actual value of $\ddot{h}_{max}$ about 10 percent below the specified maximum. A reasonable value of $\ddot{h}_{max}$ is 0.07g's = 2.25 ft/sec^2. A 10-percent reduction in this value for the Δh calculation would result in 0.063g's = 1.84 ft/sec^2. Thus, a 6000-ft/min (100 ft/sec) climb toward a preselected altitude will require capture initiation at

$$\Delta h = \frac{100^2}{2(1.84)} = 2720 \text{ feet}$$

if we seek a 0.07g = 2.25 ft/sec^2 maximum maneuver constraint.

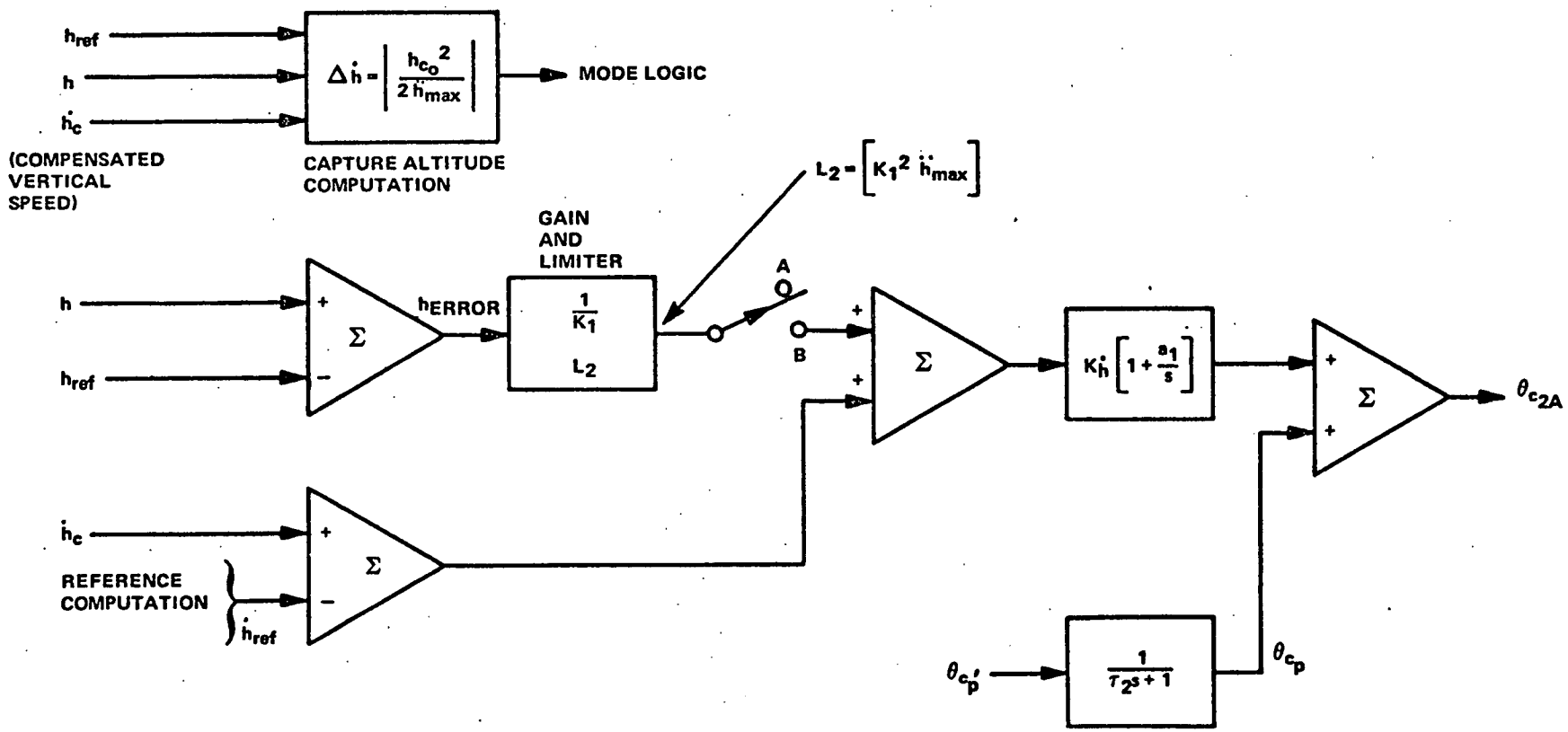

Figure 5-3
Phase A, B, Altitude Capture
Block Diagram

The first phase of the capture maneuver, designated Phase (A), occurs when the altitude error, h_e, is defined by

$$\left|\Delta h\right| \geqslant \left|h_e\right| > \left|k_1 \dot{h}\right| \tag{5-17}$$

where k_1 is a control law gain defined below. Note that this phase is required only when very large initial vertical speeds are involved. The pitch command control equation for this phase is:

$$\theta_{c_{2A}} = \left(\dot{h}_{error}\right)\left(1 + \frac{a_1}{s}\right) k_{\dot{h}} + \theta_{c_p} \tag{5-18}$$

This is seen to be the same equation as the vertical speed control law. Note also that the $\dot{h}_{error}$ signal is synthesized exactly as in equations (5-2) and (5-8). The Phase A altitude capture mode is actually a vertical speed command mode defined by:

- Equation (5-18) - Basic Control Law
- Equations (5-16), (5-17) - Initiation and Duration of Phase A
- Equation (5-8) - Programming of $\dot{h}_{ref}$ (with desired value = 0)
- Equations (5-13), (5-14), (5-15) - Computation of Predictive Pitch Command

Figure 5-3 is the block diagram illustrating the altitude capture sequence.

Phase B - Capture Flare Maneuver

The transition to Phase B should occur when h_e on Figure 5-3 comes out of limiting. At that time, the integral gain a_1 is reduced to zero and the α component of the predictive pitch command is decayed to zero through the time constant τ_2. The transition criteria for Phase B are illustrated in Figure 5-4. This is a phase plane of h and $\dot{h}$. During Phase A, we follow the constant $\ddot{h}$ trajectory. If we started the $\ddot{h}$ maneuver at the precise altitude and maintained the precise value of $\ddot{h}_{max}$, the acceleration trajectory would intersect the origin. The intersection of the acceleration trajectory with the $h + k_1\dot{h}$ switching boundary corresponds to the point at which h_e comes out of limiting (for the ideal) acceleration trajectory. When the state of the aircraft intersects (below the switching boundary), it corresponds to the case where the $h_e + k_1\dot{h}$ control law required lower

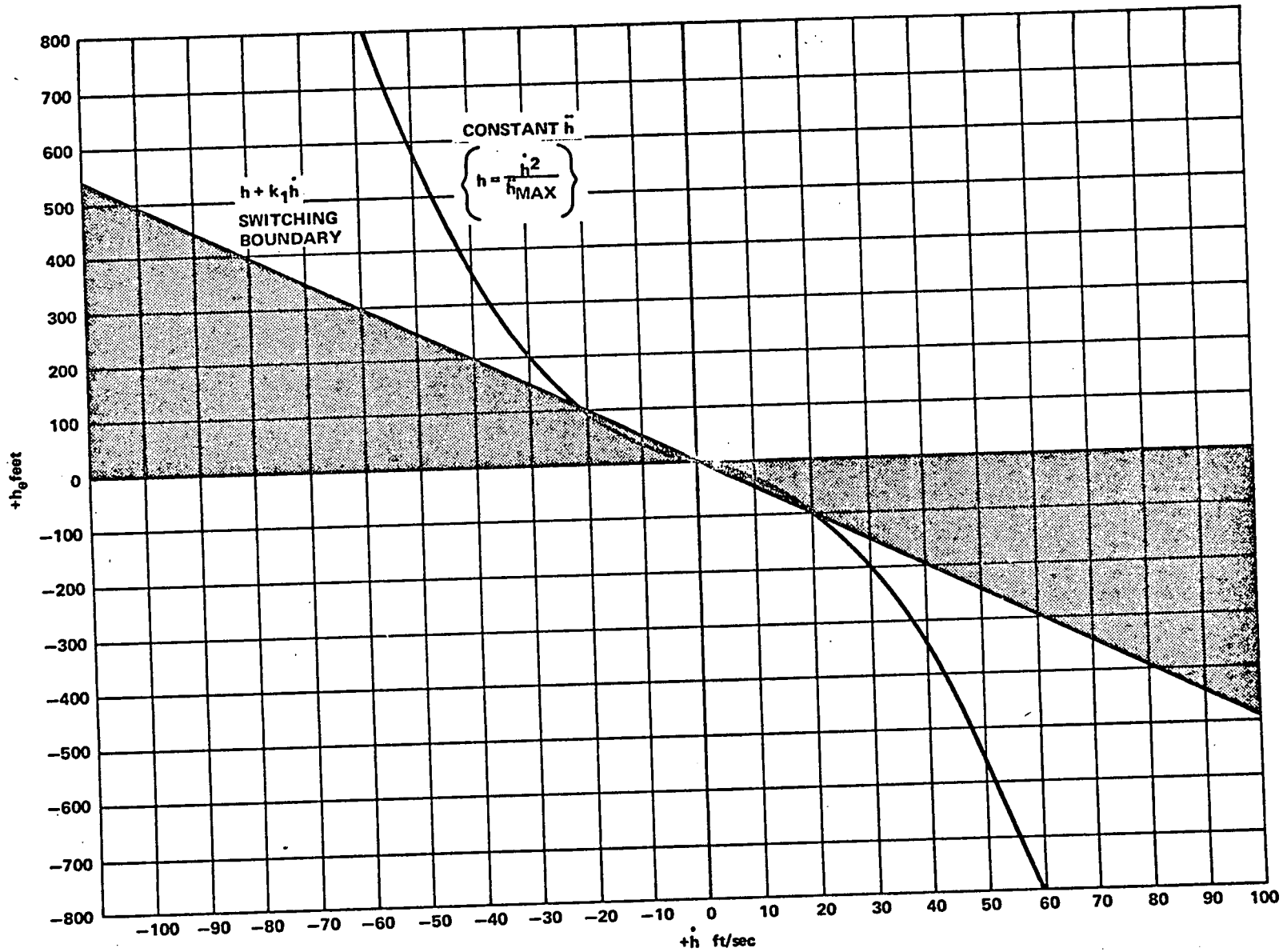

Figure 5-4
Transition from Phase A Altitude Capture
Maneuver to Phase B Altitude Capture Control Law

accelerations to reach the final state than $\ddot{h}_{max}$. The Phase B control law is initiated when the switching boundary is reached. The control law is:

$$\theta_{c_{2B}} = \left(\frac{h_e}{k_1} + \dot{h}_{error}\right) k_{\dot{h}} + \frac{\theta'_{c_p}}{\tau_2 s + 1} = \left(h_e + k_1\dot{h}\right)\left(\frac{k_{\dot{h}}}{k_1}\right) + \frac{\theta'_{c_p}}{\tau_2 s + 1} \qquad (5\text{-}19)$$

where $\theta'_{c_{P_\alpha}}$ is stepped to zero at the time of transition to Phase B while $\theta_{c_{P_\alpha}}$ is retained in θ'_{c_P}. During Phase B, the instantaneous value of $\dot{h}_{ref}$ continues to decay toward zero at the maximum acceleration constraint rate. If altitude capture is initiated from relatively low vertical speeds, then Phase A will never occur and the initial capture phase will be Phase B.

An additional criterion must be added to allow switching from the Phase A to Phase B control mode. If the acceleration maneuver is too large or started too soon, then $\dot{h} = 0$ will be reached before the terminal altitude is reached. Thus, a minimum vertical velocity criterion must be added to allow initiation of Phase B control. A reasonable value is 2 ft/sec. Thus, the Phase B transition logic is:

PB = Phase B Mode Engage

SB = Switching Boundary (Figure 5-4) has been Penetrated

HDOTMIN = $|\dot{h}| \leqslant 2$ ft/sec

HMIN = $|h_e| \geqslant 25$ ft

PB = SB · HMIN + HDOTMIN · HMIN

Note that for $|h_e| < 25$ ft, Phase C, altitude hold is initiated as described below.

It is noted that the seemingly complex computations associated with altitude capture are primarily the result of the need to constrain accelerations to acceptable values for passenger comfort. An alternative to the Phase A control law [equation (5-18)] is to start immediately with Phase B [equation (5-19)],

but to constrain $\theta_{c_{2B}}$, the total pitch command, so that the g limits are not exceeded. Thus,

$$\dot{\theta}_{c_{2B}\,max} \approx \frac{2.25 \times 57.3}{V} \tag{5-19a}$$

where 2.25 ft/sec^2 = 0.07g;s is the g constraint.

Another alternative which permits the elimination of the Phase A control law is to continuously compute the instantaneous altitude reference on the basis of the integration of the vertical speed reference. Thus, h_e in equation (5-19) is defined as

$$h_e = h - h_{ref} \tag{5-19b}$$

and

$$h_{ref} = h_o + \int_o^t \dot{h}_{ref}\, dt \tag{5-19c}$$

where h_o is the altitude at which capture is initiated. This approach allows for compensation of an off-nominal acceleration maneuver where the h_e term will act as a vernier on the $\dot{h}_{ref}$ so that the trajectory is guided toward an asymptotic intersection of the $\dot{h}_{ref} = 0$ with the selected altitude.

Phase C - Altitude Hold

At h_e less than 25 feet, the altitude hold control law is initiated. A block diagram for this phase, which involves a transition to a new control law, is shown on Figure 5-5. At transition, the pitch command synchronizer holds the last value of $\theta_{c_{2B}}$ as the initial condition for all subsequent θ_{c_3} computations. The control law is:

$$\theta_{c_3} = \left(\frac{h_e}{\tau_3 s + 1} + \frac{a_2 h_e}{s} + a_3 \dot{h}_c\right) k_h + \theta_{p_f} \tag{5-20}$$

where θ_{p_f} is a predictive command for flap deployment compensation.

An explicit value for θ_{p_f} could be computed if the airspeed were constant. However, flap deployment is associated with a planned speed reduction. The character of the speed reduction transient involves too many variables to achieve a reasonable computed value of θ_{p_f}. A compromise approach is the following simple compensation

$$\theta_{p_f} = k_f \frac{\tau_4 s}{(\tau_4 s + 1)(\tau_5 s + 1)} \cdot \alpha_F \tag{5-21}$$

The best values of k_f and τ_4 should be obtained from simulations of reasonable flap deployment programs. The approximate value of k_f is:

$$k_f \approx \frac{C_{L_{\delta_F}}}{C_{L_\alpha}} \tag{5-22}$$

The washout time constant should be about 4 seconds and the filter τ_5 should be about 0.25 second. The gain k_h should be a function of (1/V). Thus,

$$k_h = \left(\frac{200}{V}\right) k_{h_{nominal}} \tag{5-23}$$

for (V in ft/sec)

where $k_{h_{nominal}}$ is approximately 0.05 deg/ft.

4. Altitude Hold

The altitude hold control laws and block diagram are identical to those used for Phase C of the altitude capture (Figure 5-5).

5. Pitch Compensation in Turns

To minimize altitude loss in turns, a feedforward or predictive pitch command is required to provide the nose-up attitude that yields the necessary lift increment. The lift increment ΔL is:

$$\Delta L = \frac{W}{\cos\phi} - W = W\left(\frac{1 - \cos\phi}{\cos\phi}\right) \tag{5-24}$$

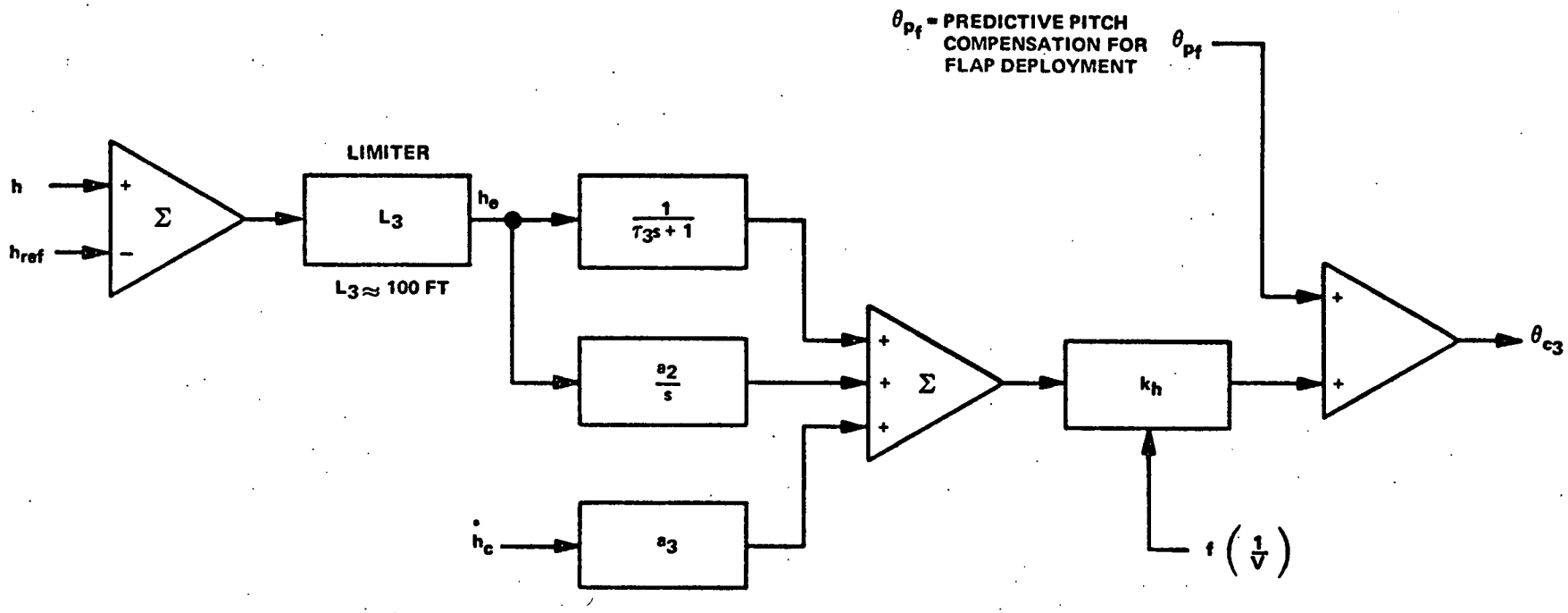

Figure 5-5
Altitude Hold Control Block Diagram

This increased lift is provided by the nose-up $\Delta\alpha$ and the associated $\Delta\delta$ in accordance with

$$\Delta L = C_{L_\alpha} \Delta\alpha QS + C_{L_{\delta_E}} \Delta\delta_E QS \tag{5-25}$$

and

$$C_{M_\alpha} \Delta\alpha + C_{M_{\delta_E}} \Delta\delta_E = 0 \tag{5-26}$$

Substituting equation (5-26) and (5-24) in (5-25) and solving for $\Delta\alpha$ yields

$$\Delta\alpha = \left[\frac{1 - \cos\phi}{\cos\phi}\right] \frac{W}{QS} \left[\frac{1}{C_{L_\alpha} - C_{L_{\delta_E}} \left(\frac{C_{m_\alpha}}{C_{m_{\delta_E}}}\right)}\right] \tag{5-27}$$

For constant flight path angle flight

$$\Delta\alpha = \Delta\theta = \theta_L \tag{5-28}$$

where θ_L is the required pitch change for lift compensation.

The predictive pitch command should be filtered so that

$$\theta_{P_L} = \frac{\theta_L}{(\tau_6 s + 1)} \tag{5-29}$$

where $\tau_6 \approx 1.0$ second.

6. Stability Considerations

a. Vertical Speed Control

Figure 5-6 shows the block diagram of the various control loops and transfer functions involved in the vertical speed mode. The vertical speed feedback loop is closed as a pitch command to the pitch stabilization inner loop. The pitch loop, $G_\theta(s)$ modifies the aircraft closed-loop response to an elevator input. Since the $\dot{h}$ error signal is converted to a pitch command (the output of $G_{\dot{h}}(s)$ is a pitch command), then to make the stability analysis loop consistent,

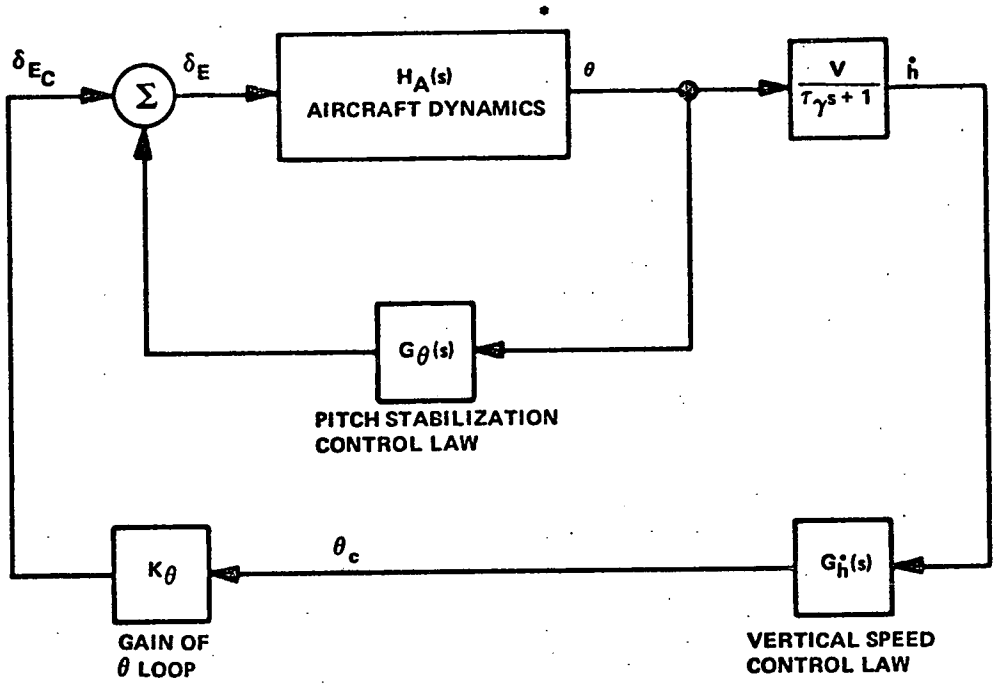

* THE PHUGOID MODE CAN BE ELIMINATED IF A GOOD AUTOTHROTTLE LOOP CLOSURE IS ASSUMED.

Figure 5-6
Stability Analysis Block Diagram
Vertical Speed Control

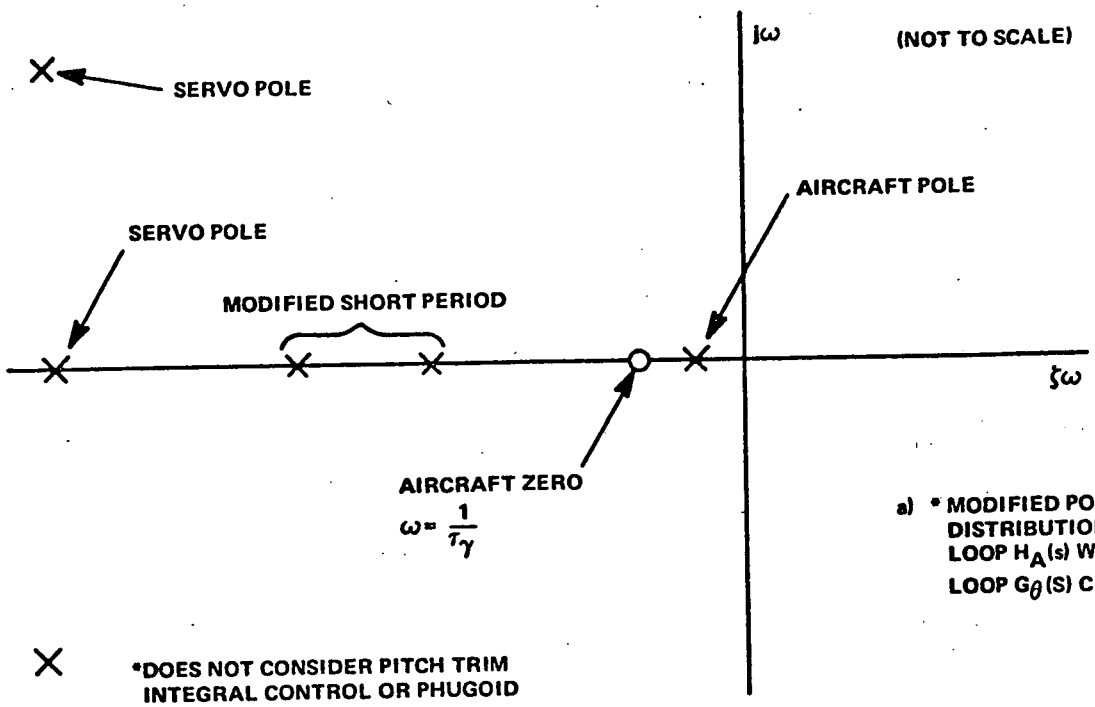

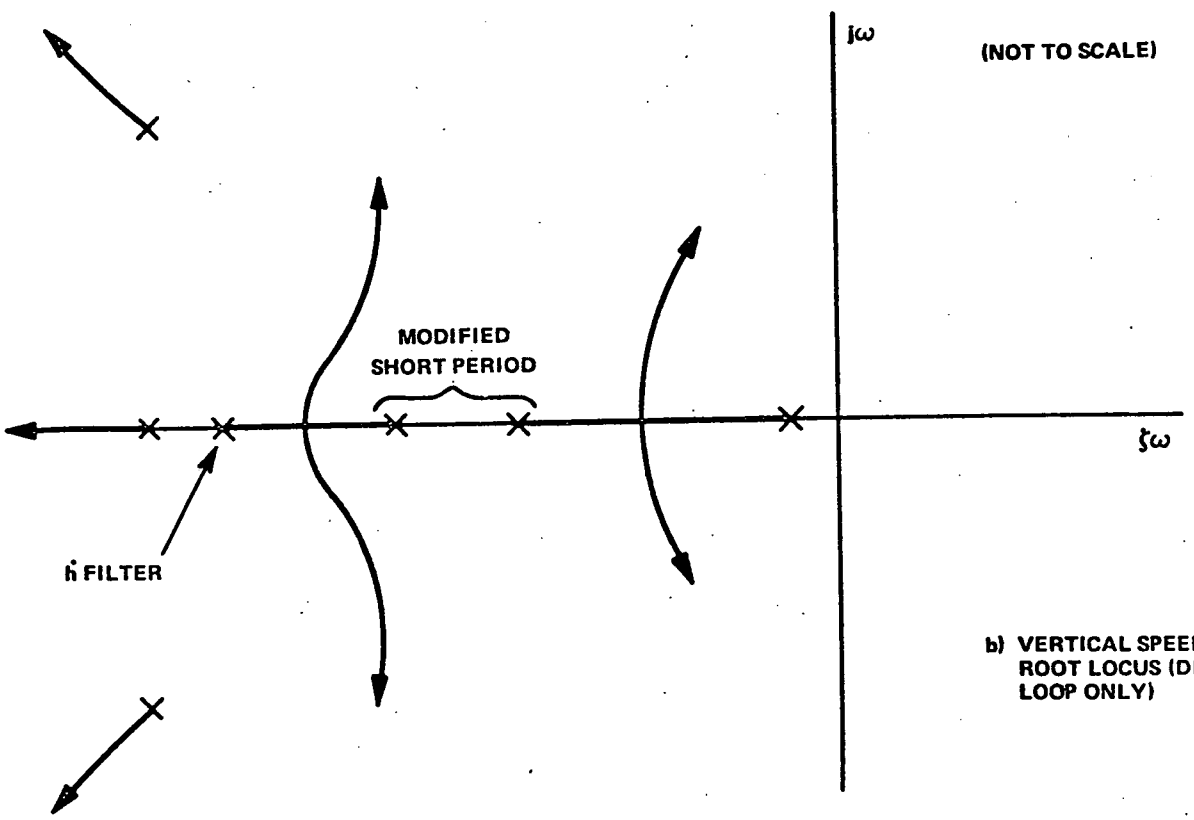

Figure 5-7
Vertical Speed Control Stability Analysis

the pitch gain K_θ must be added to the $\dot{h}$ loop as shown on Figure 5-6. The pitch feedback causes a shift in the aircraft's $[\theta/\delta_E]$ poles and zeros to the locations illustrated on Figure 5-7a. The closure of the $\dot{h}$ loop causes the root loci illustrated on Figure 5-7b. In general, excessive gains of the $\dot{h}$ loop excite relatively short period pitch oscillations. This is in contrast to excessive gains of the altitude control loop which cause longer period flight path oscillations.

b. Altitude Control

The stability analysis block diagram for the altitude control mode is shown on Figure 5-8. In this case, the modified aircraft is shown as a $[\theta/\theta_c]$ transfer function achieved by the closure of the pitch inner loop. The effect of this loop closure is approximated as a second order response $[H_A'(s)]$ defined by two real poles. A nominal displacement, integral, and rate control law $[G_h(s)]$ results in a cubic numerator and quadratic denominator. Typical ratios of integral and rate gains yield the control law zeros and poles shown on Figure 5-9. As the loop gain k_h is increased for this fixed ratio of displacement, integral and rate feedback, the loci of Figure 5-9 are obtained.

7. Summary of Control Parameters and Performance Criteria

a. Control Parameters

The control parameters identified in the control equations given in this section are specified in terms of typical minimum, nominal, and maximum values in Table 5-1.

b. Performance Criteria

(1) Vertical Speed Control Modes

(a) Vertical Speed Hold

Introduce 10 ft/sec offset or initial condition error. Response should be restricted to 15-percent overshoot. Final value should be attained within 10 seconds, with static accuracy of 2.0 percent if airspeed is maintained via the throttle loop.

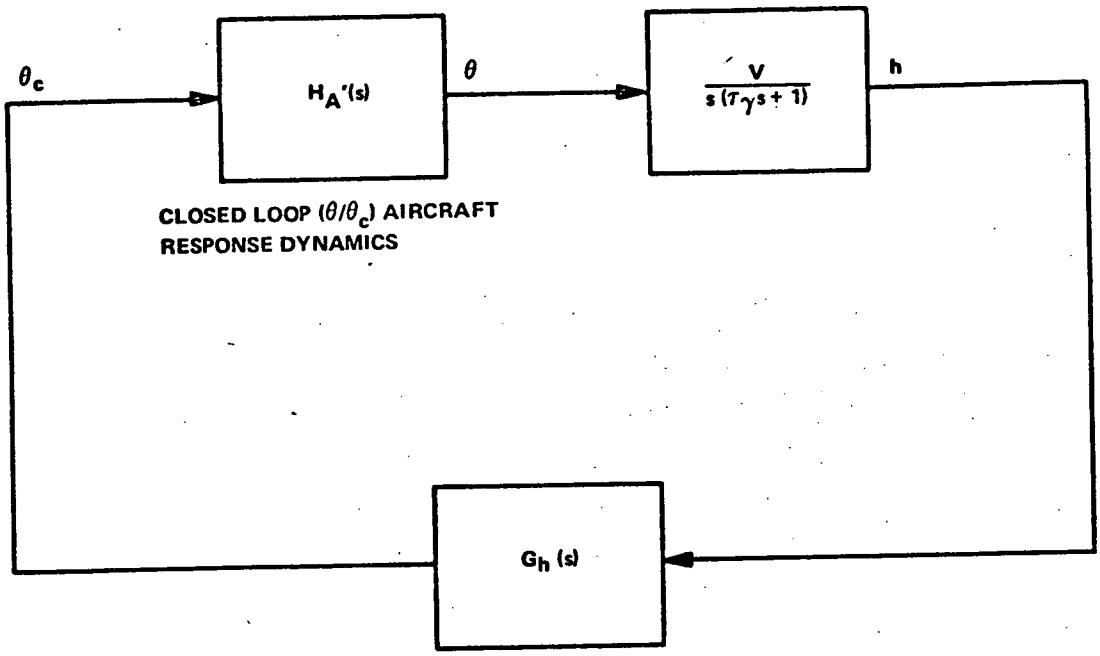

ALTITUDE CONTROL LAW

$$G_h(s) = \left[\frac{1}{\tau_3 s + 1} + \frac{a_2}{s} + s\,a_3\right] k_h$$

$$H_A'(s) = \frac{1}{(\tau_A s + 1)\,(\tau_B s + 1)}$$

WHERE $\frac{1}{\tau_A}$ AND $\frac{1}{\tau_B}$ ARE THE MODIFIED SHORT PERIOD POLES OF FIGURE 5-7a

Figure 5-8
Stability Analysis Block Diagram - Altitude Control

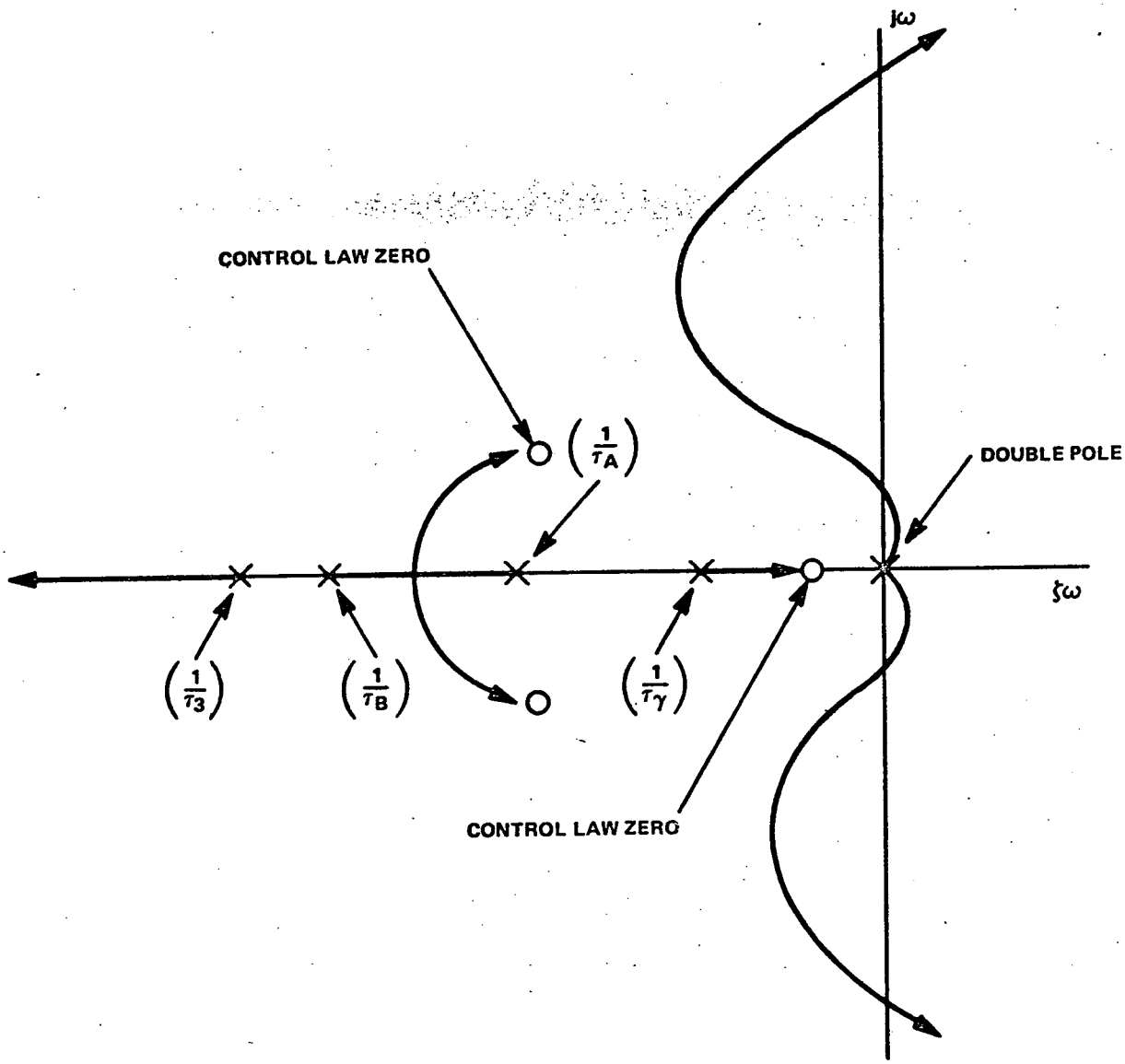

Figure 5-9
Altitude Control Root Loci
(Displacement, Rate and Integral)

TABLE 5-1

PARAMETER SUMMARY

Parameter	Typical Minimum Value	Typical Nominal Value	Typical Maximum Value	Remarks
a_1	0.20	0.30	0.50	Vertical Speed Control Integral Gain Ratio
$k_{\dot{h}}$	0.075	0.15	0.25	Vertical Speed Control Pitch Command Gain (degrees θ_c per ft/sec error) [Note gain reduction function of velocity per equations (5-4) and (5-5)]
τ_1	2.0	4.0	6.0	Vertical Speed Complementary Filter Time Constant
$\ddot{h}_{max}$	1.5 ft/sec^2	2.25 ft/sec^2 (0.07g's)	4.0 ft/sec^2	Acceleration Constraint
τ_2	0.50	1.0	1.5	Predictive Pitch Command Filter (seconds)
k_1	5	10	12	Altitude Capture Rate to Displacement Ratio
τ_3	0.30	0.50	1.0	Altitude Error Filter (seconds)
a_2	0.03	0.05	0.10	Altitude Control Integral to Displacement Ratio
a_3	0.05	1.0	4.0	Altitude Control Rate to Displacement Ratio
k_h	0.03	0.05	0.10	Altitude Control Gain - Degrees θ_c per Foot Error (Function of 1/V)
k_F	--	$\frac{C_{L_{\delta_F}}}{C_{L_\alpha}}$	--	Flap Compensation Gain
τ_4	1.0	2.0	4.0	Flap Compensation Washout (seconds)
τ_5	0.25	0.5	1.0	Flap Compensation Filter (seconds)

(b) Vertical Speed Command

From a vertical speed reference of 10 ft/sec with aircraft stabilized to that value, introduce a step reference change of 30 ft/sec to a new reference value 40 ft/sec (2400 ft/min). The normal acceleration should be restricted to within 10 percent of the maximum limit value ($\ddot{h}_{max}$). The final convergence to the new reference vertical speed should be held to an overshoot below 15 percent of the $\Delta \dot{h}_{ref}$.

(2) Altitude Capture

From an initial $\dot{h}$ of about 100 ft/sec (6000 ft/min), approach the reference altitude. Altitude capture initiate, flare to reference altitude, and final acquisition of the reference altitude should be achieved with maximum normal acceleration held to within 15 percent of the specified $\ddot{h}_{max}$. The overshoot of the reference altitude should be restricted to a maximum of about 50 feet. Convergence to within 10 feet of the reference altitude should be achieved within 12 seconds after the first overshoot if the capture trajectory overshoots. If the capture trajectory undershoots, convergence to within 10 feet of the reference altitude should be achieved within 10 seconds after the altitude error reached 50 feet.

(3) Altitude Control

(a) Transient Response

With altitude hold mode engaged and altitude error = 0, introduce 50 feet altitude error. The corrective response should have its overshoot restricted to 10 feet maximum. The reference value should be reached (within 2 feet) in 15 seconds.

(b) Turn Compensation

With altitude hold mode engaged and airspeed maintained via throttle control, bank the aircraft to a bank angle of 30 degrees at a roll rate of 5 degrees/second. The altitude error transient should not exceed 30 feet and should be reduced to within 10 feet within 10 seconds after the 30-degree bank angle is attained.

3

B. DIGITAL PROGRAM - VERTICAL GUIDANCE (NONLANDING)

1. Control Law Conversion

Four subroutines were written to implement the vertical guidance laws. They are:

MEASUR	Derives compensated vertical speed information from blend of inertial and barometric data
VERTSC	Vertical Speed Control Law
ALTHLD	Altitude Hold Control Law
HDTCMP	Vertical Speed Command Processor - Applies acceleration constraints to vertical speed reference changes

The FORTRAN namelists for MEASUR, VERTSC, ALTHLD, AND HDTCMP are given in Tables 5-2, 5-3, and 5-4, respectively. The block diagrams for these subroutines (in FORTRAN notation) are given in Figures 5-10, 5-11, 5-12, and 5-13, respectively.

TABLE 5-2

NAMELIST FOR SUBROUTINE MEASUR

Name	FORTRAN Name	Definition
$\ddot{h}_i$	(-) VDDOT	Vertical acceleration in local vertical coordinate axis
$\dot{h}_B$	ALTDTB	Barometric vertical speed
$\dot{h}_c$	HDTC	Compensated vertical speed
τ_1	TV1	Filter time constant
--	DT3	Sample time of computation interval

TABLE 5-3

VARIABLE NAMELIST FOR SUBROUTINE VERTSC

Variable	FORTRAN Name	Definition
h	ALT	Aircraft altitude above sea level
h_{ref}	ALTREF	Altitude reference
$\dot{h}_c$	HDTC	Calibrated vertical speed
$\dot{h}_{ref}'$	HDTRFC	Vertical speed reference command
V	VT	Aircraft ground speed
θ_c	THECOM	Pitch attitude command
Q	QBAR	Dynamic pressure
W	WAIT	Aircraft weight
C_{L_α}	CLALPH	Aircraft lift curve slope $\partial C_L/\partial\alpha$
$C_{L_{\delta_e}}$	CLDE	$\partial C_L/\partial\delta_e$
C_{m_α}	CMALPH	$\partial C_m/\partial\alpha$
$C_{m_{\delta_e}}$	CMDE	$\partial C_m/\partial\delta_e$
S	AREA	Reference area
k_1	KHC	Altitude capture displacement to rate ratio
$k_{\dot{h}}$	KHDT	Vertical speed control pitch command gain
a_1	A1	Vertical speed control integral gain ratio
L_1	LH1	Vertical speed command rate limit
L_2	LH2	Altitude error limit for altitude capture
$\ddot{h}_{max}$	HDDMAX	Vertical acceleration limit
τ_2	TV2	Filter time constant
	DT3	Subroutine sample time

TABLE 5-4

VARIABLE NAMELIST FOR SUBROUTINE ALTHLD

Variable	FORTRAN Name	Definition
h	ALT	Aircraft altitude above sea level
h_{ref}	ALTREF	Reference altitude
$\dot{h}_c$	HDTC	Calibrated vertical speed
δ_f	DELTF	Flap deflection angle
ϕ	PHI	Euler roll attitude angle
θ_c	THECOM	Pitch attitude command
Q	QBAR	Dynamic pressure
W	Wait	Aircraft weight
C_{L_α}	CLALPH	
$C_{L_{\delta_e}}$	CLDE	
C_{m_α}	CMALPH	
$C_{m_{\delta_e}}$	CMDE	
S	AREA	Reference area
a_2	A2	Altitude control integral to displacement ratio
a_3	A3	Altitude control rate to displacement ratio
k_h	KH	Altitude control gain
k_F	KFLAP	Flap compensation gain
L_3	LH3	Altitude error limit
τ_2	TV3	Altitude error filter time constant
τ_4	TF4	Flap compensator filter time constant
τ_5	TF5	Flap compensator filter time constant
τ_6	TC5	Roll compensator filter time constant
	R2D	Radians to degrees conversion factor
	DT3	Subroutine sample time

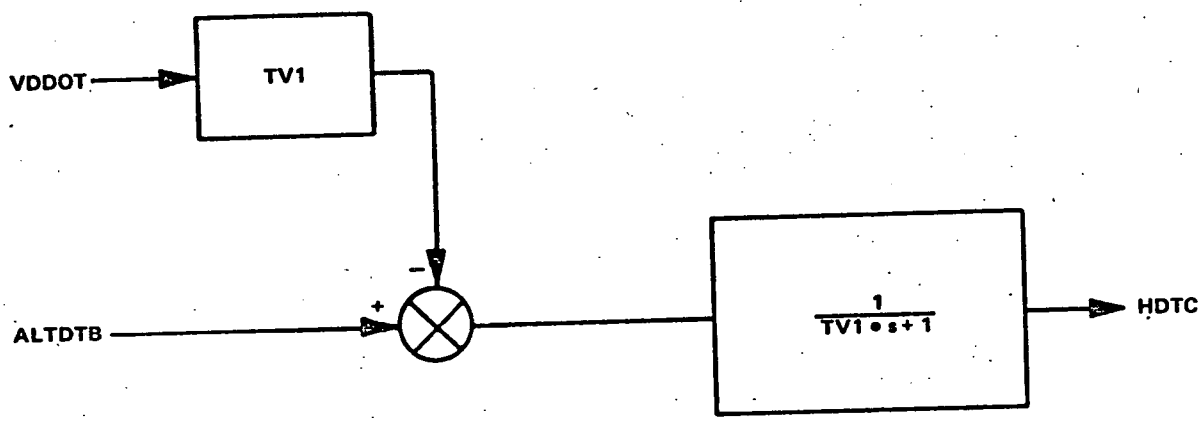

Figure 5-10
Filtered Vertical Speed Block Diagram
(Fortran Notation)

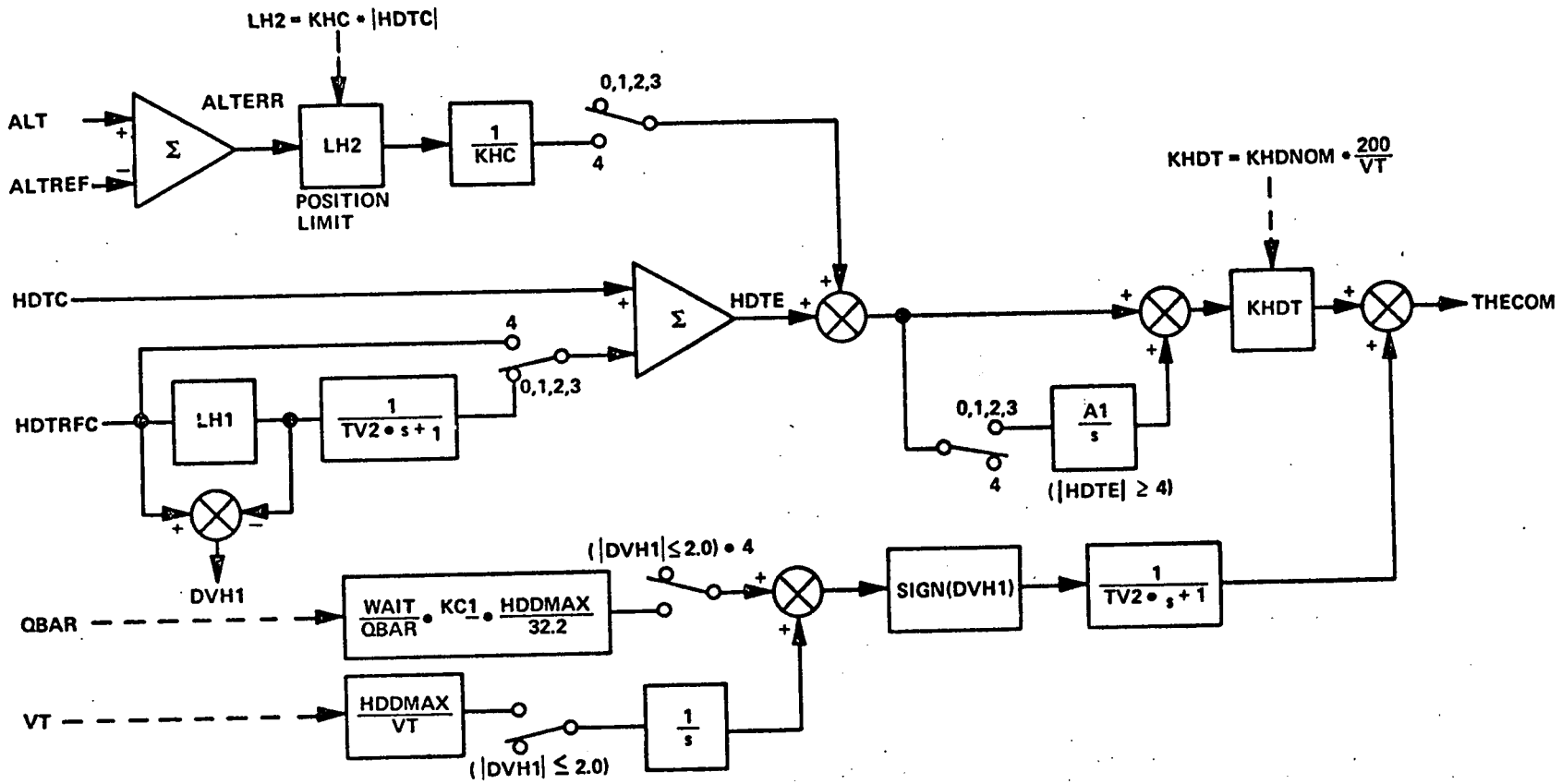

MODE CONTROL

IALTCP	CONDITION AND ACTION
0	VERTICAL SPEED HOLD OR SELECT, ALTITUDE CAPTURE NOT ARMED
1	VERTICAL SPEED HOLD OR SELECT, ALTITUDE CAPTURE ARMED: IF (ALTERR < DELH), IALTCP = 2
2	VERTICAL SPEED HOLD, SENSE CAPTURE ALTITUDE: IF [(ALTERR < DELH) ⊕ (ALTERR > LH2)] IALTCP = 3
3	PHASE A OF CAPTURE: IF [(|HDTC| ≤ 2) ⊕ (ALTERR > 25) + (AALTER < LH2))], IALTCP = 4
4	PHASE B OF CAPTURE: IF (ALTERR < 25) SWITCH TO ALTITUDE HOLD

Figure 5-11
Vertical Speed Hold, Select,
Altitude Capture Block Diagram (Fortran Notation)

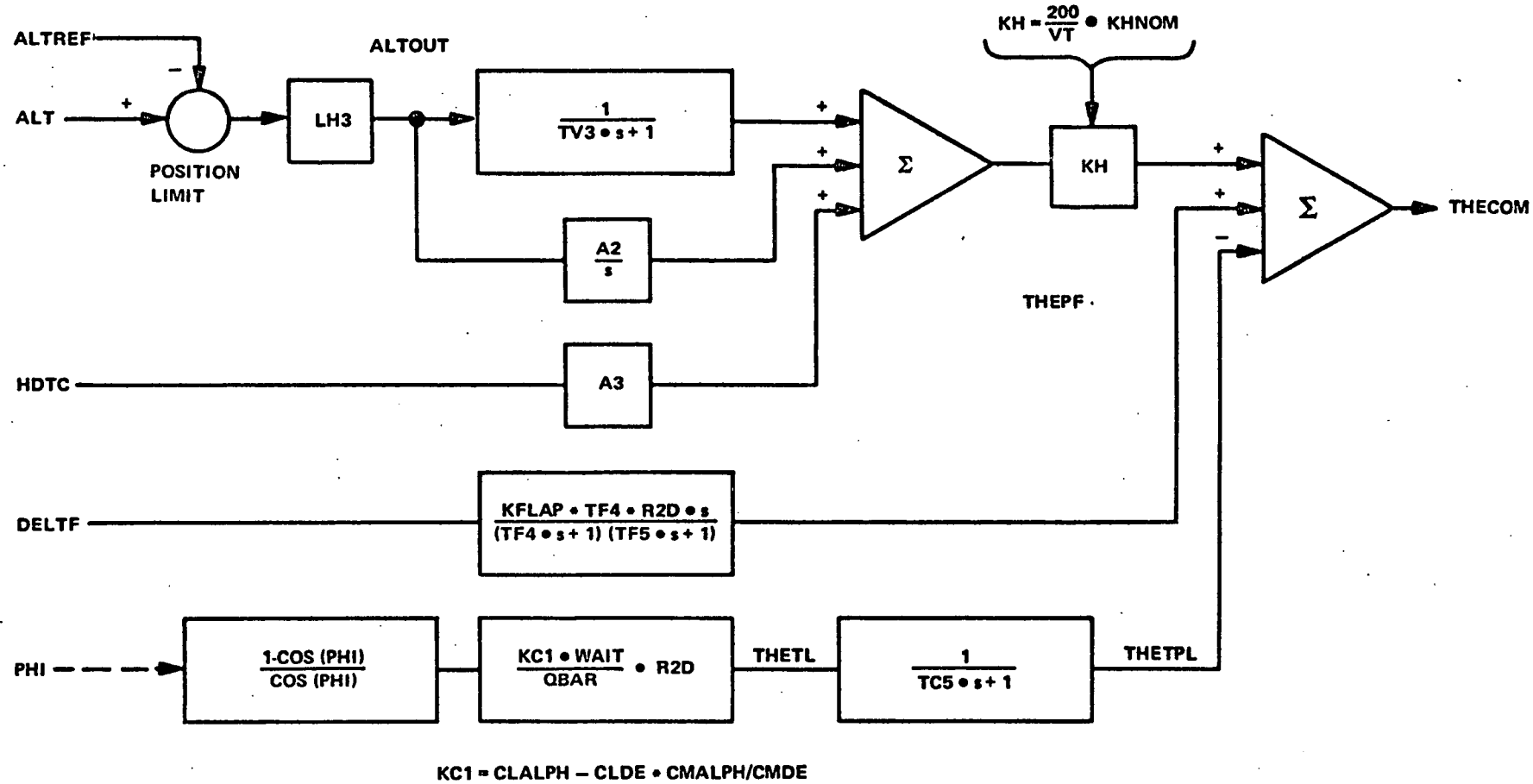

Figure 5-12
Altitude Hold Control Law Block Diagram -
Fortran Notation

2. Program Flow Chart

The initial condition computations which are performed in the SASIC subroutine for the vertical guidance modes are:

IC Calculations (MEASUR)

a) Initialize Filter

HDTCIO = 0

HDTC = ALTDOT

b) Filter Difference Equation Coefficients

CM1 = EXP (-DT3/TV1)

DM1 = 1.0 - CM1

IC Calculations (VERTSC)

a) Predictive Pitch Constants

KC1 = R2D/(CLALPH - CLDE * CMALPH/CMDE)/AREA

WC = WAIT * KC1 * HDDMAX/32.2

b) Vertical Speed Reference Rate Limit

LH1 = HDDMAX * DT3

c) Altitude Limit Term

THDDMX = 1.8 * HDDMAX

d) Control Law Gains

KHDV = KHDNOM * 200

A1T = A1 * DT3

e) Control Law Difference Equation Coefficients

CVERT1 = EXP (-DT3/TV2)

DVERT1 = 1 - CVERT1

f) Set Logic

ITEST1 = 0

ITEST2 = 0

ITEST3 = 0

IC Calculations (ALTHLD)

a) Altitude Error Filter Difference Equation Coefficients

CAH1 = EXP (-DT3/TV3)

DAH1 = 1.0 - CAH1

b) Altitude Error Integrator Gain

DAH2 = A2 * DT3

c) Roll Compensation Filter Difference Equation Coefficients

CPL1 = EXP (-DT3/TC5)

DPL1 = 1.0 - CPL1

d) Flap Compensation Filter Difference Equation Coefficients

CTF1 = EXP (-DT3/TF4) + EXP (-DT3/TF5)

CTF2 = EXP [-DT3 * (1.0/TF4 + 1.0/TF5)]

DTF = R2D/TF5 * [EXP (-DT3/TF4) - EXP (-DT3/TF5)]/(1.0/TF5 - 1.0/TF4)

e) Altitude Error Gain

KHDVA = KHNOM * 200.0

f) Initialize Synchronization Logic Variable

ITEST4 = 0

The flow charts are shown in Figures 5-14 through 5-17. The vertical speed control and altitude capture parameter values for optimum performance are:

KHC = 10.0

KHDNOM = 0.25 deg/ft/sec

A1 = 0.3

HDDMAX = 2.0 ft/sec^2

TV2 = 1.0 sec

I: BLOCK DIAGRAM

II: FLOW CHART

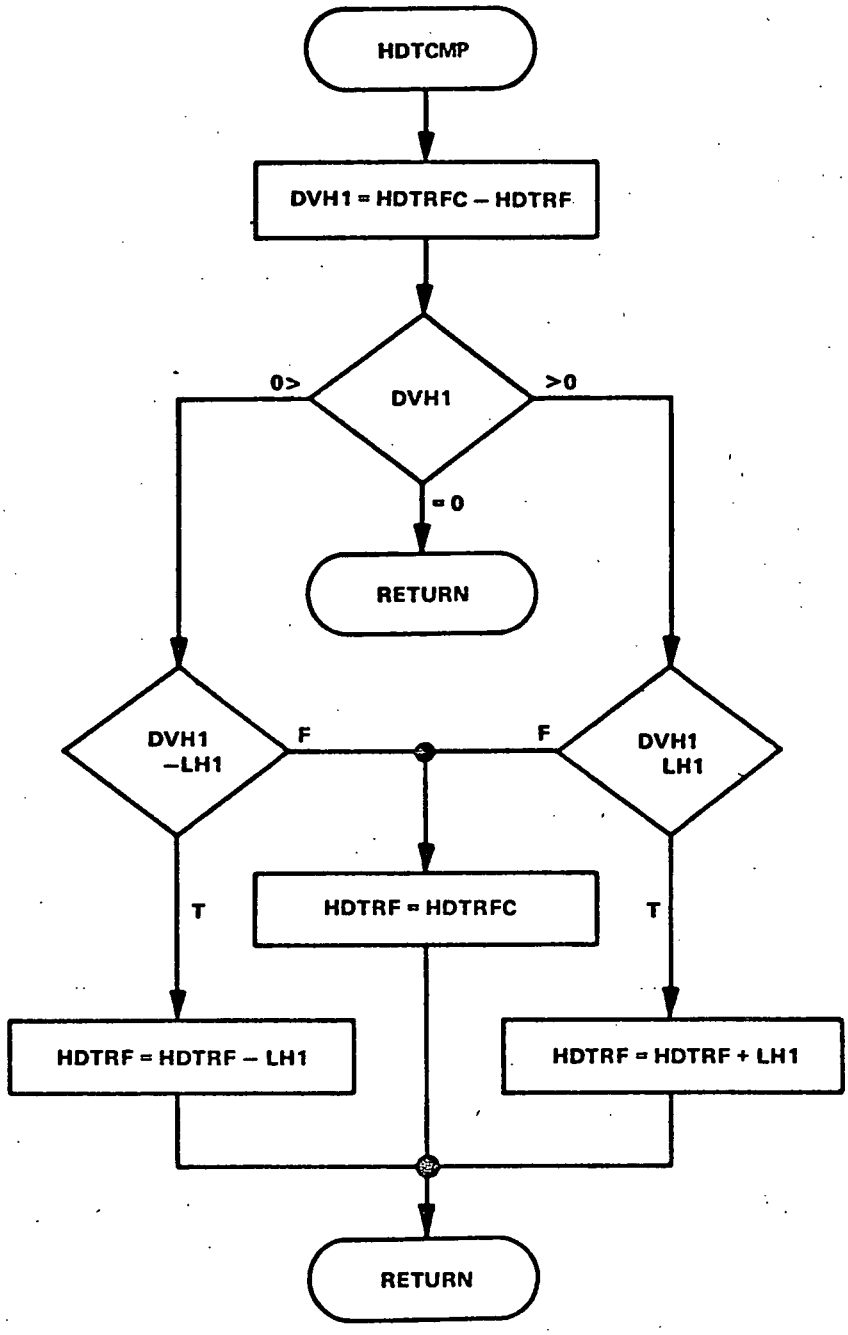

III: IC CALCULATION

LH1 = HDDMAX DT3
HDDMAX = VERTICAL ACCELERATION LIMIT
DT3 = SAMPLE TIME

Figure 5-13
Vertical Speed Reference Processor

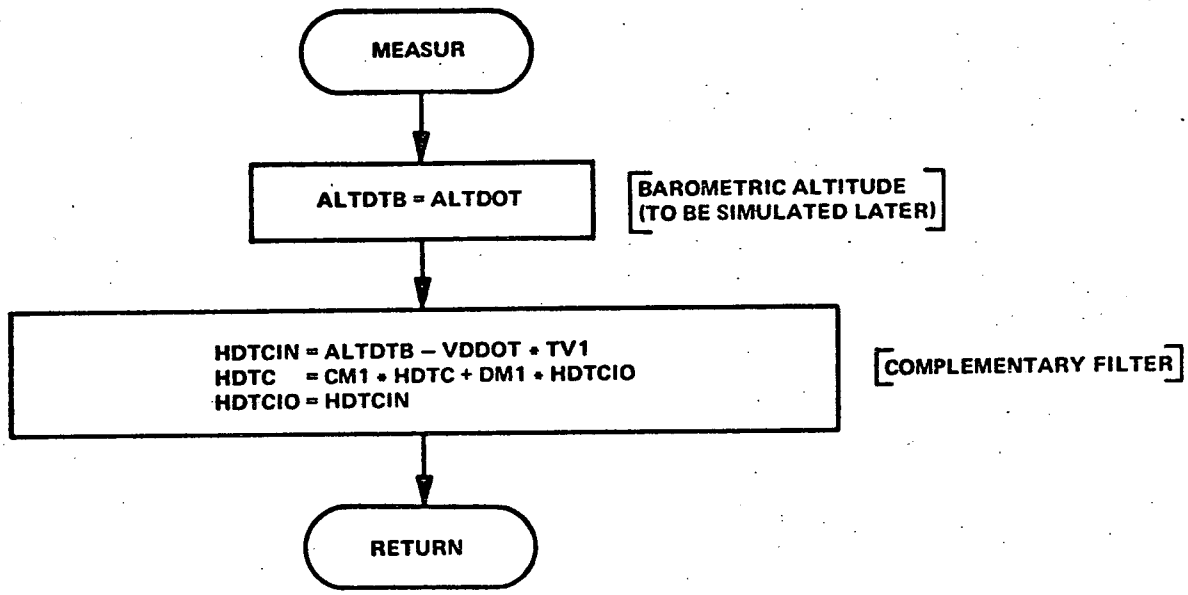

Figure 5-14
Measure Subroutine Flow Chart

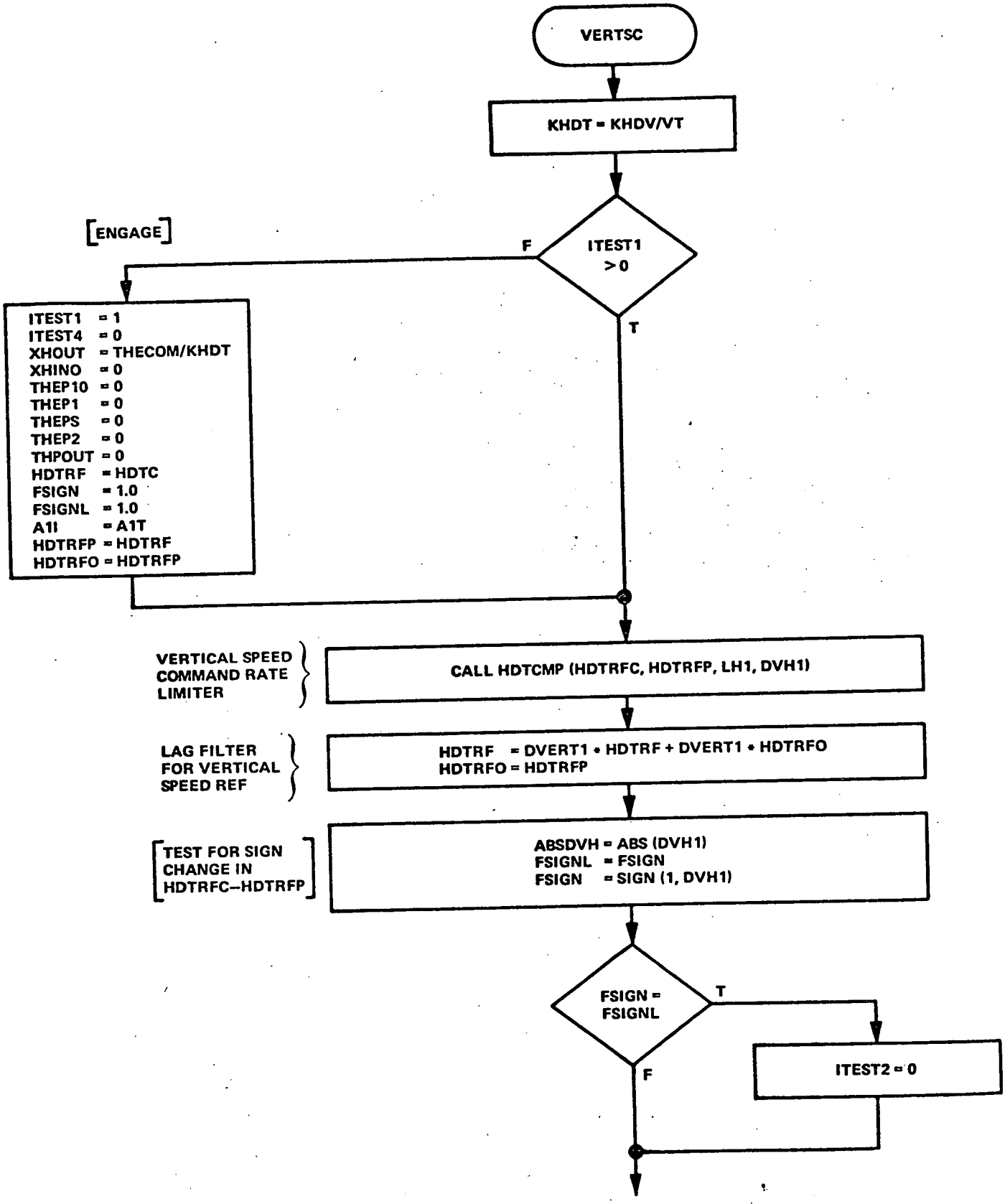

Figure 5-15a
VERTSC (Vertical Speed Control)
Flow Chart

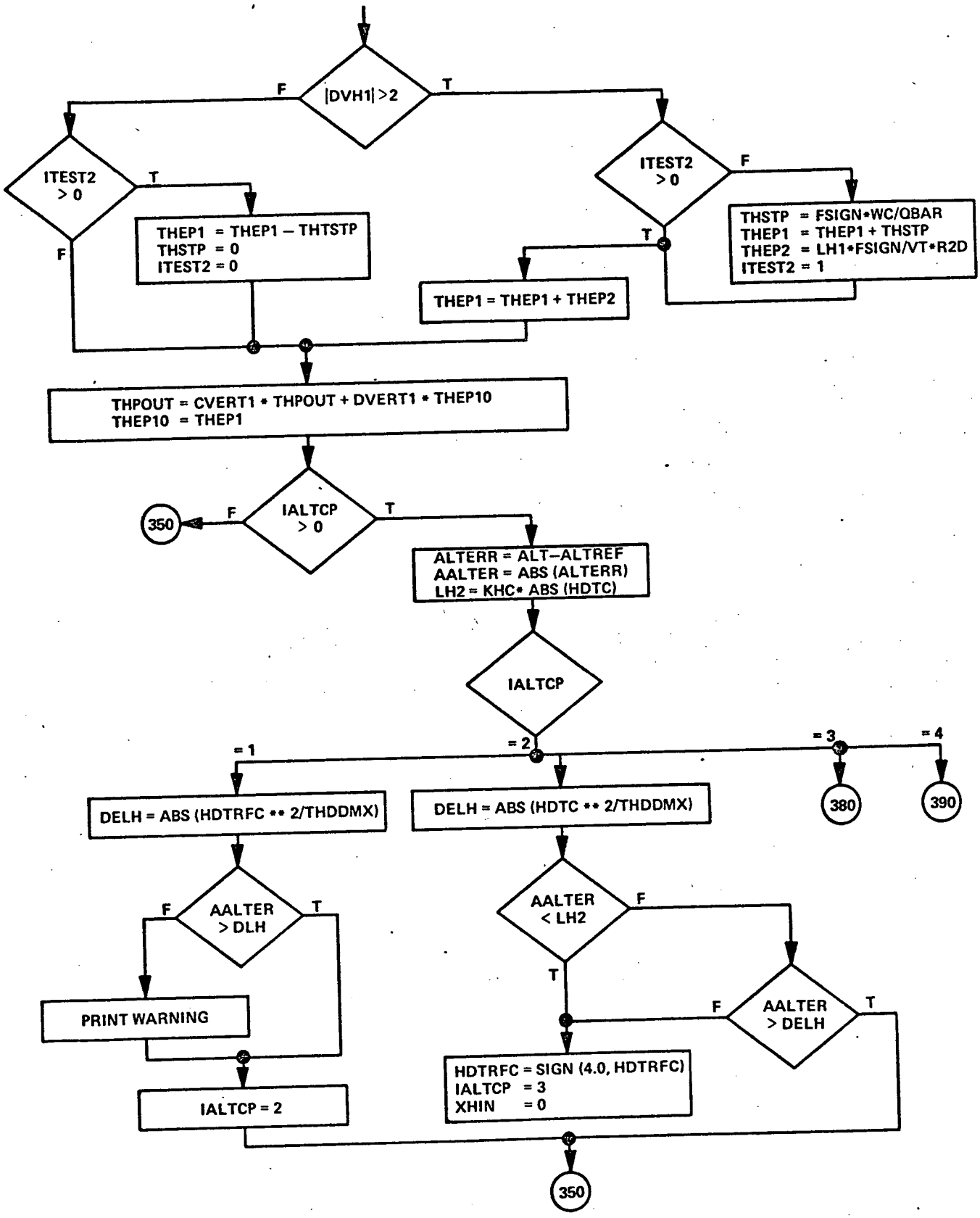

Figure 5-15b
VERTSC Flow Chart (cont)

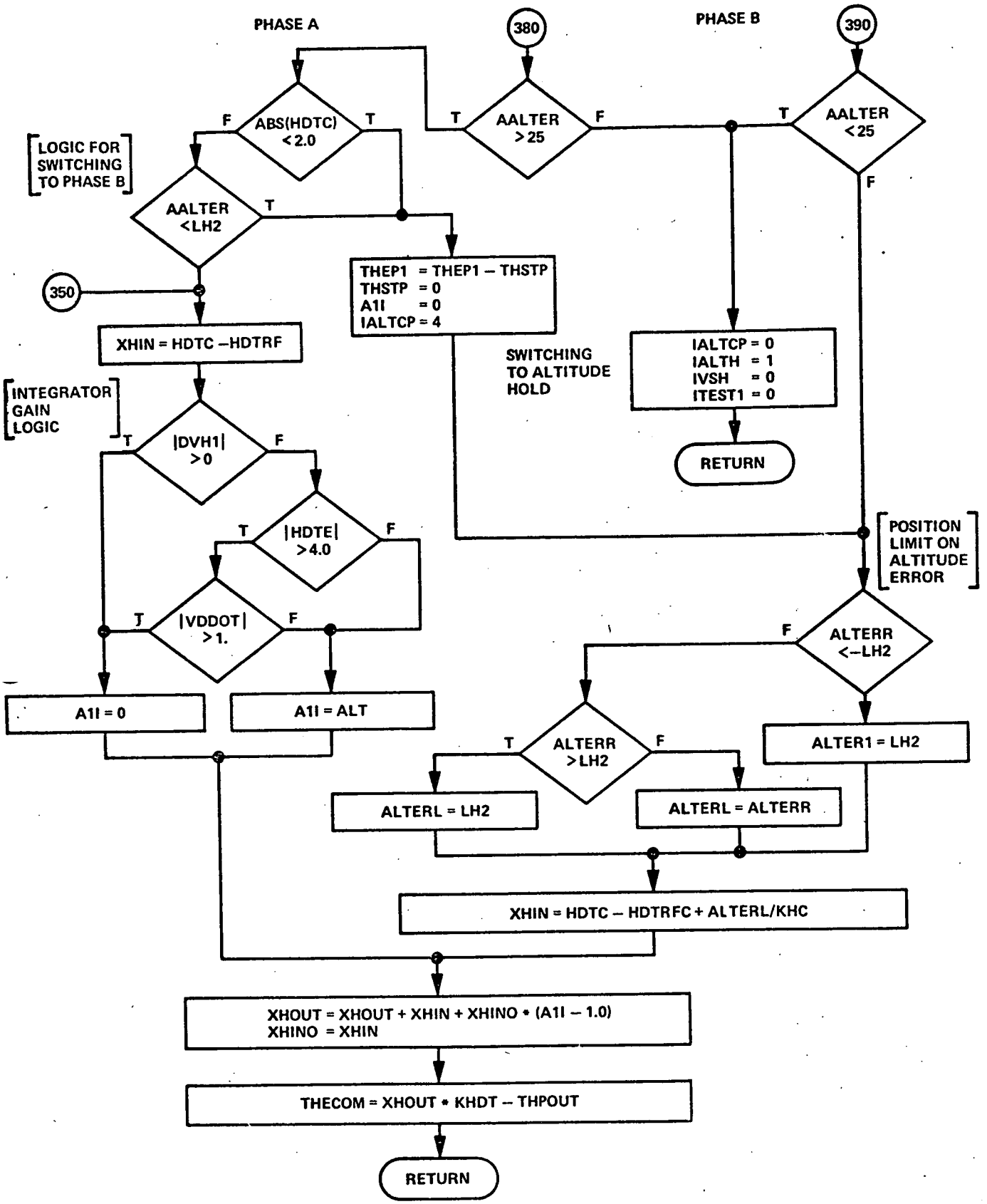

Figure 5-15c
VERTSC Flow Chart (cont)

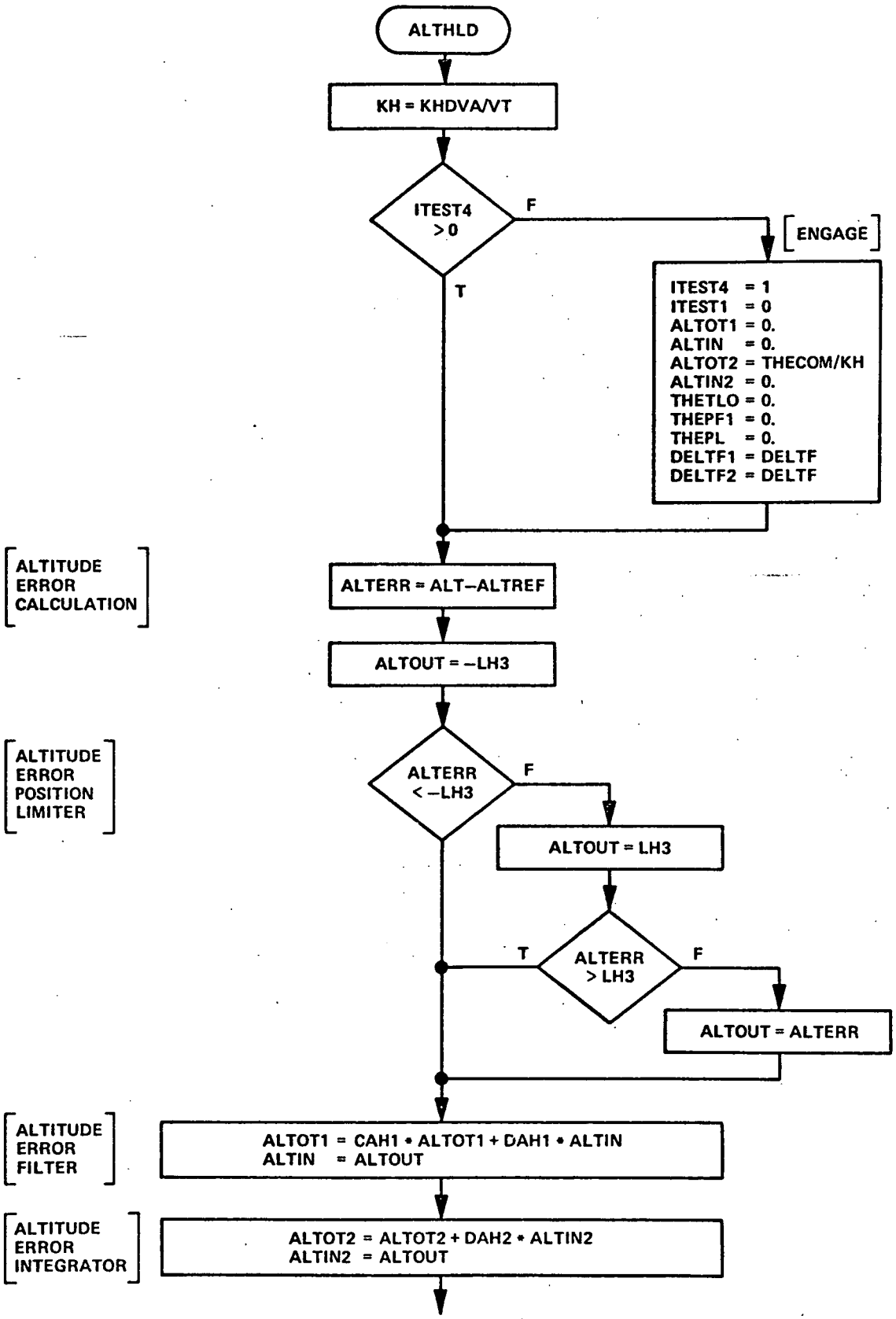

Figure 5-16a
Altitude Hold (ALT HLD) Flow Chart

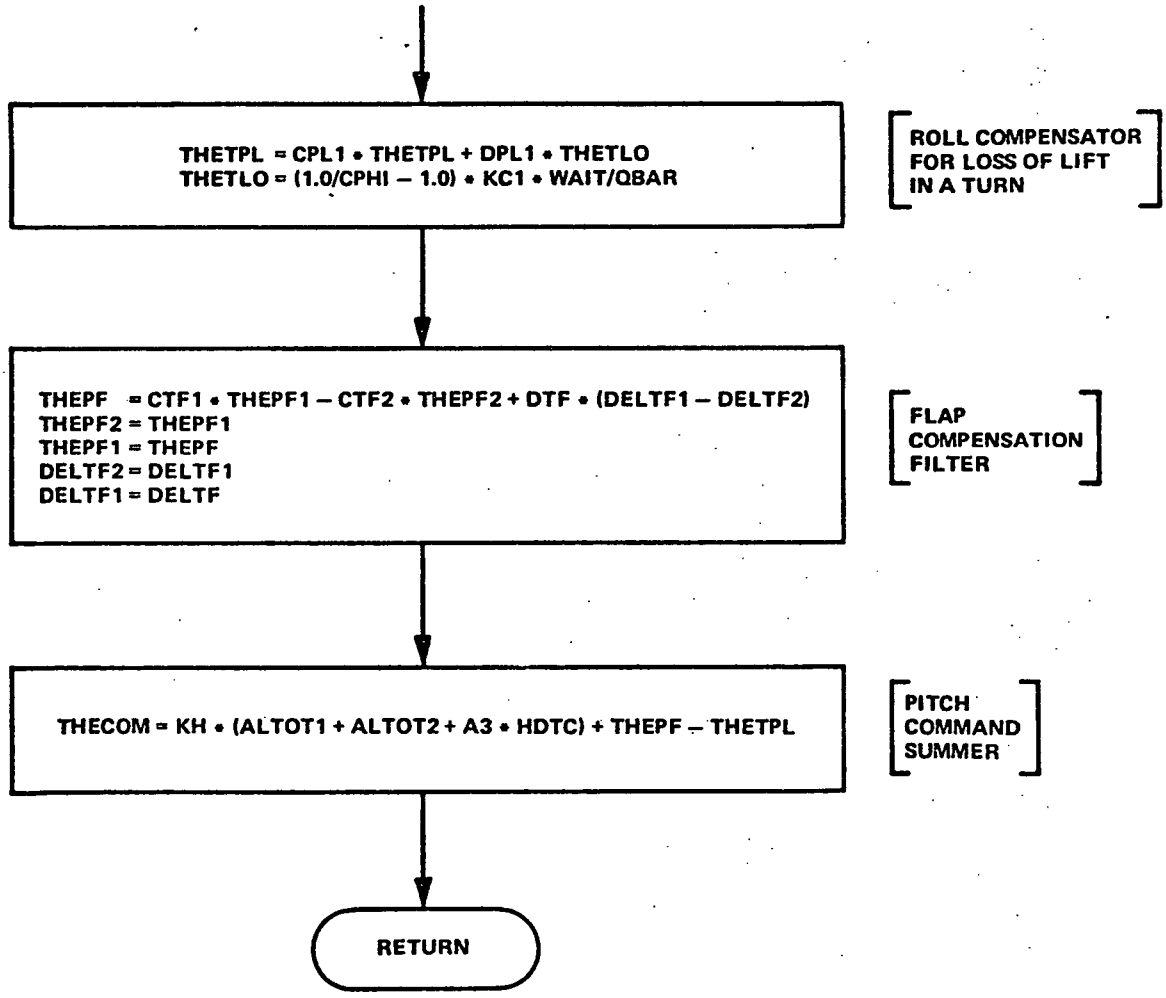

Figure 5-16b
ALTHLD Flow Chart (cont)

Figure 5-17

Intentionally Omitted

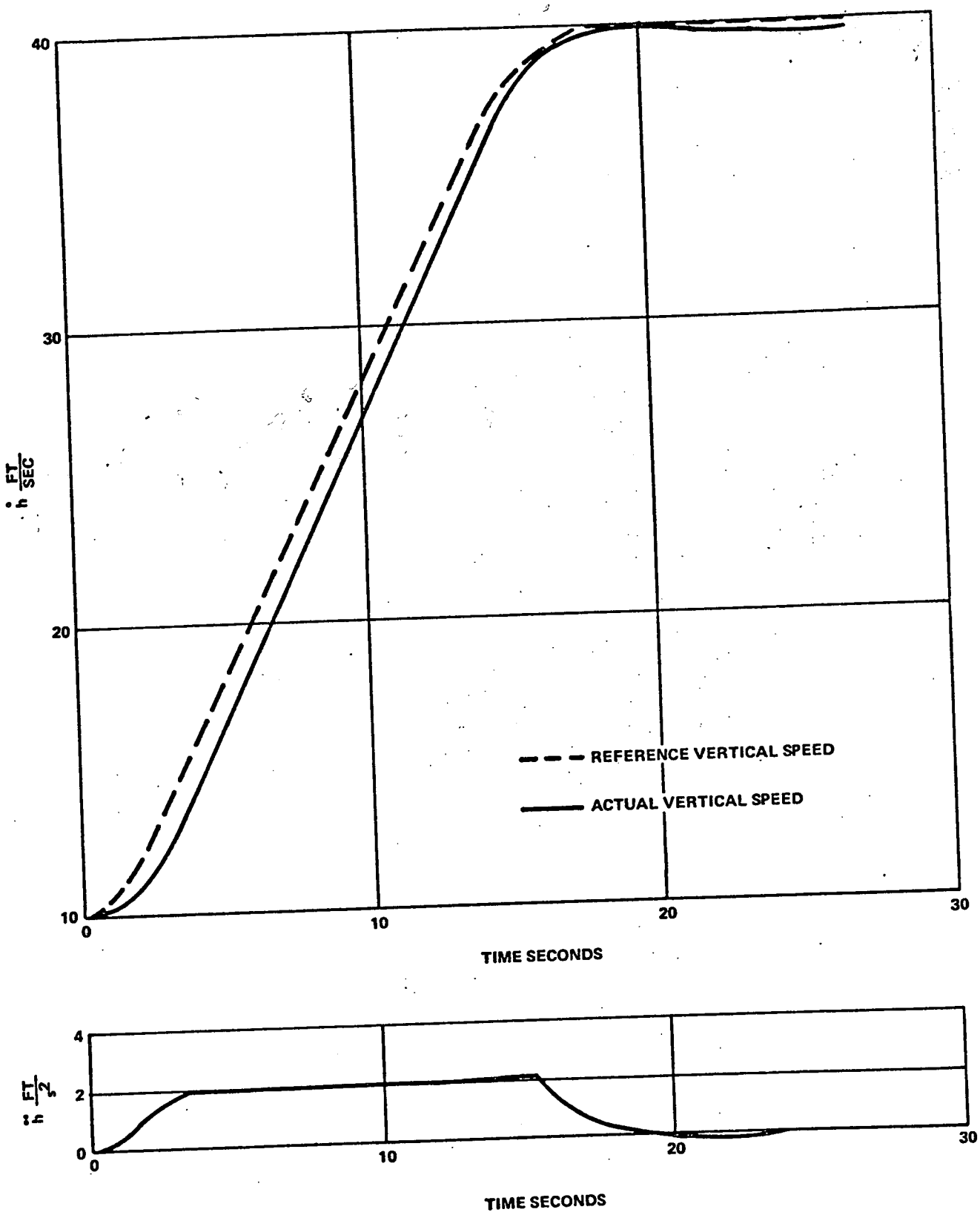

Figure 5-18
Vertical Speed Command Test

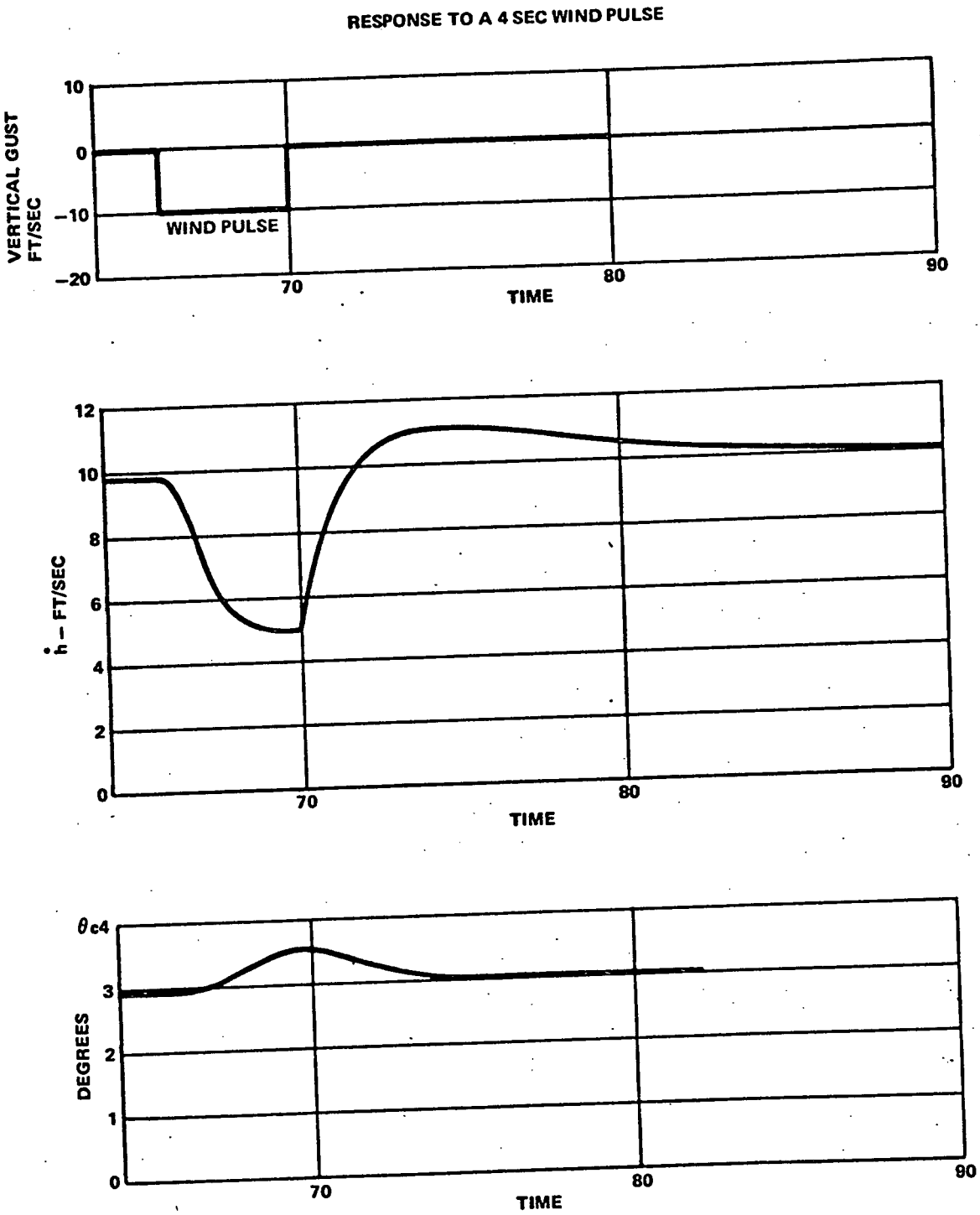

Figure 5-19
Vertical Speed Control Gust Response

C. SIMULATION TEST RESULTS - VERTICAL GUIDANCE (NONLANDING)

1. Vertical Speed Control

Figure 5-18 illustrates the vertical speed control command response. From an initial velocity of 10 ft/sec (climb) the reference is increased to 40 ft/sec. The response is almost dead-beat with the maximum error restricted to about 1.0 ft/sec. The acceleration was held to 2.0 ft/sec^2. A key factor in permitting tight tracking of the vertical speed reference is the inclusion of an additional lag filter on $\dot{h}_{ref}$. As seen on Figure 5-18, $\dot{h}_{ref}$ has a first order lag of about 1.0 second after its computation based on the $\ddot{h}$ constraint. This lag matches the basic vehicle acceleration response capability. If $\dot{h}_{ref}$ was a pure ramp, it would require infinite acceleration to maintain zero error initially.

The gust response is illustrated in Figure 5-19. During a 10 ft/sec (600 ft/min) rate of climb, a 4-second wind pulse (from above) of magnitude 10 ft/sec is introduced. The response illustrated in Figure 5-19 demonstrates that the vertical speed error is arrested by the time one half of the wind velocity has been transferred to the aircraft. The overshoot in the recovery is caused by the integration loop. Although this response is satisfactory, the overshoot could be largely eliminated by incorporating integral mode switching logic. With such an approach, the integrator gain would be held at zero unless an $[\dot{h}_{error} + k\ddot{h}]$ criterion was satisfied.

2. Altitude Capture

The final phase of altitude capture in terms of the vertical speed and acceleration responses is illustrated in Figure 5-20. An altitude overshoot of 26.9 feet occurs as the 13,000-foot altitude is penetrated. The phase B control sequence starts with an altitude rate of about 40 ft/sec. The acceleration exceeds the desired 0.07g limit value by a small and acceptable value (peak = 3 ft/sec^2).

A complete capture trajectory starting from a vertical speed of about 4800 ft/min is shown in Figure 5-21. In this case, the alternate control technique described in equations (5-19b) and (5-19c) was used. Altitude capture is initiated at an altitude of about 4500 feet. The reference altitude is 6000 feet.

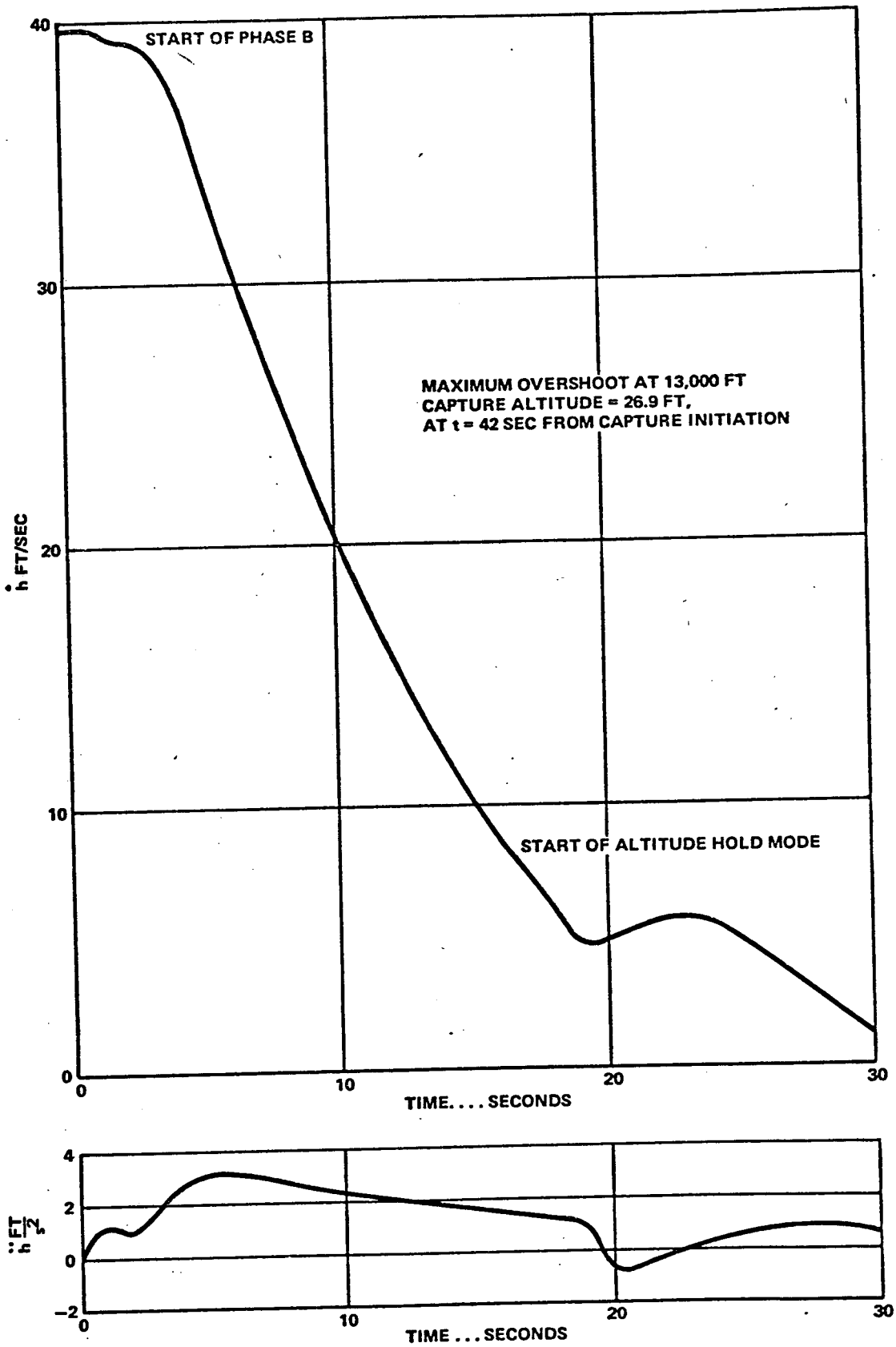

Figure 5-20
Altitude Capture Vertical Speed and
Acceleration Histories

Page intentionally left blank

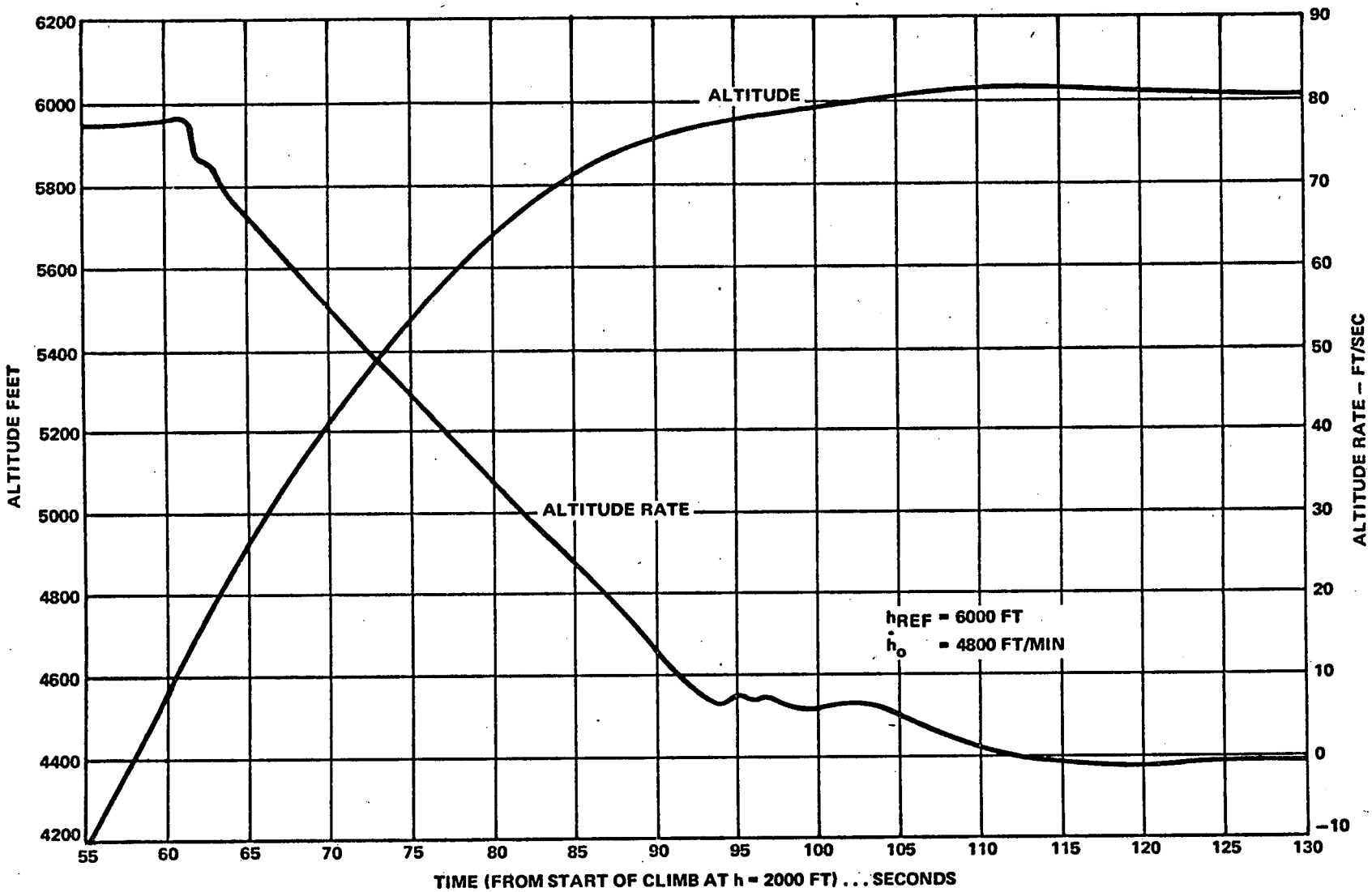

Figure 5-21
Altitude Capture Trajectory

Preceding page blank

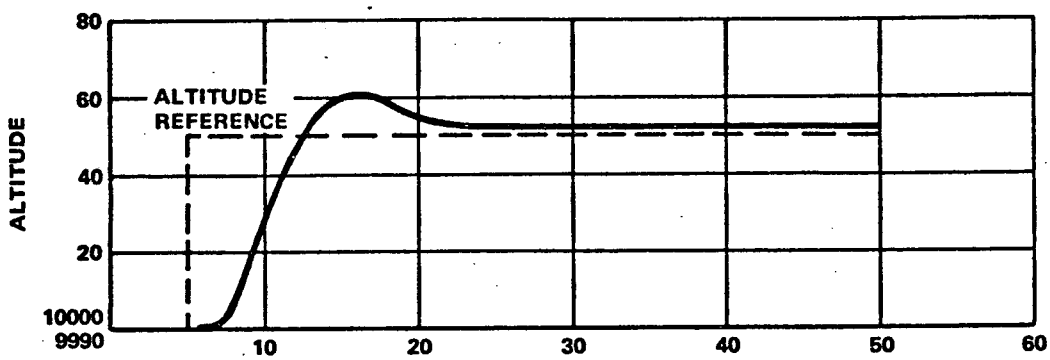

ALTITUDE HOLD PARAMETERS:

LH3	= 100 FT
TV3	= 0.5 SEC
A2	= 0.04
A3	= 1.6
KHNOM	= 0.10 DEG/FT
TC5	= 1.0 SEC
TF4	= 4.0 SEC
TF5	= 5.0 SEC

Figure 5-22
Altitude Hold Step Response Tests
V = 296 kt

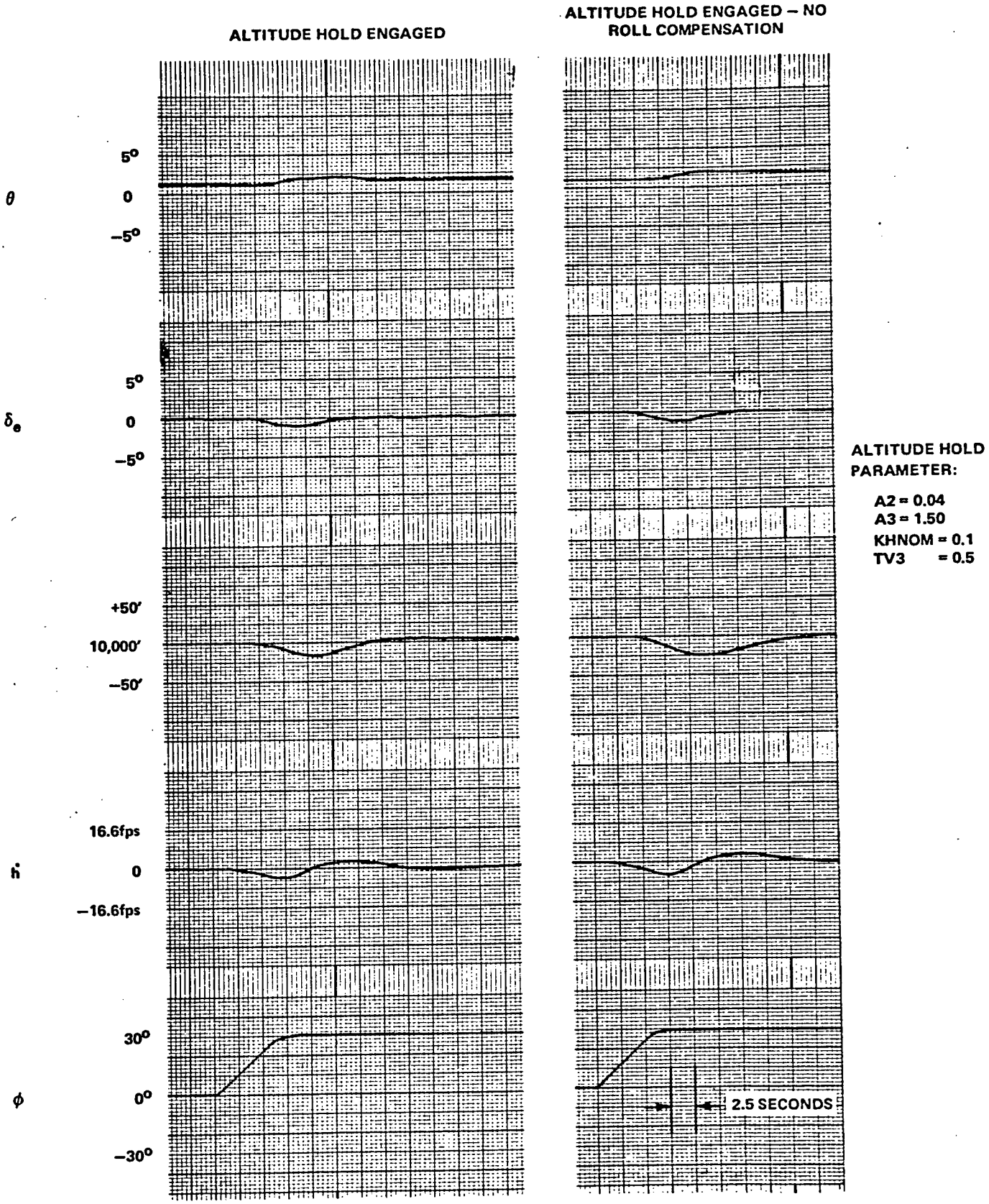

Figure 5-23
Performance of Altitude Hold During
A Turn with a 30° Bank Angle,
V = 296 Knots

SECTION VI

VERTICAL GUIDANCE - FINAL APPROACH AND LANDING

A. CONTROL LAW DEFINITION

1. General

The vertical flight path, landing guidance laws covered in this section relate to the capture or acquisition of an ILS glide path, the precise tracking of that glide path to an altitude somewhat below 100 feet, the maintenance of that path below 100 feet until a flareout initiate altitude is reached, and the flareout maneuver to achieve desired touchdown velocity and position objectives.

A large variety of guidance schemes for automatic landing have been studied and applied in actual operational systems. (See Reference 3, for example.) When viewed mathematically, these different schemes can generally be reduced to almost identical systems. The motivations for different guidance laws, however, are not usually dictated by performance benefits. System design criteria involve availability of state variable information, the quality of the available measurement and considerations related to the redundancy architecture of the total system. In this latter category, for example, the choice of sensor may be dictated by the cost of providing a triple or quadruple set to meet fail-operative and monitoring requirements. Another consideration in system design is the selection of a system configuration that minimizes or avoids the introduction of new sensors as the flight progresses toward touchdown. Thus, the activation of computation sequences requiring new sensors at flareout is undesirable because the validity and integrity of the total system, including all sensors, should have been established by actual operation prior to initiation of flareout.

The comparative evaluations of the relative merits of different guidance configurations, when viewed from such operational considerations, are beyond the scope of this report. We are concerned here only with the problem of static and dynamic performance in the presence of reasonable disturbances. Nevertheless, the

computation sequences defined herein are realistic in that they involve filters that are employed for practical considerations not apparent if one views the problem as a mathematical abstraction. The specification of synthesis procedures for developing a vertical velocity signal from inertial, barometric, and radar measurements is an example of this realistic approach. Mathematically, all that is required is a vertical velocity term, $\dot{h}$; but practically, we are defining the computer's computation load associated with generating a usable $\dot{h}$ signal.

Although some consideration is given to the problem of state variable synthesis (as mentioned above for the case of $\dot{h}$), the scope of this report does not, in general, cover the problem of state estimation. For example, any control law using vertical acceleration, $\ddot{h}$, can obtain the required function by measuring the variable directly or by employing compensators to synthesize the desired term from $\dot{h}$ data. Choosing the correct approach involves analysis of the measurement processes for noise and bandwidth characteristics. This type of analysis is, in general, beyond the scope of this report. For complete generality, the guidance laws are specified in terms of the various state variables as though these variables are measured directly. This should not preclude the ultimate consideration of compensators in place of some of these variables.

Two generic types of systems are described in this report. The first is the pitch command landing system. It is consistent with the concept of pitch steering to adjust vertical flight paths. All steering commands may be viewed as pitch commands into a pitch attitude inner loop. The other type of system eliminates the pitch attitude inner loop entirely and replaces it with a basic vertical velocity control system augmented with pitch rate feedback for damping and perhaps vertical acceleration for increased tightness (increased bandwidth). The vertical velocity system is activated at the time of glide slope capture and continues to touchdown. It has some practical advantages in the mechanization of redundant systems that must use all flareout sensors in an active manner prior to flareout initiation. It also can have some performance advantages in minimizing flight path disturbances resulting from gusts and wind shears. These performance advantages are not clearly established if compared against an optimally compensated pitch system. Both systems are described but only the pitch steering systems were simulated for this report.

2. Glide Slope Control Geometry

Figure 6-1 summarizes the geometry of an aircraft penetrating the ILS glide slope to the point where the capture maneuver is initiated. The parameters that are used in the control problem are λ, the angular deviation from the center of the beam; $\gamma_{G/S}$, the nominal beam angle (2.5 degrees for discussions in this report); and R, the range from the intercept of the glide slope with the runway. Note that the polarity of λ is positive when the aircraft is above the center of the beam. We assume knowledge of R in the airborne computer. (This assumes an area navigation capability or a DME colocated with the localizer transmitter.) The aircraft can penetrate the glide path from above or below, but it is obviously desirable to have a standard intercept procedure, usually from a constant altitude of about 1500 feet. The guidance laws defined in the subsequent paragraphs make provision for penetration at off-nominal altitudes and initial flight path angles.

3. Glide Path Capture Phase -- Pitch Command System

When the aircraft penetrates the outer boundaries of the glide slope beam, it should have reached a stable situation along the center of the localizer beam, and terminal approach speed and flap settings should have been established.

If a consistent vertical acceleration maneuver is desired for capturing the glide slope regardless of initial altitude, then the value of λ for starting the capture maneuver should vary with range R. If we make the approximation that the distance travelled from the start of the capture maneuver at λ_o to the intercept of the beam center ($\lambda = 0$) is equal to the horizontal component of that distance, Δx, then

$$\Delta x \approx \frac{R_o \lambda_o}{\gamma_{G/S}} = Vt \qquad (6\text{-}1)$$

where

Δx = distance to beam center

V = velocity (with respect to ground)

t = time to beam center

$\gamma_{G/S}$ = glide slope angle (from aircraft viewpoint)

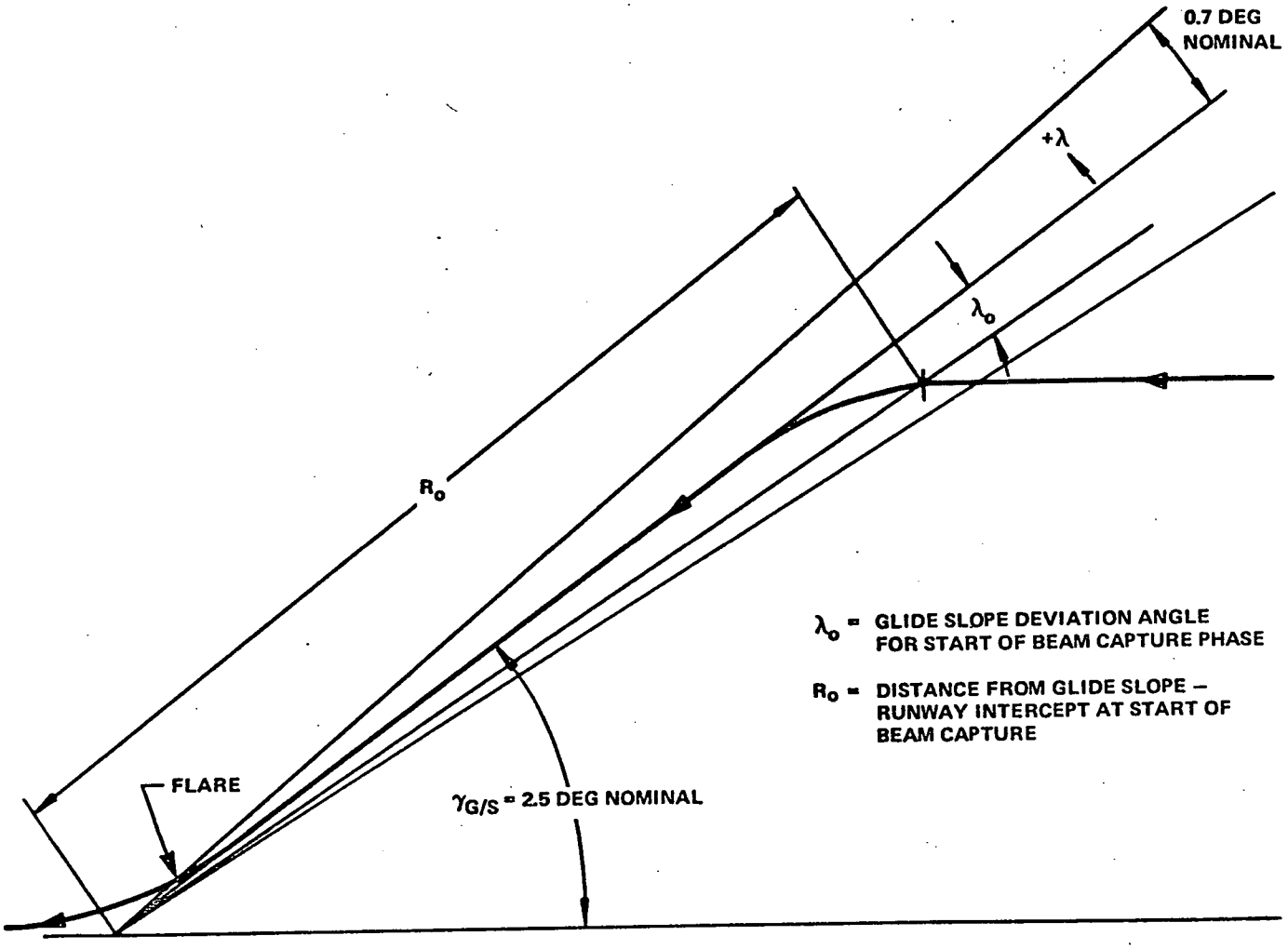

Figure 6-1
Glide Slope Control Geometry

For a constant vertical acceleration equal to $\ddot{h}_c$,

$$\frac{\ddot{h}_c t}{V} = \Delta\gamma \tag{6-2}$$

where $\Delta\gamma$ is the change in flight path angle required to align the aircraft with the beam center.

$$\Delta\gamma = \gamma_{G/S} - \gamma_o \tag{6-3}$$

where γ_o, the initial flight path angle, is zero if the intercept proceeds from a constant altitude initial condition.

Solving for λ_o from equations (6-1) and (6-2) yields

$$\lambda_o = \left(\frac{V^2}{R}\right)\left(\frac{\Delta\gamma\ \gamma_{G/S}}{\ddot{h}_c}\right) \tag{6-4}$$

A reasonable value of $\ddot{h}_c$ is 1.0 ft/sec^2. Thus, a constant altitude beam penetration at 1500 feet of altitude would define a λ_o as follows:

$$\left.\begin{aligned} V &= 238 \text{ ft/sec} \\ \Delta\gamma &= -2.5/57.3 \text{ radians} \\ \gamma_{G/S} &= -2.5/57.3 \text{ radians} \\ R &= 42{,}700 \\ \ddot{h}_c &= -1 \text{ ft/sec}^2 \end{aligned}\right\} \quad \begin{aligned} &\lambda_o = -0.145 \text{ degrees or} \\ &\frac{0.145}{0.70} \times 150 = 31.1 \\ &\text{microamperes of beam signal} \end{aligned}$$

Some additional logic must be added to the glide slope capture initiate computation to cope with unusual initial conditions. If this logic is not added, a dangerous condition can exist in which the aircraft does not capture the glide path until too low an altitude is reached. For example, if the outer boundary of the glide slope is penetrated from below while the aircraft is descending in a -2.2 degree flight path angle, the specified capture procedure would not initiate glide path capture until the aircraft is near the ground. The aircraft was descending almost parallel to the beam. A corresponding condition exists when the aircraft is above the beam at a flight path angle of about -2.8 degrees. In

these cases the capture phase should be eliminated and the glide path tracking mode should be initiated (without integral control). The logic to cope with such situations may be summarized as follows:

Engage Glide Slope Tracking Mode = G

Abort Landing = A

$$G = (\gamma < -2°) \cdot (\lambda < 0) \cdot (h > 600 \text{ ft}) \cdot (|\lambda| < 0.75|\lambda|_{max})$$

too steep a descent for reasonable glide slope intercept	below beam center	above 600 feet	not too far from beam center for reasonable acquisition

$$+ (\gamma > -2.5°) \cdot (\lambda > 0) \cdot (h > 600 \text{ ft}) \cdot (|\lambda| < 0.75|\lambda|_{max})$$

too shallow a descent for reasonable glide slope intercept	above beam center	above 600 ft	not too far from beam center

$$A = (h < 600 \text{ ft}) \cdot (\overline{G} + \overline{C})$$

below 600 ft	neither the tracking or capture mode have been initiated

Figure 6-2 illustrates the computation sequence to initiate glide slope capture [equation (6-4)]. It shows that when the capture sequence is initiated (the mode logic is defined by c) a predictive pitch command θ'_{c_1} is activated. This predictive command is equivalent to the required change in flight path angle since angle of attack and speed are assumed to remain constant through the throttle loops. Thus,

$$\theta'_{c_1} = \left[\frac{\dot{h}_{co}}{V}\right] - \gamma_{G/S} \tag{6-5}$$

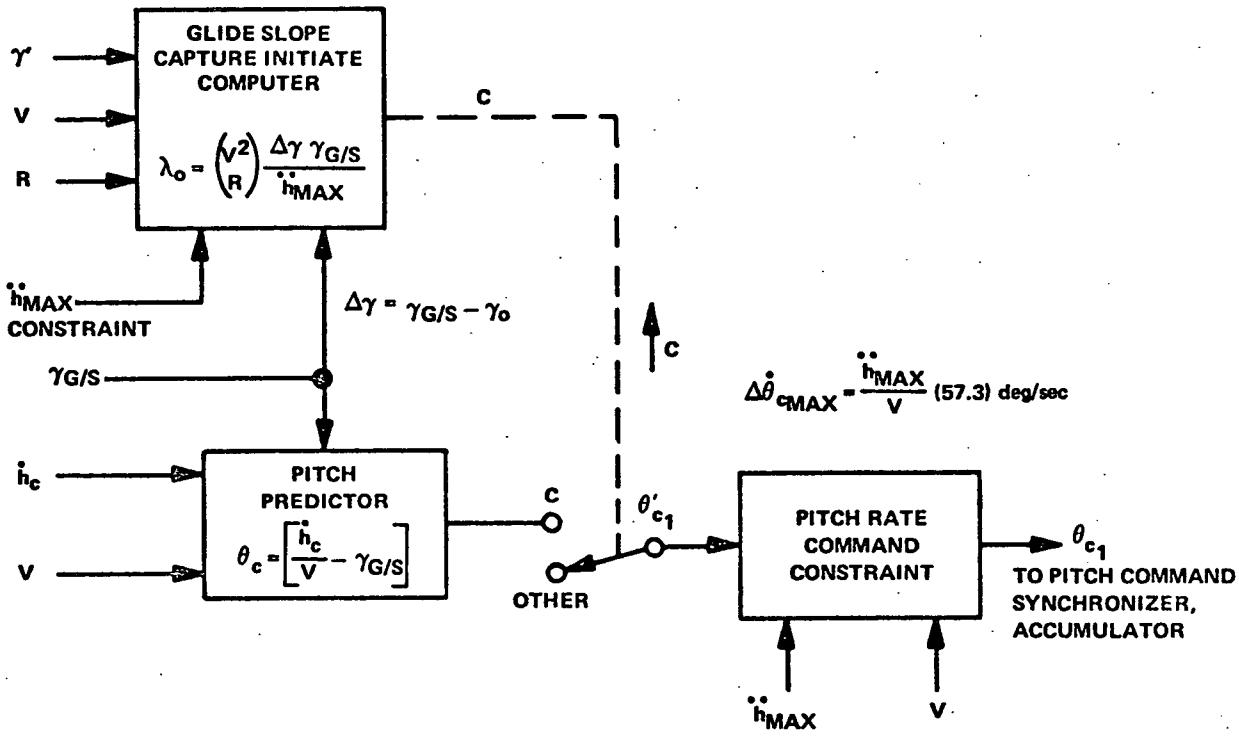

Figure 6-2
Glide Slope Capture Initiation -
Block Diagram-Pitch Command System

where $\dot{h}_{co}$ is the compensated vertical speed existing at initiation of the capture mode. Note that $\dot{h}_c$ is a compensated or synthesized vertical velocity signal generated by blending inertial and barometric data as defined in Section V on vertical guidance (non-landing).

The predictive pitch command, θ'_{c_1}, is constrained in rate to correspond to a vertical acceleration limit, $\ddot{h}_{MAX}$. Thus,

$$\Delta\dot{\theta}_{c_1} = \frac{\ddot{h}_{MAX}}{V} (57.3) \text{ deg/sec} \tag{6-6}$$

The constrained pitch command is referred to as θ_{c_1}.

At the initiation of the capture mode, c, all previously existing pitch commands, θ_c, are held at their last value prior to mode transition. In addition to the pitch command θ_{c_1}, a vertical speed mode is activated. This mode is shown in Figure 6-3 as contributing to the pitch command θ_{c_2}. The vertical speed control law that is activated at initiation of c (and remains active through the remainder of glide slope flight) is

$$\theta_{c_2} = \left[\dot{h}_c - \dot{h}_{ref}\right] k_{\dot{h}} = \left[\dot{h}_c - V\gamma_{G/S}\right] k_{\dot{h}} \tag{6-7}$$

where θ_{c_2} is rate constrained to correspond to the acceleration limit by controlling the rate of change of $\dot{h}_{ref}$ and $\dot{h}_c$ is compensated $\dot{h}$. The complete control law for capture is therefore

$$\theta_{c_{capture}} = \theta_{c_1} + \theta_{c_2} = \left(\frac{\dot{h}_{co}}{V} - \gamma_{G/S}\right) + \left[\dot{h}_c - V\gamma_{G/S}\right] k_{\dot{h}} \tag{6-8}$$

4. <u>Glide Slope Tracking -- Pitch Command System</u>

The glide slope tracking phase begins when the beam capture has been completed. The following criteria indicate that the beam has been captured:

- The reference flight path angle, $\gamma_{G/S}$, has been achieved or exceeded and λ remains negative (below beam center) -- (overshoot from above or undershoot from below).

- The reference flight path angle, $\gamma_{G/S}$, has not been fully attained, but λ reached zero or became positive -- (overshoot from below or undershoot from above).

In analog systems where failures in beam detector circuits may occur and we do not wish to abort the approach, a timing circuit is often added as a back-up to indicate glide slope tracking. Thus, if a nominal glide slope descent vertical speed of 10 ft/sec is assumed and a minimum capture maneuver of 1.0 ft/sec^2 is commanded, then the desired descent should have been established in 10 seconds so that when $t - t_o$ exceeds 10, the glide slope tracking phase G is initiated - even if the other detectors had not operated. This timing logic is included in the control logic computations, illustrated in Figure 6-3, although its utility is doubtful in the digital system. In summary, the glide slope tracking phase, G, is initiated in accordance with the following logic equation:

$$G = \left[\gamma_{error} \leq 0\right] \cdot \left[\lambda \leq 0\right]$$

$$+ \left[\gamma_{error} \geq 0\right] \cdot \left[\lambda \geq 0\right]$$

$$+ \left[t - t_o > 10 \text{ seconds}\right] \qquad (6\text{-}9)$$

(6-10)

where $\gamma_{error} = (\gamma - \gamma_{G/S}) = (\gamma + 2.5°)$.

At initiation of the glide slope tracking phase, the $\dot{h}$ loop remains closed and the λ (beam) control loop is activated as shown in Figure 6-3. The control law pitch command is:

$$\theta_{c_2} = \left(\dot{h}_c - \dot{h}_{REF}\right) k_{\dot{h}} + \lambda \left(\frac{k_\lambda}{\tau_1 s + 1}\right) + \frac{k_I}{s} \lambda \qquad (6\text{-}11)$$

where the gains k_λ and k_I are programmed as a function of radio altitude (or range to touchdown).

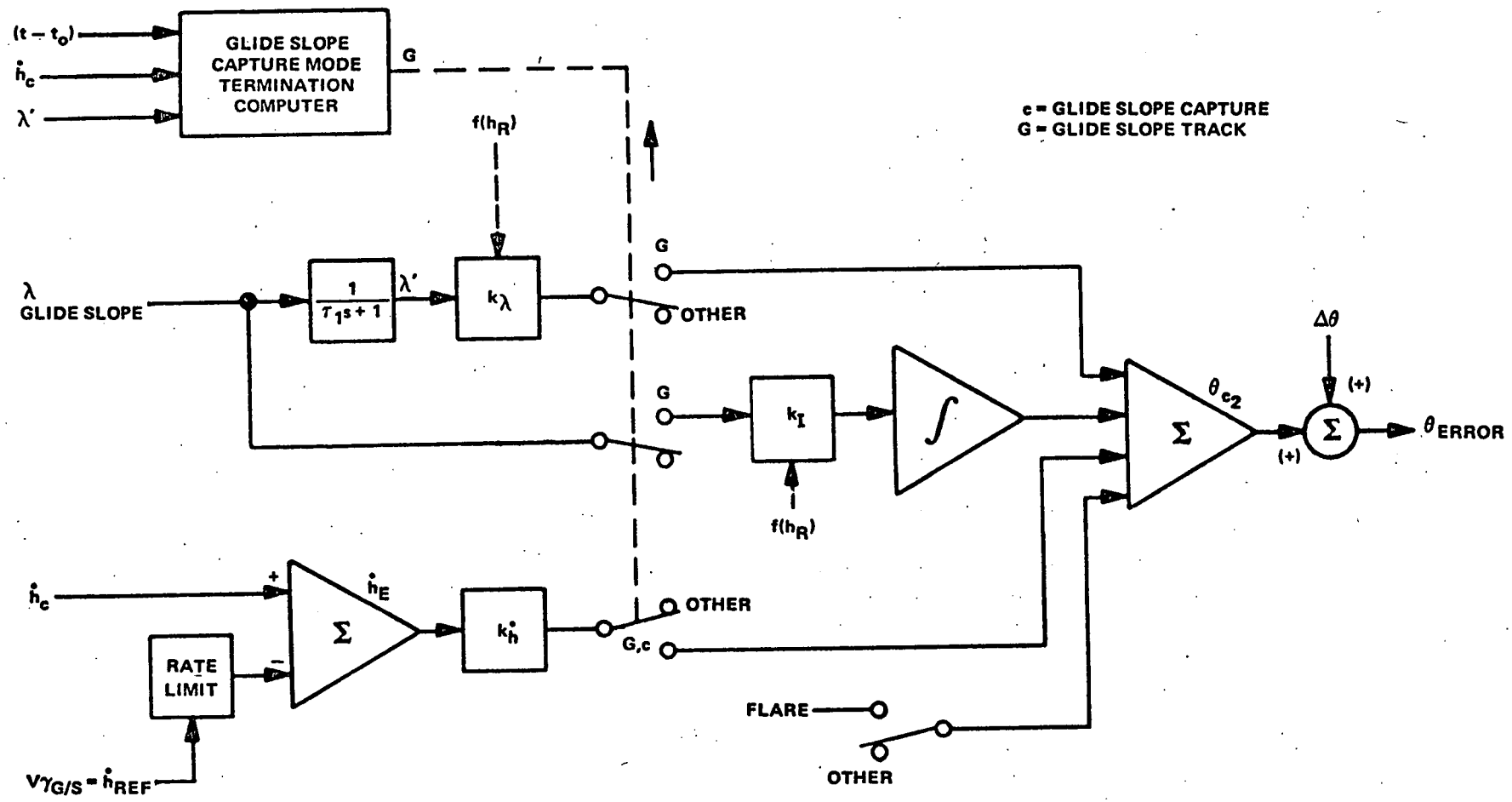

Figure 6-3
Glide Slope Tracking Block Diagram
Pitch Command System

Since a radio altimeter is needed for the flareout phase, it is desirable that it be used during the glide path tracking phase for the gain programming function. Figure 6-4 illustrates the gain function as a gain ratio versus radio altitude. Since many terrains are sufficiently irregular to question the use of such a gain programmer, some compromises are usually incorporated to minimize rough terrain problems. For example, the radio altitude sensing logic incorporates a unidirectional blocking function that does not allow the h_R input to the gain computer to increase, but always holds it at the minimum value of altitude previously attained. The function g, shown in Figure 6-4, is applied to both k_λ and k_I. Note that the integrator gain reduction must be accomplished at the input to the integrator and never at the output of the integrator. It is also noted that the integrator may be switched on and off on the basis of an integrator control logic scheme designed to improve stability. Such a logic scheme would cut out the integrator when the error plus error rate exceeds specified thresholds. This type of function is not included in this study.

Although the guidance equations have been specified with a vertical speed loop it is apparent that the vertical speed terms can be replaced directly with a flight path angle loop (with the application of the appropriate V gain adjustment). Historically, $\dot{h}$ rather than γ has been used because of such operational considerations as:

- $\dot{h}$ is available from simple analog interfaces
- V data is not generally available to the autopilot

For the digital autopilot these considerations are not as pertinent and, consequently, the γ loop is certainly an acceptable alternate.

5. Flareout Control -- Pitch Command System

As the aircraft tracks the glide slope below 100 feet, dependency upon the glide slope signal diminishes. The gain program reduces glide slope gains initially to compensate for the fact that an angular beam results in infinite gain at its origin. Below 100 feet, the validity of glide slope signals become doubtful and the gain reduction program drives k_λ and k_I to zero at an altitude of about 60 feet. The flight path control is primarily maintained by the pitch

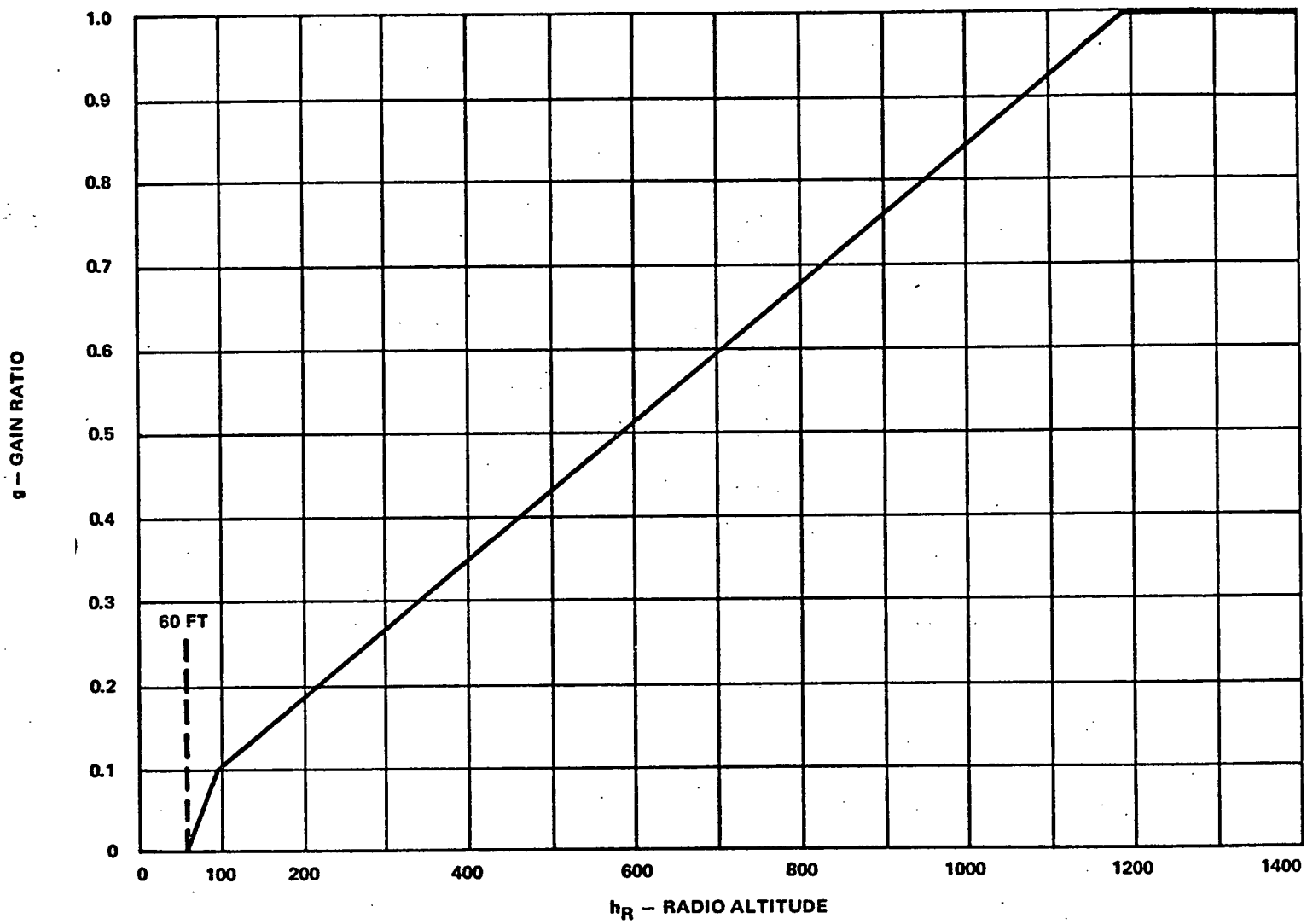

Figure 6-4
Glide Slope Gain Programming

attitude and vertical speed loops below 100 feet. The radio altimeter will activate the flareout mode at about 35 feet so that from 60 feet to 35 feet (about 2.5 seconds) no glide slope information can be used. Flareout initiates a new set of control laws shown in the block diagram in Figure 6-5. The θ_{c_2} summer switches from the previous $\dot{h}$ control loop, holding the last value of θ_{c_2} prior to mode transition.

Three types of flareout laws are described. They are illustrated in Figures 6-5a, b, and c. The first (Figure 6-5a) is the exponential flare controller.

a. Exponential Flare Controller

The control equations are:

$$\theta_{c_2} = \theta_p(t) + k_F \left\{ h + \frac{k_{\dot{h}}}{k_F} (\dot{h}_c - \dot{h}_F) \right\} \left[1 + \frac{k_2}{s} \right] + k_{\ddot{h}} \ddot{h} \qquad (6\text{-}12)$$

Vertical speed at touchdown = $\dot{h}_F$

Flare initiate altitude = h_o

$$h_o = h_1 - f\,\dot{h} \qquad (6\text{-}13)$$

Thus if $h_1 = 20$, $f = 2$, and $\dot{h} = -10$ ft/sec, the flare initiate altitude would be 40 feet. If $\dot{h}$ had been -15 ft/sec, the flare initiate altitude would be increased to 50 feet.

The predictive term or feedforward pitch command ideally creates the maneuver that satisfies the closed loop control law. The predictive commands are nose-up signals of the form:

$$\theta_p(s) = \frac{\theta_1}{\tau_2 s + 1} + \frac{\dot{\theta}_2}{s} \qquad (6\text{-}14)$$

or in the time domain,

$$\theta_p(t) = \theta_1 \left(1 - e^{-t/\tau_2}\right) + \int \dot{\theta}_2 \, dt, \qquad (6\text{-}15)$$

Where θ_1 and θ_2 are constants.

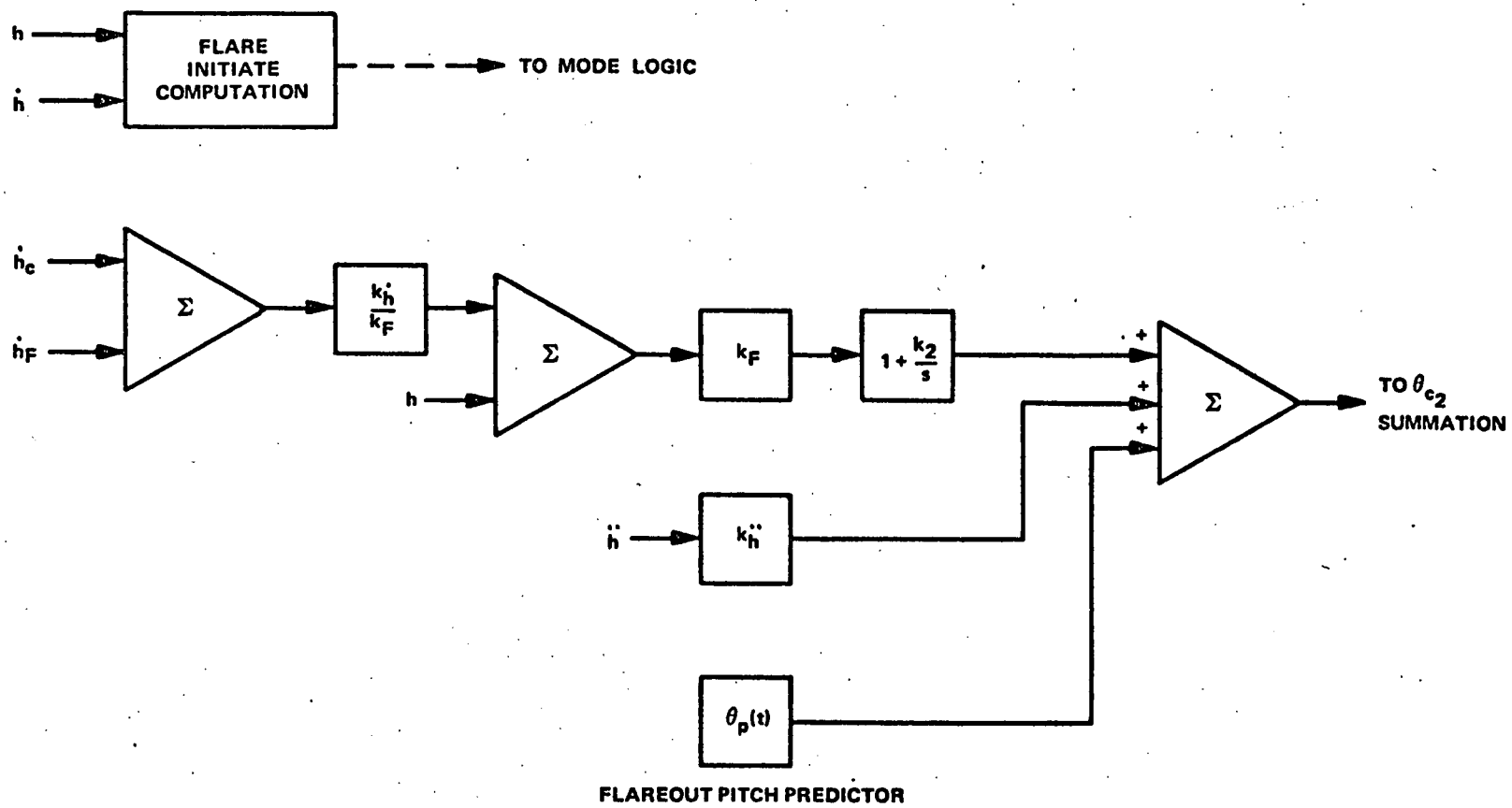

Figure 6-5a
Exponential Flareout Controller Block Diagram

NOTE: refer to 6-5b

The values of θ_1 and $\dot{\theta}_2$ are determined by the aircraft characteristics and especially the ground effect aerodynamics. Constraints should be applied to the ramp term ($\dot{\theta}_2$) so that an excessive command does not develop if the flareout produces an extended float characteristic. Thus $\dot{\theta}_2$ should be brought to zero after a specified time duration. Also, $\dot{\theta}_2$ may be changed to compensate for off nominal velocity conditions. Note that the $\ddot{h}$ term attempts to oppose the flare-out maneuver since the $\ddot{h}$ reference is zero while a finite (and changing) $\ddot{h}$ is required for the flareout. The predictive pitch commands contain the necessary bias program to compensate for the nominal $\ddot{h}$ signals. Thus, the useful $\ddot{h}$ information will be the result of deviations from the nominal trajectory. A tight $\ddot{h}$ loop is essential for minimizing flight path disturbances due to turbulence.

The touchdown reference terminal velocity is $\dot{h}_F$. A value of about -1.5 ft/sec is desirable, but values of about -2.0 ft/sec to -2.5 ft/sec are being used to minimize the downrange excursion of the aircraft during the flare.

b. Vertical Velocity Flareout Controller

The exponential controller is converted to a vertical velocity controller by removing the h input from the control law. Thus, its control equation is

$$\theta_{c_2} = \theta_p(t) + k_{\dot{h}} (\dot{h}_c - \dot{h}_F) \left[1 + \frac{k_2}{s}\right] + k_{\ddot{h}} \ddot{h} \tag{6-16}$$

The rationale for its use over the exponential controller is that it can provide tighter control to the touchdown vertical velocity, $\dot{h}_F$. It may do this, however, at the expense of fore-aft dispersion on the runway.

c. Acceleration Flareout Controller

A terminal controller that always attempts to satisfy the terminal vertical velocity requirement, $\dot{h}_F$, by computing and controlling to the precise acceleration that will allow the aircraft to fly an exponential flare to the desired terminal condition can be derived as follows:

An exponential flareout is achieved if

$$h + k_{\dot{h}} \left[\dot{h} - \dot{h}_F\right] = 0 \tag{6-17}$$

Differentiating this equation gives

$$\dot{h} + k_{\dot{h}} \ddot{h} = 0 \text{ or } \ddot{h} = -\frac{\dot{h}}{k_{\dot{h}}} \tag{6-18}$$

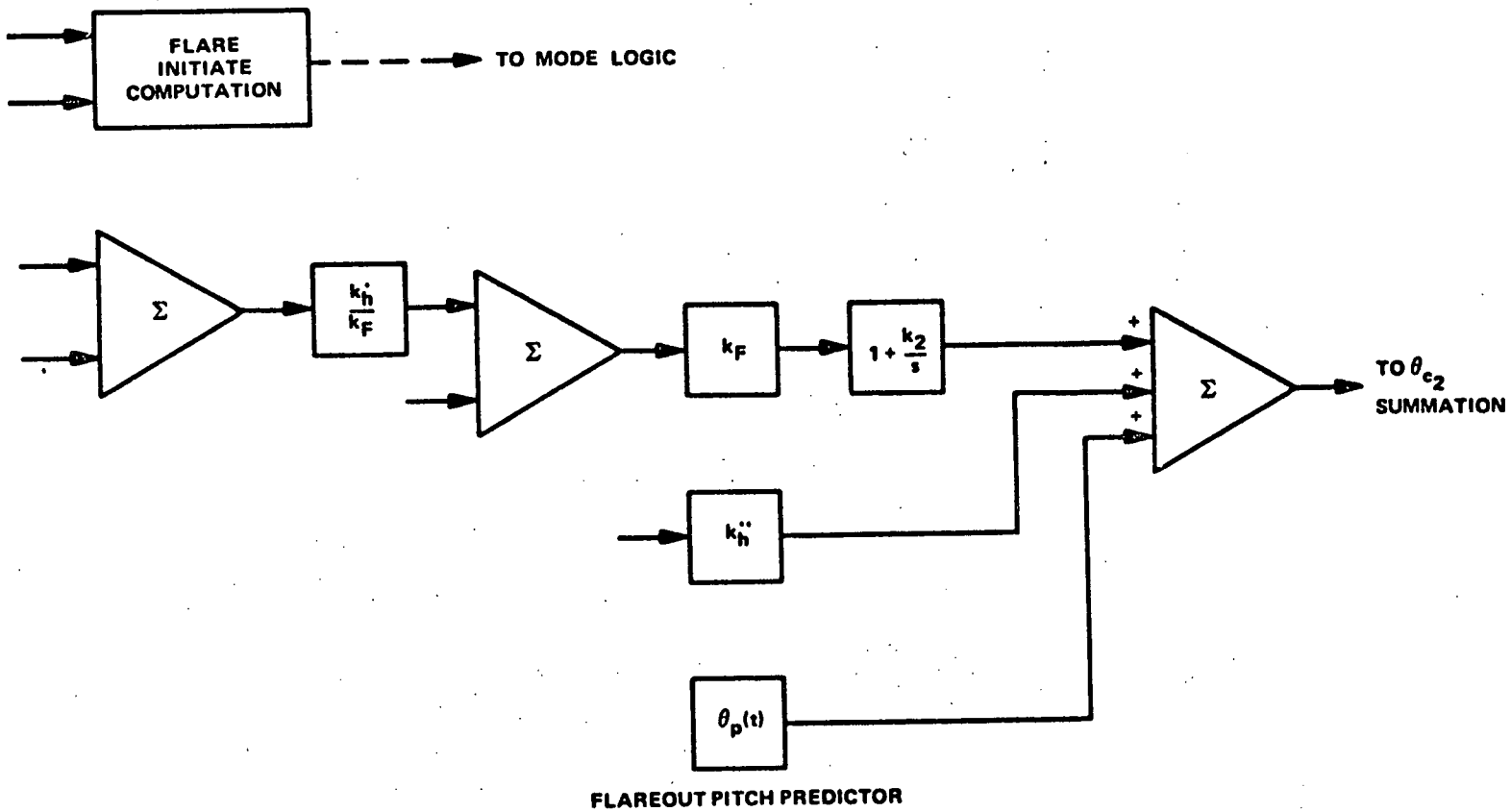

Figure 6-5b
Vertical Velocity Flareout Controller
(Same as Figure 6-5a but remove h input)

For any initial h and $\dot{h}$ state, if we wish to perform an exponential flareout that satisfies both the terminal requirements and the initial state, a specific value of $k_{\dot{h}}$ in equation (6-17) must be satisfied. From equation (6-17), it is

$$k_{\dot{h}} = \frac{-h}{\dot{h} - \dot{h}_F} \tag{6-19}$$

Substituting equation (6-19) into (6-18) gives

$$\ddot{h}_{ref} = \left[\frac{\dot{h}^2}{h} - \frac{\dot{h}_F \dot{h}}{h}\right] \tag{6-20}$$

Thus if we always flew the $\ddot{h}_{ref}$ defined by equation (6-20), we will follow an exponential path toward $\dot{h}_F$ regardless of our initial state. The computed value of $\ddot{h}_{ref}$ can be used as a reference acceleration and a tight acceleration loop closed to try to attain the value of $\ddot{h}$ computed by equation (6-20). Such a controller would be of the form

$$\theta_{c_2} = \theta_p(t) + k_{\ddot{h}} (\ddot{h} - \ddot{h}_{ref}) \tag{6-21}$$

The predictive pitch command sets up the nominal flareouts as in the previous types of flareout controllers. In this case however, for best results, the predictive term should start the flareout maneuver with $k_{\ddot{h}} = 0$ until the vertical speed is reduced to about one half its original value. Since the $\ddot{h}_{ref}$ computation diverges at h = 0, the computation is constrained by letting h = 2 be the minimum allowable value of h. Also, equation (6-20) becomes erroneous if $\dot{h}$ should become positive. To prevent this, $\ddot{h}_{ref}$ is set to zero when $\dot{h}$ reaches about -2.5 ft/sec (for $\dot{h}_F$ = -2 ft/sec). Figure 6-5c shows a block diagram of this system with the various logic computations needed to control the $\ddot{h}$ loop. The loop is closed on logic state M and the $\ddot{h}_{ref}$ is set to zero on logic state N.

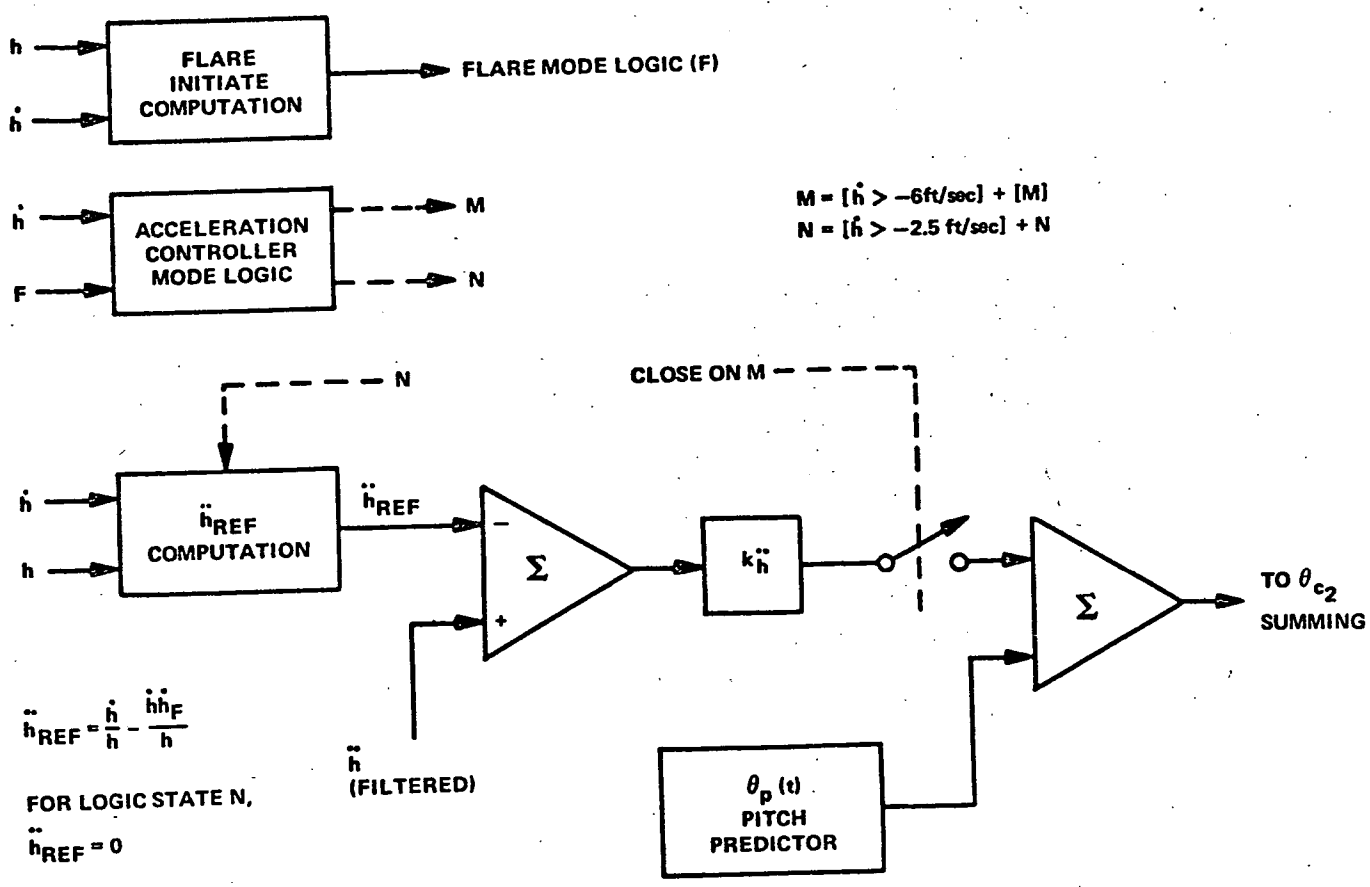

Figure 6-5c
Acceleration Flareout Controller

d. Comparison of Flareout Controllers

The three types of flareout controllers described above can provide satisfactory performance when properly optimized. It is difficult, however, to make a judgment on which is best. All three systems are actually quite similar. They depend upon the predictive term for most of the flareout maneuver while the closed loop controls act as a vernier. Ultimately, the best system is the one that provides the tightest flight path control in the presence of wind and turbulence disturbances and perhaps measurement errors. The mode of operation of all three systems can be described in terms of the h, $\dot{h}$ phase plane. Figure 6-6 shows these phase planes for each system. The exponential flareout system (Figure 6-6a) always tries to control to a fixed line on the phase plane. A large vehicle has difficulty in achieving an $h + 5\dot{h}$ line. (It typically can achieve an $h + 2\dot{h}$ line.) Also an $h + 2\dot{h}$ controller will give higher accelerations than an $h + 5\dot{h}$ system. The higher gain in $\dot{h}$ is desired for control tightness but it does not give the best trajectory. What is more significant, however, is that if the aircraft has deviated from the reference $h + k_{\dot{h}}\dot{h}$ line, it generally does not have the control bandwidth to reacquire that line in the remaining time. This is where the acceleration controller [Figure 6-6(c)] should have some advantage. It does not try to recover to the original reference line but always computes the minimum acceleration needed to complete an exponential flareout. This controller, however, is also restricted by the large aircraft's inability to achieve rapid acceleration changes.

Figure 6-6(b) shows the vertical speed controller's phase plane trajectory. It only tries to achieve the terminal $\dot{h}$ reference. It should nominally reach $\dot{h}_F$ at about 8 feet from touchdown. If it flares too high it will tend to land at $\dot{h}_F$ but with a penalty in fore-aft excursion on the runway. If it flares too low it may not reach the touchdown reference $\dot{h}$. There are techniques for adding additional intelligence to this controller so that it can minimize these penalties. Likewise, there are techniques which can improve the performance of the other two types of flareout controllers. These techniques are beyond the scope of this study. Their application would be for situations having touchdown position and $\dot{h}$ requirements more severe than those now being used for transport Category III landings.

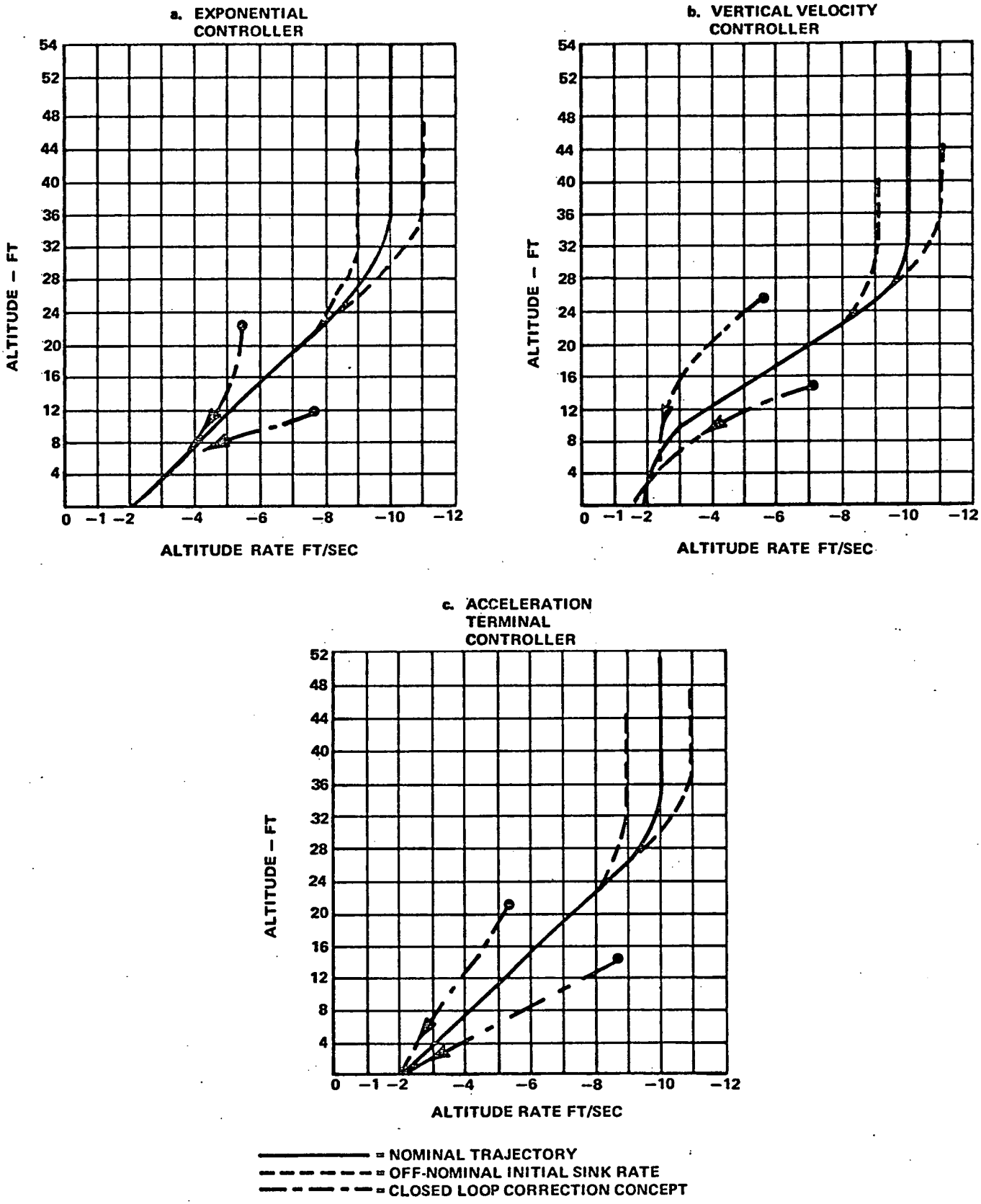

Figure 6-6
Phase Plane for Three Types of
Flareout Controllers

6. Glide Slope Capture and Tracking - Vertical Speed Control System

All of the guidance laws discussed to this point were defined as part of a pitch steering system. The basic autopilot mode is pitch attitude hold and all guidance laws are defined as pitch attitude commands. An alternate scheme uses vertical speed, $\dot{h}$, or flight path angle, γ, in place of pitch attitude as the basic autopilot mode. Pitch rate is used to damp this mode but pitch attitude feedback is not used. The elimination of the pitch attitude feedback allows tighter flight path control in the presence of turbulence and wind shears. The reason for this improved capability will be discussed later under "Stability Considerations". Consider now the implementation of such a system only for the landing modes. Thus for the cruise modes, the autopilot retains the pitch attitude steering. At the start of the glide slope capture phase, c, it completely eliminates the pitch attitude loop. As shown on Figure 6-7, the pitch loop that is used during the cruise steering modes generates a control signal, θ_E. The landing computer tracks θ_E in a synchronizer and holds the value existing at mode transition. This value is retained as δ_{E_o} in the $\delta_{E_{land}}$ summing stage. Glide slope capture starts at the time λ_o is reached where λ_o is computed as in equation (6-4) for the pitch command system. At the instant of the c mode transition, δ_E control law changes to

$$\delta_{E_{land}} = G_1(s)\ q + \delta_{E_o} + k_{\dot{h}}\ \dot{h}_{error} + k_{\ddot{h}}\ \ddot{h}_{error} \tag{6-22}$$

where $G_1(s)$ is the pitch rate control law as it existed in the pitch control system except that a gain increase may now be needed.

The notations $k_{\dot{h}}$ and $k_{\ddot{h}}$ are used for the vertical speed and acceleration gains as in the previous system, but the gains are not the same as for the pitch command system. For the capture mode

$$\dot{h}_{error} = \dot{h}_c - \dot{h}_{ref} \tag{6-23}$$

and the acceleration constraints are applied to the change in $\dot{h}_{ref}$ as in the pitch steering system.

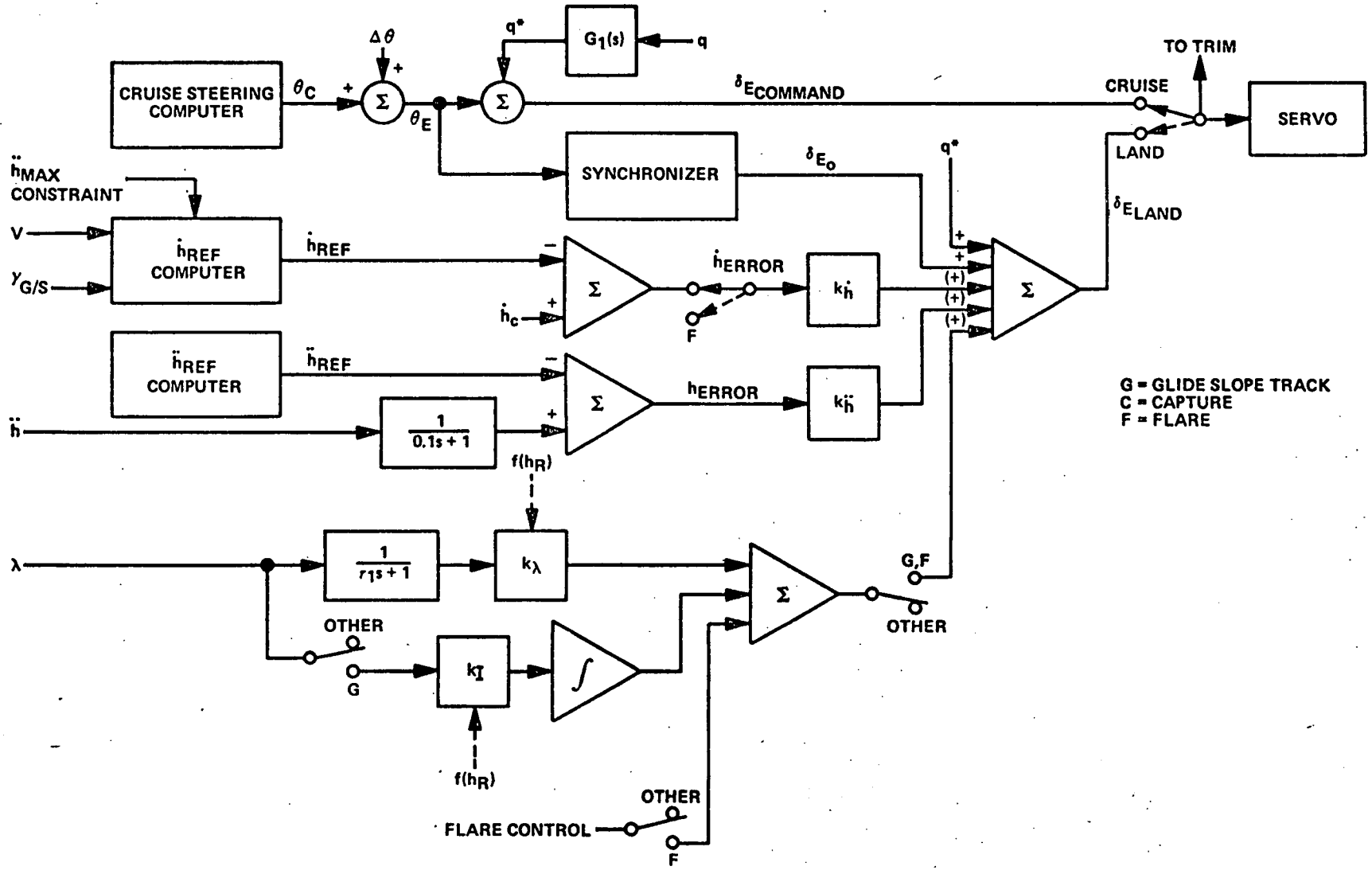

Figure 6-7
Glide Slope Capture and Tracking Block Diagram-Vertical Speed Control System

The vertical acceleration loop is added to improve control tightness (although a lead compensator on $\dot{h}$ error could have theoretically achieved the same purpose). The vertical acceleration error is

$$\ddot{h}_{error} = \ddot{h} - \ddot{h}_{ref} \tag{6-24}$$

where the computation of $\ddot{h}_{ref}$ is as follows:

$$\ddot{h}_{ref} = \left[-\text{sign } \dot{h}_{error}\right] \left|\ddot{h}_{max}\right| \tag{6-25}$$

if $\left|\dot{h}_{error}\right| > 2$ ft/sec

and

$$\ddot{h}_{ref} = 0$$

if $\left|\dot{h}_{error}\right| \leqslant 2$ ft/sec (6-26)

The criteria for terminating the capture phase are identical to those of equation (6-9). This starts the glide slope tracking or G phase. The $\delta_{E_{land}}$ control law for the G phase is:

$$\delta_{E_{land}} = qG_1(s) + \delta_{E_o} + k_{\dot{h}}\dot{h}_e + k_{\ddot{h}}\ddot{h} + \frac{k_\lambda}{\tau_1 s + 1}\lambda + \frac{k_I}{s}\lambda \tag{6-27}$$

where $\dot{h}_e$ is defined as in equation (6-24), and k_λ and k_I are programmed per radio altitude as in Figure 6-4. Note that $\ddot{h}$ reference is zero in the $\ddot{h}$ loop.

7. <u>Flareout - Vertical Speed Control System</u>

The flareout control law is switched into the summing point shown on Figure 6-7 while the previous $\dot{h}$ loop is disengaged. The new computations added for flareout are identical to those shown for the pitch command system except that here a δ_E feedforward or predictive input is used. The flareout control law is

$$\delta_{E_{land}} = qG_1(s) + \delta_{E_o} + \left[h_c + \frac{k_{\dot{h}}}{k_F}(\dot{h}_c - \dot{h}_F)\right]\left[1 + \frac{k_2}{s}\right] k_F + k_{\ddot{h}}\ddot{h}_e + \delta_{E_P} \tag{6-28}$$

The three types of flareout controllers discussed previously for the pitch steering system can be mechanized with equation (6-28) by defining the $\ddot{h}_{ref}$ and controlling the h and $\dot{h}$ feedbacks. The δ_{E_P}, if required, should be similar dynamically to the θ_p of equations (6-14) and (6-15).

8. Throttle Control Considerations

The flareout control parameters, especially the use of predictive feedforward commands, are sensitive to the throttle control program. A consistent throttle procedure is needed to assure consistent performance. Thus, all flareout control parameters must be optimized on the basis of an assumed throttle program. The following throttle control procedure is recommended for the flareout:

- At $h \approx 50$ feet when the flight path control is maintaining rate of descent, start a ramp throttle retard program. The thrust retard should be about 5.0 percent maximum rated thrust per second. The retard ramp continues to zero thrust, even beyond the normal autothrottle 10 percent lower limit.

- If thrust started at 50 percent maximum rated thrust, the retard program should end with about 10 percent maximum rated thrust remaining at touchdown. Longer flare trajectories can have zero thrust remaining at touchdown.

- Flareout starts at about 35 feet. Thus, the throttle retard program preceded flare by about 1.5 seconds.

9. Stability Considerations

a. Pitch Command System

Stability aspects of the glide slope control and flareout control are identical to those of the nonlanding vertical flight path guidance laws. The vertical speed and altitude control stability analysis was discussed in Section V, "Vertical Flight Path Guidance Laws (Nonlanding)". The vertical speed control problem appears in the glide path capture phase. The glide slope tracking phase is mathematically identical to the altitude control problem from the viewpoint of stability. The reference altitude line is slanted to the glide path angle. The stability block diagrams and associated root loci for these two modes were shown previously in Figures 5-6, 5-7, 5-8, and 5-9.

b. Vertical Speed Control System

With the attitude loop removed and the stabilization system feedbacks are the various derivatives of h, it can be shown that the basic stability problem does not differ significantly from the attitude command system.

An important point to stress is that the $\dot{h}$ and $\ddot{h}$ systems discussed here do not permit the implementation of tighter flight path control systems from the standpoint of higher position gains and higher closed loop position control frequencies. Their advantage is in the minimization of wind disturbance transients because they sense the disturbance sooner and because the new pitch attitude equilibrium in wind shear can be achieved without opposition from the pitch attitude loop. From the standpoint of command response or ability to close initial condition errors, they have no advantages over the attitude command systems. This can be demonstrated by analyzing and comparing the control laws for both types of systems. Consider first the system based on the acceleration inner loop. The simplified surface command control law will be of the form

$$\delta_{(\ddot{h})} = a_1 \int h dt + a_2 h + a_3 \dot{h} + a_4 \ddot{h} + a_5 \dot{\theta} \tag{6-29}$$

where h is the deviation from the reference path.

If we substitute

$$\gamma = \theta - \alpha = \frac{\dot{h}}{V} \tag{6-30}$$

where γ, θ, α, and $\dot{h}$ are incremental values from the equilibrium values,

$$\delta_{(\ddot{h})} = \int a_1 h dt + a_2 h + a_3 V\theta - a_3 V\alpha + a_4 \ddot{h} + a_5 \dot{\theta} \tag{6-31}$$

neglecting control surface lift effects,

$$\ddot{h} \approx \frac{C_{L_\alpha} QS\alpha}{W/g} = \frac{QC_{L_\alpha}\alpha}{W/gS} k_1 \alpha \tag{6-32}$$

$$\alpha = \alpha' + \alpha_g \tag{6-33}$$

where α' is the nondisturbed angle of attack and α_g is the equivalent gust angle of attack.

The undisturbed angle of attack has a well-defined dynamic relationship to pitch angle which can be approximated for the frequencies of interest as

$$\alpha \approx \frac{\tau_\gamma s}{\tau_\gamma s + 1} \cdot \theta = \frac{\tau_\gamma \dot{\theta}}{\tau_\gamma s + 1} \tag{6-34}$$

where

$$\tau_\gamma = MV/C_{L_\alpha} QS \qquad (M = \text{aircraft mass}) \tag{6-35}$$

Thus, for the no-gust condition when $\alpha = \alpha'$, the control law reduces to

$$\delta_{(\ddot{h})} = a_1 \int h dt + a_2 h + a_3 V\theta + a_5 \dot{\theta} + \frac{\tau_\gamma (a_4 k_1 - a_3 V)\, \dot{\theta}}{\tau_\gamma s + 1} \tag{6-36}$$

This control law can be compared with the attitude inner loop control law which is of the form

$$\delta_{(\theta)} = b_1 \int h dt + b_2 h + b_3 \theta + b_5 \dot{\theta} \qquad \text{(neglecting the } \dot{h} \text{ feedback)} \tag{6-37}$$

for glide slope control.

The two control laws differ only by a lagged $\dot{\theta}$ term. Typically $a_4 k_1 \approx a_3 V$ so that this term is relatively small. It obviously can be added to the pitch system so that both control laws would be completely identical.

The essential difference between the two control laws is in the disturbance situation where the α_g term in equation (6-33) and horizontal gusts are the significant contributor to flight path accelerations. The acceleration control system provides feedbacks proportional to the actual flight path accelerations, while the attitude based system requires integration of these accelerations until the position errors of equation (6-37) develop. Also changes in the equilibrium wind condition (wind shear) require a change in the equilibrium pitch attitude. With pitch feedback this necessitates a flight path offset that must be corrected by the integrator.

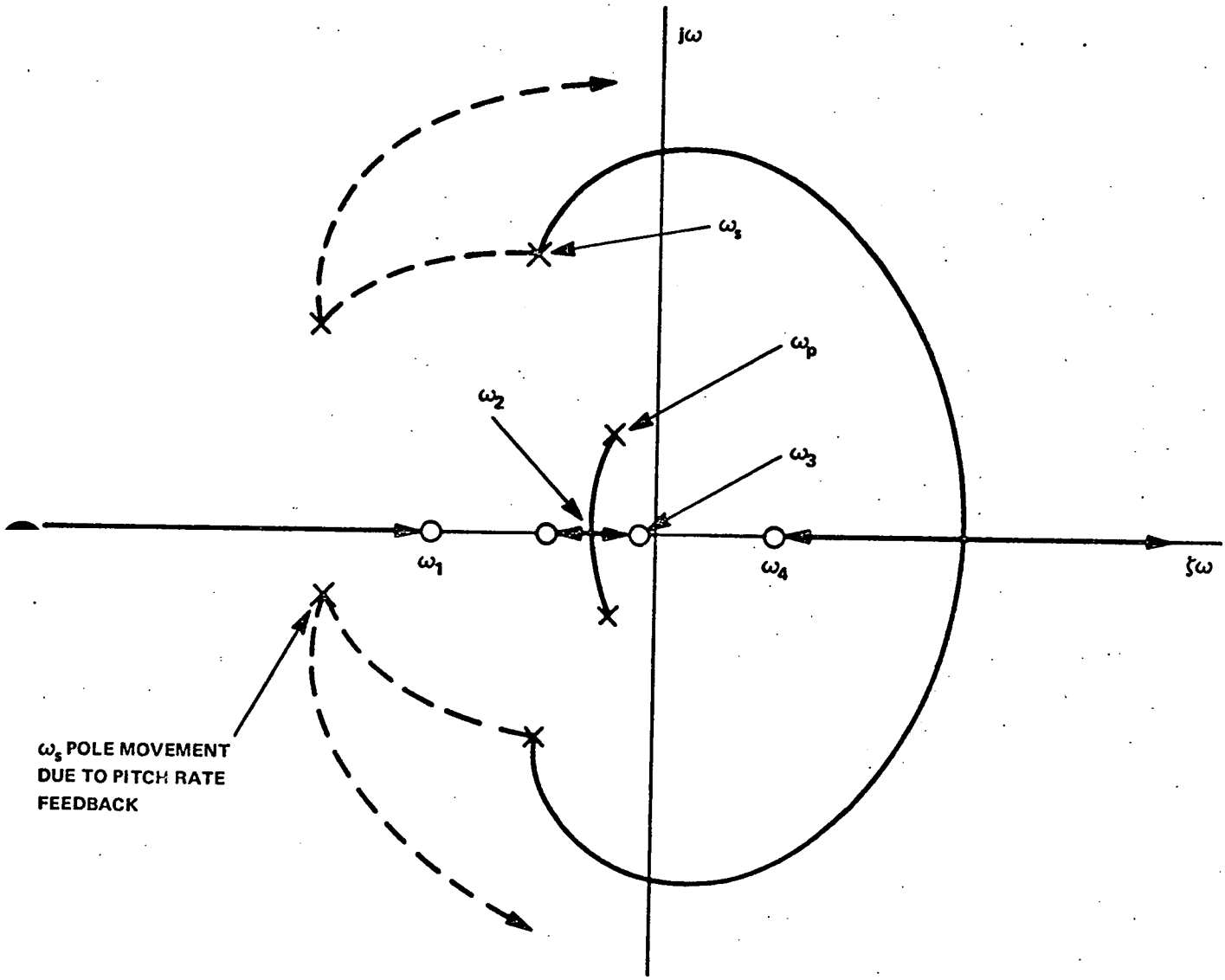

Figure 6-8
Root Locus for $\ddot{h}$ Feedback Loop
showing Effect of Right-half Plane Zero
Caused by $C_{L_{\delta_E}}$

One peculiar stability problem occurs in the $\dot{h}$, $\ddot{h}$ type of stabilization system. The preceding analysis neglected the lift due to elevator, $C_{L_{\delta_E}}$. This term, when included, results in a right-half plane zero in the $\ddot{h}/\delta_E$ transfer function. The implication of this zero is illustrated in the root locus for an $\ddot{h}/\delta_E$ transfer function (Figure 6-8) which is of the form:

$$\frac{\ddot{h}}{\delta_E}(s) = \frac{\left(\frac{s}{\omega_1}+1\right)\left(\frac{s}{\omega_2}+1\right)\left(\frac{s}{\omega_3}+1\right)\left(\frac{s}{\omega_4}-1\right)}{\left(\frac{s^2}{\omega_p^2}+\frac{2\zeta s}{\omega_p}+1\right)\left(\frac{s^2}{\omega_s^2}+\frac{2\zeta s}{\omega_s}+1\right)} \tag{6-38}$$

A high gain $\ddot{h}$ loop closure rapidly runs into instability as the short-period roots bend back into the right-half plane toward the zero, ω_4. Increasing pitch rate gain bends the locus further toward the regions of higher damping, but the pitch rate loop has its own stability limitations when it interacts with actuator dynamics not shown in Figure 6-8. Partial compensation is often achieved by moving the $\ddot{h}$ sensor forward to the pilot's station where angular acceleration at the aircraft's nose cancels some of the initial acceleration reversal resulting from a δ_E deflection. High gain acceleration loops, however, are generally more difficult to achieve in real aircraft then they are in simulators.

10. Summary of Control Parameters and Performance Criteria

a. Control Parameters

The control parameters identified in the control equations given in the previous section are specified in terms of typical minimum, maximum, and nominal values in Table 6-1.

b. Performance Criteria

(1) Glide Slope Capture

- Start aircraft at a constant altitude of 1500 feet and at the outer fringes of the glide slope beam (0.7 degree). Capture should be accomplished with less than 0.1 degree beam overshoot. If an undershoot occurs, it should occur within 0.1 degree of beam. That is, if the descent velocity $V\gamma_{G/S}$ is attained before the beam center is intercepted, it should not occur any further out than 0.1 degree of beam deflection.

TABLE 6-1

PARAMETER SUMMARY

Parameter	Typical Minimum Value	Typical Nominal Value	Typical Maximum Value	Remarks
$\gamma_{G/S}$	2.5°	2.5°	3.0°	Glide slope angle
$\ddot{h}_{max}$	0.025g	0.05g	0.1g	Maximum acceleration constraint for glide slope capture
τ_1	0.05 sec	0.10 sec	0.25 sec	Glide slope filter
k_λ	50	30	50	Glide slope displacement gain degrees θ_c per degree beam (λ)
k_I - Pitch	0.025 k_λ	0.04 k_λ	0.08 k_λ	Glide slope integral gain degrees per second θ_c per degree beam
Glide Slope $k_{\dot{h}}$ - Pitch	0.05	0.1	0.25	Vertical speed gain degree θ_c per ft/sec
$g = f(h_R)$	See Figure 6-4			Gain reduction program for k_λ and k_I (applicable to both pitch command and vertical speed systems)
k_F	0.04	0.05	1.0	Flareout gain
Flareout ($k_F k_{\dot{h}}$) - Pitch	0.10	0.20	0.40	Vertical speed gain degree θ_c per ft/sec for flareout
$k_{\ddot{h}}$	0.1	0.25	1.0	Vertical acceleration gain for flareout - degree θ_c per ft/sec^2
k_2 - Pitch	0.15	0.25	0.4	Flareout integral gain ratio
τ_2	0.5	1.0	2.0	Pitch flareout predictor time constant
θ_1	1.0	2.0	2.5	Displacement component of predictive pitch term
$\dot{\theta}_2$	0.30 deg/sec for 1st 5 sec, 0.10 deg/sec for 2nd 5 sec, or until touchdown	0.40 deg/sec for 1st 5 sec, 0.10 deg/sec for 2nd 5 sec, or until touchdown	0.50 deg/sec for 1st 5 sec, 0.15 deg/sec for 2nd 5 sec, or until touchdown	Pitch rate predictive command....(requires maximum constraint on integral output)
$k_{\dot{h}}$ (Vert Speed Guide System)	1.0	1.8	2.4	Degrees δ_E per ft/sec $\dot{h}$ error
k_λ (Vert Speed Guide System)	100	150	200	Degrees δ_E per degree beam
k_I (Vert Speed Guide System)	0.06	0.20	0.40	Degrees per second δ_E per degree beam
$k_{\ddot{h}}$ (Vert Speed Guide System)	0.8	1.25	2.5	Degree δ_E per ft/sec^2 $\ddot{h}$ error

• When the level flight capture is optimized, perform a capture with a 2.0-degree initial descent angle intercepting the beam outer boundary (0.7 degree) at 1500 feet altitude. The logic procedure defined in Appendix A should produce a successful capture with criteria the same as above.

• Perform a steep-angle capture by initializing the aircraft with a 4.0-degree descent flight path angle at the outer boundary of the beam at an altitude of 1800 feet. Overshoot and undershoot criteria are similar to those for level flight, except the limit values of λ are increased from 0.1 degree to 0.2 degree.

To optimize performance on beam capture, adjust for tightest $\dot{h}$ loop gains consistent with stability and then insert the feedforward compensation to minimize errors.

(2) Glide Slope Tracking

• Steady-state tracking errors should be reduced to λ = zero ± 0.02 degree by the time an altitude of 500 feet is reached.

• With 5 feet per second vertical gust pulses of 2-second duration, recovery to zero ± 0.02 degree beam error should occur within 12 seconds following gust removal. This transient should be inserted at h = 1000 feet, 600 feet, and 300 feet. Damping of the flight path transient or associated inner-loop modes should exceed 0.4. Damping of about 0.7 in these responses is desirable.

• At an altitude of 400 feet, introduce a wind shear of 4 knots per 100 feet. The aircraft deviation from beam center at 100 feet shall not exceed 0.12 degree.

To optimize glide slope tracking performance, use the highest gains of k_λ and k_I consistent with stability. The gain reduction program should ensure that instability does not occur below altitudes of about 200 feet. Minimum damping of flight path oscillations should be about 0.4.

(3) Flareout

- With nominal conditions (zero wind or gusts) and the aircraft aligned with the center of the glide path beam, let the aircraft fly into the ground without any flareout. Observe the change in $\dot{h}$ due to ground effect. Use the recommended throttle retard program.

- Add the predictive pitch program optimized to yield a touchdown velocity of about 2 feet per second and a minimum runway excursion beyond glide slope runway intercept. Flare should start at about 35 feet to minimize runway excursion.

- Add closed loop flareout law with tightest gains achievable without causing instability or oscillatory responses.

- Test the nominal flareout system under conditions of windshear (4 knots per 100 feet), nominal turbulence, and combinations of head wind and tail wind. Successful landings are those that have touchdown vertical speeds of less than 4 feet per second and runway dispersions of -300 feet to +1200 feet of the ILS reference point.

B. DIGITAL PROGRAM - VERTICAL GUIDANCE (LANDING)

1. Control Law Conversion

Figure 6-9 is the block diagram (in FORTRAN notation) of the glide path capture and tracking part of the vertical landing guidance laws. (Table 6-2 summarizes the FORTRAN designations.) The sequencing of functions in accordance with the mode switching logic is summarized in the table on Figure 6-9. The exponential flareout block diagram is illustrated in Figure 6-10. Note that, as mechanized here, the acceleration loop has not been included. The acceleration loop with the $\ddot{h}$ reference set to zero could tighten the system response to gust disturbances. Also note that the predictive pitch command is inserted at flare initiation which is 1.5 seconds before the closed loop $h + \dot{h}$ system is activated. This is one possible variation of this system although adequate performance can also be obtained without this delay. The rationale behind delaying initiation of closed loop control is the recognition that satisfaction of the $h + \dot{h}$ control law requires a continuous $\ddot{h}$ with the largest $\ddot{h}$ at the start of flare. Since there is a lag in the attainment of the initial $\ddot{h}$, the closed loop system tends to overcompensate. This problem can be handled with a properly shaped predictive command or by delaying initiation of closed loop control as in the particular implementation shown in Figure 6-10.

An alternate flare control system based on the computed acceleration needed to achieve the specified final value of $\dot{h}$ is shown in the FORTRAN block diagram in Figure 6-11. As in the case of the exponential flare control system, closed loop control is delayed for 1.5 seconds. Also, the control law changes to a vertical speed control if the vertical speed is arrested too rapidly.

It is noted that the specific implementations for both flare controllers illustrated in Figures 6-10 and 6-11 have weaknesses which will compromise their performance in winds and turbulence. The brief delay before closed loop control is initiated represents loss of closed loop control for part of the flare maneuver. For the nominal, no-wind case, performance can be made perfect. With steady winds, shears and gusts, the time for correction is cut short so that the system should suffer somewhat from the weaknesses of open loop systems sensitivity to disturbances. Another feature not incorporated in the implementation shown in Figures 6-10 and 6-11 is the variable flare initiation altitude based on satisfying an altitude plus altitude rate criterion. The variation in flare initiation altitude helps to minimize dispersions due to headwind and tailwind variations.

VERTICAL LANDING CONTROL, PITCH COMMAND SYSTEM SUBROUTINE VLAND1

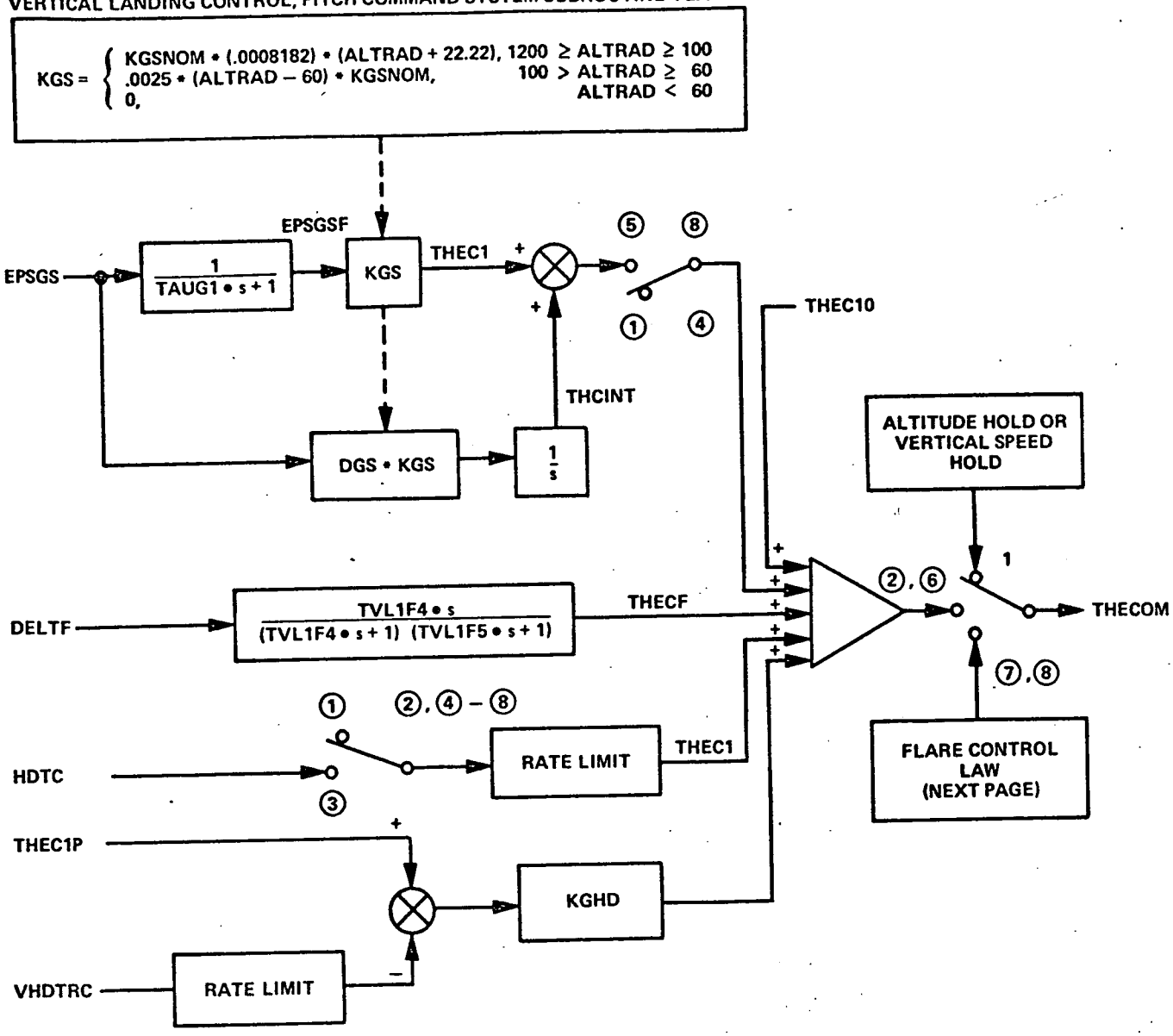

ILAND

1 CALCULATE SAFETY OF CAPTURE (SEE FLOW CHART). IF SAFE, CALCULATE AND TEST FOR CAPTURE ANGLE. WHEN REACHED, SWITCH TO 2.

2 CALCULATE: THEC1P = THECOM$_2$ GSD • HDTC/VT • R2D, VHDTRFC = VT • GS LTHEC1 = HDMAXL/VT • DT3 • R2D, SWITCH TO 3.

3 BEGIN CAPTURE MANEUVER, TEST FOR CAPTURE COMPLETION. WHEN CAPTURE IS COMPLETE, SWITCH TO 4 (SEE FLOW CHART).

4 SYNCHRONIZE GS TRACKING LAW: SET INTEGRATOR, THCINT = 0 AND BIAS THEC10, SWITCH TO 5.

5 TRACK GS, TEST FOR BEGINNING OF THRUST REDUCTION PROGRAM (ALT ≤ 50). WHEN ALT 50, SWITCH TO 6.

6 CONTINUE GS TRACKING. START THRUST REDUCTION (SEE FLOW CHART). TEST FOR FLARE INITIATION. WHEN FLARE INITIATION ALTITUDE IS REACHED, SWITCH TO 7.

7 INITIALIZE FLARE, SWITCH TO 8.

8 FLARE LAW.

Figure 6-9
Vertical Landing Guidance-Glide Slope
Control (Fortran Notation)

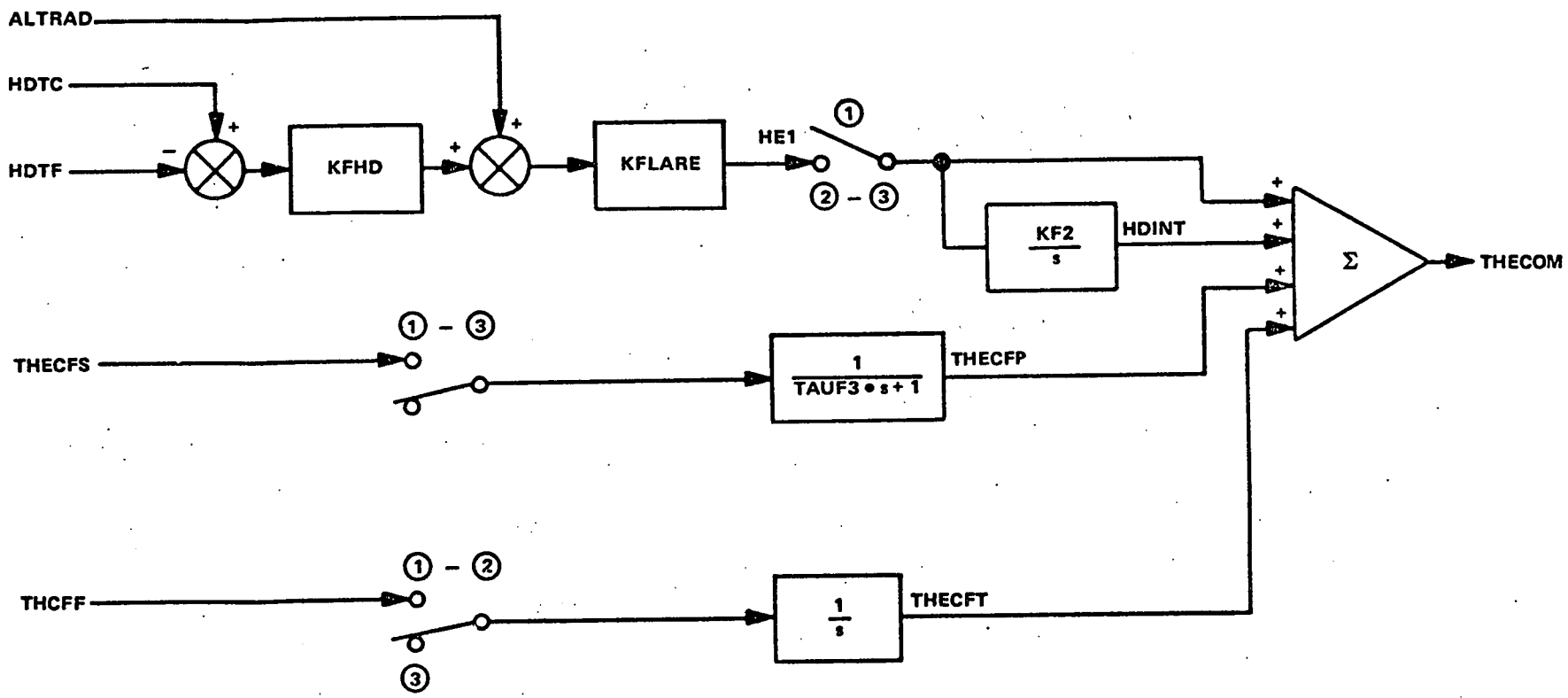

1. BEGIN FLARE: AFTER 1.5 SECONDS; SWITCH TO ③
2. ENGAGE FEEDBACK CONTROL LAW AFTER SPECIFIED DELAY TIME
3. HALT FEED FORWARD PITCH RAMP COMMAND

Figure 6-10
Standard Flare Control System
Fortran Notation

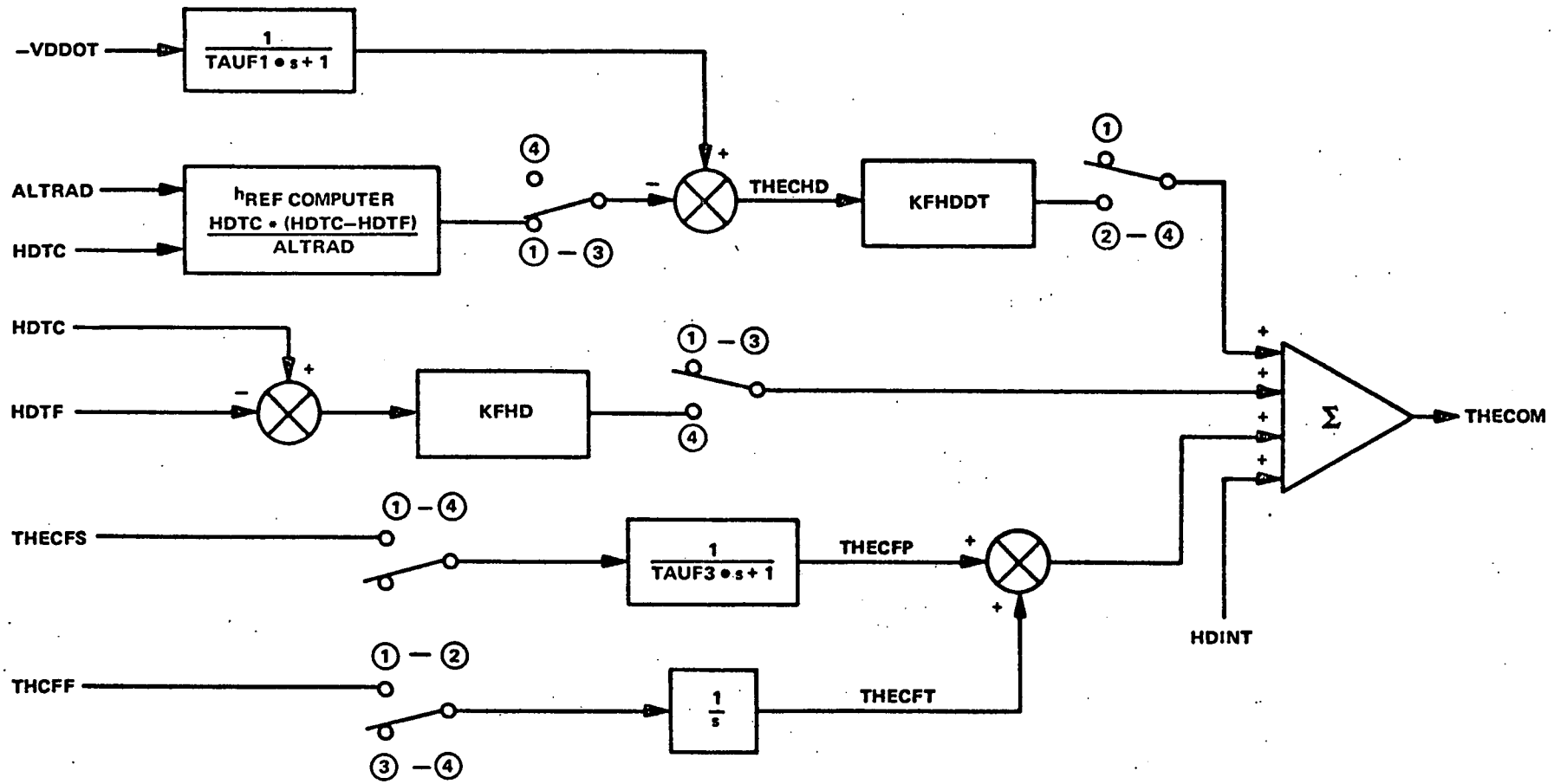

1. BEGIN FLARE: START FLARE TIMER (TRAMP). WHEN TRAMP = 1.5 SEC TO 5.0 SEC, SWITCH TO 2
2. ENGAGE FEEDBACK CONTROL LAW AFTER SPECIFIED DELAY TIME
3. HALT THE FEED FORWARD PITCH RAMP. WHEN HDTC = -2.5 FT/SEC, SWITCH TO 4
4. CONSTANT VERTICAL SPEED PORTION OF FLARE, HDTF = -2.0 FT/SEC

Figure 6-11
Flare Control System: Acceleration Feedback Control Law
Fortran Notation

TABLE 6-2

VERTICAL LANDING GUIDANCE FORTRAN NAMELIST

Variable	FORTRAN Name	Definition
h_R	ALTRAD	Aircraft radar altitude above ground
V	VT	Aircraft ground speed
λ	EPSGS	Glide slope displacement error angle
$\dot{h}_c$	HDTC	Compensated vertical speed
$\ddot{h}$	VDDOT	Vertical acceleration
γ_{GS}	THETGS	Glide slope beam angle above horizon
λ_o	EPSGSO	Glide slope error angle for capture initiation
θ'_{c_1}	THEC1P	Predictive step command for glide slope capture
$\dot{h}_{ref}$	VHDTRC	Vertical speed reference command for capture
--	TIMCP	Glide slope capture duration time
--	DTC	Thrust reduction increment
--	LTHEC1	Rate limit on θ'_c
$k_{\dot{h}}$	KGHD	Glide slope capture, tracking vertical speed error gain
k_λ	KGSNOM	Glide slope displacement error gain, nominal
k_I/k_λ	DGS (KGSINT)	Ratio of glide slope integral to displacement gain
τ_1	TAUG1	Glide slope displacement error filter time constant
τ_4, τ_5	TVL1F4, TVL1F5	Flap compensation filter time constants
δ_f	DELTF	Flap angle
θ_1	THECFS	Predictive step pitch command for flare
$\dot{\theta}_2$	THCFF, THCFR	Predictive ramp pitch command, fast and slow rates, respectively
$\dot{h}_F$	HDTF	Desired vertical speed at touchdown
$k_{\dot{h}}$	KFHD	Vertical speed error gain for flare
k_F	KFLARE	Total flare gain

TABLE 6-2 (cont)

VERTICAL LANDING GUIDANCE FORTRAN NAMELIST

Variable	FORTRAN Name	Definition
k_2	KF2	Flare integral gain
τ_3	TAUF3	Predictive pitch step command filter time constant
--	TRAMP	Predictive ramp pitch command timer
--	DELAY	Time delay for engaging feedback control law in the flare
$k_{\ddot{h}}$	KFHDDT	Vertical acceleration gain
τ_1	TAUF1	Vertical acceleration filter time constant
--	THEC10	Pitch command synchronization term
--	HDINT	Pitch command synchronization term

2. Flow Charts

The flow charts for the landing guidance program (VLAND1) are shown in Figures 6-12a through 6-12j. The initial condition calculations are summarized on Table 6-3.

TABLE 6-3

SUMMARY OF VLAND1
INITIAL CONDITION CALCULATIONS

```
LHDT1 = HDMAXL*DT3
CTF1 = EXP(-DT3/TVL1F4)+EXP(-DT3/TVL2F5)
CTF2 = EXP(-DT3*(1/TVL1F4+1/TVL1F5))
DTF = R2D/TVL1F5*(EXP(-DT3/TVL1F4)-EXP(-DT3/TVL1F5))/(1/TVL1F5-1/TVL1F4)
CG1 = EXP(-DT3/TAUG1)
DG2 = 1-CG1
CF1 = EXP(-DT3/TAUF3)
DF2 = 1-CF1
CF2 = EXP(-DT3/TAUF1)
DF3 = 1-CF2
DGS = KGS1NT*DT3
THECFF = THCFF*DT3
THECFR = THCFR*DT3
GSD = THETGS
GS = GSD*D2R
```

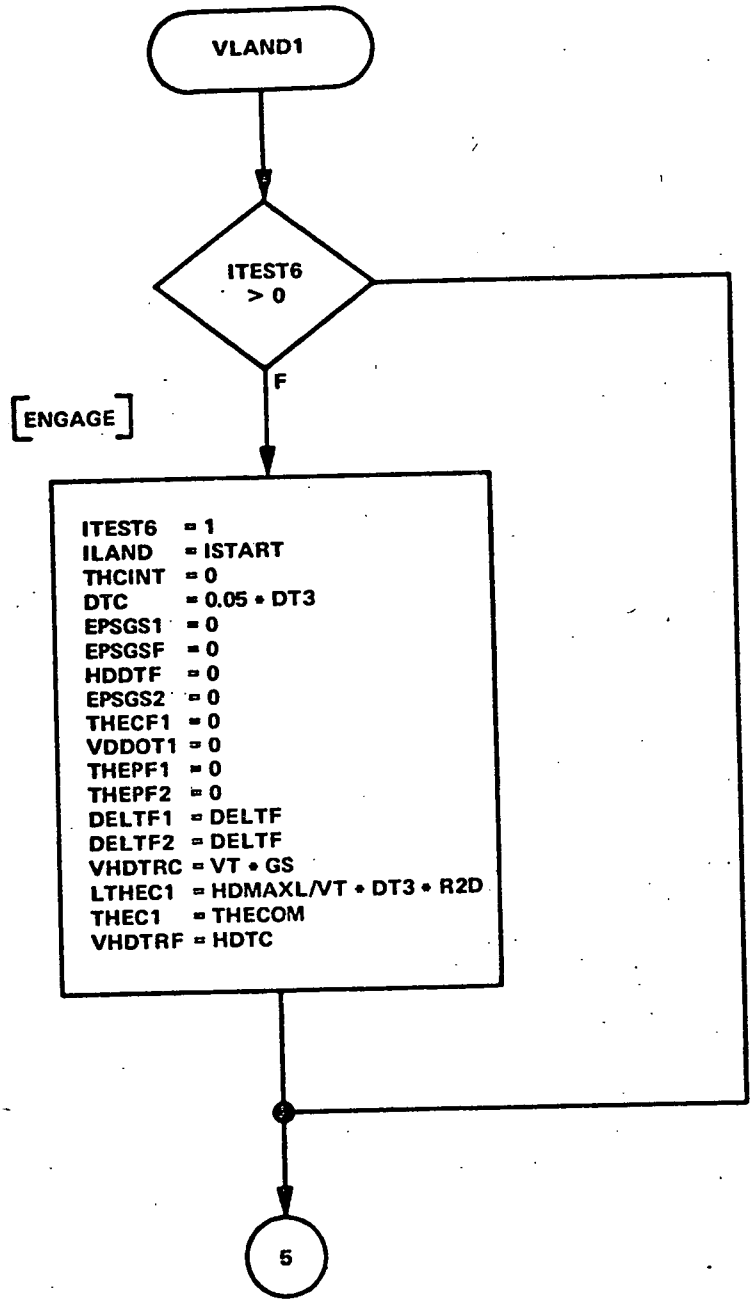

Figure 6-12a
VLAND1 Flow Chart

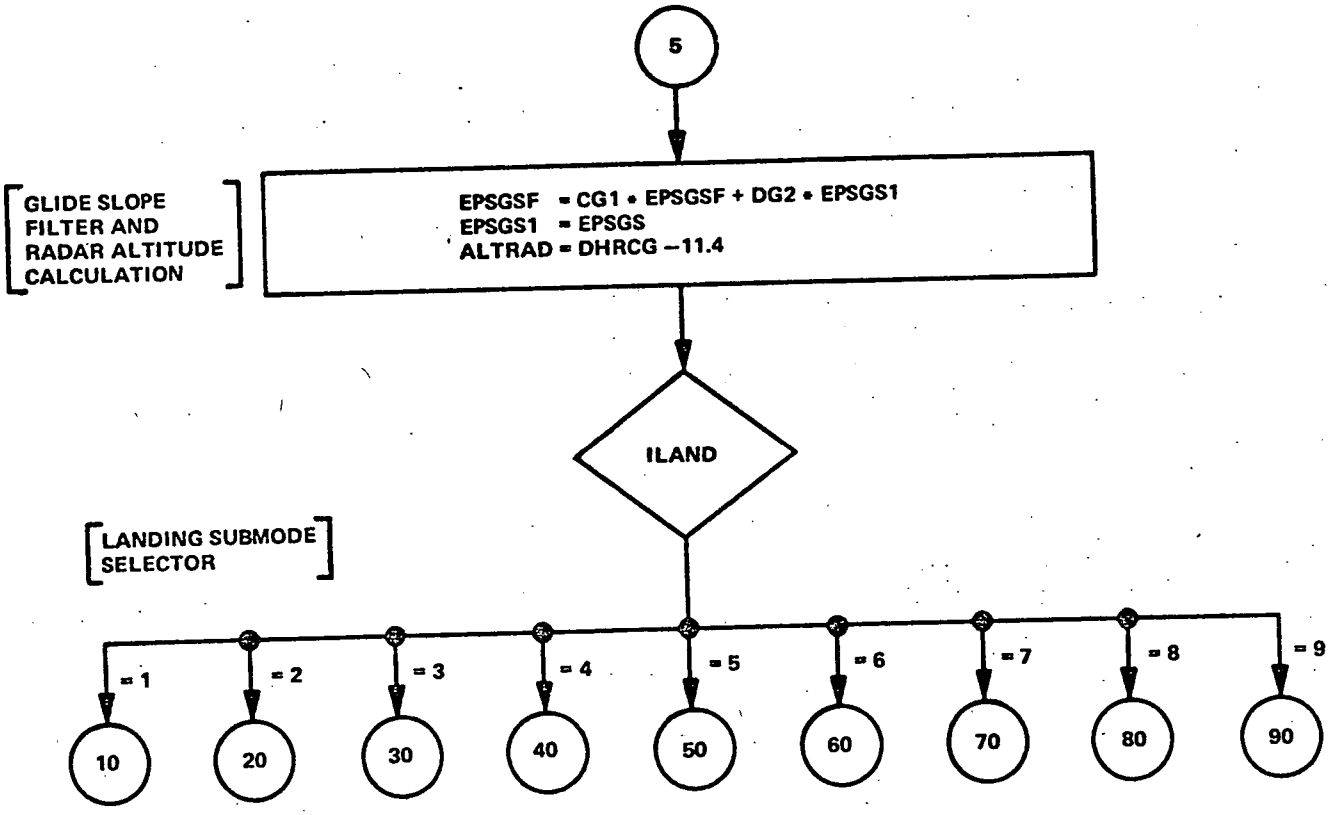

Figure 6-12b
VLANDI Flow Chart

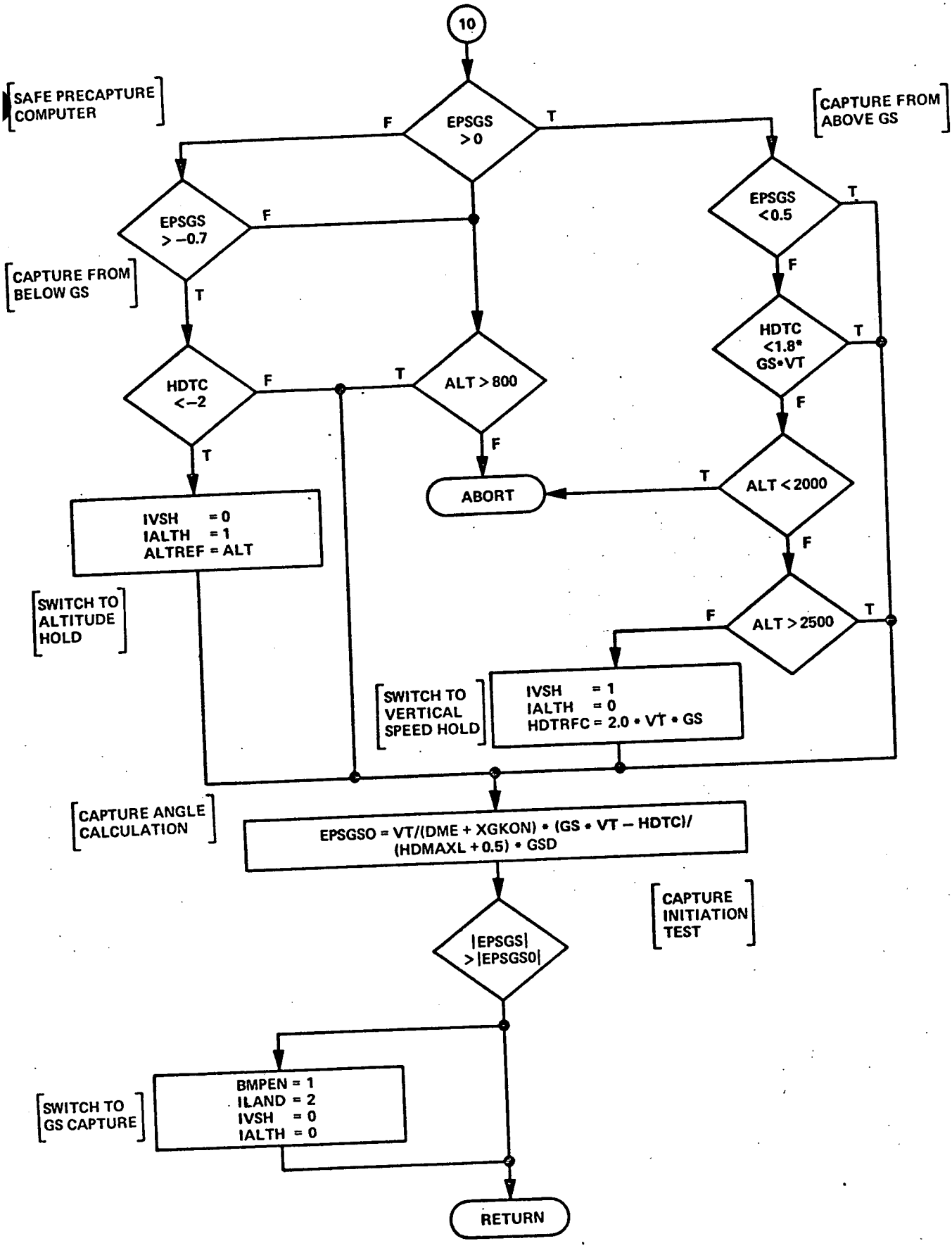

Figure 6-12c
VLAND1 Flow Chart

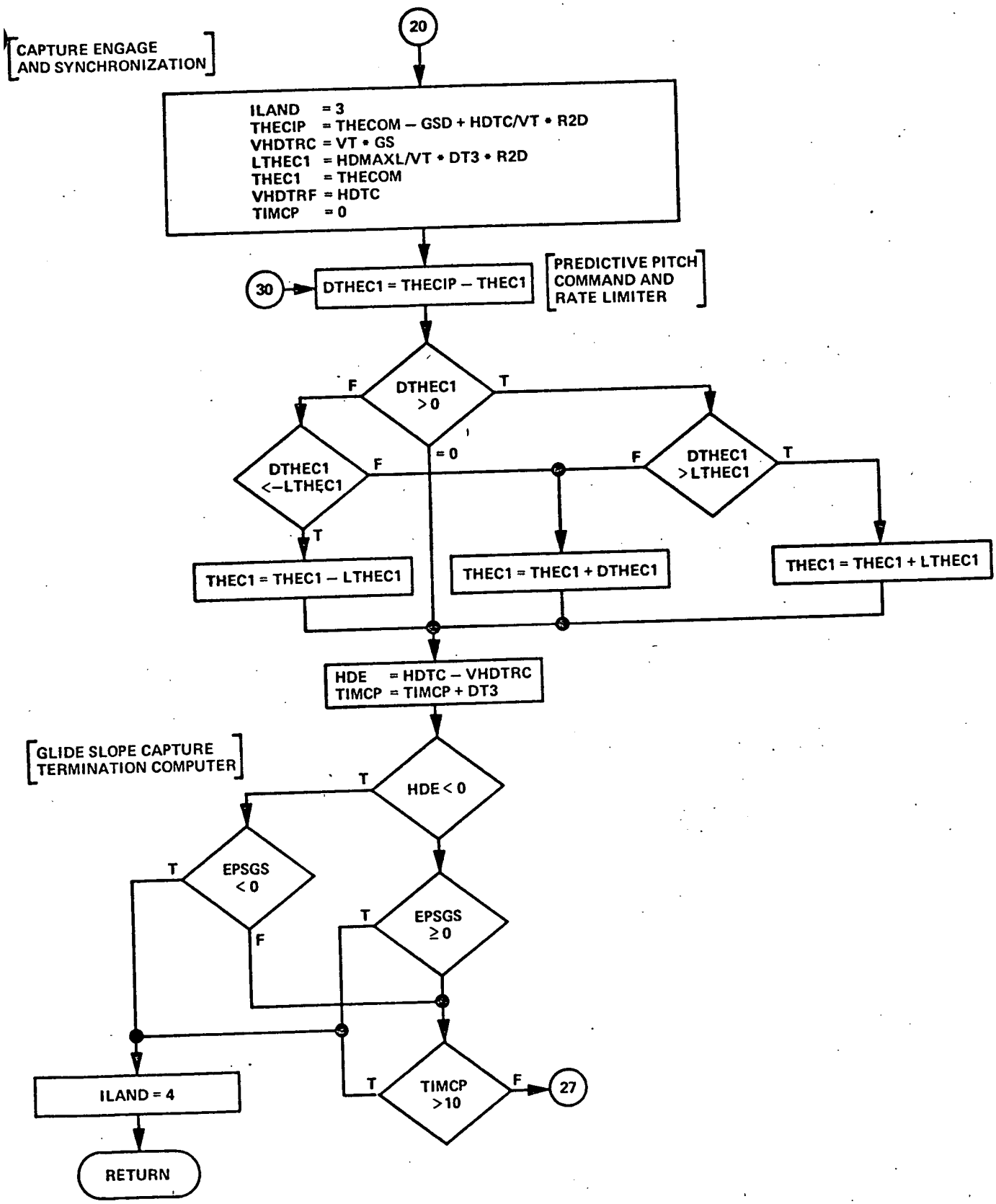

Figure 6-12d
VLAND1 Flow Chart

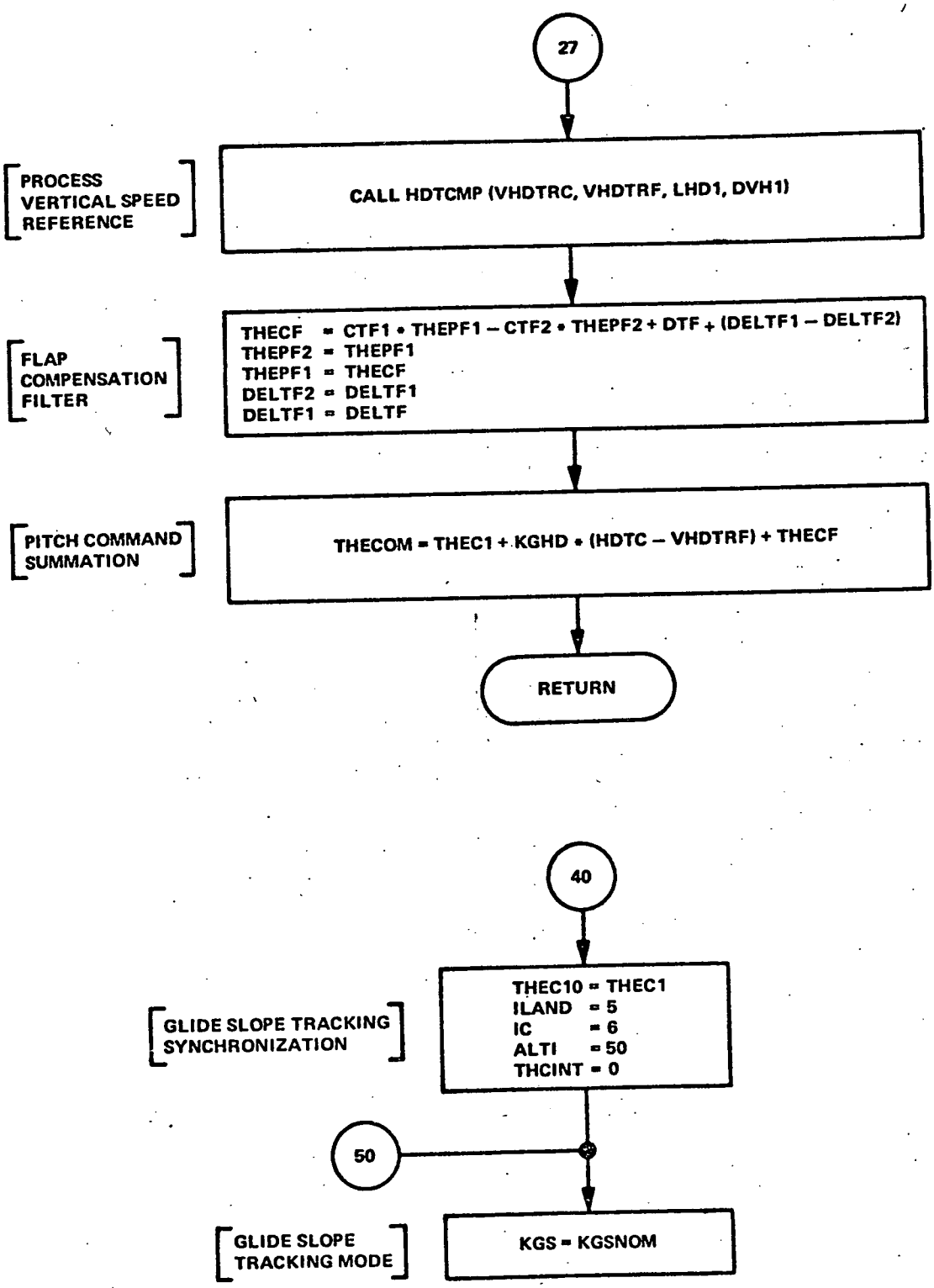

Figure 6-12e
VLAND 1 Flow Chart

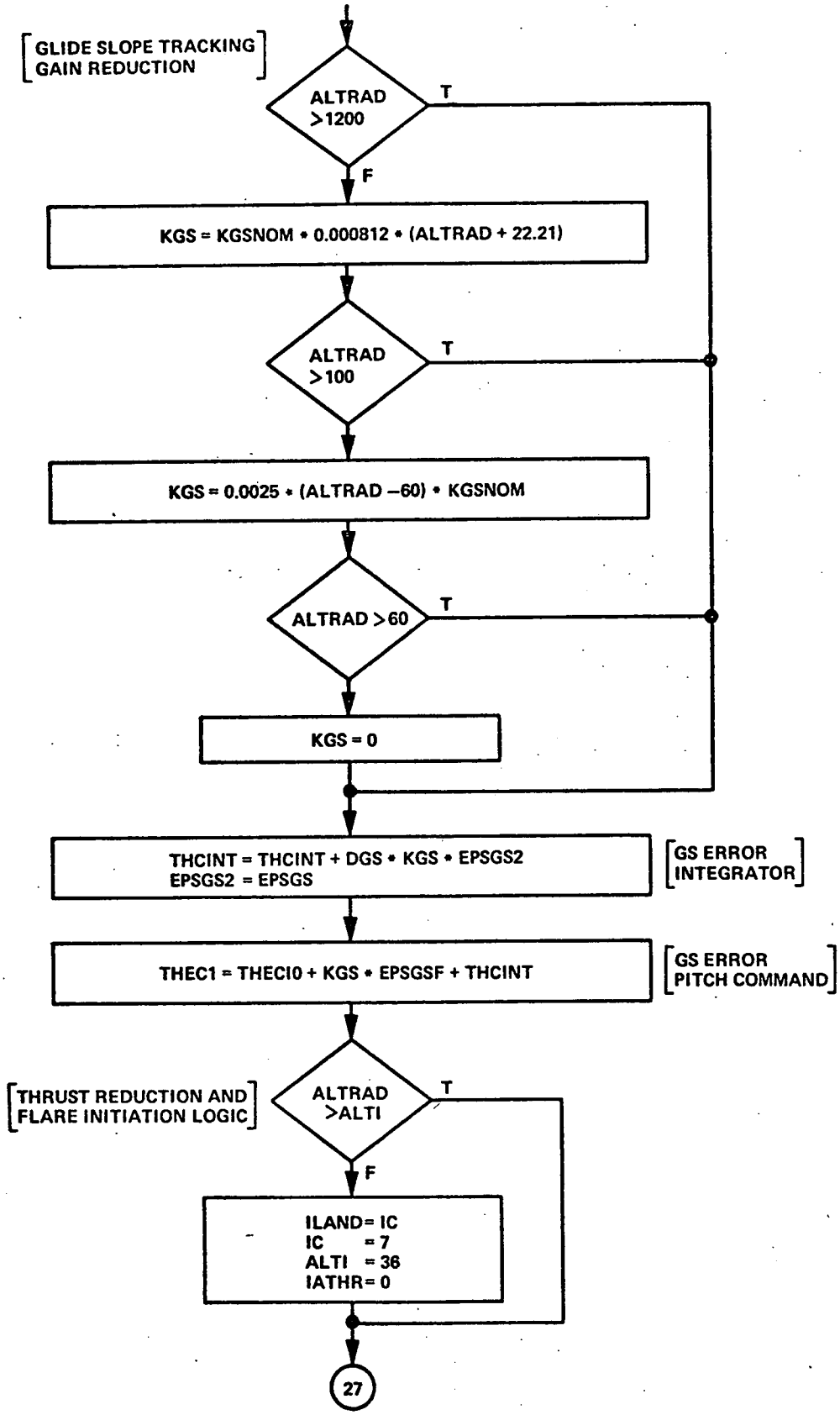

Figure 6-12f
VLAND1 Flow Chart

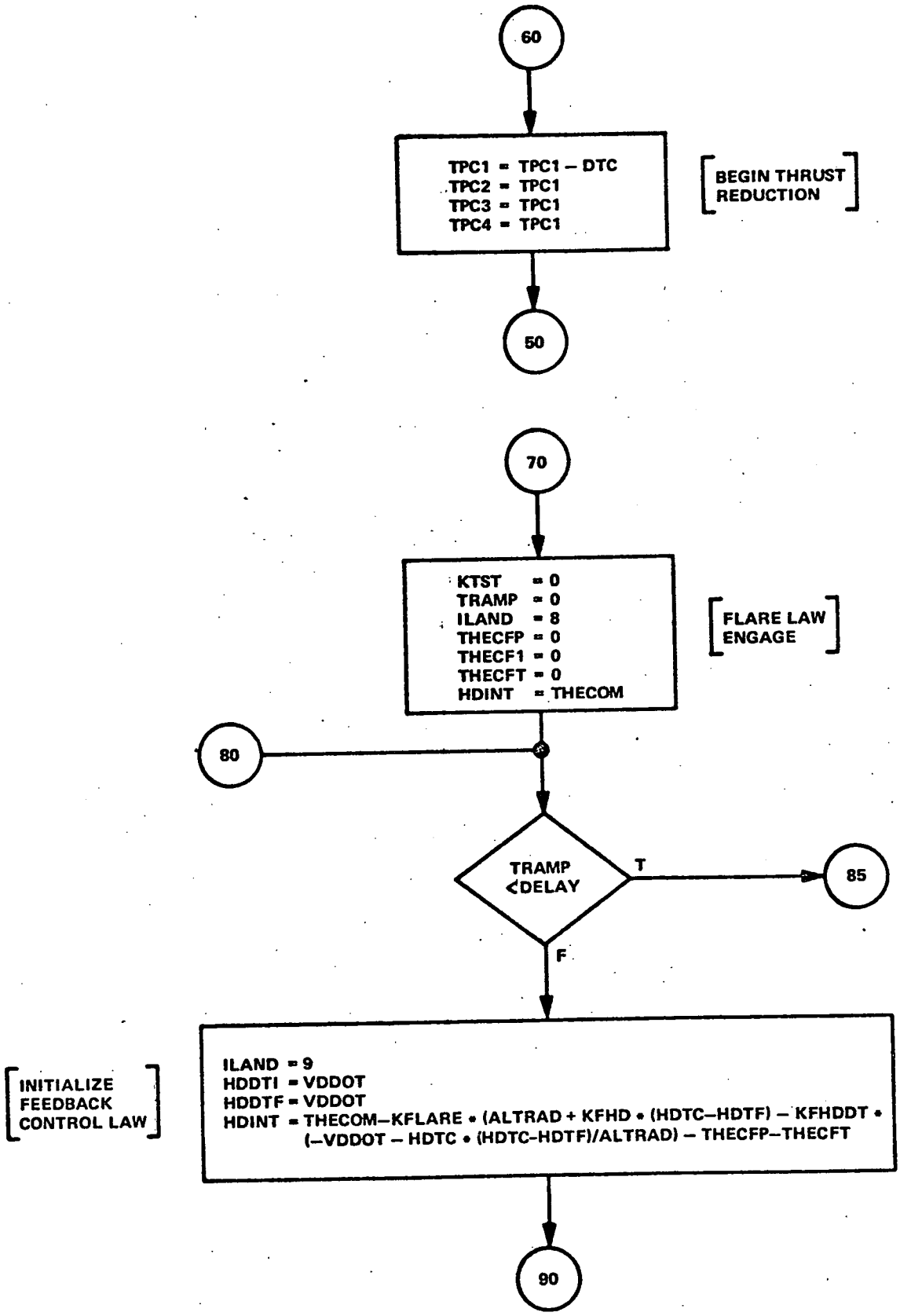

Figure 6-12g
VLAND1 Flow Chart

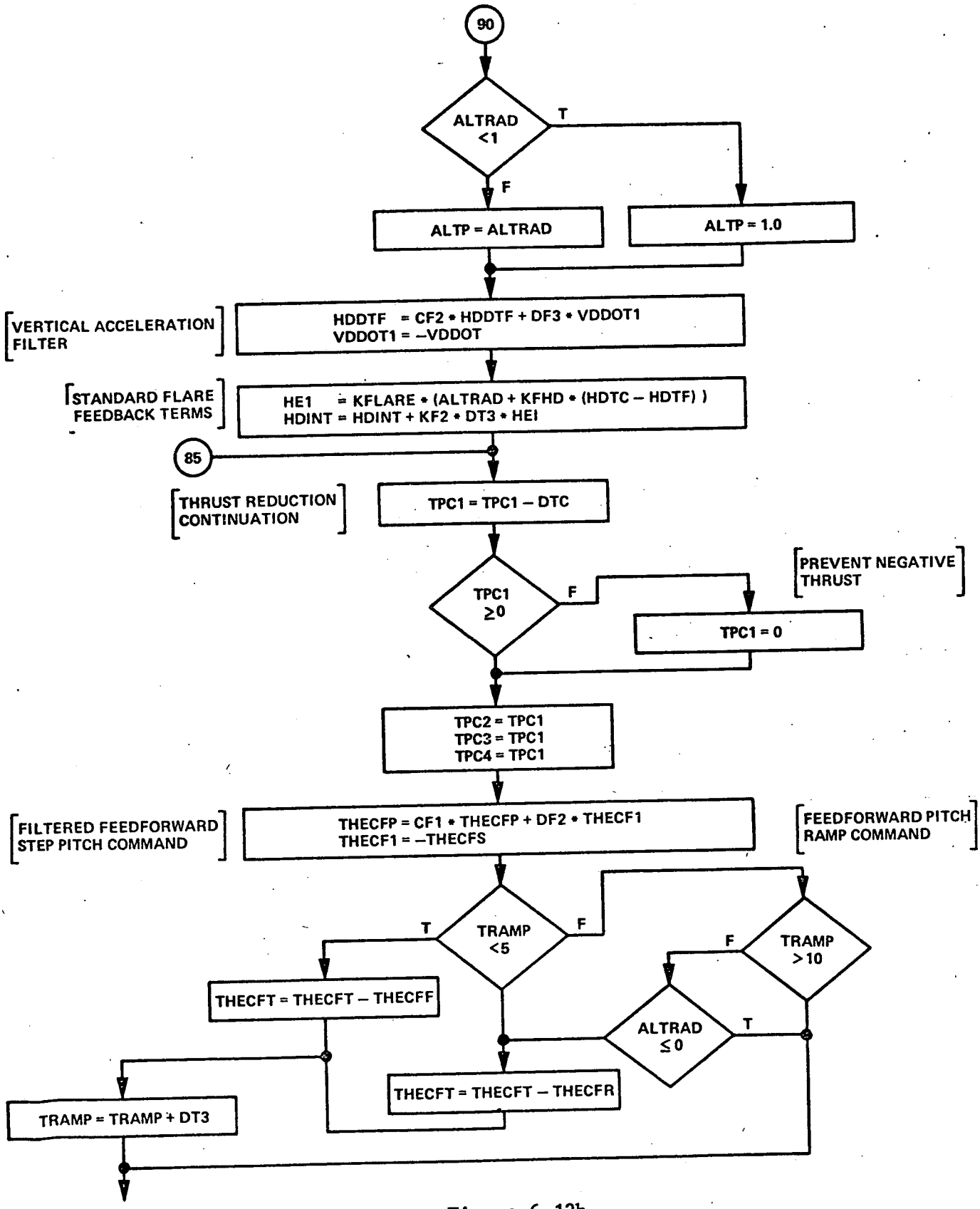

Figure 6-12h
VLAND1 Flow Chart

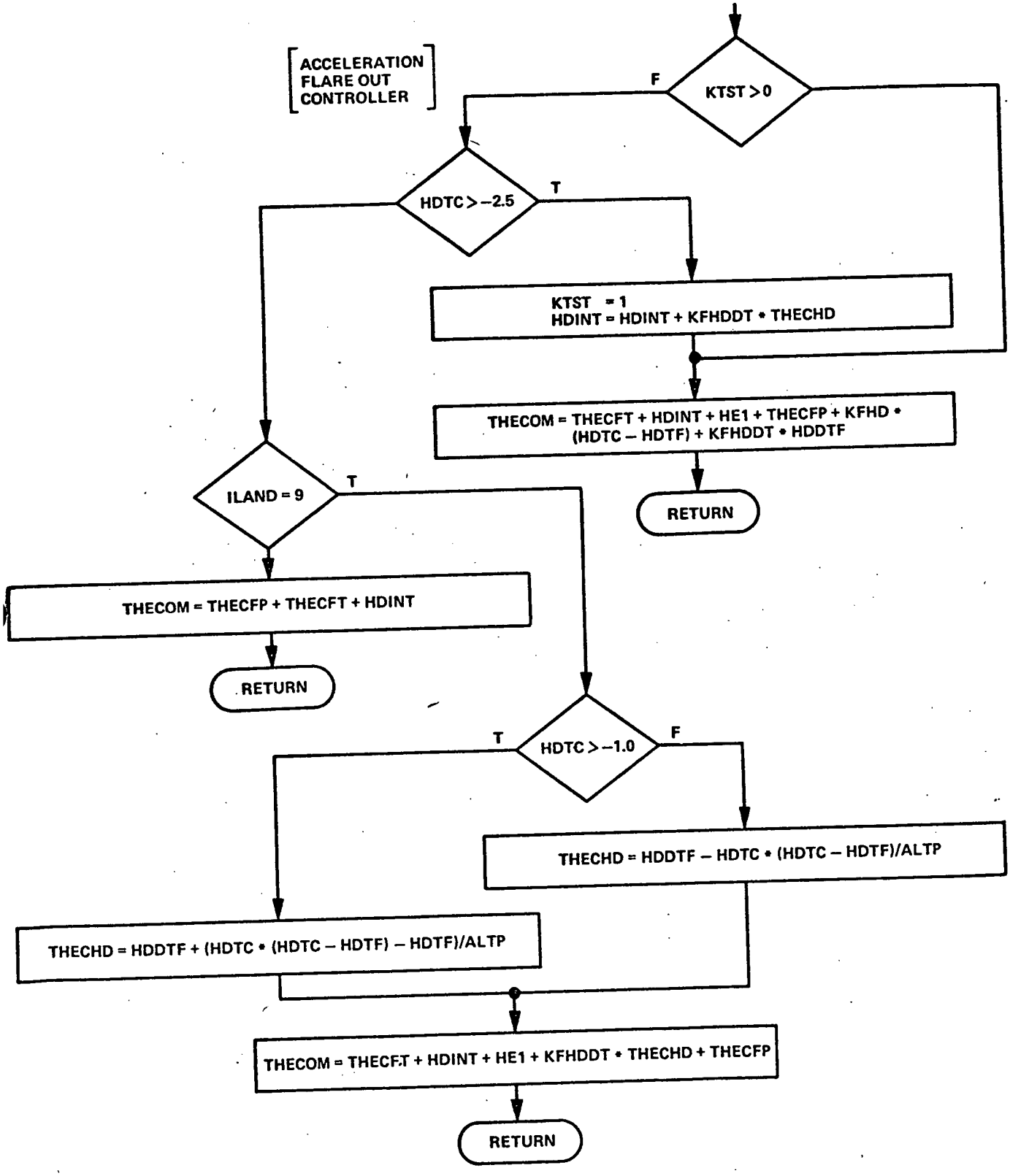

Figure 6-12i
VLAND1 Flow Chart

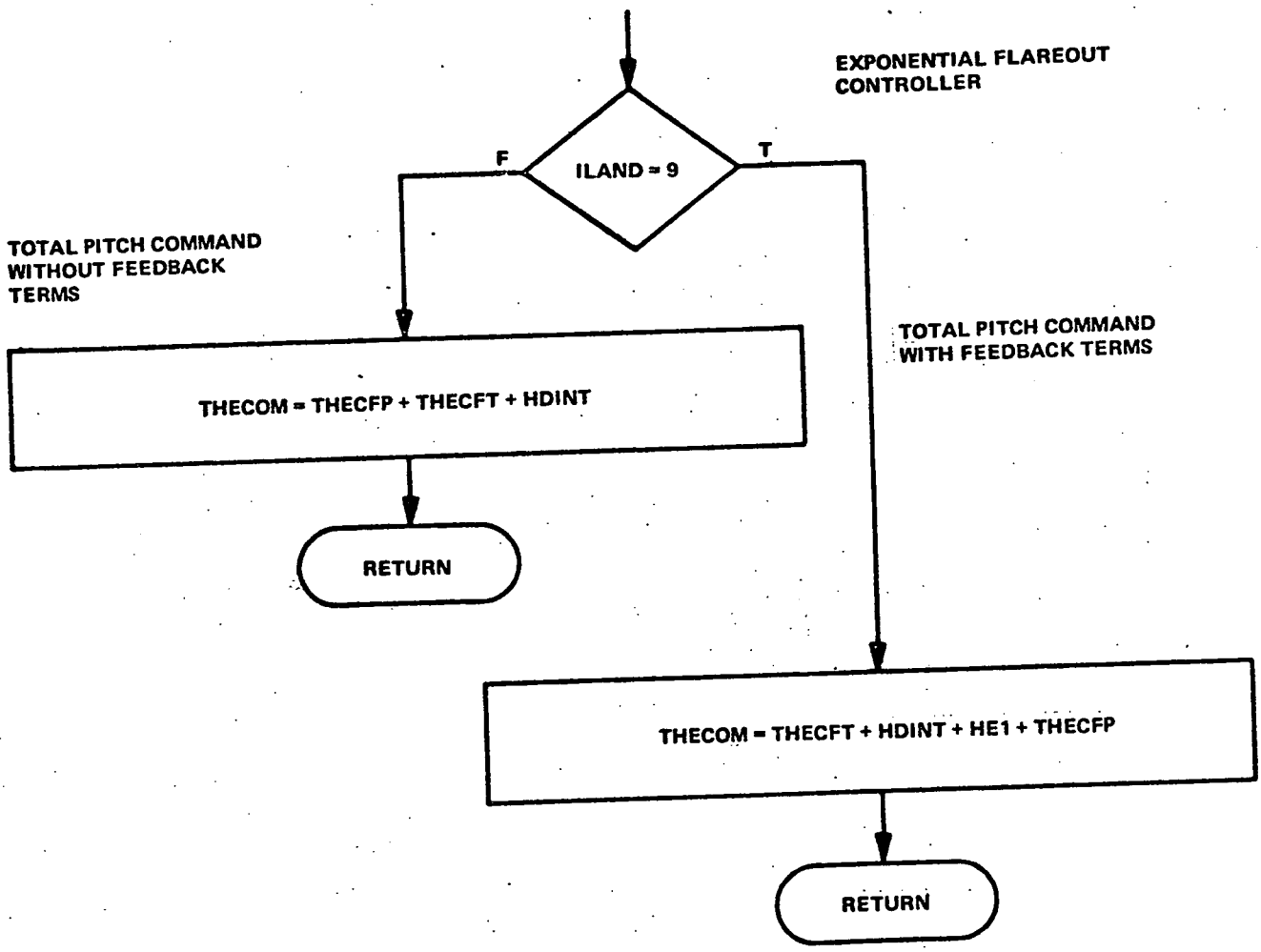

Figure 6-12j
VLAND1 Flow Chart

C. SIMULATION TEST RESULTS - VERTICAL GUIDANCE (LANDING)

1. Glide Slope Capture

Penetration and capture of a 2.5-degree glide slope from a constant altitude (1500 feet) and from an initial diving trajectory (flight path angle = -4°) is demonstrated in Figure 6-13. The two cases illustrated cover a capture of the glide slope from below and from above. In both cases overshoots are held to a maximum of about 0.015 degree of glide slope beam deviation. This overshoot would be barely discernible on the pilot's display. The acceleration constraint was only 0.025g which indicates that the glide slope capture maneuver can be achieved without detectable accelerations. The characteristics of the overshoot are typical of the integral loop. In the trajectories illustrated, glide slope tracking is initiated at offsets near 0.05 degree and the integral control law starts at that time. Delaying the start of integral control either on the basis of timing logic or error plus error rate criteria would eliminate most of this small overshoot problem.

2. Glide Slope Tracking

Response to 5-knot wind pulses applied at 1000 feet, 600 feet, and 300 feet are illustrated in Figure 6-14. Although the gust vertical velocity is about 8-1/2 feet per second, the disturbances are small relative to beam deviation angle. The overshoot in the responses is partially the result of the integration term in the control law and as discussed in previous sections this characteristic can be remedied with additional switching logic on the integral gain. What appears to be an offset tendency in Figure 6-14 is actually the consequence of the converging beam. (A constant beam displacement corresponds to a convergence toward the center of the beam in distance units.) This is apparent in the case of the wind disturbance at 300 feet of altitude. In this case, the final part of the transient occurs as the beam convergence becomes very pronounced (near 100 feet of altitude). As shown by the locus of points corresponding to a 1.0-foot offset above the beam centerline, a 1.0-foot displacement begins to look like a rapid divergence. The 100-foot decision height is reached at about t = 18 seconds. The glide slope error is about 0.02 degree at that point. The Category II and III glide slope window is 35 microamps or about 0.175 degree of beam. Thus the responses shown on Figure 6-14 are all well within Category II/III window requirements.

GLIDE SLOPE CAPTURE FROM 1500 FT ALTITUDE

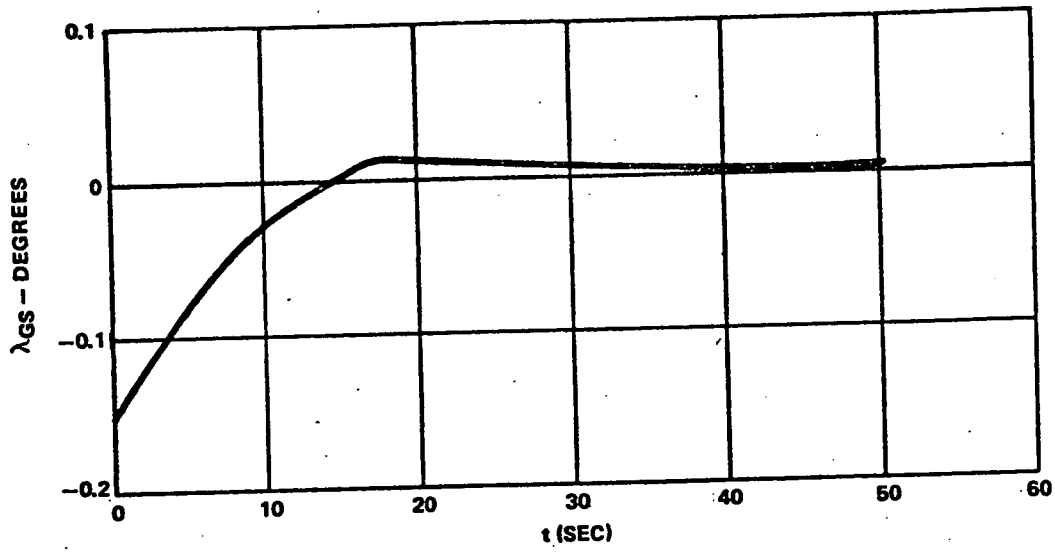

GLIDE SLOPE CAPTURE FROM ABOVE:
INITIAL FLIGHT PATH ANGLE OF −4°

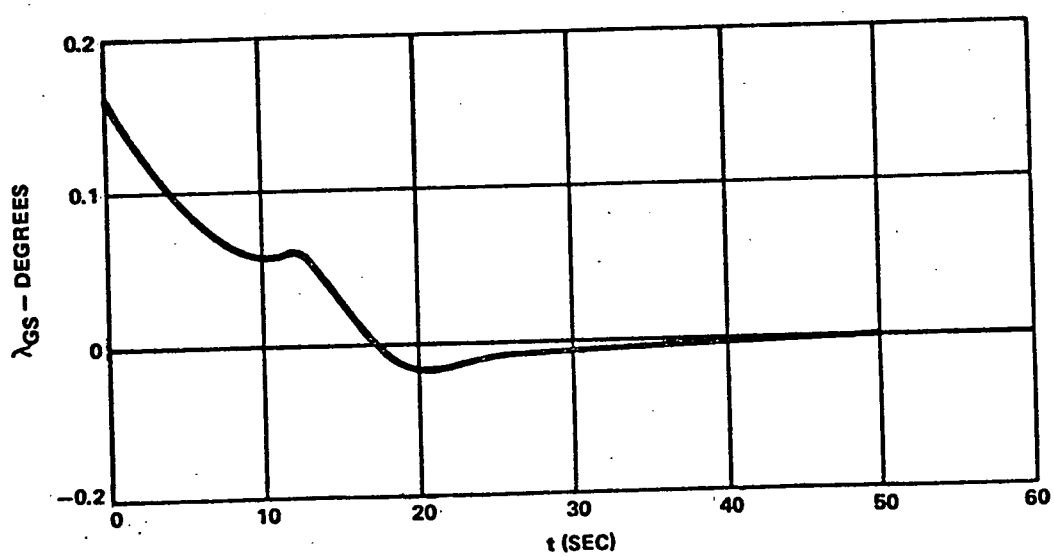

GLIDE SLOPE CAPTURE CONTROL LAW PARAMETERS

KGHD = 0.2 DEG/FT/SEC
HDMAXL = 0.8 FT/SEC^2

Figure 6-13
Glide Slope Capture Trajectories
(V = 141 knots)

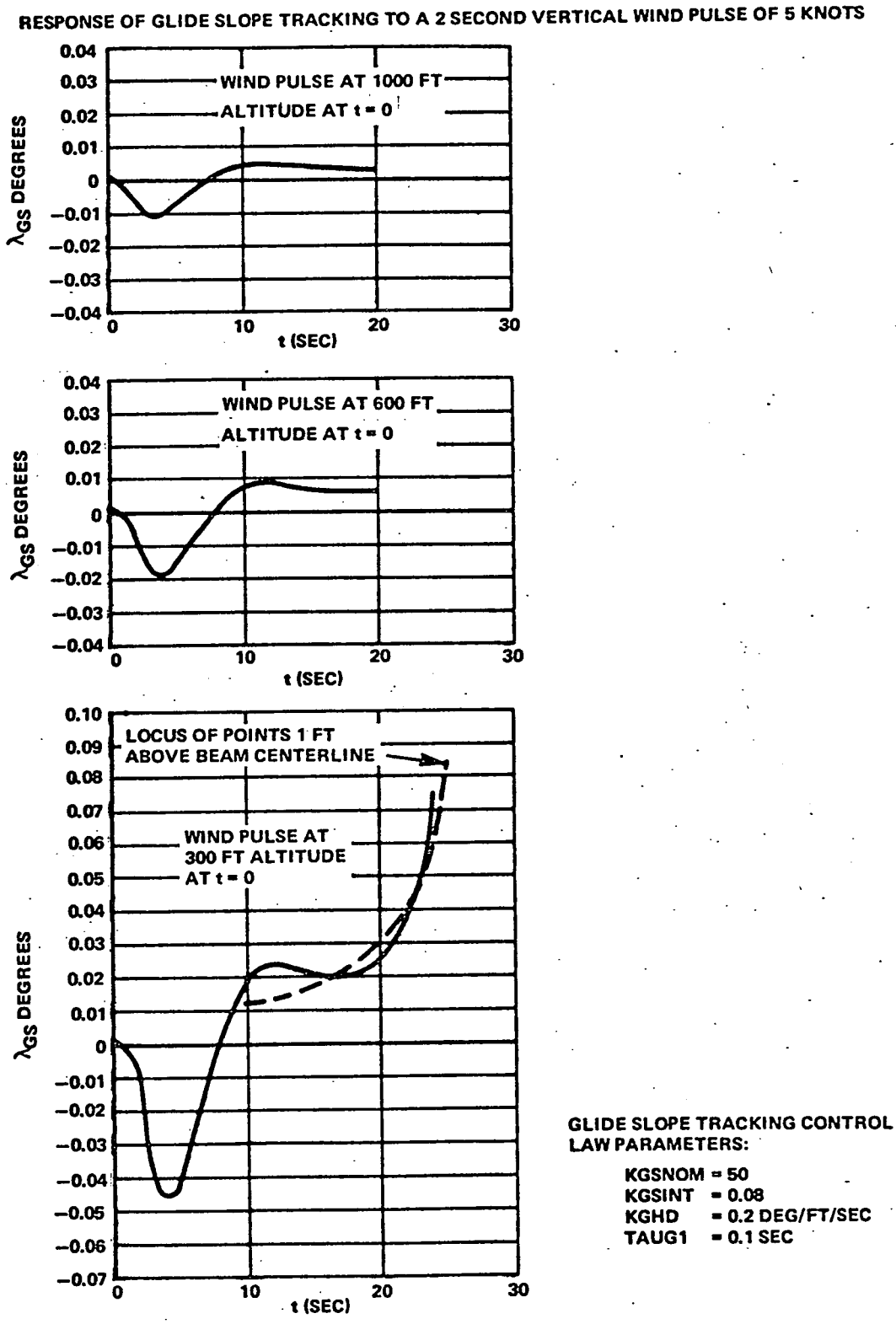

Figure 6-14
Glide Slope Tracking Transient Responses

3. Flareout Response

The nominal no-wind flareout characteristic for the exponential flare controller (standard flare) and the acceleration flare controller are illustrated as h vs $\dot{h}$ phase plane trajectories on Figure 6-15. The effectiveness of a flareout controller is determined by performance in a disturbance environment. Statistical data is needed to measure this performance. Histograms of the standard flare controller performance in turbulence (plus strong headwind) are given in Figure 6-16. One hundred runs were used to obtain this data. In general, the performance meets the FAA specified criteria in regard to touchdown dispersion (Reference 4). There are no standard criteria for maximum values of touchdown vertical velocity since this limit varies with individual aircraft. In Figure 6-16, it is seen that 78 percent of the landings had touchdown vertical velocities below 4 feet per second. No landings exceeded 6 feet per second. This would generally be considered satisfactory performance. Performance with the acceleration controller was not as successful, with touchdown $\dot{h}$ in turbulence tending to run about 30 percent higher than for the standard flare. A statistically significant sample of runs for the acceleration controller was not obtained. It is noted that σ = 6 feet per second vertical gusts represents fairly severe turbulence.

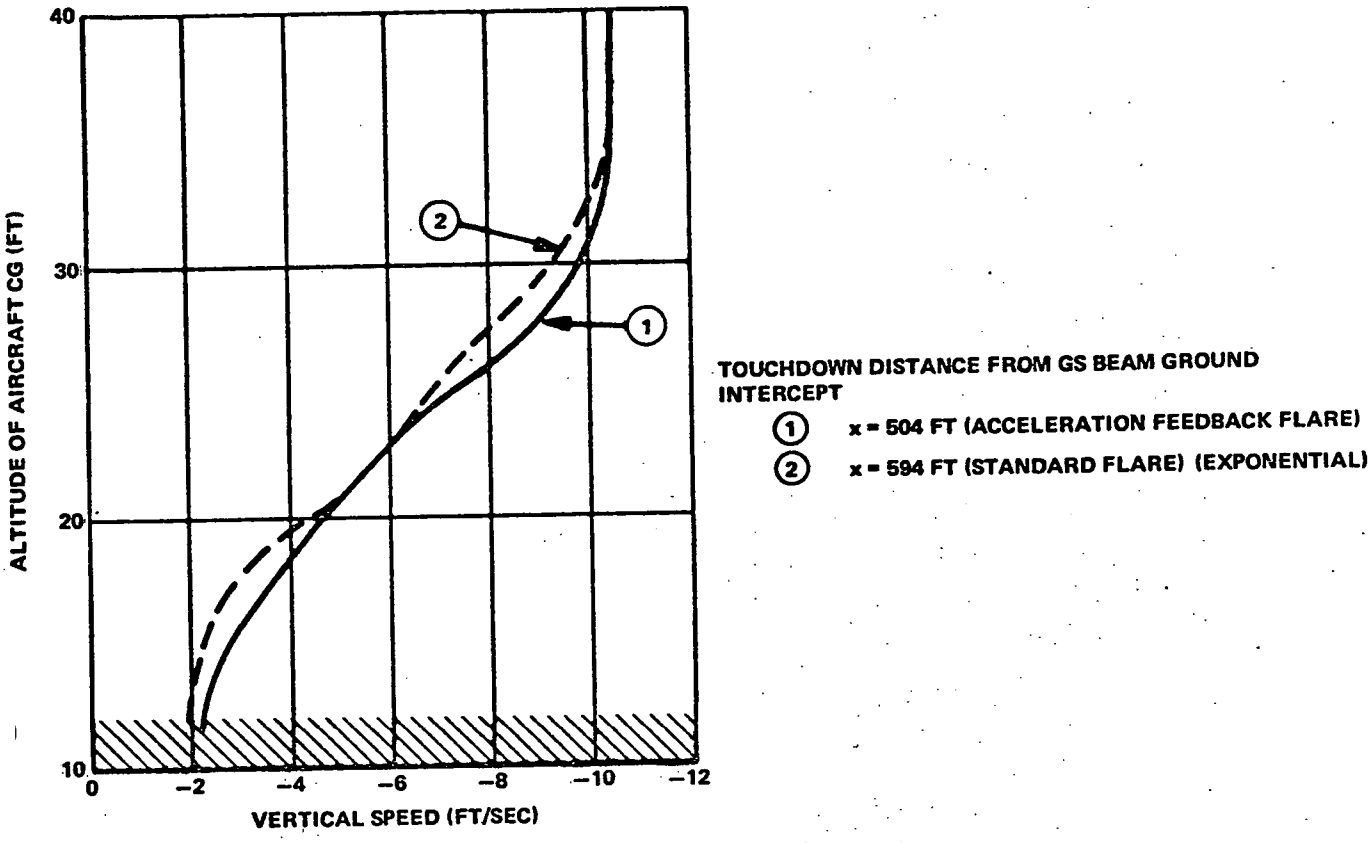

FLARE LAW PARAMETERS:

1 ACCELERATION FEEDBACK FLARE

THECFS = 2.18°
THCFF = 0.36 DEG/SEC
THCFR = 0
KFHD = 0.20
KFHDDT = 0.25
TAUF3 = 0.5

2 STANDARD FLARE

THECFS = 2.18°
THCFF = 0.36 DEG/SEC
THCFR = 0
KFLARE = 0.40
KFHD = 0.15
TAUF3 = 0.5

Figure 6-15
Nominal (No Wind) Flare Performance
(Phase Plane Trajectories)

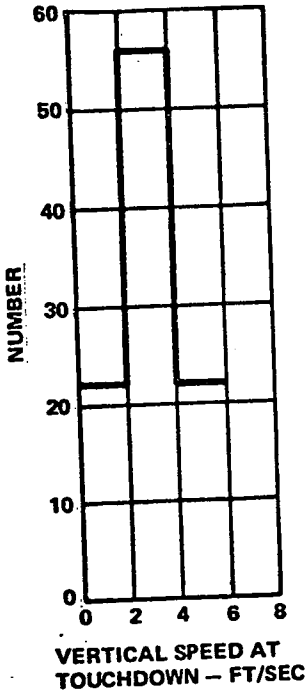

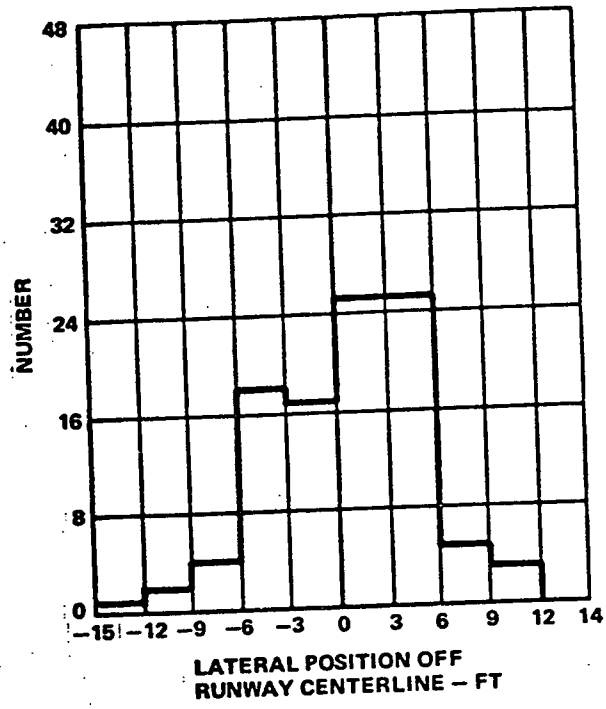

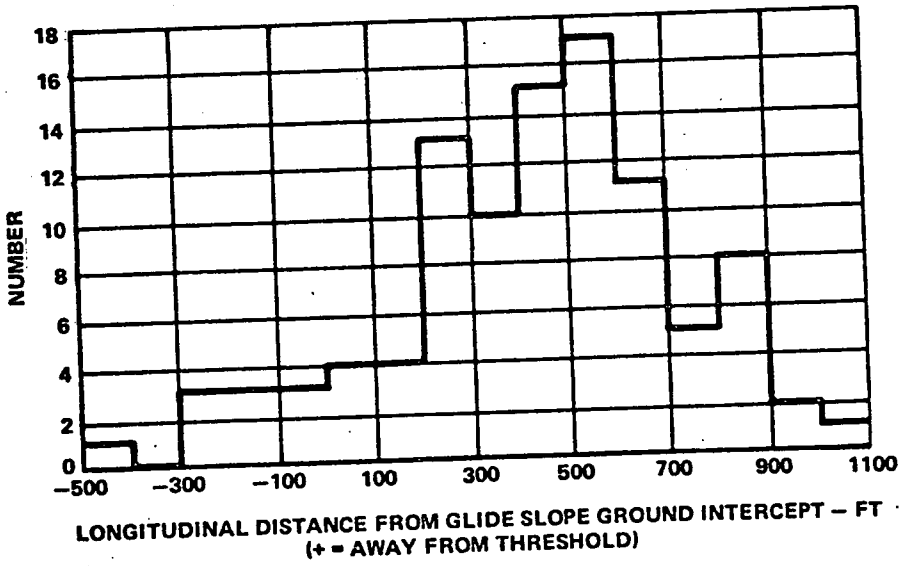

FLARE LAW PARAMETERS:
THECFS = 2.18°
THCFF = 0.36 DEG/SEC
THCFR = 0

KFLARE = 0.40
KFHD = 2.0
KF2 = 0.15
TAUF3 = 0.5

Figure 6-16
Standard Flare Touchdown Performance in Turbulence (Mean Headwind = -30 ft/sec, σ Gust = 6.0 ft/sec)

SECTION VII

LATERAL GUIDANCE

A. CONTROL LAW DEFINITION

1. Heading Control Modes

a. General

There are three heading control submodes. From the standpoint of control dynamics, they are identical. They differ because of operational procedures associated with reference data entry, mode selection, and computation requirements. The three submodes are:

- Heading hold
- Heading preselect
- Heading command

Heading hold is the basic lateral steering mode that is engaged automatically when other steering modes are not selected and manually commanded bank angles fall below a specified threshold value (about 5 degrees). The heading hold mode provides an automatic wing leveling capability. Heading preselect allows a reference heading to be entered while some other steering mode (including heading hold) is engaged. Heading preselect is not actually a control mode, but it is the initializing stage of the heading command mode (also referred to as heading select). A desired heading is entered, but control is not initiated until the heading command mode is engaged.

Provision is also made for a bank command mode. Various methods exist for manual bank angle insertion. Transport aircraft autopilots generally have turn knobs or control wheel steering sensing devices for this purpose. The computation and logic requirements associated with the manual bank modes are not covered in this report except for basic logic provisions that allow disengagement and synchronization of heading error signals when a manual bank command is received and reengagement of heading hold when bank commands are removed. Note that automatic turn coordination is implicit in the lateral/directional stabilization system. That is, all steering commands are executed to provide turn coordination by virtue of the lateral stabilization control laws defined in Section III.

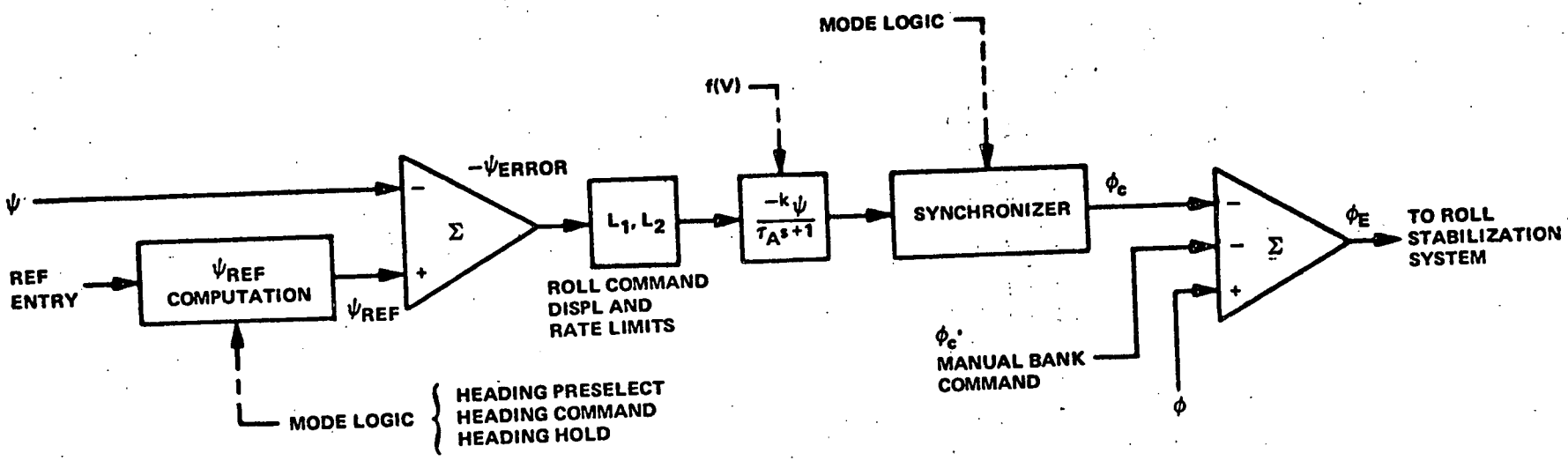

Figure 7-1
Heading Control Mode Block Diagram

b. Heading Hold Control

(1) Control Law

The basic heading control block diagram is shown in Figure 7-1. The heading control law used for all heading submodes is

$$\phi_c = -\left[\frac{k_\psi}{\tau_A s + 1}\right] \psi_{ERROR} \tag{7-1}$$

where the roll error is

$$\phi_E = (\phi - \phi_c) = \phi + \left[\frac{k_\psi}{\tau_A s + 1}\right] \psi_{ERROR} \tag{7-2}$$

The definition of ψ_{ERROR} (ψ_E) depends upon the mode logic. For the heading hold mode, ψ_E is defined as follows.

$$*\psi_E = (\psi - \psi_{REF}) \tag{7-3}$$

where

$$\psi_{REF} = \psi_o \tag{7-3a}$$

ψ_o is the heading that exists at the instant the heading hold mode is engaged. The gain k_ψ should be made a function of velocity to compensate for the change in turn rate capability with velocity. Thus,

$$k_\psi = a_1 \frac{V}{V_o} \tag{7-4}$$

where

$V_o \approx 200$ ft/sec

The limits L_1 and L_2 represent roll and roll rate command limits, respectively. A typical bank limit (L_1) is about 30 degrees, and a roll rate limit is about 5 degrees per second.

---

*See discussion of ψ_E in following paragraph on heading command mode for method of resolving the zero/360° ambiguity.

(2) Heading Hold Logic

The following symbols are used to represent mode logic states:

HH = Heading Hold Engaged

BC = Manual Bank Command Mode Engaged

BT = Bank Threshold Exceeded ($|\phi| > 5°$)

HC = Heading Command Mode Selected

$(\overline{\ })$ = Negation

$$HH = [(\overline{BC}) + (\overline{HC})] \cdot \overline{BT} + [(HH) \cdot (\overline{BC}) \cdot (\overline{HC})] \tag{7-5}$$

c. Heading Command

The heading command computation provides the heading reference storage and synchronization. Heading synchronization is performed in accordance with equation (7-3a). The elimination of the zero or 360-degree ambiguity in the computation of heading error may be accomplished as follows:

$$(\psi - \psi_{ref}) = \psi'_E \tag{7-6}$$

For $-180° < \psi'_E < +180°$, that is $|\psi'_E| < 180°$ (7-7)

$$\psi_E = \psi'_E$$

For $\psi'_E > +180°$ (7-8)

$$\psi_E = \psi'_E - 360°$$

For $\psi'_E < -180°$

$$\psi_E = \psi'_E + 360°$$

For $\psi'_E = \pm 180°$ (7-9)

$$\psi_E = +180°, \text{ if } \phi < 0 \text{ (left bank)}$$

or

$$\psi_E = -180°, \text{ if } \phi > 0 \text{ (right bank)}$$

To illustrate the above, consider the case where $\psi_{ref} = 30°$ and ψ, the aircraft heading = 340°

$$\psi'_E = \psi - \psi_{REF} = 340° - 30° = 310°$$

since

$$\psi_E' > 180°$$

$$\psi_E = 310° - 360° = -50°$$

Thus, to reach the heading reference, the aircraft will command a bank angle in accordance with equation (7-1). For the case illustrated, ϕ_c will be

$$\phi_c = -\frac{k_\psi}{\tau_A s + 1}(-50) = +\frac{50\ k_\psi}{\tau_A s + 1}$$

which is a right bank angle command.

d. Synchronization - Data Hold

The block identified as the synchronizer on Figure 7-1 provides the necessary mode engage and disengage smoothing. At the time of any mode transition, the existing value of bank command (ϕ_c) resulting from a previously computed error signal is decayed to zero as follows:

$$\phi_{C_R} = \phi_{C_o} \frac{\tau_B s}{\tau_B s + 1} \tag{7-10}$$

where ϕ_{C_R} is the residual roll command that is to be reduced to zero, and ϕ_{C_0} is the value of roll command at the instant of mode transition.

e. Stability Considerations

Heading control by rolling the aircraft to correct heading errors involves a single integration loop (associated with turning kinematics) plus the roll stabilization dynamics and filter lag (Figure 7-2a). Note that the lag filter, τ_A, on the heading error is used primarily to decouple any residual dutch roll oscillatory tendencies not fully compensated by the yaw damper and roll stabilization loops. This filter also helps prevent excessive rolling as a result of turbulence. The penalty for this filter is a significant lag (1 to 2 seconds) and a compromise in attainable gain. The typical root locus is shown in Figure 7-2b.

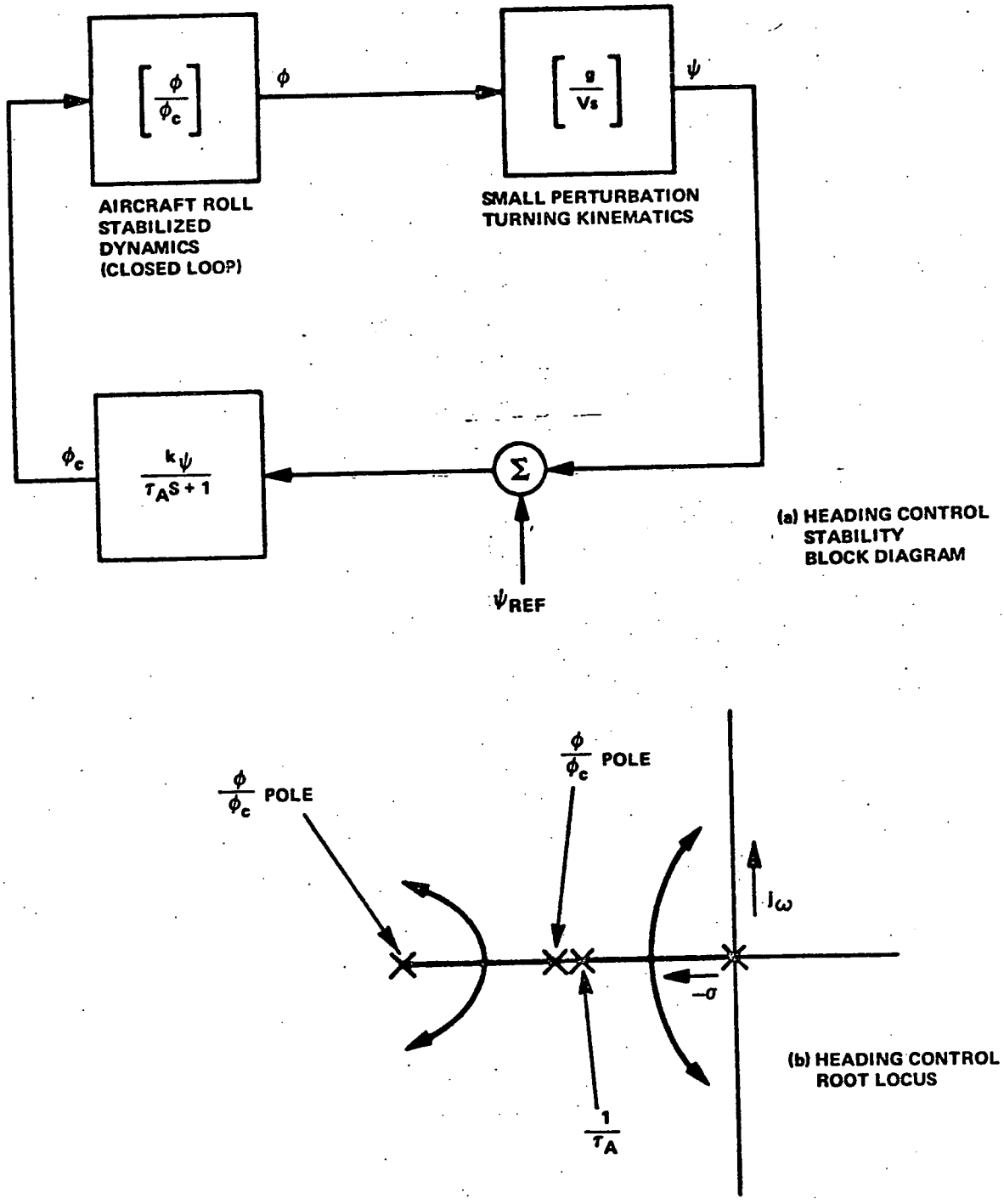

Figure 7-2
Heading Control Stability Analysis

The heading control loop gain should be made proportional to velocity to compensate for the velocity term in the aircraft's turning kinematics (ψ/ϕ). In some applications, heading error integral is used to improve heading control static accuracy. Asymmetric thrust would result in a heading standoff (with a resultant wing-down condition). The use of integral control could prevent the heading standoff error. It is not recommended because the heading mode does not generally have stringent accuracy requirements. A good guidance system readily recomputes the heading correction needed to correct a flight path error caused by a condition such as asymmetric thrust.

An important factor in the analysis of heading control stability is the definition of the heading angle ψ. If ψ is the euler angle determined by a yaw, pitch, roll sequence of rotations from a local vertical coordinate frame, then the heading control laws given in equations (7-1) and (7-3) are not adequately represented by the stability analysis (Figure 7-2) for large angles of attack and large bank angles. The problem results from the fact that the turning kinematics are only an approximation of the azimuth change experienced by the aircraft's X axis. To illustrate the problem without the required derivation of the geometrical relationships, consider the hypothetical case of an aircraft in horizontal flight with a 90-degree angle of attack (pitch angle = +90 degrees). Now perform a zero sideslip bank about the velocity vector. A bank about the velocity vector is all body axis yaw rate and zero body axis roll rate. Let the roll angle change about the velocity vector be 90 degrees. The initial result is that the angle of attack remains 90 degrees (no change in velocity vector) but the azimuth angle ψ has changed 90 degrees. This corresponds to a case where the azimuth rate is the rate of roll about the velocity vector rather than $g/V \tan \phi$, the relationship defined by the turning kinematics.

Thus if the control laws specified in this report are implemented using euler angle ψ, then serious stability problems can occur for high angle-of-attack flight conditions (at high velocities). To overcome this problem, the angle ψ can be interpreted as inertial velocity vector heading defined as:

$$\psi = \tan^{-1} V_{north}/V_{east}$$

f. Control Parameter Summary

The control parameters identified in the control equations given in the previous paragraphs are specified in terms of typical minimum, nominal, and maximum values in Table 7-1.

TABLE 7-1

CONTROL PARAMETER SUMMARY

Parameter	Typical Minimum Value	Typical Nominal Value	Typical Maximum Value	Remarks
a_1	0.50	1.0	1.5	Heading control gain at velocity V_o
V_o	--	200 ft/sec	--	Normalizing velocity
τ_A	0.70	1.0	2.0	Heading error filter
L_1	20 deg	30 deg	40 deg	Roll displacement command limit
L_2	3.0 deg/sec	5 deg/sec	8 deg/sec	Roll rate command limit
τ_B	1.0 sec	2.0 sec	4.0 sec	Mode transition smoothing

g. Performance Criteria

Heading Control Transient Response

a. At an aircraft velocity of about 200 to 300 feet per second, apply a 45-degree step heading change command.

b. The roll rate limit should be held within ±10 percent and the bank angle increased to the maximum value (L_1) with a maximum overshoot of about 3 degrees.

c. Sideslip should never exceed a value equivalent to a lateral acceleration of 0.08g.

d. Roll out to the desired heading should be achieved with a heading overshoot restricted to about 2 degrees.

e. When stabilized on the reference heading, apply a step rudder command of about 5 to 10 degrees δ_R for about 5.0 seconds. Remove the rudder command and allow the aircraft to settle to the reference heading. The heading error should be less than 0.5 degrees within 10 seconds after release of the disturbance. The corrective response should have a maximum of one overshoot.

2. Localizer and Landing Guidance

a. General

The ILS steering functions covered in this report relate to the capture and tracking of the ILS localizer radio beam from the initial intercept path to landing. Two important aspects of the ILS control problem are avoided by the simplified statement of control equations given herein. The first involves the terminal area navigation problem associated with establishing the proper localizer intercept trajectory. The availability of range and bearing to the localizer transmitter (VOR and DME source located near localizer transmitter) could permit the automatic computation of optimum terminal area flight paths. For example, the aircraft could be guided toward the proper intercept path and then automatically turned to that intercept heading when the downrange distance is considered optimum. This terminal area navigation and guidance system would use the aircraft turning radius constraints to compute a fixed bank angle maneuver that yields a flight path tangent to the desired localizer intercept heading. In effect, a circle of radius given by

$$R = \frac{V^2}{g \tan \phi_M} \tag{7-11}$$

(where ϕ_M = the maximum permissible bank angle) could be located so that it is tangent to the desired intercept heading. Automatic programs that provide this navigation function are not covered in the present report. The problem is started on the heading select mode where the selected heading is the desired beam intercept angle and the point of intersection is sufficiently far from touchdown to permit beam capture without excessive overshoots.

The other aspect of the localizer steering problem that is not covered in this report involves the considerable complication associated with redundancy and reliability considerations for sensors. In a Category III, fail-operative control system, the sensors and other reference devices used for flight path control must be operating in a properly monitored and redundant configuration. If some of these sensors fail during earlier phases of the flight, an automatically coupled ILS approach should not be precluded. Thus, if the Inertial Navigation System (INS) provides information used in the control laws, should a loss of that INS data eliminate the automatic approach capability? Systems in operation today have answered this question by providing back-up modes in the event of the loss of such data. The following is a brief summary of typical compromises that have been made in operational autopilots in order to cope with practical problems of this type:

- Localizer beams that meet Category II (or higher) standards are able to provide adequate lateral velocity information. However, the airborne systems must also operate with Category I (or poorer) beams, where beam noise precludes the derivation of satisfactory lateral velocity data. Hence, autopilots mechanize compromise control laws which derive lateral velocity inertially from aircraft heading.

- Systems using heading derived lateral velocity contain large crosswind errors. These errors are minimized or eliminated by the type of control law used. The crosswind error can be eliminated if drift angle correction is derived from the INS computer. If a localizer steering control law depends upon true velocity vector heading, then the loss of the INS will force a breakdown of the steering law. Hence, in typical operational systems, back-up steering laws are implemented to cope with an invalid INS, but these steering laws are only activated upon loss of the INS.

- Localizer gains are programmed downward during the final approach phase. The gain programming is often made a function of radio altitude. If the radio altimeter is not "valid", a back-up gain program is activated. This back-up gain program may be a function of time, or it may be a function of marker beacon signals.

The activation of an alternate gain reduction program can permit penetration to lower altitudes although not to flare-out altitudes.

In this report, the concepts of back-up control laws and alternate sensing schemes are not considered. It is assumed that all of the required data is available. It is also assumed, however, that the localizer radio signal is not of ideal quality. Hence, its use in deriving lateral rates is restricted to reasonable applications that minimize noise effects. The dominant lateral velocity source for the specified control laws is drift angle corrected heading. An idealized source of gain programming is obtained from range to localizer. Such information is not generally available today and a radio altimeter would be a more reasonable source of such information. The altimeter, however, is a compromise choice because of its dependence upon a smooth terrain along the final approach path.

b. Localizer Geometry and Control Phases

There are five phases of lateral beam steering in regard to control laws used. They are:

1. Intercept - Heading select mode on a constant beam intercept heading.

2. Capture - Proper penetration of the beam has been sensed and the aircraft is turned to align with the beam center line.

3. On-Course - Alignment has been satisifed with regard to position and rate errors, and tight tracking of the beam is initiated.

4. On-Course/Final Approach - The final phase of the localizer tracking is initiated (usually at glide slope penetration) and downward gain programming of the beam signal is initiated.

5. Decrab - The aircraft nose is aligned with the runway center line immediately prior to touchdown.

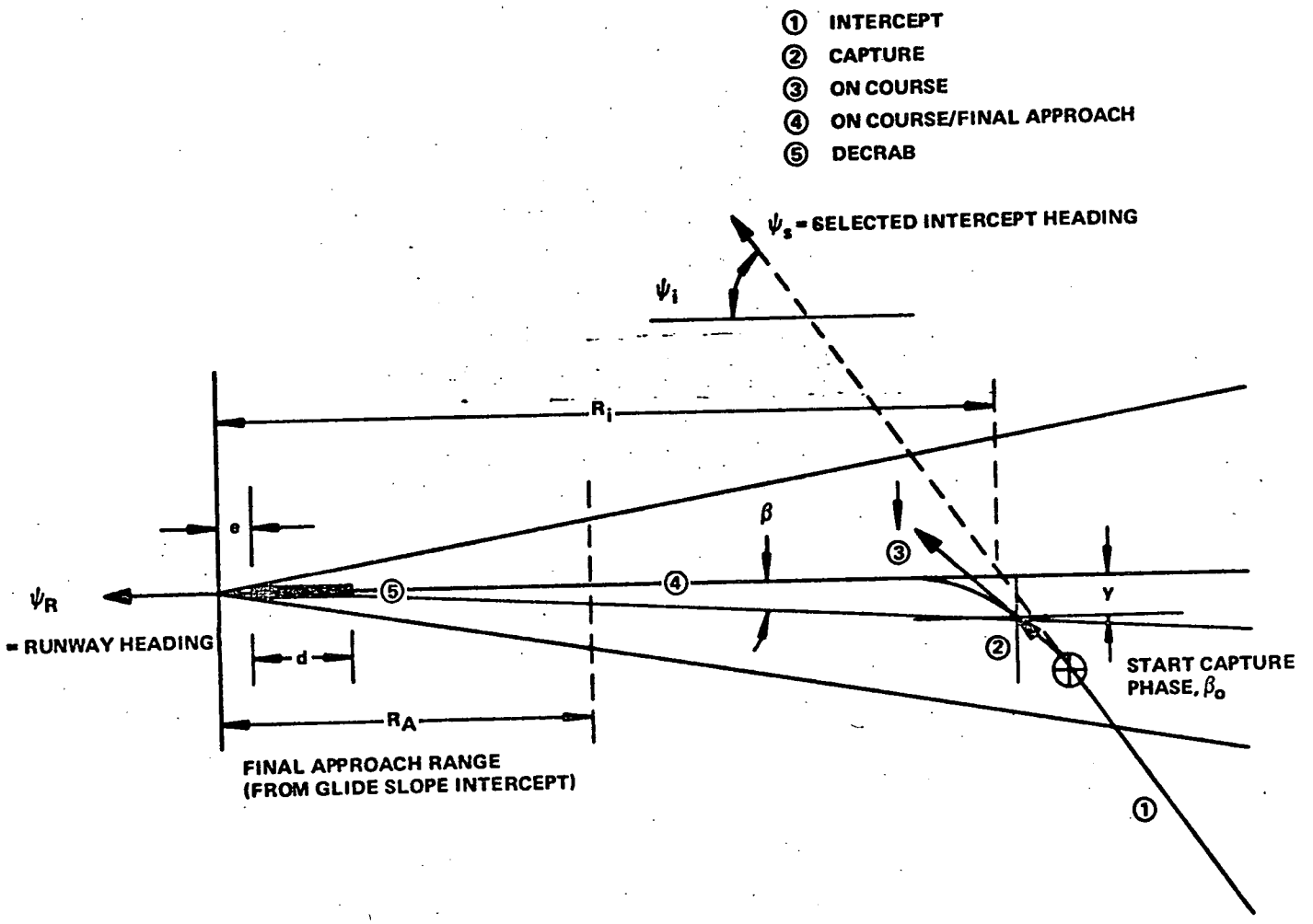

Figure 7-3
Localizer Capture and Tracking Geometry

Figure 7-3 illustrates these control phases in terms of the localizer beam geometry. Note that for consistently good performance, the intercept range, R_i, should be greater than 12 nautical miles if bank angle limits of about 25 degrees are to be imposed. (For a 10,000-foot runway, an R_i of 12 nautical miles represents an intercept about 10 nautical miles from the runway threshold.) The intercept angle is ψ_i. It should be about 45 degrees. Intercept angles as large as 90 degrees are acceptable if the intercept range is increased to greater than 14 nautical miles. The capture phase will automatically start when the beam is penetrated to a value β_o. This capture point is computed as a function of position and rate so that it will vary with distance from the runway and the steepness of the intercept. For large intercept angles, capture starts near the outer boundary of the beam; while for shallow intercept angles, capture is delayed until the aircraft is near the beam center (small β_o).

A standard localizer beam for a 10,000-foot runway is assumed for the calculation of all nominal parameters. Such a beam is 3.6 degrees wide (7.2 degrees total). Figure 7-4 illustrates how this converging beam produces an increasing sensitivity as the runway is approached. From the point of the penetration of the glide path center (28,000 feet for 1,500 feet of altitude and a 3.0-degree glide path) to touchdown, the localizer sensitivity increases by a factor of nearly 5 to 1.0.

R = DISTANCE FROM TRANSMITTER
R' = R– (d + e) = DISTANCE FROM RUNWAY THRESHOLD
β = LOCALIZER DEVIATION . . . DEGREES
β_{MAX} = LOCALIZER COURSE SECTOR ANGLE = 3.6° FOR 10,000 FT RUNWAY (d = 10,000; e = 1,000)
y = POSITION DEVIATION

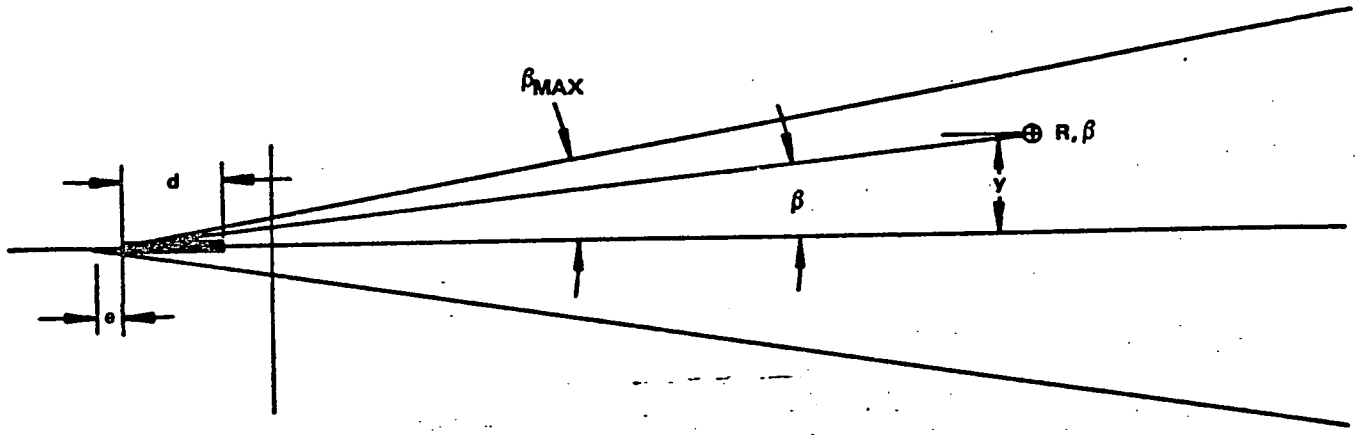

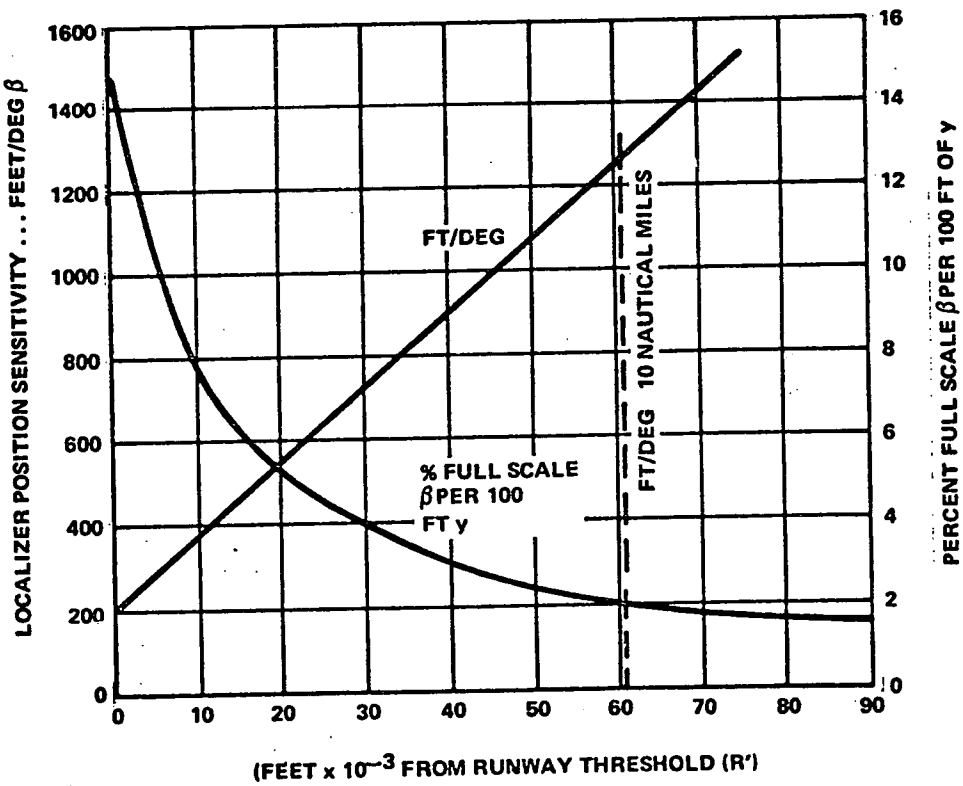

Figure 7-4
Localizer Position Measuring Sensitivity

c. Control Laws

(1) Localizer Capture

The control law block diagram for all phases of localizer control is illustrated in Figure 7-5. The problem starts on the heading select mode where the steering law is

$$(\psi_V - \psi_S)\left[\frac{1}{\tau_5 s + 1}\right] = -\phi_C' \tag{7-12}$$

where ψ_V is the velocity vector heading

$$\psi_V = \psi + \psi_D \tag{7-13}$$

and ψ_S is the selected beam intercept heading. If ψ_R is the runway heading, the intercept angle, ψ_i, is

$$(\psi_R - \psi_S) = \psi_i \tag{7-14}$$

(Note that the polarity of roll error summing is $\phi_E = \phi - \phi_C$.) The heading select control laws have been described in equations (7-2) through (7-9).

The aircraft is maintained on the selected heading while the capture computer sums weighted beam displacement, beam rate, and heading error in accordance with either of the following equations: [Note that (7-15a) or (7-15b) can be optimized for good performance but with different combinations of constants c_1, c_2 and c_3.]

$$c_1 \sin \psi_E + \frac{c_2 \beta s}{(\tau_2 s + 1)(\tau_3 s + 1)} + \frac{c_3 \beta}{\tau_4 s + 1} = \epsilon \tag{7-15a}$$

or

$$c_1 (1 - \cos \psi_E) + \frac{c_2 \beta s}{(\tau_2 s + 1)(\tau_3 s + 1)} + \frac{c_3 \beta}{\tau_4 s + 1} = \epsilon \tag{7-15b}$$

where $\psi_E = \psi_V - \psi_R$ (7-16)

and the following sign conventions are observed: ψ_E, β, $\dot{\beta}$ are positive for those conditions that displace the aircraft or cause a rate of change of displacement to the right of the beam (from the viewpoint of the pilot). The angle β is therefore positive if it is defined as counterclockwise when viewed from the localizer transmitter. (In Figure 7-3, ψ_E and $\dot{\beta}$ are positive and β is negative at the capture angle β_o. The capture phase starts when $\epsilon = 0$.

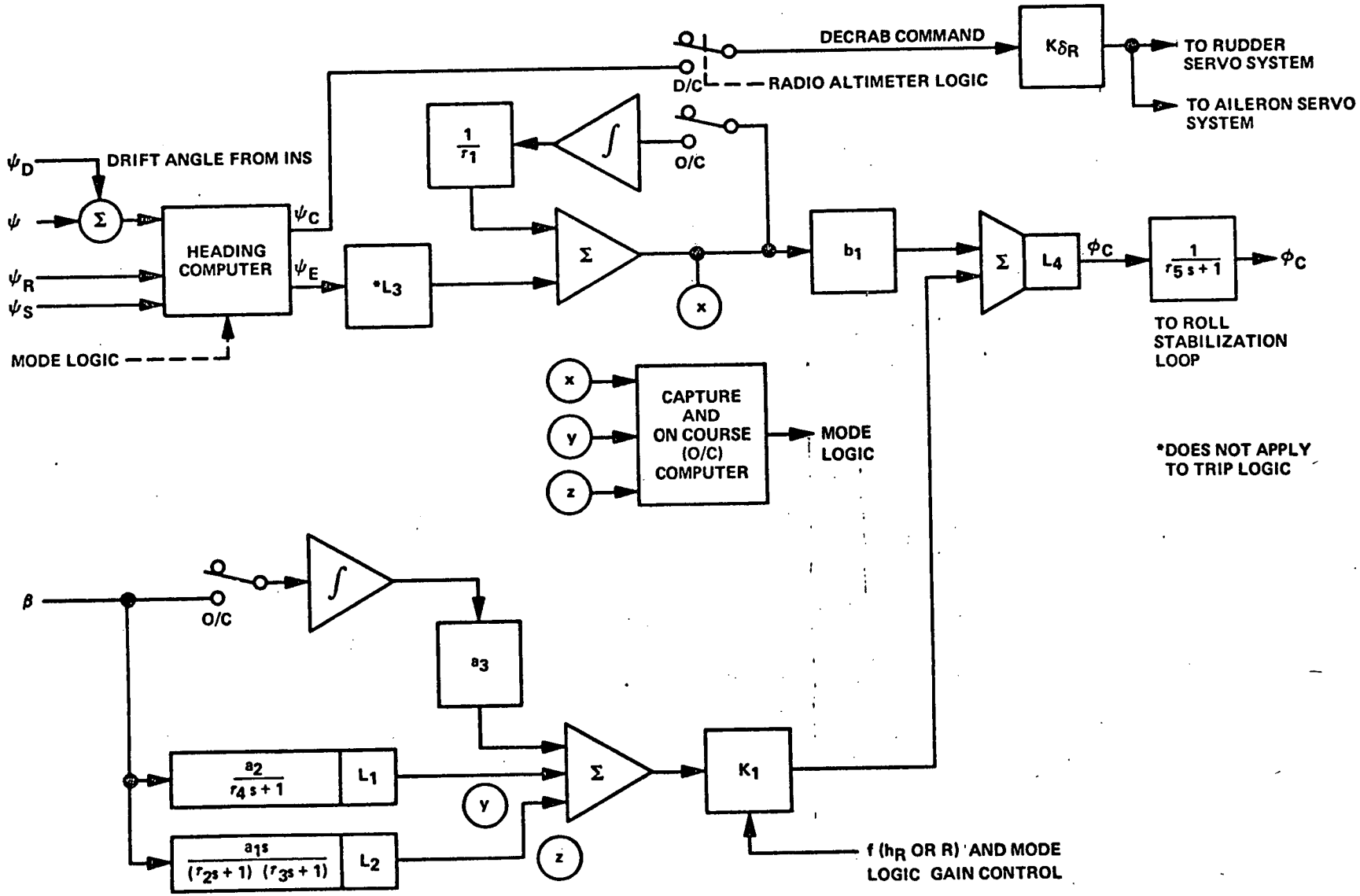

Figure 7-5
Localizer Control Block Diagram

The heading select mode is disengaged and any residual bank angle command decayed to zero in accordance with equation (7-10). The localizer capture control law is now activated. It is

$$b_1 \psi_E + \frac{a_1 s}{(\tau_2 s + 1)(\tau_3 s + 1)} \beta + \frac{a_2 \beta}{\tau_4 s + 1} = - \phi_C \tag{7-17}$$

(2) On-Course (O/C) Tracking

The capture equation (7-17) aligns the aircraft with the localizer beam. The on-course computer senses beam displacement beam rate and bank angle and, when these parameters satisfy certain specified minima, the O/C phase will begin. The O/C sensing logic equation is

$$O/C = \left\{ \left| \frac{\beta}{\beta_{MAX}} \right| < \epsilon \cdot \left| \frac{\dot{\beta}}{\beta_{MAX}} \right| < \epsilon_2 \cdot |\phi| < \epsilon_3 \right\} \tag{7-18}$$

When the O/C logic equation is satisfied, the control law switches to the O/C parameters. Note that control variables do not change; only the computations performed on these variables change. Hence, there is no need for any mode transition synchronization or data smoothing. The O/C control law is

$$b_1 \psi_E \frac{\tau_1 s}{\tau_1 s + 1} + \frac{a_1 s \beta}{(\tau_2 s + 1)(\tau_3 s + 1)} + \frac{a_2 \beta}{\tau_4 s + 1} + a_3 \int \beta \, dt = - \phi_C \tag{7-19}$$

As the O/C control law is activated, bank limits are usually reduced from 25 to 30 degrees to about 10 degrees. Likewise, roll rate command limits are reduced.

(3) On-Course (O/C) Tracking - Final Approach

This phase starts with penetration of the glide slope center line. The control law remains identical to equation (7-19) except that the gains are now changed and programmed. Thus, for this final phase, the control law may be expressed as:

$$b_1 \psi_E \left[\frac{\tau_1 s}{\tau_1 s + 1} \right] + \left[\frac{a_2 s \beta}{(\tau_2 s + 1)(\tau_3 s + 1)} + \frac{a_2 \beta}{\tau_4 s + 1} + a_3 \int \beta \, dt \right] k(R') = - \phi_C \tag{7-20}$$

where the individual constants, b_1, a_1, a_2, a_3, may also be modified, but the gain reduction program k(R') is activated. The gain reduction is of the form

$$k(R') = 1 - \left(\frac{R'_{G/S} - R'}{R'_{G/S}}\right) k \qquad (7\text{-}21)$$

where

R' = distance to runway threshold

$R'_{G/S}$ = distance from glide slope intercept point to runway threshold (see Figure 7-4)

k = localizer control attenuation factor

Thus, if k = 0.5, the localizer gain at the runway threshold will be half the gain at the glide slope intercept point.

(4) Decrab (D/C)

Two techniques for automatic runway alignment have resulted from work in automatic landing. These are the skid decrab and the forward slip decrab.

Skid Decrab

This technique involves roll control to track the lateral path through coordinated turns (zero sideslip down to a "decrab" altitude of approximately 8 feet. In the presence of cross winds, a zero sideslip crab angle will develop. At the decrab altitude, the lateral guidance commands are removed and zero roll angle is commanded. At the same time, rudder commands are used to align the aircraft with the runway heading (decrab). Predictive commands are added to both the rudder and aileron channels to provide surface deflections that will compensate for roll and yaw moments resulting from the sideslip developed during the maneuver. The system is normally designed so that touchdown occurs when approximately 70 to 80 percent of the crab angle is removed. At this time, the crab angle is small and the aircraft has a yaw rate established in the direction of the remaining crab angle. This results in low side forces on the gear at touchdown and does not allow time for the aircraft to develop a significant cross runway drift velocity.

Forward Slip

The "forward slip" technique involves aligning the aircraft heading with the runway heading by applying roll and yaw commands at an altitude

of approximately 200 feet. The roll commands used for lateral guidance combined with the rudder commands used for alignment result in a sideslip equal to the original crab angle. The vehicle can be landed on one gear truck in the forward slip configuration provided maximum bank angle constraints (imposed by wing scrape limitations) are observed. In fact, this is the normal manual landing technique for transport aircraft. Because of restrictions on roll attitude resulting from wing and engine pod clearances, techniques have been developed to reduce the touchdown roll attitude to an acceptable value with an additional skid maneuver. Systems have been developed combining the forward slip and the skid decrab maneuver.

The forward slip maneuver is the preferred runway alignment technique for manual control. Pilots have found it easier to minimize lateral drift with this technique than with the skid decrab. For the skid decrab to be done properly, a critical and precise sequence of rudder and roll commands must occur in the final three seconds prior to touchdown. Automatic systems can, in general, perform this maneuver with less difficulty than a pilot because they can utilize precise measurements and computations to develop the necessary roll and yaw controls.

For automatic control, the forward slip maneuver has the disadvantage of interacting with the lateral guidance. While rudder control is maintained to keep the vehicle heading aligned with the runway heading, roll commands are used to command sideslip for lateral guidance. To avoid large lateral errors in the presence of wind shear and gusts, cross feed is required between the rudder channel and the roll channel. Experience has shown that the definition of these cross-feed terms is critical and that small errors in these parameters can result in lateral guidance errors which are more dangerous than incorrect runway alignment at touchdown.

In this study the skid decrab was selected for implementation because of its simplicity. It is acknowledged that pilots tend to prefer the other approach for manual control but a skid decrab should be adequate for most aircraft when precise automatic control is feasible. The recommended decrab control laws are:

$$\delta_{R_{COM}} = k_{\delta_R} \left[\left(\psi - \psi_R \right) \left(1 + \frac{C_1}{s} \right) \right] + k_r \gamma + \delta_{RP} \tag{7-22}$$

where ψ_R is the runway heading and δ_{RP} is the predictive rudder command.

$$\delta_{RP} = f\left[(\psi_o - \psi_R),\ C_{N_{\delta_R}},\ C_{N_\beta}\right] \tag{7-23}$$

where

ψ_o = crab angle at decrab initiate

$$-\delta_{A_{COM}} = k_7\left[\phi + \frac{a_1}{\tau_7 s + 1}\,p\right] + \delta_{AP} \tag{7-24}$$

where δ_{AP} is a predictive or feedforward compensation used to help keep wings level in the presence of sideslip build-up or even to drop the wing in the direction of the wind to partially compensate for the lateral drift.

$$\delta_{AP} = k_{\delta A}\,(\psi_o - \psi_R) \tag{7-25}$$

where

$$k_{\delta_A} = f\left[C_{\ell_\beta},\ C_{\ell_{\delta_A}},\ C_{N_\beta},\ C_{\ell_{\delta_R}}\right]$$

The decrab initiate altitude should be adjusted as a function of lateral error and vertical velocity. If $h_{D/C}$ is the altitude at which decrab is initiated, it should be defined as follows:

$$h_{D/C} = h_{D/C\ \mathrm{NOMINAL}} + f\,(\Delta\dot{h},\ \psi - \psi_R,\ y,\ \dot{y}) \tag{7-26}$$

d. Stability Considerations - Lateral Guidance (Landing)

The stability of the flight path control loop used to track the localizer is described by the dynamics shown in Figure 7-6. Note that control laws using β, $\dot{\beta}$, and ψ_E are forms of y and $\dot{y}$ in accordance with the following:

$$\beta = \frac{y}{R} = \frac{y}{R' + (d + e)} \tag{7-27}$$

$$\dot{\beta} = \frac{\dot{y}}{R} - \frac{\dot{R}}{R^2} \tag{7-28}$$

$$\psi_E = \sin^{-1}\frac{\dot{y}}{V} \approx \frac{\dot{y}}{V} \tag{7-29}$$

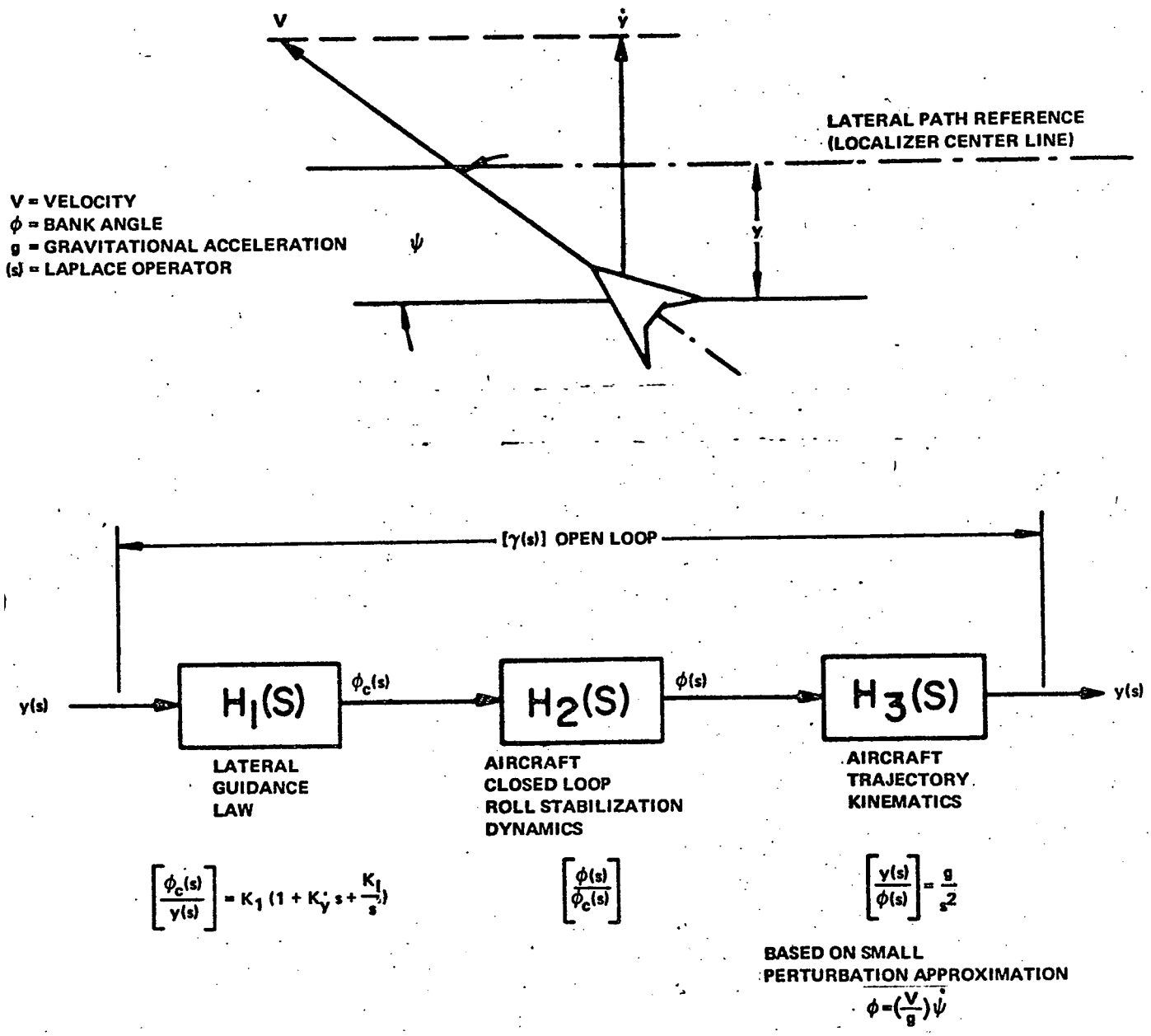

Figure 7-6
Lateral Flight Path Stability Parameters

Thus, equation 7-19, expressed in terms of y and $\dot{y}$, would be

$$\left[\frac{b_1}{V}\left(\frac{\tau_1 s}{\tau_1 s + 1}\right) + \frac{a_1}{R}\frac{1}{(\tau_2 s + 1)(\tau_3 s + 1)}\right] sy + \frac{a_2}{R} y + \frac{a_3}{R}\frac{y}{s} = -\phi_C \qquad (7\text{-}30)$$

(Note that equation (7-30) neglects the $\dot{R}$ part of $\dot{\beta}$.)

Figure 7-6 simplifies equation (7-30) by assuming that the filters do not have a dominant effect on closed-loop stability. The form of the root loci, with and without integral control, is shown in Figure 7-7. Since the gains vary with R, it is seen that the loop (with integral control) tends toward conditional stability when gains are too low. Low gains correspond to large values of R. The effects of the low frequency modes associated with the integral part of the control law can be minimized by engaging the integrator only when errors are very small. The O/C engage logic is used to ensure that this condition is met.

The most important factor involving stability of localizer control is the increasing gain as R approaches zero [equation (7-30) and Figure 7-4]. The gain reduction program used in the O/C - final approach phase helps compensate for this problem. When the damping term ($\dot{y}$) is obtained from heading, then the gain of that term does not increase as the runway is approached. Hence, the ratio of rate to displacement decreases as the displacement gain rises. This is one reason why beam rate (a_1 term) is used as well as heading. However, the effectiveness of the beam rate damping is limited in bandwidth because of the required filtering. Hence, if the total y and $\dot{y}$ gain is allowed to go too high for small R, the closed loop frequency will reach a region where the lags in the beam rate filter become destabilizing. The effect of these lags is not shown in Figure 7-7. If they were included, the dominant roots would turn into the right-half plane as gain is increased.

e. Control Parameters Summary - Localizer and Landing Guidance

The control parameters identified in the control law equations given in the previous paragraphs are specified in terms of typical minimum, nominal, and maximum values in Table 7-2.

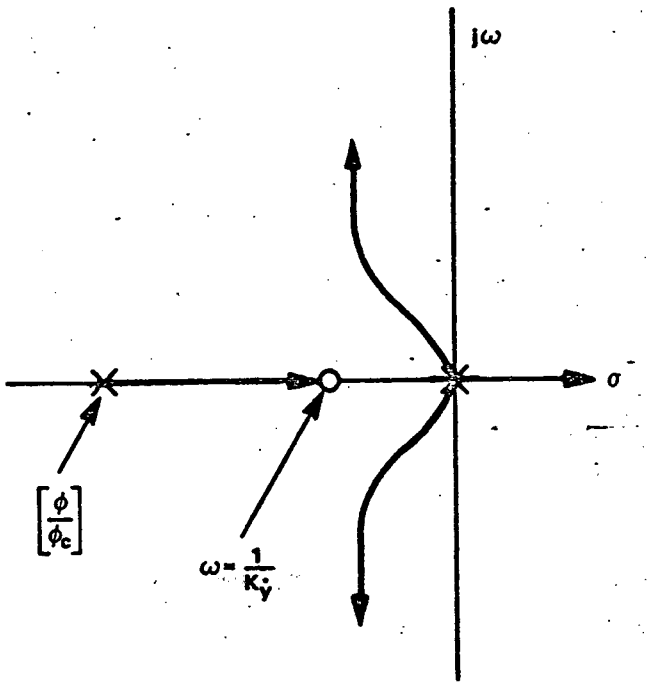

$$[Y(s)]_{\substack{\text{OPEN}\\\text{LOOP}}} = K_{1g}\,\frac{[K_{\dot{y}}s + 1]}{s^2}\left[\frac{\phi}{\phi_c}\right]$$

(a) LATERAL PATH CONTROL ROOT LOCUS WITHOUT INTEGRAL CONTROL

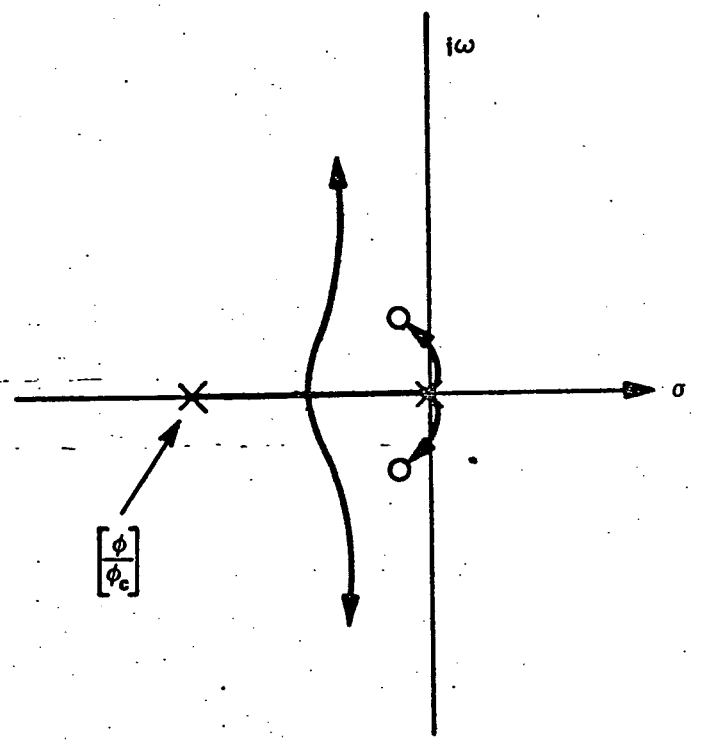

$$[Y(s)]_{\substack{\text{OPEN}\\\text{LOOP}}} = K_{1g}\,\frac{[K_I + s + K_{\dot{y}}s^2]}{s^3}\left[\frac{\phi}{\phi_c}\right]$$

(b) LATERAL PATH CONTROL ROOT LOCUS WITH INTEGRAL CONTROL

Figure 7-7
Stability Analysis of Lateral Flight Path Control

TABLE 7-2

LOCALIZER AND LANDING GUIDANCE
PARAMETER SUMMARY

Parameter	Typical Minimum Value	Typical Nominal Value	Typical Maximum Value	Remarks
c_1	2.0	2.5	3.0	LOC capture sensor trip logic heading gain
c_2	4.0	7.0	10.0	LOC capture sensor trip logic $\dot{\beta}$ gain
c_3	$0.5 \times \frac{R}{72,000}$	$1.0 \times \frac{R}{72,000}$	$2.0 \times \frac{R}{72,000}$	LOC capture displ (β) trip lag
τ_2	0.5	1.0	1.5	$\dot{\beta}$ filter time constant (seconds)
τ_3	0.1	0.2	0.4	$\dot{\beta}$ filter time constant (seconds)
τ_4	0.10	0.25	0.50	β filter time constant (seconds)
b_1 (Capture)	1.0	1.5	2.0	Heading gain - deg ϕ_C per deg ψ_C
a_1 (Capture)	3	5	10	Beam rate gain - deg ϕ_C per deg per sec β
a_2 (Capture)	18	20	25	Beam displacement gain - deg ϕ_C per deg β
b_1 (O/C)	1.0	1.5	2.0	Same units as above
a_1 (O/C)	3	5	10	Same units as above
a_2 (O/C)	18	20	25	Same units as above
a_3 (O/C)	0.20	0.30	0.40	Beam integral gain - deg ϕ_C per sec per deg β
τ_1	25	30	40	Heading washout time constant (seconds)
b_1 (O/C Final)	1.8	2.2	2.5	Same units as above
a_1 (O/C Final)	3	5	10	Same units as above
a_2 (O/C Final)	18	20	25	Same units as above
a_3 (O/C Final)	0.20	0.30	0.40	Same units as above
k	0.25	0.5	0.70	Gain attenuation factor

TABLE 7-2 (cont)

LOCALIZER AND LANDING GUIDANCE
PARAMETER SUMMARY

Parameter	Typical Minimum Value	Typical Nominal Value	Typical Maximum Value	Remarks
k_{δ_R}	1	2 deg δ_R per deg ψ_C	4	Linear decrab rudder gain deg δ_R per deg ψ_C
C_1	0.05	0.10	0.20	Decrab integral ratio
L_1 (Capture)	1.0	1.5 deg	2.0	Beam displacement limiter (deg β)
L_2 (Capture)	—	None	—	Beam rate limiter
L_1 (O/C)	1.0	1.5 deg	2.0	Same as above
L_2 (O/C)	—	None	—	Same as above
L_3 (Capture)	20°	25°	30°	Heading error limiter
L_3 (O/C)	20°	25°	30°	Heading error limiter
L_4 Displ (Capture)	25°	30°	36°	Roll command limit
L_4 Displ (O/C)	8°	10°	15°	Roll command limit
L_4 Rate (Capture)	5 deg/sec	7 deg/sec	10 deg/sec	Roll command rate limit
L_4 Rate (O/C)	3 deg/sec	4 deg/sec	8 deg/sec	Roll command rate limit
ϵ_1	0.15	0.25	0.30	O/C sensor trip logic β/β_{MAX}
ϵ_2	0.010	0.013	0.015	O/C sensor trip logic $\dot{\beta}/\beta_{MAX}$
ϵ_3	2 deg	3 deg	5 deg	O/C sensor trip logic ϕ
$h_{D/C}$	4	6	10	Nominal decrab altitude - wheels above ground

f. Performance Criteria

(1) Localizer Capture

(a) Initialize aircraft on a 45-degree beam intercept heading 12 nautical miles from runway threshold. The localizer should be captured with less than 10 percent overshoot. The on-course (O/C) sensor should operate before the aircraft is 9.0 nautical miles from touchdown.

(b) Initialize aircraft on a 90-degree beam intercept heading 14 nautical miles from runway threshold. The same performance as in (a) above should be achieved.

(2) Localizer On Course

(a) Initialize aircraft so that β = 1.0 degree and $\dot{\beta}$ = 0 at 6 nautical miles and 2 nautical miles from runway threshold. (Zero crosswind should be maintained.) The aircraft should converge to the beam center (β = 0) with less than 20 percent overshoot. The steady value of β should be reduced to below 0.36 degree within 20 seconds. The steady-state response should be within 0.10 degree by the time the runway threshold has been reached.

(b) With on-course parameters set, initialize the aircraft so that β = 0 and $\dot{\beta}$ = 0 at a distance of 8 miles from the runway threshold. Apply a 10-knot crosswind step. The peak β error should be below 1.0 degree and a steady-state value below 0.1 degree should be attained with overshoot held to below 20 percent of the peak error. The β error should be below 0.36 degree within 30 seconds after insertion of the step crosswind.

(3) Decrab

Decrab performance can only be evaluated in conjunction with flareout tests.

(a) Establish the nominal time required for the aircraft to descend from the nominal decrab altitude to touchdown.

(b) Establish a steady-state descent with 5 degrees of crab angle. The decrab should be accomplished with the following touchdown criteria:

- Landing gear drift velocity should be below 3 feet per second at touchdown.
- Lateral drift from initiation of decrab should be below 20 feet.

B. DIGITAL PROGRAM - LATERAL GUIDANCE

1. Control Law Conversion

The representation of the lateral guidance block diagram and control laws in FORTRAN notation is summarized in Figure 7-8 with a tabulation of the FORTRAN namelist given in Table 7-3.

TABLE 7-3

VARIABLE LIST FOR SUBROUTINE LGUIDE

Variable	FORTRAN Name	Description
a_1	ALG1	Localizer beam rate gain
a_2	ALG2	Localizer beam displacement gain
a_3	ALG3	Localizer beam displacement integral gain
b_1	BL1	Heading error gain
--	BMPEN	Glide-slope beam penetration logic variable
--	CB	Capture localizer beam logic variable
ϵ	CBTEST	Localizer capture trip logic level
--	CBTHLD	Localizer capture trip logic threshold
R'	DME	Range to runway threshold
$R'_{G/S}$	DMEGS	Range to runway threshold at glide-slope penetration
ϵ_1	EPLB1	On-course trip logic - $\dot{\beta}$ threshold
ϵ_2	EPLB2	On-course trip logic - β threshold
ϵ_3	EPL3	On-course trip logic - ϕ threshold
β	EPSLOC	Localizer beam displacement in degrees
--	HH	Heading hold logic variable
C_1	KCL1	Localizer capture trip logic: heading error gain
C_2	KCL2	Localizer capture trip logic: $\dot{\beta}$ gain
C_3	KCL3	Localizer capture trip logic: β gain
$k(R')$	KLDCT	Attenuation factor for localizer gain reduction

TABLE 7-3 (cont)

VARIABLE LIST FOR SUBROUTINE LGUIDE

Variable	FORTRAN Name	Description
K_ψ	APSI	Heading hold gain
L_1	LGL1	Localizer displacement signal limiter
L_3	LGL3	Heading error limiter
$L_4(P)$	LGL4P	Roll command position limit
$L_4(R)$	LGL4R	Roll command rate limit
k	LOCATN	Attenuation factor for localizer gain reduction
β_{max}	LOCMAX	Localizer beam width in degrees
--	ONC	On course logic variable
ϕ	PHI	Roll angle
ϕ_C	PHICOM	Roll angle command
--	PHIMAN	Manual bank angle command
ψ	PSI	Heading angle
ψ_D	PSIDRF	Aircraft drift angle
ψ_{ref}	PSIREF	Heading reference angle
ψ_R	THETRK	Runway heading
τ_2	THH	Synchronizer time constant
τ_1	TLG1	Heading error washout filter time constant
τ_2	TLG2	$\dot{\beta}$ filter time constant
τ_3	TLG3	$\dot{\beta}$ filter time constant
τ_4	TLG4	β filter time constant
--	DT3	Subroutine sample time
--	ANGLE	Input error angle } Heading error processor
--	ANS	Output error angle } Heading error processor

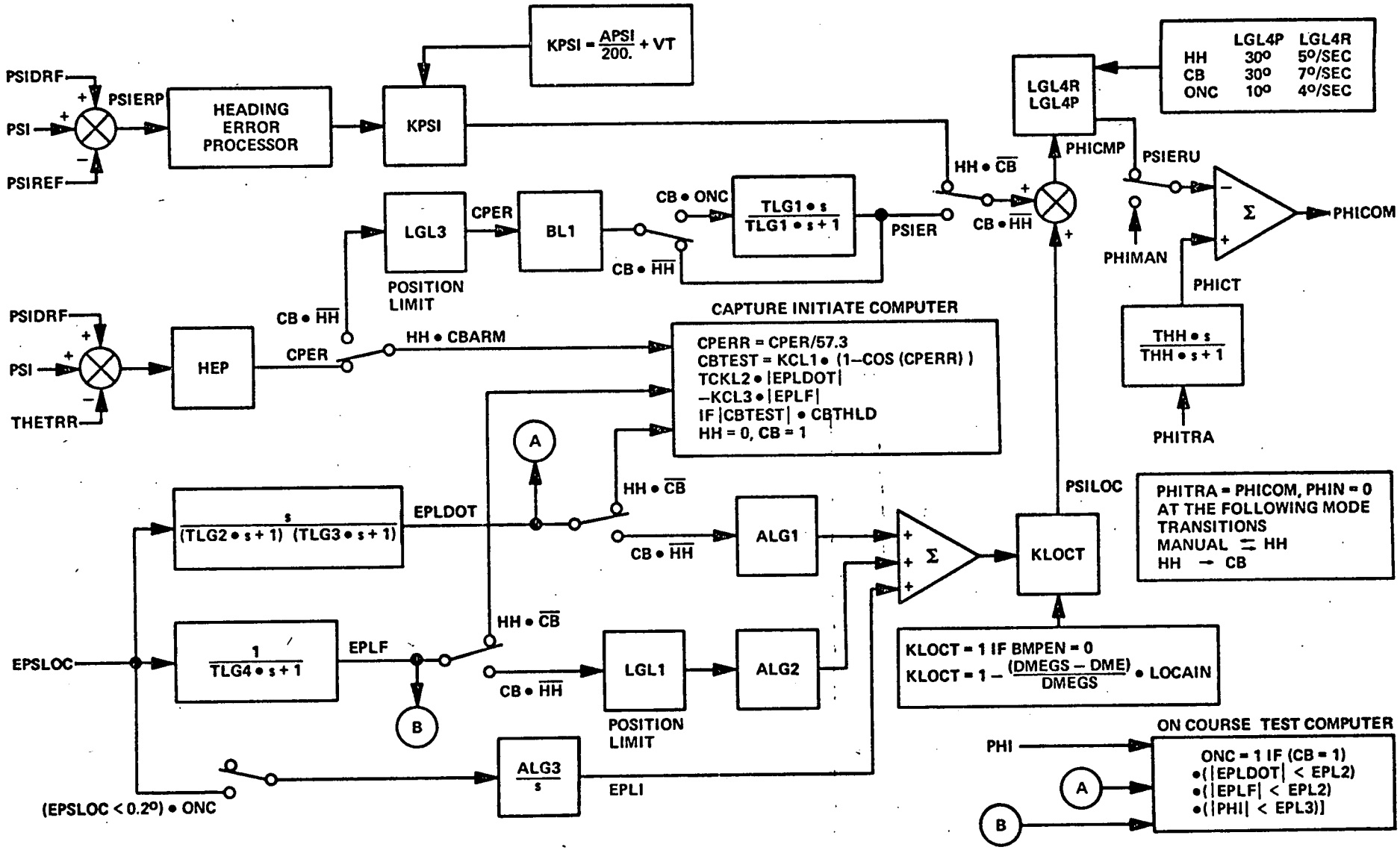

Figure 7-8
Lateral Guidance Block Diagram -
Fortran Notation

2. Program Flow Chart

The sequences of operations associated with the LGUIDE subroutine are:

a. Initial Condition Calculations

b. Heading Hold Gain Calculation

KPSI = APSI/200.0

c. Localizer On-Course Test Thresholds

EPL1 = EPLB1 * LOCMAX

EPL2 = EPLB2 * LOCMAX

d. Difference Equation Coefficients

Heading Error Washout Filter

CPSI = EXP (-DT3/TLG1)

Localizer Beam Displacement Rate Filter

CEPL1 = EXP (-DT3/TLG2) + EXP (-DT3/TLG3)

CEPL2 = EXP [-DT3 * (1.0/TLG2 + 1.0/TLG3)]

DEPL2 = [EXP (-DT3/TLG2) - EXP (-DT3/TLG3)]
* (1.0/TLG2/TLG3)/(1.0/TLG3 - 1.0/TLG2)

Localizer Beam Displacement Filter

CEPF = EXP (-DT3/TLG4)

DEPF - 1.0 - CEPF

Roll Angle Command Synchronizer Washout Filter

CPH1 - EXP (-DT3/THH)

Localizer Beam Displacement Integrator

DEPLI = ALG3 * DT3

The control law parameters for localizer on-course tracking are summarized on the figures depicting the transient responses. The localizer capture parameters that gave best results are:

LGL3 = 25°
BL2 = 3.0
TLG1 = 40 sec
KCL1 = 2.5
KCL2 = 2.8
KCL3 = 1.05 * (12 NM/R)
TLG2 = 1.0
TLG3 = 0.2
TLG4 = 0.25
ALG1 = 50
ALG2 = 50
ALG3 = 0.2

The flow diagrams for lateral guidance are summarized on Figures 7-9(a) through 7-9(h).

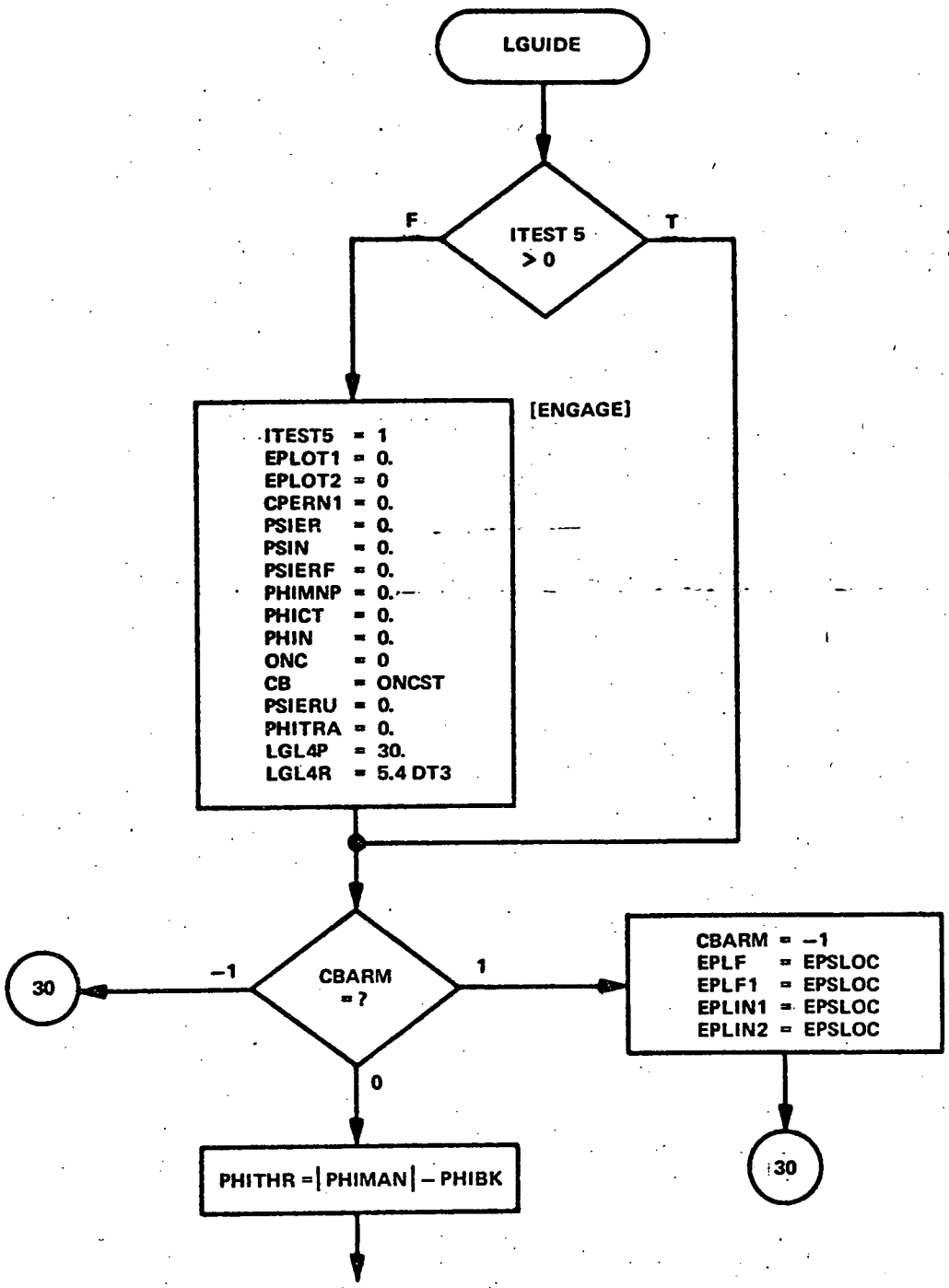

Figure 7-9a
LGUIDE Flow Chart

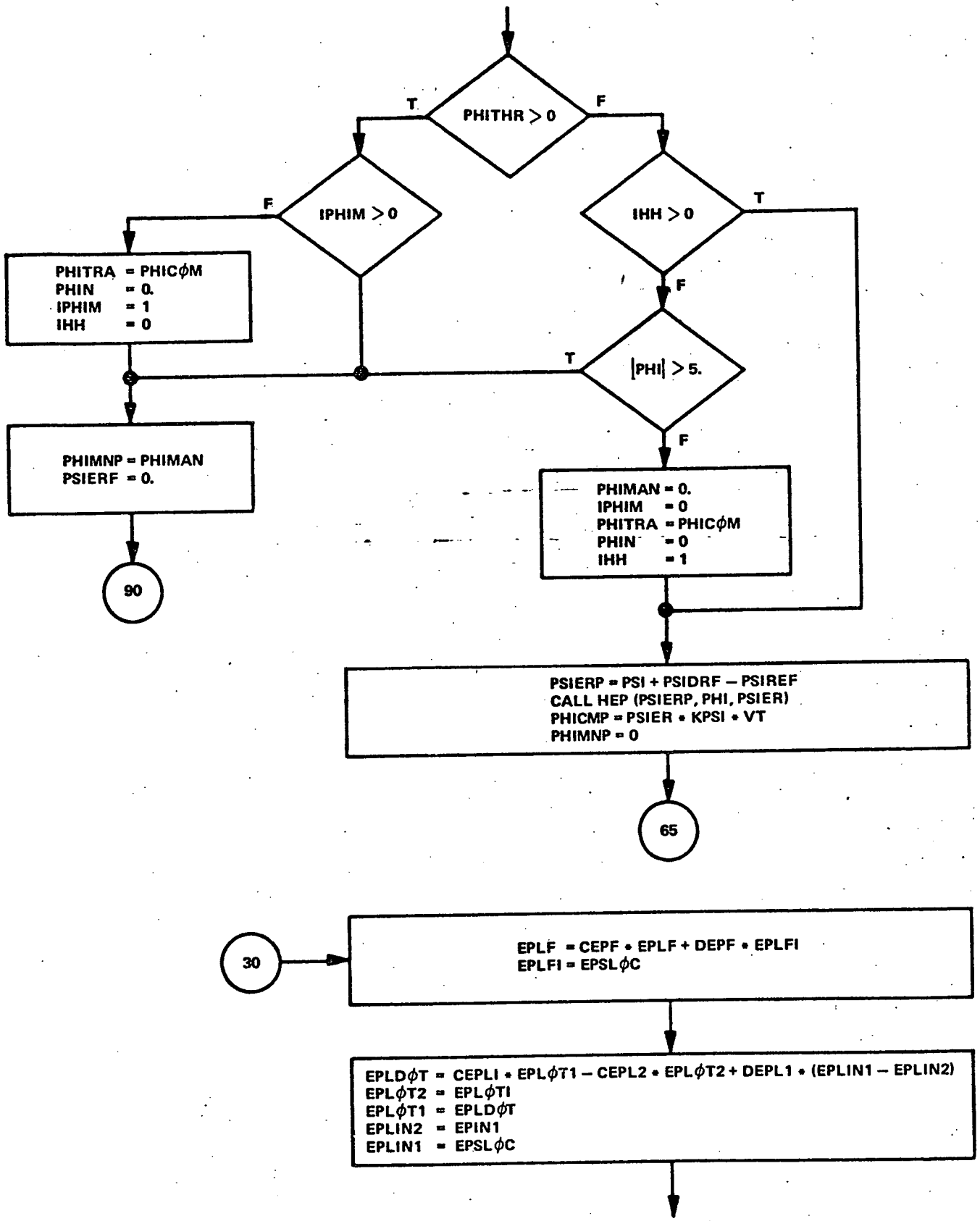

Figure 7-9b
LGUIDE Flow Chart

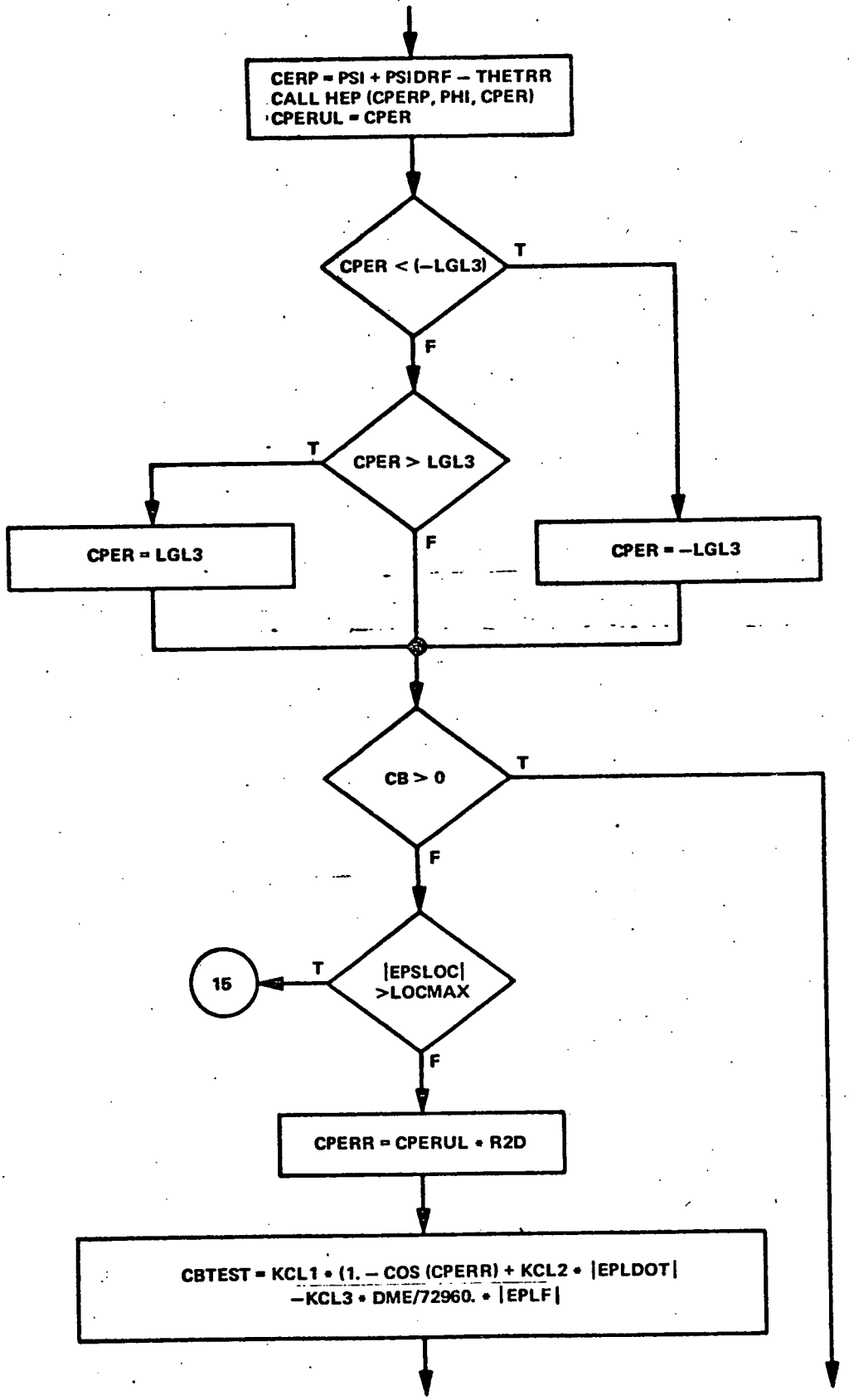

Figure 7-9c
LGUIDE Flow Chart

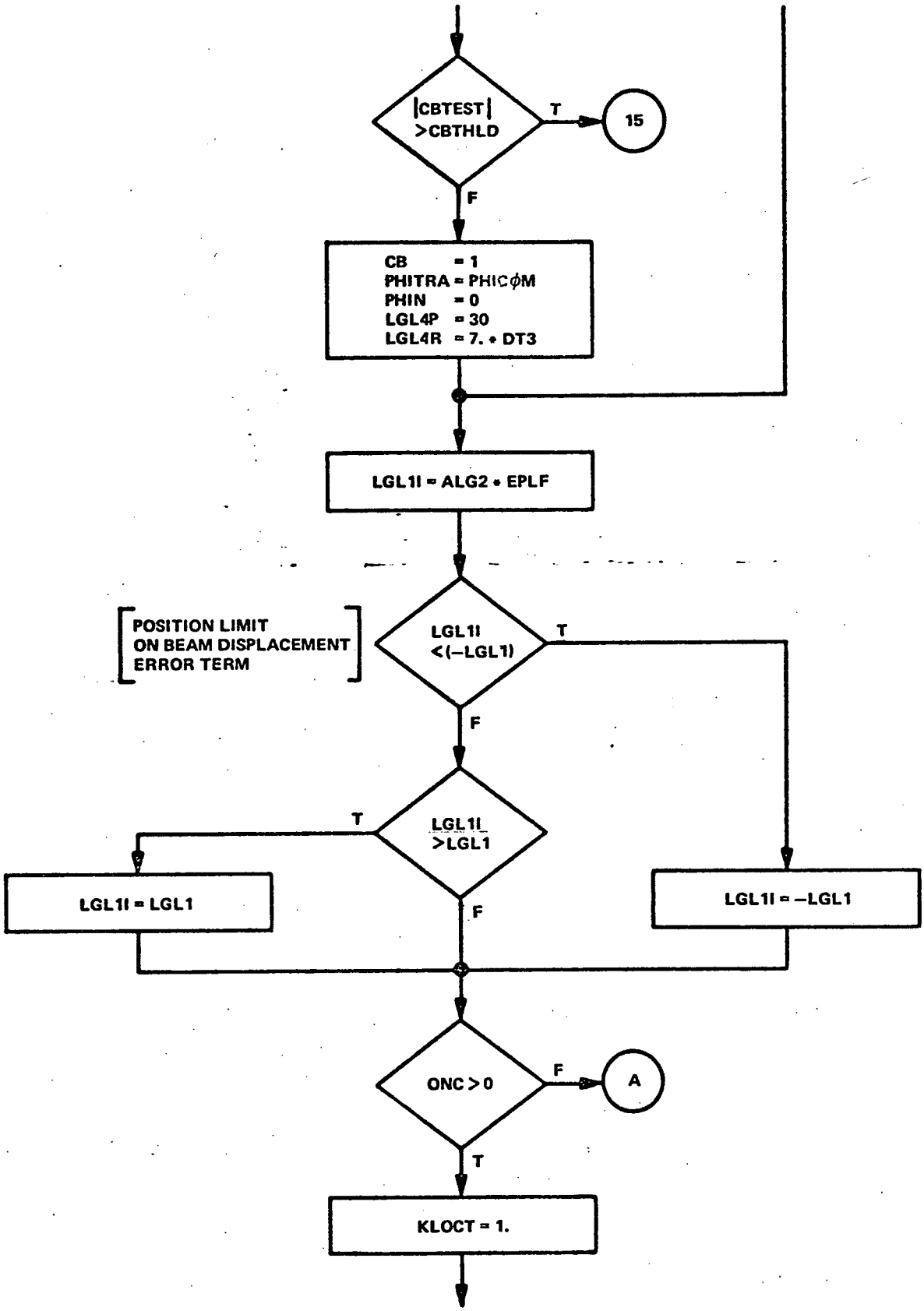

Figure 7-9d
LGUIDE Flow Chart

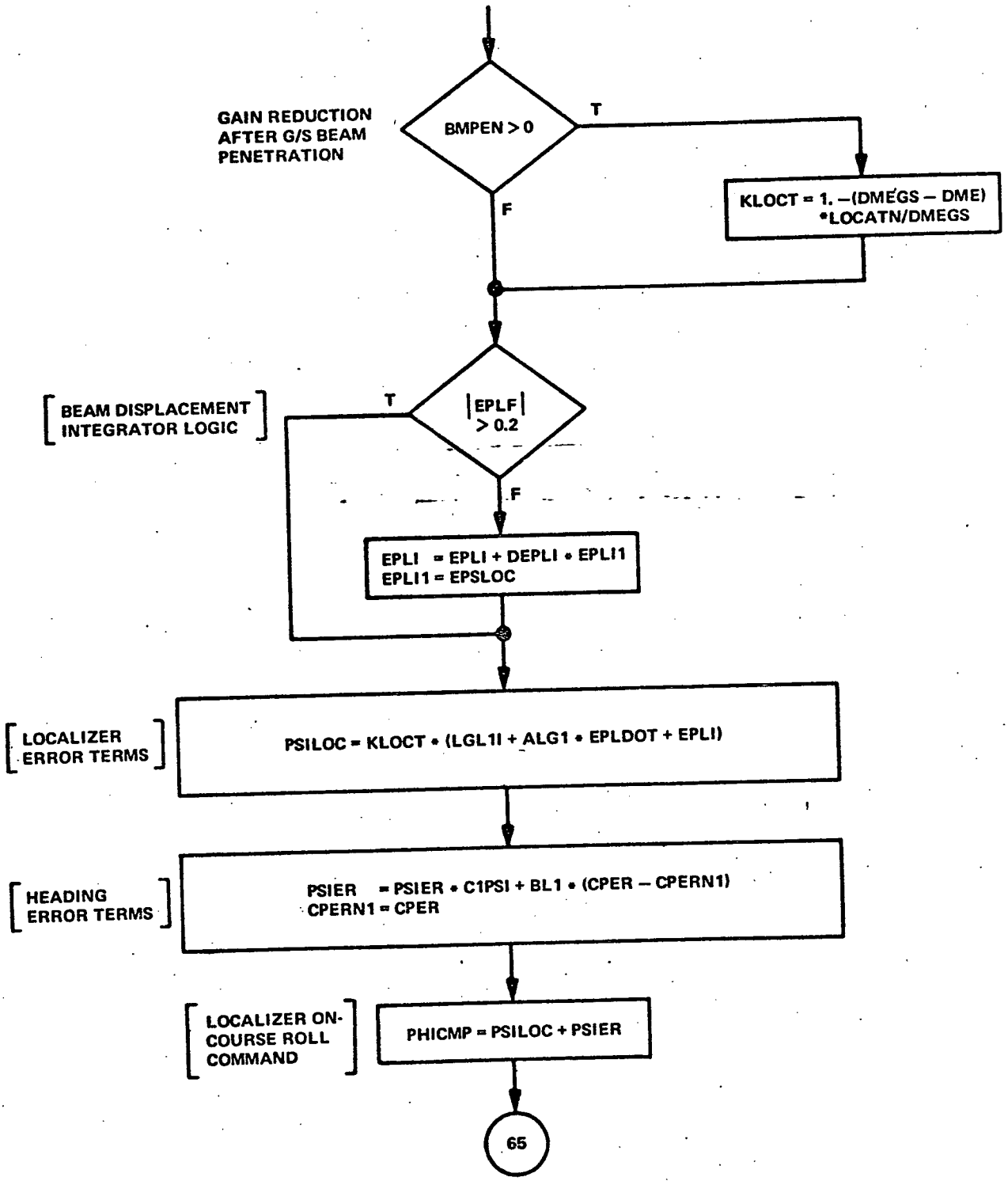

Figure 7-9e
LGUIDE Flow Chart

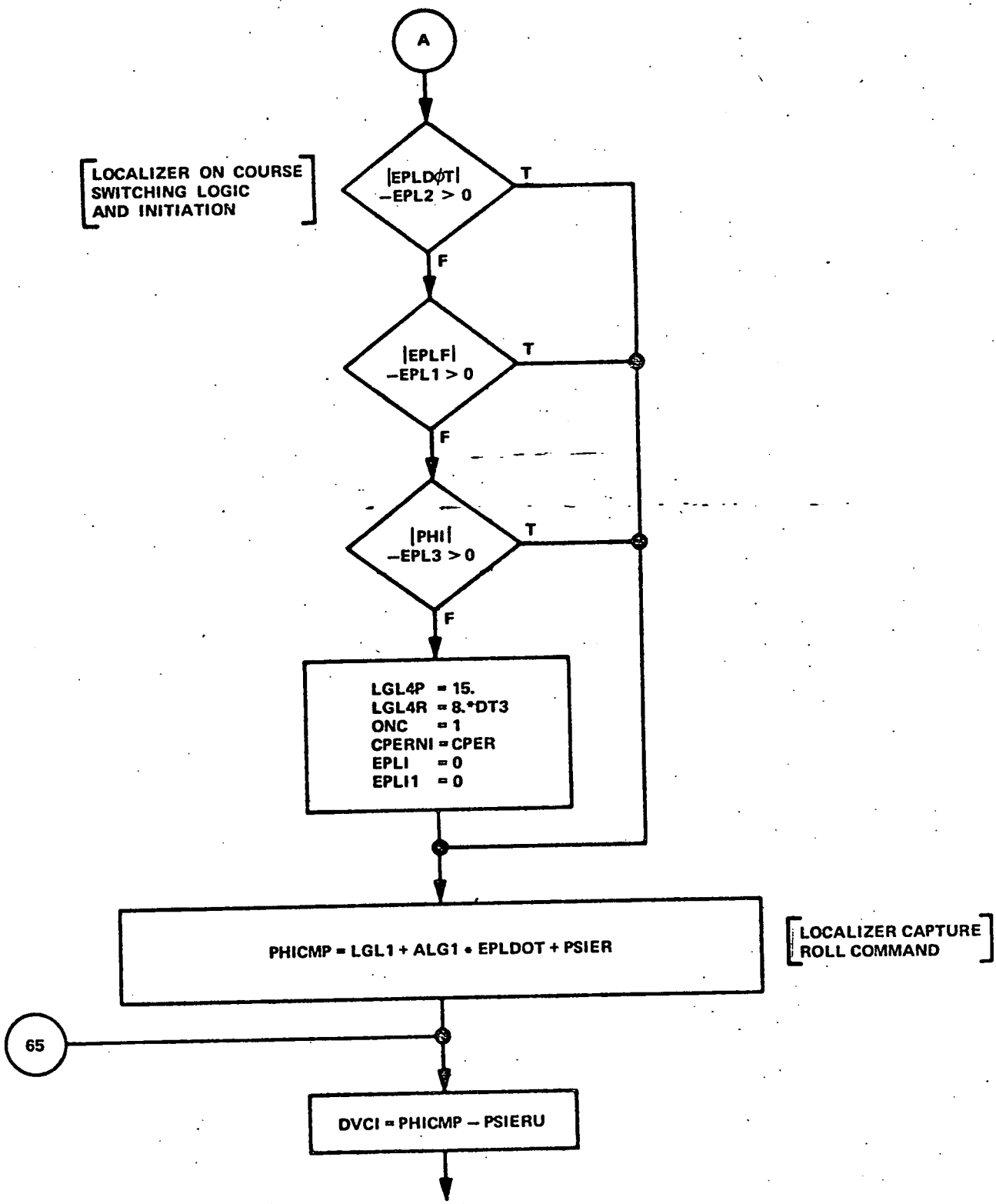

Figure 7-9f
LGUIDE Flow Chart

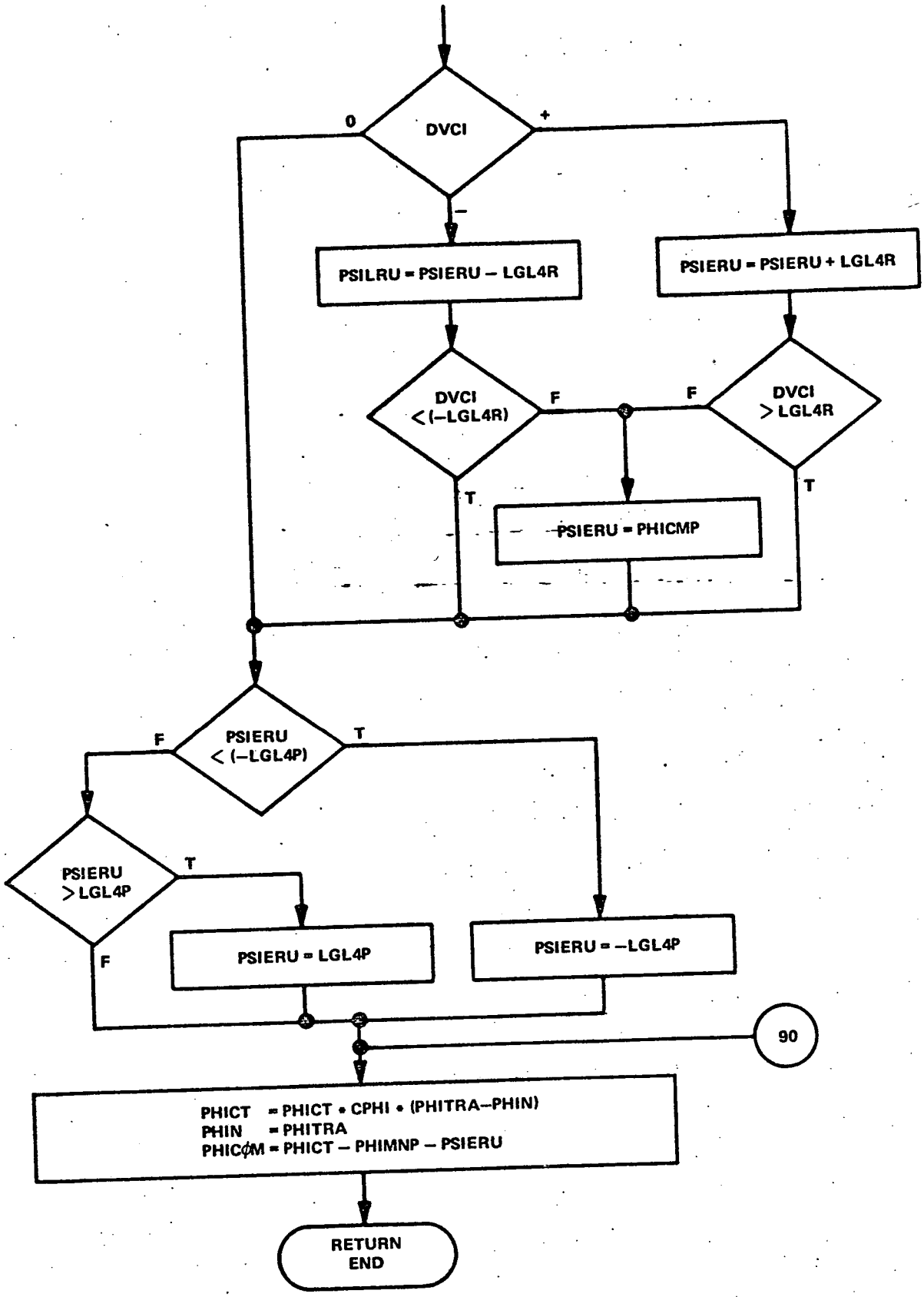

Figure 7-9g
LGUIDE Flow Chart

C. SIMULATION TEST RESULTS

1. Heading Control

Figure 7-10 illustrates heading control transient responses which meet the performance criteria specified in section 7-A-1f. A 5-degree step rudder held for 5 seconds causes a yaw transient of 5.5 degrees. Ninety percent of the recovery is achieved in about 6 seconds and the response is well damped.

Heading command response is almost entirely defined by the process kinematics and the control system constraints as illustrated in Figure 7-10. The initial response to a step 45-degree heading change command is dictated by the 5-degree-per-second roll rate command constraint, the 30-degree bank command limit and the coordinated turn rate achieved by the 30-degree bank angle. When 15 degrees of heading error remains, the control comes out of the command limit and the linear system takes over to provide a well-damped acquisition of the reference heading. The peak miscoordination is 0.03g, well within the specified criteria.

2. Localizer Capture

Excellent capture responses for a 90-degree and a 45-degree intercept are illustrated in Figure 7-11. In the 90-degree intercept case the overshoot is an imperceptible 0.05 degree of beam while in the 45-degree intercept case, on-course control starts when the beam error is about 0.1 degree and the overshoot is less than 0.05 degree. In both cases the overshoots would not be perceptible on the pilot's display instrument.

3. Localizer On-Course Transient Responses

The fact that accurate localizer control is more a measurement than a control problem is illustrated by the responses in Figure 7-12. The aircraft is initialized parallel to the beam but offset 1 degree of beam angle. The recovery for this position error 6 nautical miles and 2 nautical miles from touchdown is shown on this figure. Case (2) includes the washout filter in the control law while case (1) eliminates the washout filter from the heading feedback term. Obviously, when we eliminate the washout we can obtain an excellent, almost dead-beat, response. The washout degrades the transient response with an effect analogous to increasing the gain of the integral loop. It is used to compensate for inaccuracy in the measurement and computation of heading. In a lateral

guidance law with lateral velocity weighted 20 times lateral displacement ($y + 20\dot{y} = K\phi_C$), a 1.0 foot per second error in measuring $\dot{y}$ can cause a 20-foot offset in y. Note that 1.0 foot per second lateral velocity error is about 0.2 degree of heading error at approach speeds. If heading can be measured to 0.05 degree (or lateral velocity to about 0.25 foot per second) then the washout will not be needed. With velocity vector heading accuracies of 0.05 to 0.2 degree, the washout may be eliminated if sufficient beam rate compensation can be used. The restriction on the use of beam rate (ALG2 in Figure 7-8) is related to beam noise and the type of servo system used in the autopilot.

A summary of transient responses at 8 nautical miles, 6 nautical miles, and 2 nautical miles from touchdown is given in Figure 7-13. All of these results show adequate responses that should allow convergence of all errors to within a few feet of the runway centerline at touchdown. These results were obtained by eliminating the washout from the heading feedback term.

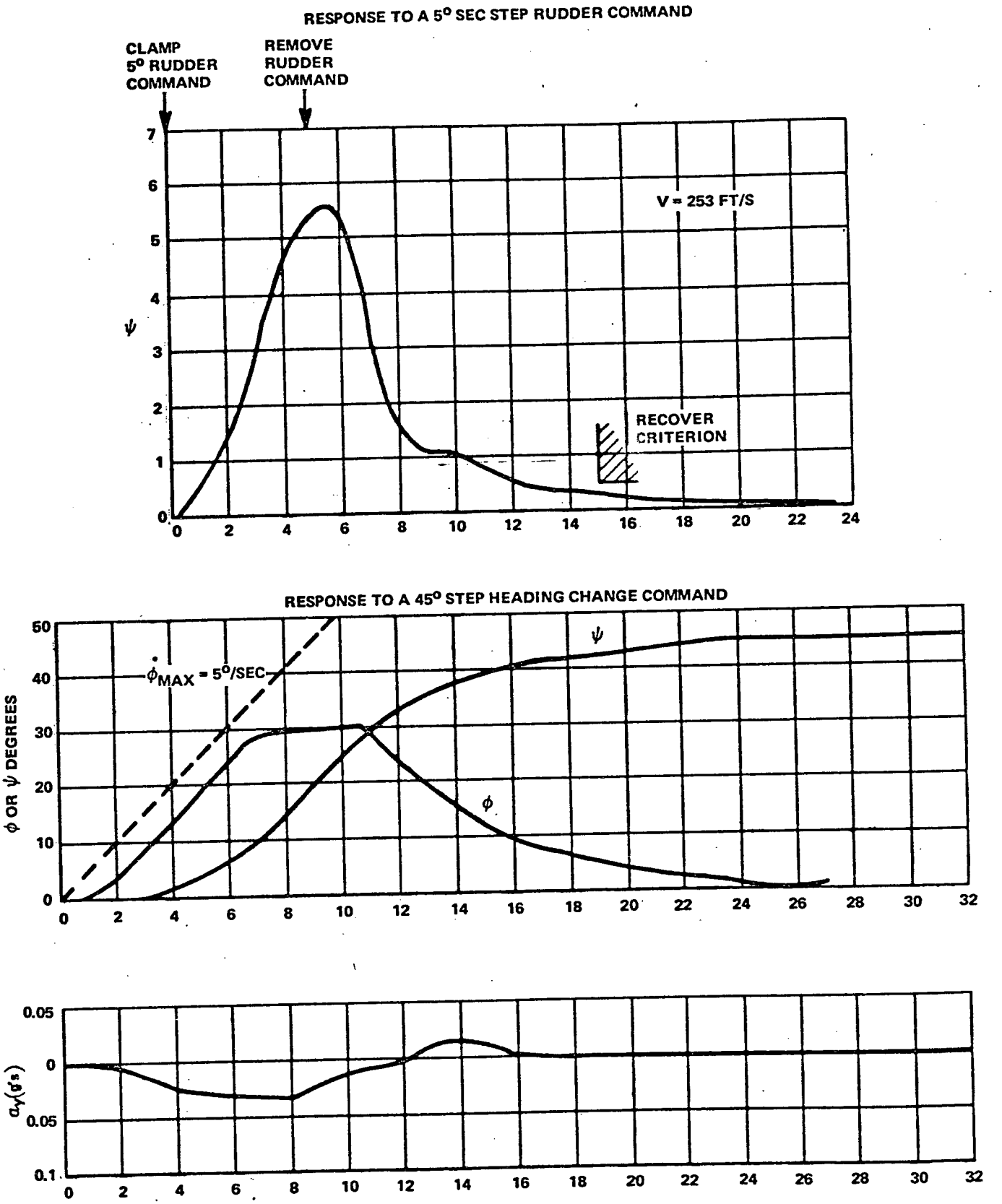

Figure 7-10
Heading Control Transient Response

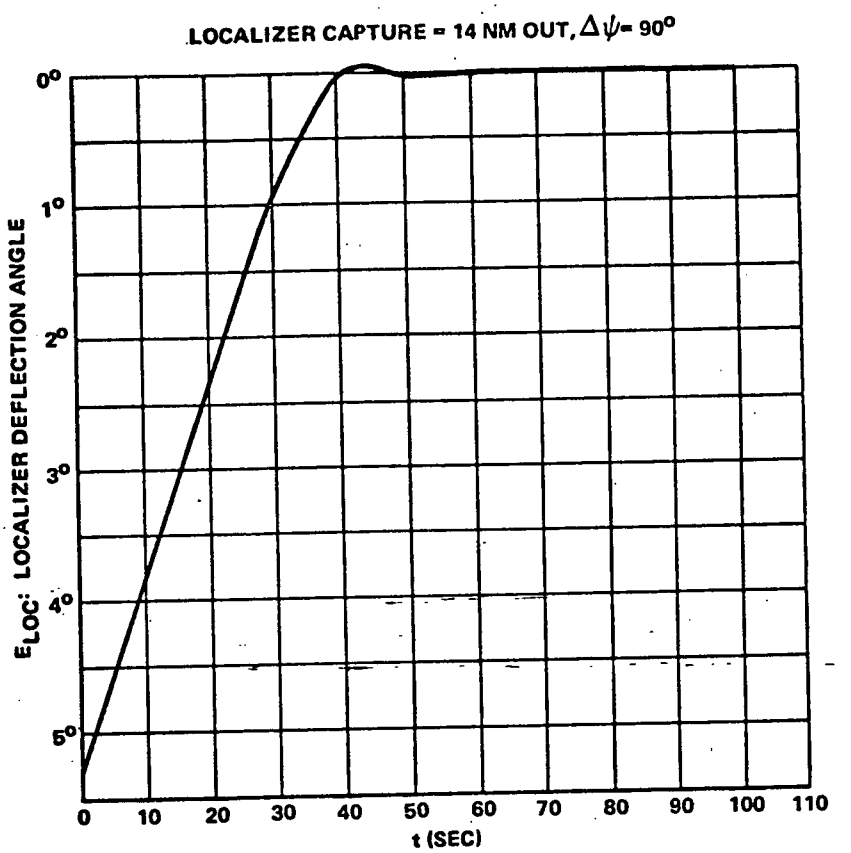

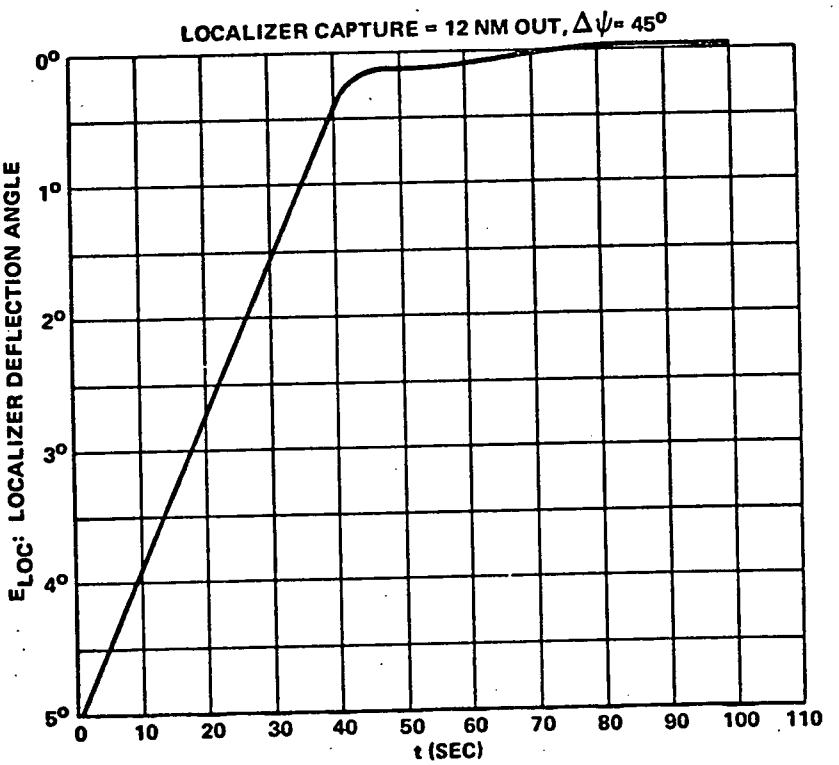

Figure 7-11
Localizer Capture Responses
(90° and 45° Intercepts)

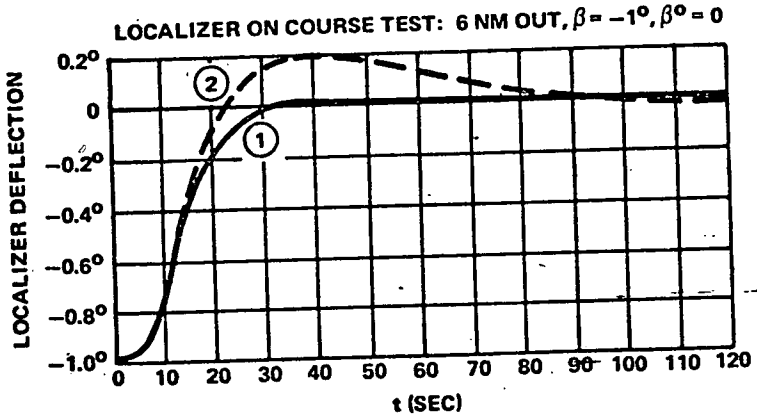

(1) INS VELOCITY VECTOR HEADING USED NO HEADING ERROR WASH-OUT FILTER. PARAMETER VALUES:
ALG1 = 10.
ALG2 = 30.
ALG3 = 0.2
BL1 = 2.0

(2) HEADING WASHOUT FILTER IN PARAMETER VALUES:
ALG1 = 20.
ALG2 = 50.
ALG3 = 0.2
BL1 = 2.8

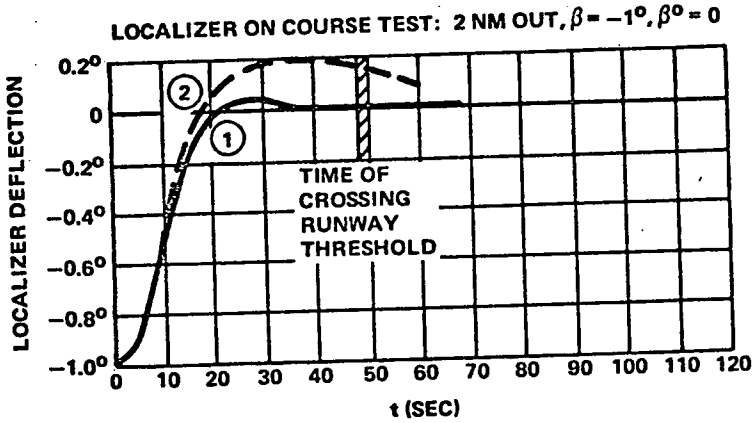

(1) SAME AS (1) ABOVE

(2) HEADING WASHOUT FILTER IN PARAMETER VALUES:
ALG1 = 50.
ALG2 = 50.
ALG3 = 0.2
BL1 = 2.8

Figure 7-12
Localizer Transient Responses with and without Heading Washout Filter

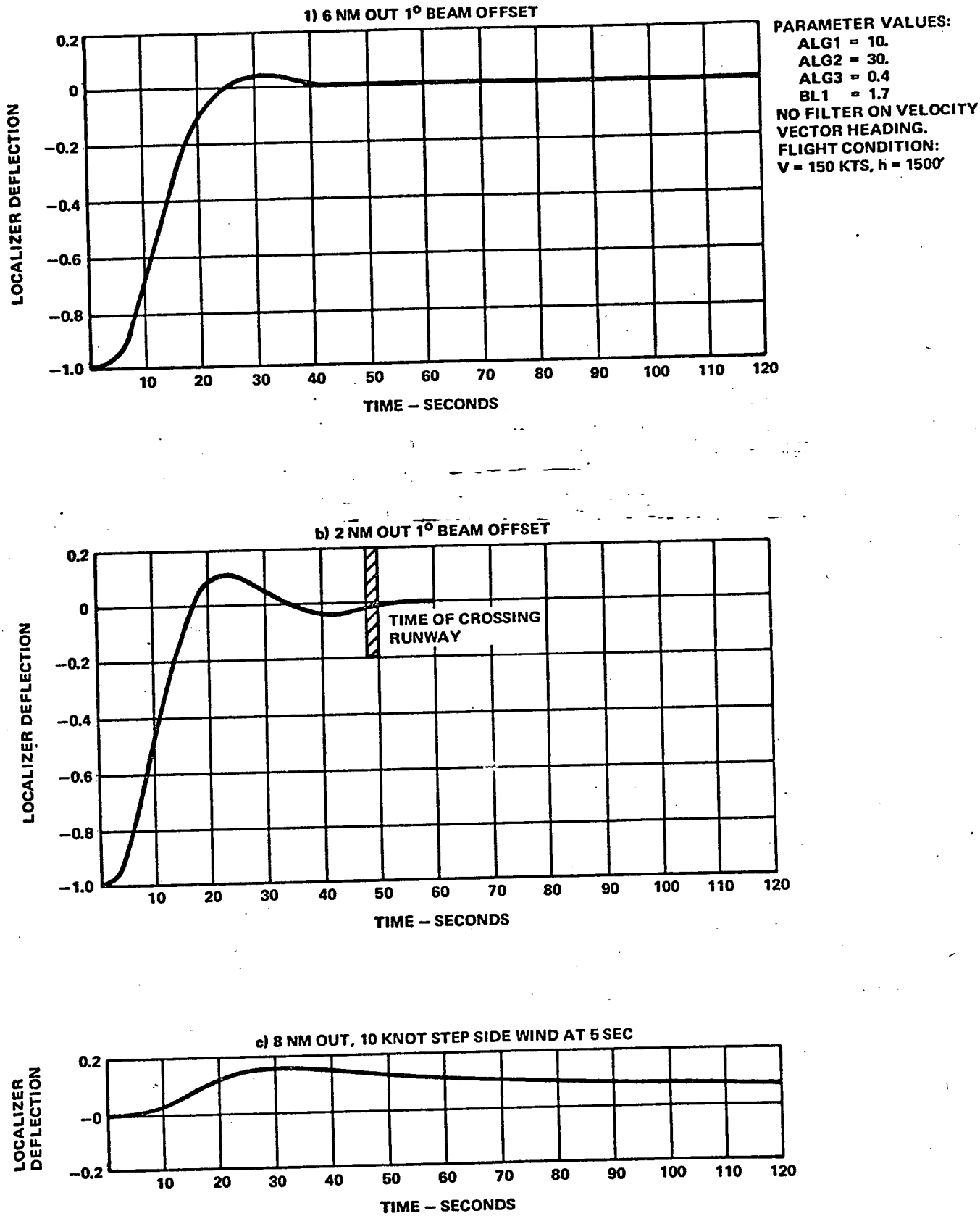

Figure 7-13
Localizer On-Course Transient Responses

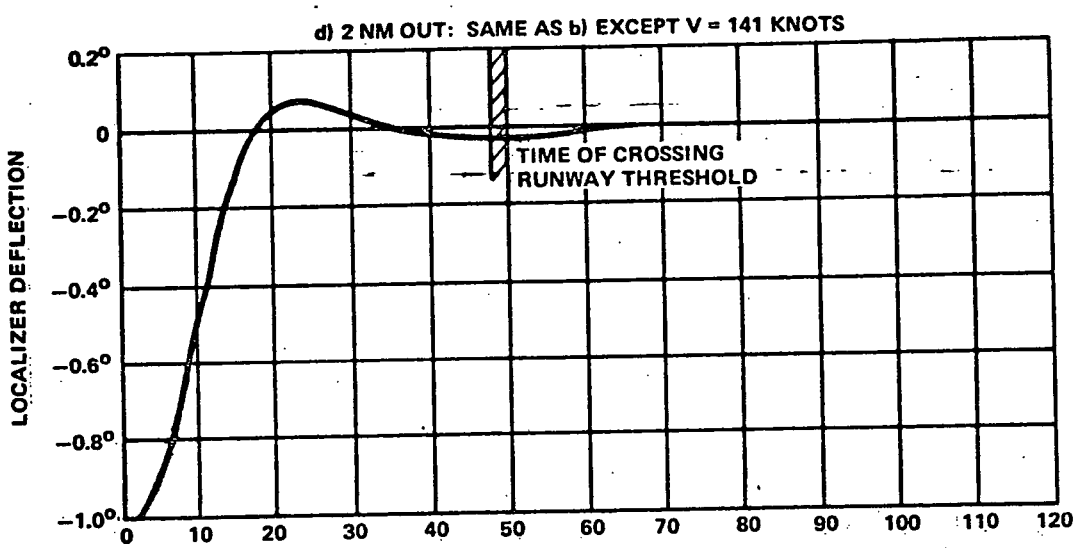

Figure 7-13
Localizer On-Course Transient Responses (cont)

SECTION VIII

MODE SELECTION AND DATA ENTRY

A. INTRODUCTION

The subject of mode selection and data entry for a digital autopilot involves operational procedures and data transmission programming that is beyond the scope of this report. Nevertheless some comments on these requirements are pertinent.

The flow chart for a mode select panel is one of the more complicated parts of a digital autopilot. A strategy for scanning the status of all input-output devices each computation cycle must be established. In a practical mechanization the data coding scheme and transmission format to and from the panel is an essential part of the system design. The versatility of the data entry and display devices enters into the software design requirements. In this discussion, the operational requirements for the altitude select and vertical speed select functions are presented as typical examples of procedures and techniques that are applicable to this problem. In place of the panel and numerical keyboard concept described, one could easily envision an alphanumeric keyboard and CRT interactive terminal.

B. OPERATIONAL CONSIDERATIONS AND MODE LOGIC

To utilize the various guidance modes described in this report, the pilot must have a means of entering desired references and a means of selecting a desired control mode. The elements of such a mode control panel for accomplishing the non-landing vertical guidance mode functions are shown in Figure 8-1. The requirements are a keyboard for entering numerical references, a display for transferring a verified keyboard entry to the appropriate control law parameter, and mode engage switches. For example, on Figure 8-1, the following procedure is used to set an altitude reference and then proceed to the desired altitude:

- The desired altitude is 12,500 feet.
- Set 1-2-5-0-0 on the keyboard. 12500 will appear on the keyboard display.
- Depress SET button under altitude reference window.
- 12500 transfers to reference altitude window (also is entered as h_{REF}).
- Depress altitude select mode switch.

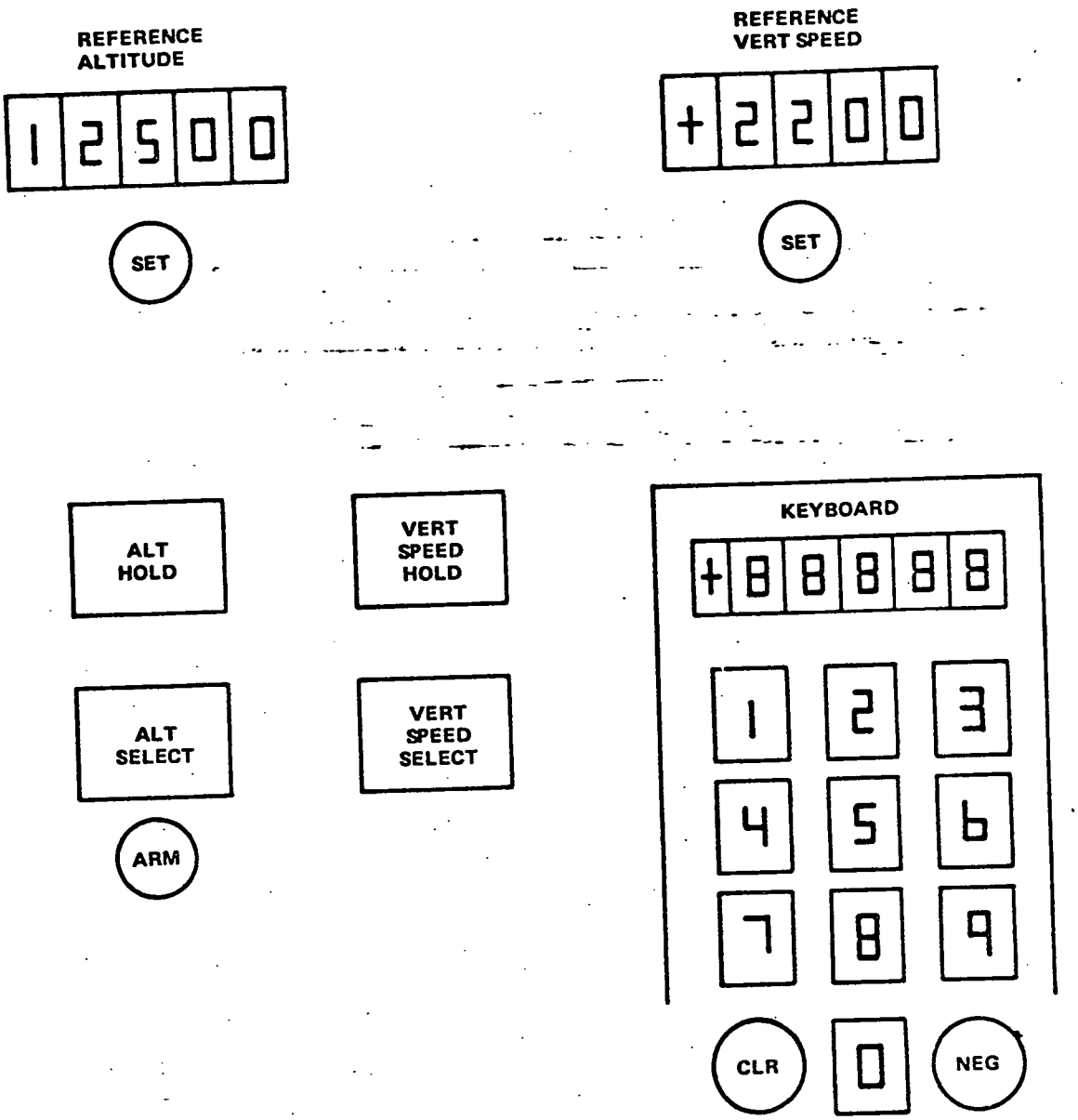

Figure 8-1
Mode Select Panel Requirements For
Vertical Guidance Modes

The aircraft will be maneuvered toward the desired altitude automatically in accordance with the following mode sequencing logic:

- If altitude hold was previously engaged, that mode is automatically disengaged and the vertical speed command mode is automatically engaged.

- A reference nominal vertical speed is automatically selected. A suggested nominal vertical speed is the one that points toward the reference altitude with a 2.0-degree flight path angle.

- The vertical speed command mode remains engaged until the Δh of the altitude select [Section V, equation (5-16)] is attained.

- The altitude select armed light is illuminated following depression of the altitude select engage switch. When capture to the reference altitude is initiated, the "armed" light is extinguished and the altitude select mode is now considered engaged.

- If the pilot wishes to change the vertical speed reference from the value automatically selected, he need only follow the normal procedure of entering a new vertical speed via the keyboard and the reference vertical speed SET button.

- If the altitude hold mode were not initially engaged when the altitude select switch was depressed, an automatic vertical speed steering program will not be commanded if the aircraft is already heading toward the desired altitude. However, if the aircraft is moving away from the desired altitude, then the vertical speed command sequence described above will be activated.

It is apparent that many computation and logic sequences must be programmed in the general-purpose digital autopilot computer to accomplish these functions. Included in these programs are the logic and computations that examine the reasonableness of the data entries (selected altitudes above allowable operating limits, for example) and the compatibility of selected modes (altitude select or altitude hold cannot be engaged while in an automatic approach and

landing sequence). The displays and warning sequences following mode select or data entry errors are an important part of the autopilot program.

The other functions which must be handled in a manner similar to that described for altitude select and vertical speed select are:

- Heading select
- Airspeed select (for autothrottle or pitch control modes)
- VOR course select
- Various mode engage functions.

Proper programming of these functions are dictated by the cockpit display and control concepts which are beyond the scope of this report.

REFERENCES

1. "Dynamics of the Airframe", Bureau of Aeronautics Report AE61-4-II, September 1952.

2. Jackson, C. T. and Snyder, C. T., "Validation of a Research Simulator for Investigating Jet Transport Handling Qualities and Airworthiness Criteria During Takeoffs", NASA TN D-3563, October 1966.

3. Osder, S. S., "Avionics Requirements for All Weather Landing of Advanced SST's, Volume I, Analysis of System Concepts and Operational Problems and Volume II, State-of-the-Art Review of All Weather Landing System Techniques", NASA CR73092 and CR73093, April 1967.

4. "Automatic Landing Systems", FAA Advisory Circular, AC N020-57A, 12 January 1971.

5. Neuman, F. and Foster, J. D., "Investigation of a Digital Automatic Landing System in Turbulence", NASA TN D-6066, October 1970.

6. Tou, J. T., "Digital and Sampled Data Control Systems", Book, McGraw Hill, 1959.

APPENDIX A

DESCRIPTION OF DIGITAL AUTOPILOT PROGRAM

The stabilization and control subroutines are written in FORTRAN IV. This makes the program less efficient, but makes it independent of the computer, and also makes it more accessible to the design engineer.

Each subroutine is organized in three different sections, initial conditions (IC), engage, and operate. The linear filter portions of the control laws are calculated in the same manner as described in Reference 5 by using difference equations. The IC calculations include the difference equation and rate limiter coefficients, which are determined as a function of the filter parameters and the sampling time interval. When a control mode is engaged, the engage section of the corresponding subroutine is entered once to initialize filters and integrators. The operate section of the control subroutine is entered once each loop time interval and contains the control logic and filters. A list of subroutines is given in Table A-1.

TABLE A-1

SUBROUTINE LIST

PITCHS	Longitudinal stabilization and automatic trim
AUTOTH	Autothrottle
LATSTB	Lateral stabilization Roll stabilization Yaw Damper Turn coordination
ALTHLD	Altitude hold
VERTSC	Vertical speed hold Vertical speed select Altitude capture
LGUIDE	Heading hold Heading Select Localizer capture Localizer tracking Decrab
VTLAND	Glide-slope capture Glide-slope tracking Flare
MEASURE	Compensated vertical speed computer
HDTCMP	Vertical speed command processor
HEP	Heading error processor
SASIC	Difference equation coefficient calculations for most control modes

APPENDIX B

DIGITAL SIMULATION OF REFERENCE JET TRANSPORT (RJT)

The reference jet transport simulation used as the test vehicle for the autopilot design and evaluation is that of a current transport aircraft with the substitution of hydraulically powered surfaces in place of aerodynamically boosted controls used in the actual aircraft. Elevator, aileron, rudder and throttle control servos are modeled as 2nd order systems with a damping ratio of 0.7 and a natural frequency of 20 rad/sec. The surface power boost actuators are modeled as first order lags with time constant of 0.067 second. The engine response is modeled as a first order lag with a time constant of 1.25 seconds. Flaps are operated at a fixed rate of 2 degrees/second and the horizontal stabilizer is driven (by the automatic system only) at a fixed rate of 0.06 degree/second.

The simulation includes ground effect, landing gear dynamics, and uses polynominals for non-linear aero dynamic derivatives.

The equations of motion are programmed in FORTRAN IV to run in nonreal time on the IBM 360/67, with line printer output. The simulation is also available on the EAI 8400 computer for real time flight evaluation, which includes a full scale cab with motion simulation and D/A outputs of all variables of interest. The digital program is divided into three basic loops. They consist of:

1. Body axis accelerations, Euler angle rates, transformation elements, part of landing gear.

2. Rotational dynamics, and remainder of landing gear.

3. Translational Dynamics

For the EAI 8400 an executive timing routine controls the order and point in time of execution of these loops. The relationship of the timing of these loops can be varied: At the present time the relationship used is 1:1:2. (0.05 sec :0.05 sec :0.1 sec).

The automatic control system is interfaced with the RJT by FORTRAN calls from the second and third loops. The actual location depends upon the particular function of the variable being considered. No interface has yet been provided in the simulator cab for pilot selection of modes or reference control variables. At this time, mode control is accomplished by means of special purpose programs for testing individual control modes and mode transitions.

APPENDIX C

RELATIONSHIP BETWEEN ZERO SIDESLIP AND ZERO LATERAL ACCELERATION

From Reference 2, Appendix B or any text on aircraft stability and control

The aircraft lateral acceleration (a_y) is:

$$a_y = g \sin \phi + \frac{QS}{m} \left(C_{y_\beta} \beta + C_{y_{\delta_R}} \delta_R \right) - \frac{1}{m} T_\beta \tag{C-1}$$

or

$$a_y = g \sin \phi + \frac{QS}{m} C_{y_{\delta_R}} \delta_R + \frac{QS}{m} \left(C_{y_\beta} - \frac{T}{QS} \right) \beta \tag{C-2}$$

A body-mounted lateral accelerometer provides an output proportional to A_y.

$$A_y = a_y - g \sin \phi \tag{C-3}$$

The condition for $\beta = 0$ [from Equation (C-2)] is

$$a_y = g \sin \phi + \frac{QS}{m} C_{y_{\delta_R}} \delta_R \tag{C-4}$$

The condition for $A_y = 0$ is [from Equation (C-3)]

$$a_y = g \sin \phi \tag{C-5}$$

Therefore, the condition for simultaneous equality of zero sideslip and zero lateral accelerometer output is:

$$C_{y_{\delta_R}} \delta_R \equiv 0 \tag{C-6}$$

This condition is approached for aircraft with large stable values of C_{n_β} (positive) where sideslip is near zero in a turn with zero rudder.